Role of nuclear transport receptor KPNB1 in the pathophysiology of spinocerebellar ataxia type 3

Dissertation

zur Erlangung des Grades eines
Doktors der Naturwissenschaften

der Mathematisch-Naturwissenschaftlichen Fakultät
und
der Medizinischen Fakultät
der Eberhard-Karls-Universität Tübingen

vorgelegt
von

Mahkameh Abeditashi
aus Teheran, Iran

2025

Tag der mündlichen Prüfung:	28.07.2025
Dekan der Math.-Nat. Fakultät:	Prof. Dr. Thilo Stehle
Dekan der Medizinischen Fakultät:	Prof. Dr. Bernd Pichler
1. Berichterstatter:	PD Dr. Thorsten Schmidt
2. Berichterstatter:	Prof. Dr. Ludger Schöls
Prüfungskommission:	PD Dr. Thorsten Schmidt
	Prof. Dr. Ludger Schöls
	Prof. Dr. Olaf Rieß
	Prof. Dr. Stefan Liebau

Erklärung / Declaration:

Ich erkläre, dass ich die zur Promotion eingereichte Arbeit mit dem Titel:

“Role of nuclear transport receptor KPNB1 in the pathophysiology of spinocerebellar ataxia type 3”

selbständig verfasst, nur die angegebenen Quellen und Hilfsmittel benutzt und wörtlich oder inhaltlich übernommene Stellen als solche gekennzeichnet habe. Ich versichere an Eides statt, dass diese Angaben wahr sind und dass ich nichts verschwiegen habe. Mir ist bekannt, dass die falsche Abgabe einer Versicherung an Eides statt mit Freiheitsstrafe bis zu drei Jahren oder mit Geldstrafe bestraft wird.

I hereby declare that I have produced the work entitled “Role of nuclear transport receptor KPNB1 in the pathophysiology of spinocerebellar ataxia type 3”, submitted for the award of a doctorate, on my own (without external help), have used only the sources and aids indicated and have marked passages included from other works, whether verbatim or in content, as such. I swear upon oath that these statements are true and that I have not concealed anything. I am aware that making a false declaration under oath is punishable by a term of imprisonment of up to three years or by a fine.

Tübingen, den ....

Datum / Date Unterschrift /Signature

In memory of my beloved mother

Table of contents

Abbreviations

AD	Alzheimer’s disease
ALS	Amyotrophic lateral sclerosis
AR	Androgen receptor
ASO	Antisense oligonucleotide
BafA1	Bafilomycin A1
CaMKII	Calcium-calmodulin-dependent kinase II
CAS	Cellular apoptosis susceptibility
Chk1	Checkpoint kinase 1
CI-III	Calpain inhibitor III
CK2	Serine-threonine casein kinase 2
CLPP	Clp protease proteolytic subunit
COA7	Cytochrome C oxidase assembly factor 7
CRM1	Chromosome region maintenance 1 protein
DRPLA	Dentatorubral-pallidoluysian atrophy
DUB	Deubiquitinating enzyme
EPO	External progressive ophthalmoplegia
ER	Endoplasmic reticulum
ERAD	Endoplasmic reticulum-associated degradation
esiRNA	Endoribonuclease-prepared siRNA
FDR	False discovery rate
FTD	Frontotemporal dementia
GFP	Green fluorescent protein
GSK3β	Glycogen synthase kinase-3β
GST	Glutathione S-transferase
GWAS	Genome-wide association study
HD	Huntington's disease
HDAC	Histone deacetylase
HEK	Human Embryonic Kidney
Hsp	Heat shock protein

Abbreviations

HTT	Huntingtin
IM	Ionomycin
IPA	Ingenuity Pathway Analysis
iPSC	Induced pluripotent stem cell
IPTG	Isopropyl β-D-1-thiogalactopyranoside
IPZ	Importazole
JD	Josephin domain
KPNA2	Karyopherin α-2
KPNA3	Karyopherin α-3
KPNB1	Karyopherin β-1
Lac	Lactacystin
LC3	Autophagosomal microtubule-associated protein light chain 3
LDS	Lithium dodecyl sulfate
LLPS	Liquid-liquid phase separation
MBNL1	Muscleblind-like 1
MDC1	Mediator of DNA damage checkpoint protein 1
miRNA	MicroRNA
MJD	Machado-Joseph disease
MS	Mass spectrometry
mtDNA	Mitochondrial DNA
NES	Nuclear export signal
NLS	Nuclear localization signal
NPC	Nuclear pore complex
NUP	Nucleoporin
p53	Tumor protein 53
PCR	Polymerase chain reaction
PD	Parkinson's disease
PE	Phosphatidylethanolamine
PKI	Protein kinase inhibitor
PNA	Peptide nucleic acid
PNKP	Polynucleotide kinase 3'-phosphatase

PolyQ	Polyglutamine
PTM	Post-translational modification
Ran	Ras-related nuclear protein
RanGAP1	RanGTPase activating protein-1
RanGEF	Ran guanine nucleotide exchange factor
REAP	Rapid, Efficient And Practical
ROS	Reactive oxygen species
SBMA	Spinobulbar muscular atrophy
SCA3	Spinocerebellar ataxia type 3
SDHB	Succinate dehydrogenase (ubiquinone) iron-sulfur subunit
SDS-PAGE	Sodium dodecylsulfate polyacrylamide gel electrophoresis
shRNA	Short hairpin RNA
SNP	Single nucleotide polymorphism
SV40	Simian virus 40
TDP-43	TAR DNA-binding protein of 43 kDa
TRIM29	Tripartite motif containing protein 29
UIM	Ubiquitin-interacting motif
UPR^{mt}	Mitochondrial unfolded protein response
UPS	Ubiquitin-proteasome system
VCP	Valosin-containing protein

Abstract

Spinocerebellar ataxia type 3 (SCA3), also known as Machado-Joseph disease (MJD), is the most common form of autosomal dominant hereditary ataxias and characterized by a pathological expansion of the polyglutamine (polyQ) tract within the ataxin-3 protein. Ataxin-3 is mainly a cytoplasmic protein, although polyQ-expanded ataxin-3 accumulates in the nucleus of affected neurons and forms intranuclear aggregates, leading to neurotoxicity and cell death. Unravelling the underlying mechanisms in the nuclear localization of polyQ-expanded ataxin-3 and its involvement in neurotoxicity can provide insight into the pathogenesis of this disease and the development of novel therapeutic strategies. In this respect, investigation of the nucleocytoplasmic transport machinery and its implication for the pathogenesis of SCA3 and other polyQ diseases has gathered attention. Our lab has previously indicated the critical importance of karyopherin α-3 (KPNA3), a nuclear transport receptor, in the nuclear transport of ataxin-3 and its implication in the pathogenesis of SCA3. Since KPNA3 functions as an adaptor protein for karyopherin β-1 (KPNB1) in the nuclear transport of protein cargos, we aimed to explore the role of KPNB1 in the pathogenesis of SCA3 as well.

Here, we report on SCA3 cell model-based analysis of the nuclear transport receptor KPNB1 and its implications for the pathogenesis of SCA3. We figured out that KPNB1 interacts directly with both wild-type and polyQ-expanded ataxin-3. However, modulating KPNB1 levels did not change the subcellular distribution of ataxin-3. Interestingly, KPNB1 overexpression reduced protein levels and aggregation of ataxin-3 and promoted its cleavage, whereas its knockdown and pharmacological inhibition led to an increase in soluble and insoluble levels of ataxin-3. Our data revealed that modulation of ataxin-3 was apparently based on protein fragmentation, independent of the classical SCA3-associated proteolytic pathways. Label-free quantitative proteomics and knockdown experiments indicated mitochondrial protease CLPP as a potential mediator of the ataxin-3-degrading effect induced by KPNB1 overexpression. We confirmed a reduction of KPNB1 protein levels in SCA3 by analyzing two SCA3 transgenic mouse models and induced pluripotent stem cells (iPSCs) derived from SCA3 patients. Our findings suggested a yet undescribed regulatory function of KPNB1 in modulating ataxin-3, thereby highlighting a new potential target of therapeutic value for SCA3.

1. Introduction

1.1 Spinocerebellar ataxia type 3

Neurodegenerative diseases are sporadic or hereditary disorders that characterized by progressive degeneration of the structure and function of selective populations of neurons (Dugger and Dickson, 2017; Reith, 2018). Spinocerebellar ataxia type 3 (SCA3), also known as Machado-Joseph disease (MJD), is a hereditary neurodegenerative disease and the most prevalent autosomal dominant ataxia in the world (approximately 1:50,000–100,000) (Hersheson et al., 2012; Klockgether et al., 2019; McLoughlin et al., 2020). It impacts males and females equally and prominently degenerates the central nervous system (CNS) (Fan et al., 2014).

For the first time, a heritable ataxia was recognized in several Portuguese families of Azorean ancestry in the 1970s and considered independent diseases (Coutinho and Andrade, 1978). Two of the affected families were descended from William Machado and Antone Joseph, leading to the disease designation Machado-Joseph disease. Two decades later, the responsible mutation for the disease was identified and mapped to the long arm of chromosome 14 (14q24.3-q32.45) by Takiyama and colleagues. The mutation was present in all affected people of a pathologically confirmed MJD family, and the discovery led to the unification of MJD and SCA3 (Dürr et al., 1996; Kawaguchi et al., 1994; Takiyama et al., 1993). A worldwide haplotype-based study of SCA3 patients suggested that the disease may be evoked by two main founder mutations, one occurring in Asians with an estimated age of 5,800 years and another in Portuguese individuals that occurred almost 1,400 years ago. Even though it is believed that the prevalence of SCA3 is attributed to the Portuguese descent (Gaspar et al., 2001).

1.1.1 Classification and epidemiology of SCA3

SCA3 belongs to the class of spinocerebellar ataxias (SCAs) that represent autosomal dominantly inherited diseases. SCAs are remarkebly heterogeneous, with a complex genotype-phenotype spectrum, and more than 40 distinct genetic subtypes of SCA have been identified. SCAs are numbered in the chronological order in which their genetic loci were discovered (Klockgether et al., 2019). The clinical feature of all SCAs is a progressive loss of

balance and coordination known as ataxia, which arises from the progressive degeneration of the cerebellum accompanied by visual and speech problems (Sullivan et al., 2019). The age at onset is usually in mid-adulthood; however, manifestations in childhood and old age can occur (Durr, 2010). In general, SCAs are considered rare diseases, with prevalence estimates of about 0.3–2.0 per 100,000 (van de Warrenburg et al., 2002). SCA3 is the most common SCA in the world (20–50% of all types of SCAs) and shows geographical and ethnic variability (Table 1.1), which can be mainly explained by founder effects (Klockgether et al., 2019; Sequeiros et al., 2012).

Table 1.1 Overview of the prevalence of SCA3 in different countries, which is the most common SCA worldwide (Klockgether et al., 2019).

Country	**% SCA3 to all SCAs**
Portugal	58–74%
Brazil	69–92%
Singapore	53%
China	48–49%
The Netherlands	44%
Germany	42%
Japan	28–63%
USA and Canada	21–24%
France	20%
Mexico	12%
Australia	12%
India	5–14%
South Africa	4%
Italy	1%

Genetically, the SCAs fall into three major categories: 1) polyglutamine ataxias, which are caused by dynamic CAG repeat expansion mutations coding for a pure repeat of amino acid glutamine in the disease proteins; 2) non-coding repeat ataxias, which are caused by repeat expansions outside of the coding region of the respective disease genes; and 3) ataxias caused by conventional mutations (non-repeat mutations) in specific genes (Soong and Paulson, 2007).

1.1.2 The group of polyglutamine diseases

Seven spinocerebellar ataxias (SCA1, SCA2, SCA3, SCA6, SCA7, SCA17, and dentatorubral-pallidoluysian atrophy; DRPLA) belong to the class of polyglutamine (polyQ) diseases, along with Huntington's disease (HD) and spinobulbar muscular atrophy (SBMA) (Table 1.2), that are a major cause of neurodegeneration worldwide (Klockgether et al., 2019; Zoghbi and Orr, 2000).

Table 1.2 Characteristics of polyglutamine (polyQ) diseases. They are a group of nine hereditary neurodegenerative diseases that are caused by a CAG repeat expansion, coding for an abnormally long polyQ tract in the respective disease proteins. Modified from Shao and Diamond, 2007; Lieberman et al., 2019; Klockgether et al., 2019.

Disease	Protein	Normal repeat	Pathogenic repeat	Affected brain regions
HD	Huntingtin	6–35	36–121	Striatum, cerebral cortex
SBMA	Androgen receptor	6–36	38–≤ 70	Anterior horn and bulbar neurons, dorsal root ganglia
DRPLA	Atrophin-1	3–38	49–88	Cerebellum, cerebral cortex, basal ganglia, Luys body
SCA1	Ataxin-1	6–34	38–85	Purkinje cells, dentate nucleus, brainstem
SCA2	Ataxin-2	14–31	36–100	Purkinje cells, brain stem, frontotemporal lobes
SCA3	Ataxin-3	12–40	60–87	Dentate neurons, basal ganglia, brain stem, spinal cord
SCA6	Voltage-dependent P/Q-type calcium channel subunit alpha-1A	4–18	21–33	Purkinje cells, dentate nucleus, inferior olive
SCA7	Ataxin-7	7–18	38–200	Cerebellum, brain stem, macula, visual cortex
SCA17	TATA box binding protein	25–43	45–63	Purkinje cells, inferior olive

PolyQ diseases are developed by a dynamic expansion of a CAG trinucleotide repeat in the causative genes, coding for an abnormally long repeat of amino acid glutamine in the respective disease proteins (Bauer and Nukina, 2009; Klockgether et al., 2019; Shao and Diamond, 2007). SBMA, also known as Kennedy disease, was the first CAG trinucleotide repeat disease described in 1991, which is caused by a CAG repeat expansion in the androgen

receptor (AR) gene (La Spada et al., 1991). Apart from SBMA, which is X-linked, all polyQ diseases are dominantly inherited (Gatchel and Zoghbi, 2005). PloyQ diseases present anticipation, which is defined as a decreasing age of onset from generation to generation (Rudnicki and Margolis, 2003).

Despite the common mutation, the neuronal toxicity and clinical features are remarkably heterogeneous among polyQ diseases, which can be explained by the unique protein context of each disease. PolyQ diseases are mainly late-onset, relentlessly progressive, give rise to neurological and physical impairments in the patients, and are ultimately fatal (Rudnicki and Margolis, 2003). These diseases share some similarities in clinical, pathological, and genetic features that propose common mechanisms of pathogenesis amongst them. A common pathological hallmark of polyQ diseases is the accumulation of the polyQ-expanded protein in large inclusions, most often within the nuclei of the neurons, which plays a critical role in their pathogenesis (Cummings and Zoghbi, 2000). Additionally, proteolytic cleavage, impairment of protein degradation, mitochondrial dysfunction, and transcription dysregulation are implicated in the pathogenesis of polyQ diseases (Stoyas and La Spada, 2018).

1.1.3 Clinical features of SCA3

The average age at onset is 30–50 years, and the mean survival time is considered around 21 years for patients with SCA3 (Bettencourt and Lima, 2011). The prominent clinical hallmark of SCA3 is progressive ataxia which is due to the dysfunction of cerebellum and brainstem and affects gait, balance, speech, and gaze. However, the phenotypic presentation of this polyQ disease is highly pleomorphic and varies greatly among patients, even within the same family. SCA3 patients usually manifest the symptoms in the early to mid adult years with slow progression over the years. Whithin a few years, a wide range of clinical features might be developed, including speech difficulties, abnormal gait, nystagmus, jerky ocular pursuits, disconjugate eye movements, and external progressive ophthalmoplegia (EPO). Eventually, in the advanced stages of disease, patients are wheelchair-bound and have severe dysarthria and dysphagia and may present facial and temporal atrophy, dystonia, spasticity and amyotrophy (Paulson, 2007). There is also evidence for nonmotor symptoms in affected people, including sleep problems (such as restless leg disorder), mildly depressed mood, and

mild cognitive impairment in executive function and memory (Kawai et al., 2004; Lopes et al., 2013; Schöls et al., 1998). According to the manifestations of the disease and neurological signs, four SCA3 subtypes have been defined (Paulson, 2012). Moreover, Sakai and Kawakami reported two siblings that presented spastic paraplegia without cerebellar ataxia and proposed the fifth type for SCA3 (Table 1.3) (Sakai and Kawakami, 1996).

Table 1.3 Overview of the age at onset and manifestations of five different subtypes of SCA3 (Paulson, 2012; Sakai and Kawakami, 1996).

SCA3 subtype	Age at onset	Manifestations
Type I	10–30 years	Bradykinesia, spasticity, rigidity, minimal ataxia
Type II	20–50 years	Upper motor neuron signs, progressive ataxia
Type III	40–75 years	Ataxia, peripheral neuropathy, amyotrophy, generalized areflexia
Type IV	Variable onset	Parkinsonism
Type V		Spastic paraplegia without cerebellar ataxia

Like other polyQ diseases, there is no effective treatment available for SCA3. Current pharmacologic therapeutics are only able to offer symptomatic relief to promote the quality of life for patients. To date, only a few clinical trials have been carried out; however, the outcomes have not been very impactful. Given that dysfunction of the CNS of individuals carrying mutation begins many years before the manifestation of symptoms, the development of approaches to delay or prevent disease onset is beneficial (Da Silva et al., 2019; Duarte-Silva and Maciel, 2018). Therefore, unravelling the key molecular players implicated in the neuropathology of SCA3 is essential for the development of efficient therapeutic strategies.

In general, current potential therapeutic strategies for SCA3 can be divided into two categories, including: (1) those that target and eliminate the underlying cause of the disease (expanded ataxin-3) directly, such as gene silencing, promotion of protein clearance, inhibition of proteolytic cleavage and aggregation formation, and stabilization of native conformation of proteins; and (2) those that mitigate the downstream toxic effects of the expanded ataxin-3, such as mitochondrial dysfunction and oxidative stress, the impairment of autophagy and ubiquitin-proteasome system, transcriptional dysfunction, and activation of neuronal cell death (Duarte-Silva and Maciel, 2018; Wang, 2018).

1.1.4 Neuropathological features of SCA3

The pattern of widespread neuronal loss of the CNS in SCA3 patients demonstrates the heterogeneity of disease manifestations. The motor impairments in SCA3 patients are mainly due to neuronal dysfunction and death in multiple neuronal systems, such as the somatosensory and motor nuclei of the striatum, thalamus, brainstem, cerebellum, and spinal cord. Particularly, neurodegeneration occurs in the dentate nucleus of the cerebellum with relative preservation of the Purkinje cells of the cerebellar cortex, as well as subregions of the basal ganglia, including the globus pallidus, subthalamic nuclei, the substantia nigra, and the motor nuclei. Additionally, neurodegeneration also affects the medial longitudinal fasciculus, vestibular nucleus, various pontine nuclei, superior and middle cerebellar peduncles, anterior horn cells, posterior columns, and posterior root ganglia. The cerebral cortex, olivary nuclei, and corticospinal tracts are often spared in SCA3 (Da Silva et al., 2019; Raj and Akundi, 2021; Rüb et al., 2008).

Neuroimaging using magnetic resonance imaging (MRI) has been considered a promising tool for the study and diagnosis of SCA3. An MRI of SCA3 patients showed atrophy and abnormality of the basal ganglia, pontocerebellar atrophy, midbrain, brainstem, and medulla oblongata with a dilated fourth ventricle. The degree of abnormalities correlates with the CAG repeat length, and patients with longer repeats are more likely to show progressive atrophy on MRI (Paulson, 2012; Tokumaru et al., 2003). Moreover, magnetic resonance spectroscopy (MRS) studies of SCA3 patients have indicated neurochemical alterations in SCA3 patients and premanifest mutation carriers (Adanyeguh et al., 2015; Joers et al., 2018).

1.1.5 Genetic features of SCA3

SCA3 is caused by a CAG repeat expansion in the coding region of thre *ATXN3/MJD1* gene, leading to the elongation of the polyQ tract in ataxin-3 protein (Schöls et al., 2004). The *ATXN3/MJD1* gene spans almost 48 kb and is constituted of 11 exons, and 56 alternative transcript variants for this gene were identified (Bettencourt et al., 2010). The CAG repeat resides in exon 10 and encodes a polyQ tract close to the C-terminal of ataxin-3 protein (Ichikawa et al., 2001). Normal populations carry 12–40 CAG repeats in the *ATXN3/MJD1* gene, while in affected individuals, the CAG repeat ranges between 60 and 87. Intermediate repeats between 45 and 59 are rare with incomplete penetrance and are associated with

milder manifestations of the disease (Klockgether et al., 2019; Maciel et al., 2001; Takiyama et al., 1995). Homozygote SCA3 patients with two mutant alleles have more severe manifestations than heterozygote ones (Carvalho et al., 2008).

As in all polyQ diseases, the age at onset differs widely in SCA3 patients, and there is an inverse correlation between the age at onset and the CAG repeat length; larger expansions tend to cause earlier disease onset (Maciel et al., 1995). Moreover, it is anticipated that the age at onset decreases by approximately 10 years from generation to generation due to the tendency of expanded repeats to get larger in subsequent generations, a phenomenon referred to as “genetic anticipation”, which is a shared characteristic of all polyQ diseases (Friedman, 2011; Takiyama et al., 1995). The size of repeat expansion also affects the progression of disease and severity of neuropathy in SCA3 patients; larger repeats cause a broader range of manifestations. The affected people with type I typically have larger repeats than those with types II and III of SCA3, whereas the so-called type IV with parkinsonism does not easily conform to a specific repeat range. It is believed that the largest CAG repeats are often associated with pyramidal signs and dystonia, even though the smallest repeats with peripheral neuropathy (Jardim et al., 2001; Schöls et al., 1996). Indeed, the phenotypic variance of SCA3 is partially (less than 50%) explained by the size of the CAG repeat, and it appears that other modifying factors are involved (van de Warrenburg et al., 2005). A genome-wide association study (GWAS) indicated nine additional modifying factors that influence the age at onset in SCA3 patients. The strongest signals were identified in genes implicated in vesicle transport, olfactory signaling, synaptic pathways, and DNA repair, such as recombination activating genes (*RAG1* and *RAG2*), and tripartite motif containing protein 29 (*TRIM29*) (Akçimen et al., 2020).

1.1.6 Structure of the ataxin-3 protein

The protein context and aberrant function of disease proteins play a pivotal role in the pathogenesis of polyQ diseases. Therefore, understanding the disease protein is important to unravel the underlying mechanisms involved in the pathogenesis of these neurodegenerative diseases (La Spada and Taylor, 2003). The *ATXN3/MJD1* gene encodes for the ataxin-3 protein (UniProt ID P54252). The most common form of ataxin-3 has 361 amino acids with an estimated molecular weight of 42 kDa for normal individuals. It is an evolutionarily conserved

protein that is ubiquitously expressed in neuronal and non-neuronal tissues. Ataxin-3 is widely expressed throughout the brain at different protein levels for subpopulations of neurons and is not limited to the affected regions (Trottier et al., 1998). Given the ubiquitous expression of ataxin-3 throughout the body, the restricted neuropathology of SCA3 cannot be explained by cellular expression of the disease protein, and various factors are involved (Ichikawa et al., 2001; Paulson et al., 1997a).

Ataxin-3 has two structural features, including a globular N-terminal Josephin domain (JD) (amino acid residues 1–182) with highly evolutionarily conserved amino acids and deubiquitylase activity and a more flexible and unstructured C-terminal tail that harbors two or three ubiquitin-interacting motifs (UIMs) and also comprises a polyQ tract (Figure 1.1) (Da Silva et al., 2019). Ataxin-3 is subjected to different post-translational modifications (PTMs), comprising ubiquitination at K117, phosphorylation, and SUMOylation, which affect and regulate its stability, subcellular localization, and cellular function (Mueller et al., 2009; Todi et al., 2009; Zhou et al., 2013).

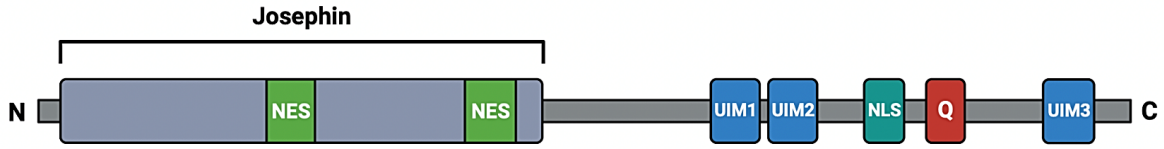

Figure 1.1 Schematic representation of the ataxin-3 protein. The most common form of the ataxin-3 protein has 361 amino acids. It is composed of a globular N-terminal, termed the Josephin domain (JD), that contains two nuclear export signals (NES), and an unstructured C-terminal tail that contains three ubiquitin-interacting motifs (UIMs), a nuclear localization signal (NLS), and a polyglutamine (polyQ) repeat. Two UIMs are located upstream, and the third UIM, which is isoform-specific, is located downstream of the polyQ repeat. Q = polyQ. Created with BioRender.com. Modified from Evers et al., 2014.

Different isoforms of ataxin-3 have been identified in which the C-terminal region is mainly variable (Bettencourt et al., 2013; Goto et al., 1997). At least two major isoforms of ataxin-3 (ataxin-3aL (long) and ataxin-3c) are generated through alternate splicing with a difference in the number of UIMs. Furthermore, the third isoform of ataxin-3 (ataxin-3aS (short)) is the result of a stop SNP in the *ATXN3/MJD1* gene that introduces a premature stop codon in exon 10 of the ataxin-3aL isoform. Each of these isoforms differs in its stability, subcellular localization, enzymatic deubiquitination activity, and interaction with proteins. Notably,

ataxin-3c appears to be the most abundant isoform expressed in the human and murine brains (Harris et al., 2010; Weishäupl et al., 2019).

1.1.7 Functions of the ataxin-3 protein

Ubiquitination is a protein post-translational modification process in which poly-ubiquitin chains are added to the ε-amino group of lysine residues of proteins and determines the fate of proteins, such as proteasomal degradation. It is a cascade of processes composed of E1 activating enzymes, E2 ubiquitin carrier/conjugating enzymes, and E3 ubiquitin ligases. Cysteine proteases known as deubiquitinating enzymes (DUBs) are considered regulators of the ubiquitin-proteasome system (UPS). They are involved in the disassembly of poly-ubiquitin chains and recycling of ubiquitin, which are believed to be critical for protein degradation, endocytosis, transcriptional regulation, cell cycle progression, and maintenance of cellular homeostasis (Burnett et al., 2003; Chung and Baek, 1999; Thrower et al., 2000). Mutations in the regulators of UPS are linked to various neurodegenerative diseases characterized by protein aggregation (Sherman and Goldberg, 2001; Taylor et al., 2002).

The exact physiological role of ataxin-3 is still not well appreciated. Ataxin-3 belongs to the family of cysteine proteases, and functions as a DUB in the UPS, and is proposed to be implicated in the proteasomal degradation of ubiquitylated proteins and protein quality control. It binds to K48/K63-linked (preferentially for K63) poly-ubiquitin chains (containing four or more ubiquitin molecules) of the substrates through its UIMs and cleaves the ubiquitin chains. Notably, mutations in the UIMs inhibit the ubiquitin binding of ataxin-3. Having UIMs can restrict the type of chains that can be cleaved, and this DUB enzyme can bind to excessively long and also particular types of poly-ubiquitin chains and functions on heavily ubiquitinated substrates, whereas most DUBs do not have any UIMs (Chai et al., 2004; Winborn et al., 2008). It has been shown that mutation of catalytic cysteine 14 in the active site of ataxin-3 results in the loss of deubiquitinating activity of this protein (Burnett et al., 2003; Costa Mdo and Paulson, 2012). Moreover, there is an increase in the ubiquitinated protein level in ataxin-3 knockout mice, verifying the DUB function of ataxin-3 *in vivo* (Schmitt et al., 2007).

Ataxin-3 interacts directly with parkin, which is an E3 ubiquitin ligase and mutated in autosomal recessive juvenile parkinsonism (AR-JP) (Durcan et al., 2012; Kitada et al., 1998;

Shimura et al., 2000). It has been indicated that parkin is able to ubiquitinate ataxin-3, and ataxin-3 can deubiquitinate parkin. Additionally, polyQ-expanded ataxin-3 promotes the autophagic degradation of parkin and increases its turnover, which might be responsible for the parkinsonian phenotype observed in some SCA3 patients (Durcan and Fon, 2011; Tsai et al., 2003).

Moreover, ataxin-3 binds to the valosin-containing protein (VCP/p97), probably via the VCP/p97 binding domain that has been mapped prior to the polyQ tract. They form a multi-functional complex involved mainly in endoplasmic reticulum-associated degradation (ERAD), a cellular process that regulates the degradation of misfolded proteins in the endoplasmic reticulum (ER) (Boeddrich et al., 2006; Zhong and Pittman, 2006).

The function of ataxin-3 extends beyond the UPS, and it is shown to be implicated in other cellular processes including transcriptional regulation, aggresome formation, cytoskeletal organization, DNA damage repair, and the maintenance of genome integrity (Burnett et al., 2003; Costa Mdo and Paulson, 2012; Li et al., 2002).

1.2 Mechanisms of SCA3 pathogenesis

Despite a mass of significant knowledge, the precise physiological mechanism by which expanded ataxin-3 elicits neurotoxicity is still far from clear. However, accumulating evidence indicates that the expanded polyQ tract induces dysfunction in the different cellular processes and evokes the formation of intranuclear aggregates, inhibition of protein degradation, susceptibility to proteolytic cleavage, destabilization of functional conformation, leading to abnormal protein-protein interactions, transcriptional dysregulation, RNA toxicity, mitochondrial dysfunction, and ultimately activation of cell death programs (Figure 1.2) (Costa Mdo and Paulson, 2012).

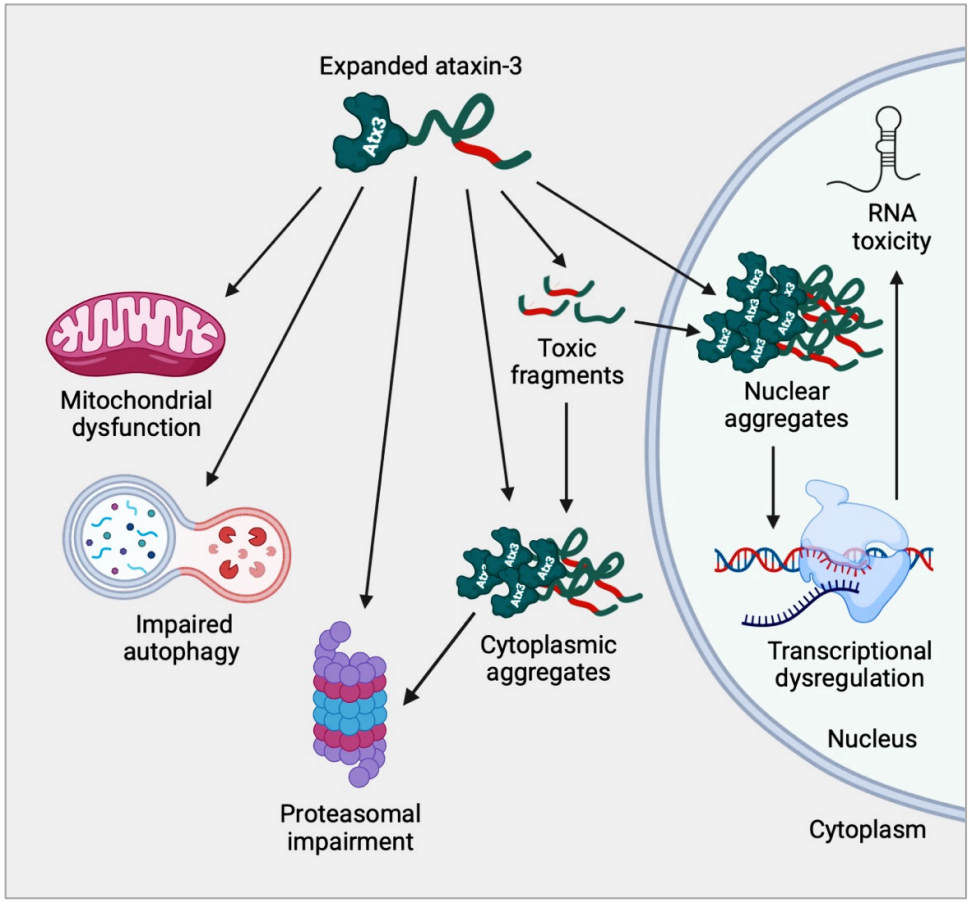

Figure 1.2 Schematic representation of cellular pathogenesis in SCA3. The expanded polyQ tract leads to conformational changes and the abnormal folding of ataxin-3. PolyQ-expanded ataxin-3 can be proteolytically cleaved, giving rise to the formation of aggregation-prone fragments. Full-length and cleavage products of polyQ-expanded ataxin-3 form insoluble aggregates, both in the nucleus and in the cytoplasm of the neurons. Other cellular pathogenesis of SCA3 include impaired autophagy and proteasomal degradation, mitochondrial dysfunction, transcriptional dysregulation, and RNA toxicity. Created with BioRender.com. Modified from Evers et al., 2014.

1.2.1 Ataxin-3 misfolding and aggregation

Dysfunction in protein homeostasis results in the accumulation of aberrant proteins as toxic aggregates in the cells; particularly, post-mitotic cells, such as neurons, are the most affected ones (Hipp et al., 2019). The formation of intraneuronal inclusions containing the expanded and misfolded proteins, most commonly in the nuclear compartment, is the histopathological hallmark of SCA3 and other polyQ diseases (Ross and Poirier, 2004; Taylor et al., 2002). The expansion of polyQ tract causes the abnormal and non-native conformation of proteins and the formation of toxic oligomers and SDS-resistant aggregates, leading to neurodegeneration by still unclear mechanisms (Breuer et al., 2010). The propensity of expanded proteins to aggregate is attributed to the polyQ repeat length, and longer tracts tend to accumulate

intensely, both *in vitro* and *in vivo*, and show faster aggregation kinetics (Teixeira-Castro et al., 2011; Yushchenko et al., 2018). Intracellular aggregates constitute mainly the expanded proteins and recruit some other proteins, including molecular chaperones, ubiquitin, heat shock proteins, proteasome subunits, transcription factors, and non-expanded wild-type ataxin-3. It is believed that the sequestration of regulators involved in protein quality control into aggregates may contribute to the pathogenesis of SCA3 and other polyQ diseases (Alves-Rodrigues et al., 1998; Cummings et al., 1998; Perez et al., 1998).

The distribution of intraneuronal inclusions is associated rather poorly with the affected brain regions in polyQ diseases. Histopathological examinations of the post-mortem brains of SCA3 patients displayed protein aggregates in the nucleus of neuronal cells of the affected brain regions, even though is not always accompanied by significant inclusions. Moreover, the aggregates were also detected in the brain regions that are spared from neurodegeneration (Paulson et al., 1997b; Schmidt et al., 1998; Yamada et al., 2001). The formation of aggregates is not restricted to the nucleus. Widespread axonal aggregates have been observed in the brains of SCA3 patients. These axonal aggregates can be detrimental to axonal transport, leading to the disruption of normal cell functions and neuronal death (Seidel et al., 2010). An increased understanding of the mechanisms implicated in the structural changes and aggregation of expanded proteins and their effects on neuronal survival may offer new and effective therapeutic leads.

1.2.2 Ataxin-3 proteolytic cleavage and formation of toxic fragments

The involvement of proteolytic pathways has been suggested extensively in the pathogenesis of various neurodegenerative diseases with abnormally aggregated proteins, such as Alzheimer's disease (AD), Parkinson's disease (PD), and polyQ diseases (De Strooper, 2010; Weber et al., 2014; Xilouri et al., 2013). In 1997, Wellington and Hayden introduced the so-called "toxic fragment hypothesis", which predicts that proteolytic cleavage of polyQ-expanded protein initiates the aggregation process and formation of intracellular inclusions and is a prerequisite for the manifestation of polyQ diseases (Wellington and Hayden, 1997). Several investigations display proteolytic cleavage as a source of the generation of cytotoxic and aggregation-prone soluble fragments of polyQ-expanded proteins, which have been detected in all polyQ diseases (Haacke et al., 2006; Wellington et al., 1998). Proteolytic

processing of polyQ-expanded proteins, which are predominantly cytoplasmic, results in the generation of small truncated proteins that are able to enter the nucleus and promote nuclear accumulation and dysfunction (Havel et al., 2009).

Ataxin-3-derived C-terminal fragments were detected both in the brains of SCA3 patients and in a transgenic SCA3 mouse model and were displayed to be enriched in the affected brain regions of SCA3 patients, such as the cerebellum and substantia nigra (Goti et al., 2004). PolyQ-expanded protein-derived fragments are highly susceptible to aggregation and able to induce cellular toxicity to a greater extent than full-length polyQ-expanded proteins (Ross et al., 1999). Proteolytic processing of ataxin-3 is thought to generate aggregation-prone fragments, primarily in the nucleus, which favors cytotoxicity (Simões et al., 2012; Weber et al., 2017).

Proteolytic cleavage of polyQ-expanded proteins, mainly by two families of proteases, caspase and calpain enzymes, leading to the generation of potentially toxic fragments, has been proposed to be implicated in the pathogenesis of polyQ diseases, such as HD and SCAs (Berke et al., 2004; Hübener et al., 2013; Ona et al., 1999). The caspase family are cysteine proteases that are able to cleave proteins after C-terminal aspartate residues and play a critical role in apoptosis and inflammatory pathways (Earnshaw et al., 1999; Li and Yuan, 2008). The involvement of caspases in the cleavage of ataxin-3 is controversially discussed, and there is no conclusive evidence for that, whereas increasing evidence points to the calpains as responsible proteases for the generation of ataxin-3 cleavage fragments (Haacke et al., 2007). Calpains are calcium-dependent cysteine proteolytic enzymes that are involved in a variety of cellular functions, such as remodeling of cytoskeletal, signal transduction pathways, and apoptosis. The best-characterized members of this family consist of calpain-1 and calpain-2, which are activated by calcium (Goll et al., 2003; Hübener et al., 2013). It has been indicated that pharmacological inhibition of calpains using N-acetyl-L-leucyl-L-leucyl-L-norleucinal (ALLN) or calpeptin resulted in the disappearance of expanded ataxin-3 aggregates in induced pluripotent stem cell (iPSC)-derived neurons (Koch et al., 2011). Conversely, overexpression of calpastatin, the endogenous inhibitor of calpains, can abolish the proteolytic cleavage, nuclear localization, and aggregation formation of expanded ataxin-3 both *in vitro* and *in vivo* (Haacke et al., 2007; Simões et al., 2012). Of interest, four calpain cleavage sites (main sites at amino acids D208 and S256) have been identified in ataxin-3

protein, and mutation at cleavage sites can prevent ataxin-3 proteolysis (Weber et al., 2017), confirming a key role for this proteolytic enzyme in SCA3 pathology.

1.2.3 Impaired protein degradation in SCA3

Maintenance of proteostasis is achieved by the degradation of misfolded or defective proteins in all eukaryotic cells (Matyskiela and Martin, 2013). Disruption of protein homeostasis and impairment of protein quality control pathways, including the ubiquitin-proteasome system, chaperone-mediated protein folding, and autophagy, have been implicated in SCA3 and other polyQ diseases (Klockgether et al., 2019). The aggregated pathological proteins are usually highly ubiquitylated and in many cases associated with components of the ubiquitin-proteasome system, which displays an attempt at their clearance. Moreover, it has been demonstrated that various components of the proteasomal machinery can be sequestered in intraneuronal aggregates in SCA3 patients and mouse models, which has a profound effect on ubiquitin signaling in the neurons (Chai et al., 1999; Paulson et al., 1997b; Seidel et al., 2010).

Additionally, chaperone-mediated protein folding has a critical role in cellular protein quality control and modulation of these misfolded and aggregated proteins. However, in SCA3 and other polyQ diseases, there is an imbalance between the production of misfolded proteins and the degradative capacity of the cells, which promotes toxicity (Sakahira et al., 2002). Some co-chaperones and ubiquitin ligases, such as CHIP (C-terminus of Hsp70-interacting protein), link the chaperone-mediated protein folding to the ubiquitin-dependent protein quality control in the cells. An *in vivo* study using an SCA3 transgenic mouse model demonstrated that genetic reduction of CHIP enhances the disease phenotype and results in the remarkable accumulation of ataxin-3 microaggregates (Williams et al., 2009). In general, overexpression of numerous chaperons is accompanied by mitigation of disease features in SCA3 models (McLoughlin et al., 2020).

In recent years, a link between autophagy and polyQ diseases has emerged. The impairment of the autophagy pathway, in which cellular components and proteins are degraded through lysosomal machinery, has been suggested in SCA3. Sequestration of components involved in the autophagy pathway, such as beclin-1, which is a key protein, has been demonstrated in ataxin-3 aggregates in SCA3 patients (Nascimento-Ferreira et al., 2011). Furthermore, polyQ-

expanded ataxin-3 binds to beclin-1 as well as wild-type ataxin-3, which appears to facilitate its degradation via the proteasome, leading to reduced levels of beclin-1 (Ashkenazi et al., 2017). Dysregulation of various autophagy proteins has been observed in the post-mortem brains of SCA3 patients, implying the perturbation of autophagy in this disease (Sittler et al., 2018).

1.2.4 Mitochondrial dysfunction in SCA3

Mitochondria play a critical role in different metabolic processes like cellular energy metabolism, cellular signaling, and apoptotic pathways (Chandel, 2015; Kroemer and Reed, 2000). Accordingly, mitochondrial dysfunction and alteration of mitochondrial bioenergetics are the commonality of neurodegenerative diseases and aging (Lin and Beal, 2006; Osiewacz and Bernhardt, 2013).

Indeed, regulation of mitochondrial proteostasis is crucial for the integrity and homeostasis of mitochondria, and mitochondrial proteases, or mitoproteases, function as key regulatory components in this process. Apart from the quality control and degradation of damaged proteins, these proteases are implicated in mitochondrial biogenesis, mitophagy, and apoptosis (Quirós et al., 2015). It has been demonstrated that the impairment and dysregulation of mitoproteases are linked to aging, neurodegenerative diseases, cancer, and metabolic syndromes (Bulteau and Bayot, 2011; Rugarli and Langer, 2012).

Reactive oxygen species (ROS) are mainly produced in the respiratory chain of mitochondria and have strong reactivity against other molecules, leading to tissue damages, especially in the central nervous system. Under normal physiological conditions, 1–2% of the consumed O_2 is converted to ROS, and there is a balance between its generation and elimination (Emerit et al., 2004). The accumulation of oxidative products has been verified to be a contributory factor in the progression of various neurodegenerative diseases, such as polyQ diseases, inducing defects in the morphology and function of mitochondrial and CNS energy metabolism. Notably, the level of ROS in mitochondria increases in Huntington's disease, leading to oxidative damage and eventually neuronal cell death (Browne and Beal, 2006; Evers et al., 2014; Miyata et al., 2008). Several investigations have shown that polyQ-expanded proteins can impair mitochondrial trafficking in mammalian neurons. Moreover,

mitochondrial-mediated activation of caspases and cell death plays a role in the pathogenesis of polyQ diseases (Choo et al., 2004; Trushina et al., 2004; Tsai et al., 2004).

Wild-type and expanded ataxin-3 have been found in mitochondria, and some of the mitochondrial resident proteins, including cytochrome C oxidase subunit NDUFA4 (NDUFA4), succinate dehydrogenase (ubiquinone) iron-sulfur subunit (SDHB), and cytochrome C oxidase assembly factor 7 (COA7), are ataxin-3 interaction partners (Kristensen et al., 2018; Pozzi et al., 2008). Like other neurodegenerative diseases, mitochondrial dysfunction has been identified in SCA3 (Harmuth et al., 2022). Mitochondrial DNA (mtDNA) damage and alteration, including a decrease in copy number and deletion, have been observed in the initial stages of the disease in an SCA3 transgenic mouse model (Kazachkova et al., 2013). In addition, expanded ataxin-3 is able to decrease the energy supply and the activity of antioxidant enzymes, such as catalase, glutathione reductase, and superoxide dismutase, and it can promote mtDNA damage and depletion *in vitro*, implying the impairment of mitochondrial function (Yu et al., 2009). Moderate disruption of mitochondrial respiratory chain complex II activity has been displayed in SCA3 cell and mouse models as well as in human SCA3 peripheral cells (Laço et al., 2012).

1.2.5 DNA damage and apoptosis in SCA3

Accumulation of damaged or improperly repaired DNA in neurons is a central feature of aging, even though it has been observed in neurodegenerative diseases, such as AD, PD, and HD (Ferlazzo et al., 2014; Milanese et al., 2018; Shanbhag et al., 2019). Several lines of evidence suggest the contribution of dysregulated DNA damage response pathways and apoptosis to SCA3 pathogenesis. Indeed, increased DNA damage has been observed both in SCA3 patients and SCA3 mouse models (Chatterjee et al., 2015; Kazachkova et al., 2013). Aberrant polyQ expansion of ataxin-3 leads to a reduction in DNA repair efficiency, impairment in multiple DNA repair processes and accumulation of DNA damage, activation of pro-apoptotic signaling and vulnerability to neuronal death, although the exact mechanism is still unclear (Liu et al., 2016).

Consistently, many studies have reported that wild-type ataxin-3 has a principal role in DNA damage response proper function and interacts with several DNA damage response regulators, including polynucleotide kinase 3’-phosphatase (PNKP), the mediator of DNA

damage checkpoint protein 1 (MDC1), checkpoint kinase 1 (Chk1), Huntingtin (HTT), Ku70, DNA-PKcs, 53BP1, and p97. PNKP is a nucleotide-processing enzyme implicated in the DNA strand break repair process. Wild-type ataxin-3 interacts directly with PNKP and stimulates its activity, leading to enhanced DNA repair, whereas expanded ataxin-3 inhibits the 3'-phosphatase activity of PNKP, presumably by its recruitment into ataxin-3 aggregates, and enhances the accumulation of DNA damage (Figure 1.3a) (Chatterjee et al., 2015; Gao et al., 2015; Singh et al., 2019; Tu et al., 2020).

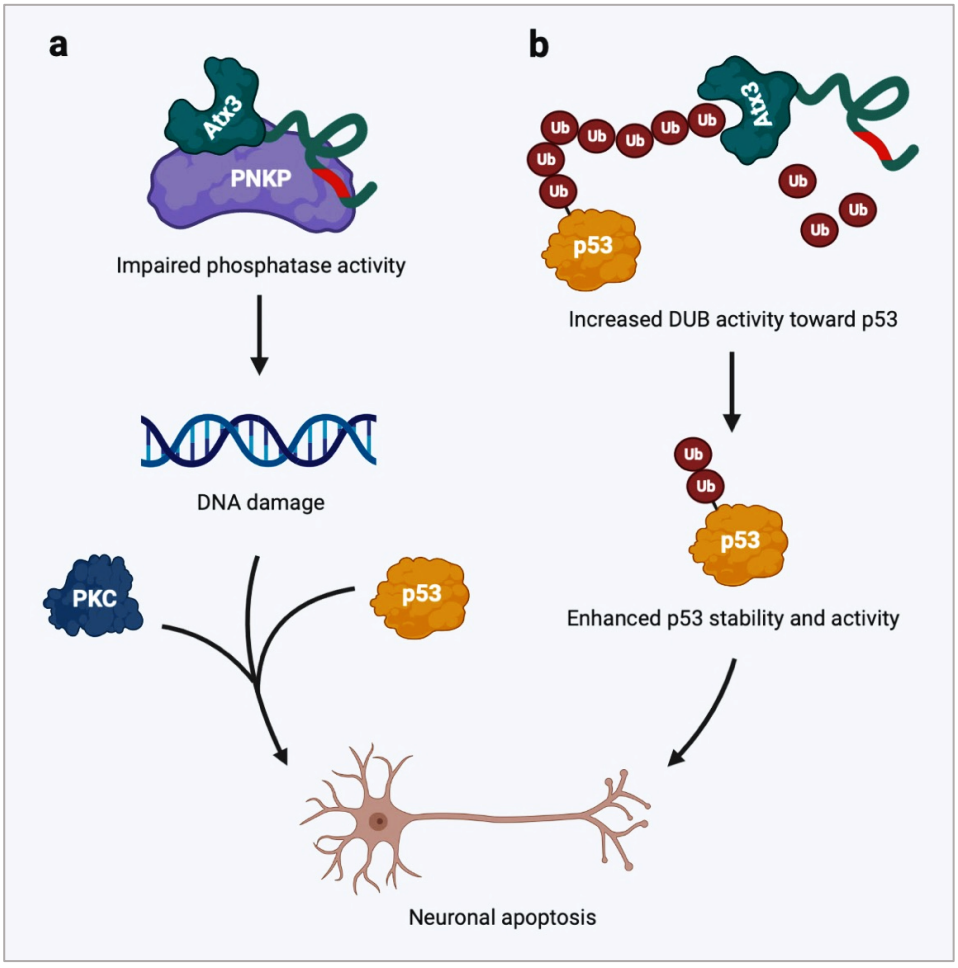

Figure 1.3 PolyQ-expanded ataxin-3 triggers neuronal apoptosis. (**a**) Expanded ataxin-3 inhibits the 3'-phosphatase activity of polynucleotide kinase 3'-phosphatase (PNKP), resulting in the activation of the apoptosis pathway mediated by tumor protein 53 (p53) and protein kinase C (PKC) after prolonged accumulation of DNA damage. (**b**) Expanded ataxin-3 also has a higher deubiquitinase activity toward p53, leading to the enhanced stability of this protein and p53-mediated neuronal apoptosis. Created with BioRender.com. Modified from Tu et al., 2020.

DNA damage response signaling pathways guarantee genome integrity and are orchestrated by two DNA kinases, ATM (ataxia-telangiectasia mutated) or ATR (ATM-and Rad3-Related)

kinase. Wild-type ataxin-3, as a DUB, stabilizes the ATR or ATR downstream targets, such as Chk1 and tumor protein 53 (p53), which regulate checkpoint signaling and promote DNA repair. Wild-type ataxin-3 regulates the stabilization and pro-apoptotic function of p53, whereas an *in vivo* study demonstrated that polyQ-expanded ataxin-3 has a higher affinity for p53, which results in the prolonged activation of p53 and promotion of p53-dependent apoptosis (Figure 1.3b) (Liu et al., 2016; Maréchal and Zou, 2013; Tu et al., 2017).

1.2.6 Transcriptional dysregulation in SCA3

Beside the role of ataxin-3 in protein degradation, ataxin-3 can bind to DNA and several transcriptional factors and is implicated in modulating the transcriptional process. It has been strongly proposed that expanded ataxin-3 can disrupt gene expression and induce transcriptional dysregulation, which might be implicated in the pathogenesis of SCA3 (Riley and Orr, 2006). In addition, transcription factors can be sequestered into intranuclear aggregates in polyQ diseases, resulting in the disruption of their functions (Perez et al., 1998). An altered pattern of gene expression has been identified both in SCA3 mouse and cell models, particularly in genes involved in neurotransmission, calcium signaling, cell surface-associated proteins, neuronal survival and differentiation, and inflammatory processes (Chou et al., 2008; Evert et al., 2001). Wild-type ataxin-3 represses transcription via interaction with histone deacetylase 3 (HDAC3) and deacetylation of histones, although expansion of the polyQ tract disrupts this function, leading to increased acetylation of total histone H3 and aberrant activation of gene transcription (Evert et al., 2006).

1.2.7 RNA toxicity in SCA3

Rising evidence indicates that, in addition to the contribution of protein toxicity in the pathogenesis of polyQ diseases, RNA toxicity may play an important role as well (Birman, 2008; Li et al., 2008). Numerous investigations have postulated that RNA toxicity induced by expanded CAG might occur through different mechanisms functioning as alternative splicing, bidirectional transcription, involvement of the RNA interference pathway, and repeat-associated non-ATG-initiated translation (Evers et al., 2014), however, the exact mechanism remains elusive.

Notably, RNA molecules containing expanded CAG/CUG repeats can form stable RNA hairpin structures, which can sequester RNA splicing factors, such as muscleblind-like 1 (MBNL1) in the intranuclear RNA foci, leading to alternative splicing aberrations (Mykowska et al., 2011). Li and colleagues demonstrated the upregulation of MBNL1 in a Drosophila model of SCA3 and suggested this RNA splicing factor as a modifier of polyQ degeneration. Additionally, they showed that interruption of CAG repeats by CAA triplets within the polyQ-encoding region can reduce the toxicity and alleviate the phenotype in the Drosophila model of SCA3 (Li et al., 2008).

MicroRNAs (miRNAs) are small, non-coding single-stranded RNA molecules that seem to play an essential role in the modulation of gene expression, and their involvement in the pathogenesis of polyQ diseases has been proposed (O'Brien et al., 2018). In one study, it was revealed that 54 miRNAs are dysregulated in the post-mortem brains of HD patients, which may contribute to the toxicity observed in this polyQ disease (Sinha et al., 2012). Furthermore, inhibition of miRNA processing can boost toxicity induced by expanded ataxin-3 in both Drosophila and human cells (Bilen et al., 2006).

1.2.8 Nuclear localization of ataxin-3 as a pathological mechanism in SCA3

The preferential accumulation of polyQ-expanded proteins in the nucleus of the neurons and the formation of intranuclear inclusions is a common pathological feature in all polyQ diseases, leading to neuropathology (Havel et al., 2009). Nevertheless, the role of nuclear accumulation in the pathology of polyQ diseases is not well characterized. It is evident that nuclear accumulation of polyQ-expanded proteins induces aberrant interaction with nuclear proteins, such as transcription factors, and could also sequester them, leading to transcriptional dysregulation and disruption of nuclear function (Friedman et al., 2007; Li et al., 2007). It has been suggested that the intrinsically low activity of the neuronal nuclear ubiquitin-proteasome system may account for the nuclear accumulation of polyQ-expanded proteins (Tydlacka et al., 2008). Moreover, it was shown that the efficient nuclear export of polyQ-expanded proteins is disrupted in polyQ diseases, implying a defect in the nucleocytoplasmic transport of expanded proteins (Cornett et al., 2005; Taylor et al., 2006).

Indeed, ataxin-3 is a ubiquitous protein and is normally found in both the cytoplasm and nucleus of cells; however, in neurons, it is predominantly located in the cytoplasm (Tait et al., 1998; Trottier et al., 1998). Even though mounting evidence points to the nucleus as a preferential site of aggregation, cellular toxicity, and pathology of expanded ataxin-3, suggesting that some nuclear functions are perturbed in SCA3 (Schmidt et al., 1998; Yang et al., 2002). It is believed that the nuclear presence of expanded ataxin-3 plays a prominent role in the manifestation of symptoms, although the involved mechanisms and molecular determinants for the nucleocytoplasmic transport of ataxin-3 have remained enigmatic. Intriguingly, inhibition of nuclear localization of expanded ataxin-3 alleviates many disease features, and promotion of nuclear localization has the opposite effects (Bichelmeier et al., 2007). Live-cell imaging demonstrates that the dynamics of polyQ-expanded ataxin-3 are slower than those of the wild-type, which contributes to a defect in the nuclear export of expanded ataxin-3 (Chai et al., 2002). Furthermore, the concentration of expanded ataxin-3 has an important implication for aggregation formation, which tends to be higher in the cell nucleus compared to the cytoplasm (Pozzi et al., 2008).

Ataxin-3 possesses a putative nuclear localization signal (NLS) located upstream the polyQ tract (amino acids 282–285), although it has been shown that mutation or deletion of this region has no impact on subcellular localization of ataxin-3, thus questioning its importance in the cellular distribution of this protein. Additionally, six potential nuclear export signals (NESs) have been identified in ataxin-3, of which two, within the Josephin domain (amino acids 77–99 and 141–158), were shown to be active and facilitate the nuclear export of ataxin-3 through nuclear pore complexes (NPCs) (Albrecht et al., 2004; Antony et al., 2009; Breuer et al., 2010). An *in vitro* study has shown that nuclear shuttling of ataxin-3 is an active process mediated by the classical transport pathway, and inhibition of nuclear export receptor CRM1 leads to the accumulation of ataxin-3 in the cell nucleus, suggesting the implication of this nuclear export receptor in the nuclear export of ataxin-3 (Macedo-Ribeiro et al., 2009). In addition, karyopherin α-3 (KPNA3) was identified as being implicated in the nuclear localization and aggregation of ataxin-3. It was demonstrated *in vitro* and *in vivo* that knockout of this nuclear transport receptor ameliorates the molecular, neuropathological, and behavioral disturbances of SCA3 by reducing nuclear localization of expanded ataxin-3 (Sowa et al., 2018).

Interestingly, the subcellular localization of ataxin-3 can also be influenced by post-translational modification. It is known that ataxin-3 is subjected to phosphorylation by two kinases, serine-threonine casein kinase 2 (CK2) and glycogen synthase kinase-3β (GSK3β). It seems that phosphorylation of serines 236, 340, and 352 by CK2 implicates a role in the nuclear localization of ataxin-3, and pharmacological inhibition of CK2 mitigates the nuclear inclusions, even though phosphorylation of other serines has less effect (Fei et al., 2007; Mueller et al., 2009).

1.3 Nucleocytoplasmic transport

The transport of macromolecules, including proteins and RNAs, between the cytoplasm and the nucleus is a tightly regulated process. It plays a critical role in various cell physiological and pathophysiological processes, such as regulation of gene expression, RNA processing, signal transduction, cell cycle progression, and oncogenesis (Jeffries and Capobianco, 2000; Takizawa and Morgan, 2000). Nuclear transport, including import and export, proceeds through large proteinaceous structures perforating the nuclear envelope called nuclear pore complexes (NPCs), which limit the traffic of macromolecules. Although NPCs allow passive diffusion of small molecules (< ~40 kDa), such as small proteins, ions, salts, and nucleotides, between the cytoplasmic and nuclear compartments, large substrates are shuttled by an active process that is highly selective and bidirectional (Kim et al., 2017; Patel et al., 2007). The main components implicated in nuclear transport are NPCs, RanGTPase, and nuclear transport receptors known as karyopherins (importins and exportins).

1.3.1 Nuclear pore complexes (NPCs)

Nuclear pore complexes (NPCs) are the main gateways connecting the nucleus and cytoplasm of cells. Structural studies have revealed that NPCs have a cylindrical structure with an octagonal symmetry, and their architecture seems to be highly conserved across all eukaryotes. The NPCs are large multiprotein assemblies with an estimated molecular mass of 125 MDa in mammalian cells. The main structure of NPCs is composed of the inner pore ring, nuclear and cytoplasmic rings, nuclear and cytoplasmic baskets, and a central aqueous channel (~30 nm in diameter and ~50 nm in length) that connects between the nucleoplasm and cytoplasm (Ryan and Wente, 2000; Stoffler et al., 1999; Wente and Rout, 2010). NPCs consist of proteins termed nucleoporins (NUPs). Proteomic analysis displayed that each NPC

includes multiple copies of 30–50 different NUPs. NUPs are involved in the regulation of nuclear permeability, and most of them are functionally conserved from yeast to mammals (Cronshaw et al., 2002). A subset of NUPs contains domains or repeats rich in the phenylalanine-glycine amino acids (FXFG, FG, or GLFG), which serve as docking sites for nuclear transport receptors. These repeating sequences line the central channel of NPCs and facilitate the trafficking of cargo across the nuclear envelope (Balasundaram et al., 1999; Ryan and Wente, 2000).

1.3.2 RanGTPase

Cargo uptake and release are modulated by the interaction of transport receptors with Ran, a Ras-related GTPase that binds to GTP or GDP. The RanGTP-RanGDP gradient across the two faces of the nuclear membrane is the key determinant of the directionality of nucleocytoplasmic transport and allows the accumulation of cargos against their activity gradients. The concentration of RanGTP is almost 100-fold higher in the nucleoplasm than in the cytoplasm because of the localization of the RanGTPase activating protein-1 (RanGAP1) predominantly in the cytoplasm. Indeed, RanGAP1 catalyzes the hydrolysis of GTP in the cytoplasm (Figure 1.4). Furthermore, Ran guanine nucleotide exchange factor (RanGEF), also called RCC1 in human cells, converts RanGDP into RanGTP in the nucleus and plays an essential role in the regulation of the nucleotide-bound state of Ran (Figure 1.4) (Bischoff et al., 1995; Bischoff and Ponstingl, 1995; Conti and Izaurralde, 2001; Kalab et al., 2002). *In vitro* binding studies demonstrate that RanGTPase interacts directly with the karyopherin/cargo complex and regulates its association and dissociation. Binding of RanGTPase to importins leads to the dissociation of cargos, whereas its interaction with exportins promotes cargo binding and moves the complex out of the nucleus (Floer et al., 1997; Rexach and Blobel, 1995).

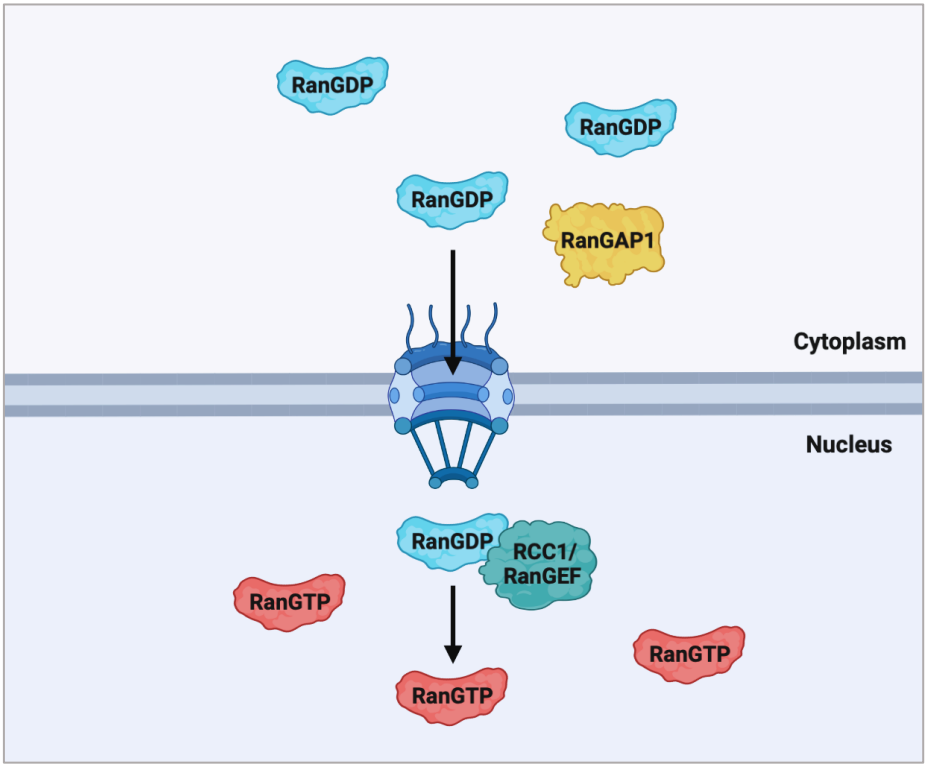

Figure 1.4 The nuclear and cytoplasmic RanGTP-RanGDP gradient. The RanGTPase activating protein-1 (RanGAP1) is mainly cytoplasmic and causes Ran to hydrolyze its GTP to GDP. The Ran guanine nucleotide exchange factor (RanGEF), also known as RCC1, is a chromatin-bound protein that converts RanGDP to the GTP-bound form (RanGTP) in the nucleus. Therefore, nuclear Ran is predominantly in the GTP state, and cytoplasmic Ran is in the GDP state. Created with BioRender.com. Modified from Harel and Forbes, 2004.

1.3.3 Nuclear transport receptors (karyopherins)

Translocation of cargos between the nucleus and cytoplasm is mediated by soluble transport receptors known as karyopherins that shuttle through NPCs. There are different classes of nuclear transport receptors that are able to bind to both NUPs and cargos and modulate their traffic through NPCs. Generally, karyopherins are classified into karyopherin α and karyopherin β families (Cautain et al., 2015).

Karyopherin α, also known as importin α, was first identified as an adaptor protein linking NLS-bearing cargos with karyopherin β. Seven isoforms of karyopherin α have been identified in humans, which are classified into three subfamilies known as α1, α2, and α3, based on their primary amino acid sequences. These subfamilies display distinct cargo specificities (Table 1.4) (Köhler et al., 1999; Pumroy and Cingolani, 2015). Karyopherin α orthologues are characterized by an N-terminal importin β-binding (IBB) domain for binding to karyopherin β, a conserved architecture consisting of 10 helical armadillo (ARM) repeats of a relatively

hydrophobic sequence of approximately 42–43 amino acids that recognize the nuclear localization signal (NLS) of cargos, and a C-terminal region that binds to the export factor chromosome segregation 1 like (CSE1L/CAS) (Oka and Yoneda, 2018; Pasha et al., 2021; Pumroy and Cingolani, 2015).

Table 1.4 Overview of all known members of the human karyopherin α which are categorized into 3 subfamilies and some of their specific cargos. TDP-43 = TAR DNA binding protein 43; NF-κB = nuclear factor-κB; RCC1 = nuclear regulator of chromosome condensation 1; STAT1 = signal transducer and activator of transcription 1; STAT2 = signal transducer and activator of transcription 2; n/a = not applicable. Modified from Pumroy and Cingolani, 2015; Pasha et al., 2021.

Subfamily	Human karyopherin α	Example of known cargo(s)
α1	Importin α-1/Karyopherin α-2	TDP-43, NF-κB (p65)
	Importin α-8/Karyopherin α-7	n/a
α2	Importin α-3/Karyopherin α-4	TDP-43, NF-κB (p50/p65; p52), ataxin-3, α1ACT, RCC1
	Importin α-4/Karyopherin α-3	TDP-43, NF-κB (p50/p65; p52), RCC1, ribosomal protein S3a
α3	Importin α-5/Karyopherin α-1	TDP-43, NF-κB (p50/p65; c-Rel; p52; RelB), STAT1, STAT2
	Importin α-6/Karyopherin α-5	TDP-43, NF-κB (p50/p65; c-Rel; p52; RelB)
	Importin α-7/Karyopherin α-6	TDP-43, NF-κB (c-Rel; RelB)

The largest class of nuclear transport receptors belongs to a conserved family of proteins known as the karyopherin β superfamily, which accounts for most of the nuclear trafficking. In mammals, it has been identified that 11 karyopherin βs are implicated in the import or bidirectional transport of cargos, which are termed importins or transportins, and 8 karyopherin βs play a role in the export of cargo called exportins (Fried and Kutay, 2003; Pemberton and Paschal, 2005). The karyopherin β family has been categorized into 15 subfamilies according to the evolutionary analysis, and most members recognize their own specific cargos (Table 1.5), although there are some redundancies (Chook and Blobel, 2001; Mühlhäusser et al., 2001; Wente and Rout, 2010). Furthermore, some transport receptors have a tissue- cell-specific expression that regulate the shuttling of distinct cargos (Jans et al., 2000). The direction of nuclear shuttling by Karyopherin βs is controlled by their association with RanGTP. Generally, importins recognize and associate with the cargos in the cytoplasm and release them in the nucleus upon interaction with RanGTP. Conversely, exportins bind to

their cargos in the nucleus, in the presence of RanGTP, and release them in the cytoplasm upon hydrolysis of GTP. Both importins and exportins are recycled to allow another round of nucleocytoplasmic transport of cargos (Görlich and Kutay, 1999; Mattaj and Englmeier, 1998).

Table 1.5 Overview of all known members of the human karyopherin β superfamily, which are categorized into 15 subfamilies and some of their specific cargos. SREBP-2 = sterol regulatory element-binding protein 2; n/a = not applicable. Modified from Harel and Forbes, 2004; Chook and Süel, 2011.

Subfamily	Human karyopherin β	Example of known cargo(s)
IMB1	Importin β/Karyopherin β-1	Imports via importin α adaptor proteins with NLS; Imports via snurportin the UsnRNPs; with no adaptor, Cargos: SREBP-2, HIV Rev, HIV TAT, cyclin B
IMB2	Karyopherin β-2/Transportin-1	PY-NLS proteins, mRNA-binding proteins, histones, ribosomal proteins
IMB3	Importin-5/RanBP5/ Karyopherin β-3	Histones, ribosomal proteins
IMB4	Importin-4/RanBP4	Transition Protein 2, histones, ribosomal protein S3a
IPO8	Importin-7/RanBP7	Smad, ERK, GR, ribosomal proteins
	Importin-8/RanBP8	SRP19, Smad
IMB5	Importin-9	Histones, ribosomal proteins
KA120	Importin-11	n/a
TNPO3	Transportin-SR1/-SR2/-3/TNPO3	SR proteins, HuR
	Importin-13	Imports UBC9, Y14; exports eIF1A
XPO4	Exportin-4	Imports SOX2, SRY; exports Smad3, eIF5A
XPO5	Exportin-5	Exports pre-miRNA
XPO6	Exportin-6	Exports profilin, actin
XPO7	Exportin-7/RanBP16	Exports p50-RhoGAP
XPOT	Exportin-t/Xpo-t	Exports tRNAs
XPO1	CRM1/Exportin-1	Exports proteins with leucine-rich NES, 60S ribosomal subunits (via NMD3 adaptor), 40S ribosomal subunits
XPO2	CAS	Importin αs

Karyopherin βs are able to consort with various adaptor proteins ranging from karyopherin α members to snurportin or other karyopherin β members to shuttle certain cargos (Harel and Forbes, 2004). They possess a similar molecular weight (90–150 kDa) and an acidic isoelectric point (PI = 4.0–5.0), although the sequence identity is low among the family members (10–20%) (Chook and Blobel, 2001). Karyopherin βs have a middle NPC-binding domain that

interacts with the FG-Nups transiently, and they share a binding domain for RanGTPase at their N-terminal, which has the most amino acid similarity between the karyopherin βs and drives active nucleocytoplasmic transport (Macara, 2001; Quimby and Dasso, 2003). High-resolution structural studies of karyopherin βs revealed that they all have a similar overall architecture consisting of multiple tandem helical repeats termed HEAT (huntingtin, elongation factor 3, the A subunit of protein phosphatase 2A, and the yeast PI3-kinase TOR1) repeats located in the C-terminal region. Each HEAT repeat is composed of almost 40 hydrophobic amino acids, which are folded into two antiparallel helices A and B connected by a short turn (Figure 1.5). These HEAT repeats are responsible for binding to importin α and cargos (Andrade and Bork, 1995; Conti and Izaurralde, 2001; Di Francesco et al., 2018).

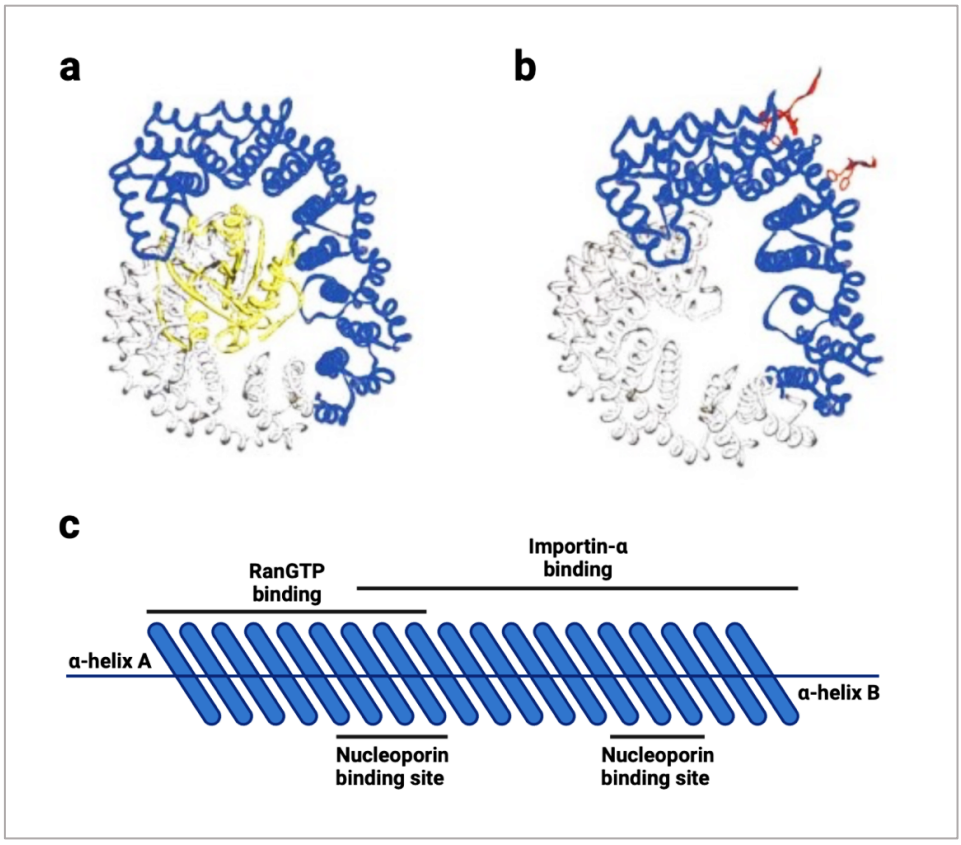

Figure 1.5 The structure of karyopherin β and its binding domains. (**a**) Structure of karyopherin β (1–462) bound to RanGTP, which is shown in blue and yellow, respectively. (**b**) Structure of karyopherin β (1–442) bound to FxFG cores of nucleoporins, which are shown in blue and red, respectively. (**c**) Karyopherin β consists of 19 tandem HEAT repeats. Each HEAT repeat consists of two α-helices, A and B. Created with BioRender.com. Modified from Harel and Forbes, 2004; Weis, 2003.

1.3.3.1 Nuclear transport receptors as cytoplasmic chaperones

Nuclear transport receptors fulfill a dual function, and aside from their canonical role as central players in the transport of cargos, they are also able to act as cytoplasmic chaperones for the exposed basic domains. Numerous importins are involved in the shielding of basic patches on the cargos, such as histones, ribosomal proteins, and FG-Nups. In fact, they can suppress the cytoplasmic aggregation of these proteins in the presence of polyanionic macromolecules (Jäkel et al., 2002; Milles et al., 2013).

In terms of neurodegenerative diseases, it has been suggested that importins not only serve as nuclear transporters for the RNA-binding protein FUS, which is involved in the pathology of amyotrophic lateral sclerosis (ALS) and frontotemporal dementia (FTD), but also have a chaperone-like activity and prevent cytoplasmic aggregation of this protein (Fallini et al., 2020; Mikhaleva and Lemke, 2018). Several independent studies, both *in vitro* and *in vivo*, have indicated that karyopherin β-2/Transportin-1 (TNPO1) interacts with FUS protein and abrogates its liquid-liquid phase separation (LLPS) and fibrillization. Moreover, overexpression of TNPO1 decreases the number of cytoplasmic FUS foci (Guo et al., 2018; Hofweber et al., 2018; Yoshizawa et al., 2018). Additionally, it was shown that the karyopherin α/β complex can mitigate fibrillization of TAR DNA-binding protein of 43 kDa (TDP-43) remarkably by binding to its NLS (Guo et al., 2018).

1.3.4 Nuclear transport signals

Nuclear transport mediated by karyopherins is a highly specific process and restricted to cargos bearing intrinsic import or export signals, which are referred to as nuclear localization signals (NLSs) or nuclear export signals (NESs), respectively. Each karyopherin is able to recognize a set of NLSs or NESs (Pemberton et al., 1998). Most transport signals cannot be categorized into a well-defined consensus, although general properties, such as length, charge, and hydrophobicity of the sequences are considered important (Fried and Kutay, 2003). The first defined NLS sequences are the classical NLS (cNLS) motifs, which contain monopartite or bipartite signals that can be recognized and bound by importin αs. Monopartite signals are a single stretch of basic amino acids, such as lysine (K) and/or arginine (R), and usually on the surface of the proteins (Dingwall and Laskey, 1991). The first characterized monopartite NLS is the simian virus 40 (SV40) large-T antigen NLS (PKKKRKV)

(Kalderon et al., 1984; McLane and Corbett, 2009). Many proteins carry bipartite NLSs, which are more complex and constitute of two clusters of positively charged amino acids separated by 10–13 non-conserved amino acids (Dingwall et al., 1988). Nonclassical NLSs have various amino acid sequences, such as proline-tyrosine NLS (PY-NLSs), that can be recognized directly by different members of the karyopherin β family (Chook and Süel, 2011; Soniat and Chook, 2015). NESs are highly diverse and usually contain four to five hydrophobic amino acids, such as leucine. They were first identified in HIV-1 Rev and heat-stable protein kinase inhibitor (PKI) (Fischer et al., 1995; Wen et al., 1995).

1.3.5 Classical import and export pathways

The classical import pathway is mediated by the importin α and importin β families and is well described. In the first step of an import cycle, importins recognize the NLSs of cargos and form an importin(s)/cargo complex in the cytoplasm where the RanGTP level is low. Importin α is an adaptor protein that recognizes the classical NLS of cargo, and then interacts with importin β via its N-terminal (importin β binding domain). However, importin β is able to bind and import proteins with extended basic stretches, such as ribosomal proteins, independently of an adaptor protein. In the next step, the resulting trimeric complex consisting of cargo/importin α/importin β can translocate into the nucleus via recruitment of importin β to the NPCs. Upon arrival in the nucleus, RanGTP binds to importin β in the trimeric complex, which causes the release and dissociation of the cargo/importin α complex. In the absence of importin β binding, the affinity of importin α for cargo reduces, leading to the release of cargo in the nucleoplasm (Figure 1.7a). Finally, the RanGTP bound to importin β is recycled back to the cytoplasm through NPCs for further rounds of import. Importin α recycling is mediated by the exportin CAS and RanGTP. Thus, at least two GTP molecules are hydrolyzed per classical import pathway (Chook and Blobel, 2001; Görlich and Kutay, 1999; Pemberton et al., 1998; Weis, 2003).

An analogous process is involved in the export pathway, which is facilitated by exportins. In the nucleoplasm, exportins recognize NES-bearing cargos and form a complex with RanGTP, which increases the affinity of the exportins to the cargos. The exportin/cargo/RanGTP complex interacts with the NPCs and ferries through them. The GTP bound to Ran is hydrolyzed by RanGAP1, which is more abundant in the cytoplasm, leading to the dissociation

of cargo, and RanGDP is shuttled to the nucleoplasm (Figure 1.7b) (Kau et al., 2004; Kim et al., 2017). Chromosome region maintenance 1 protein (CRM1) is the most versatile exportin and implicated in the nuclear export of various proteins with NES, including cycle regulators, transcription factors, and RNA-binding proteins (Fornerod et al., 1997; Fried and Kutay, 2003).

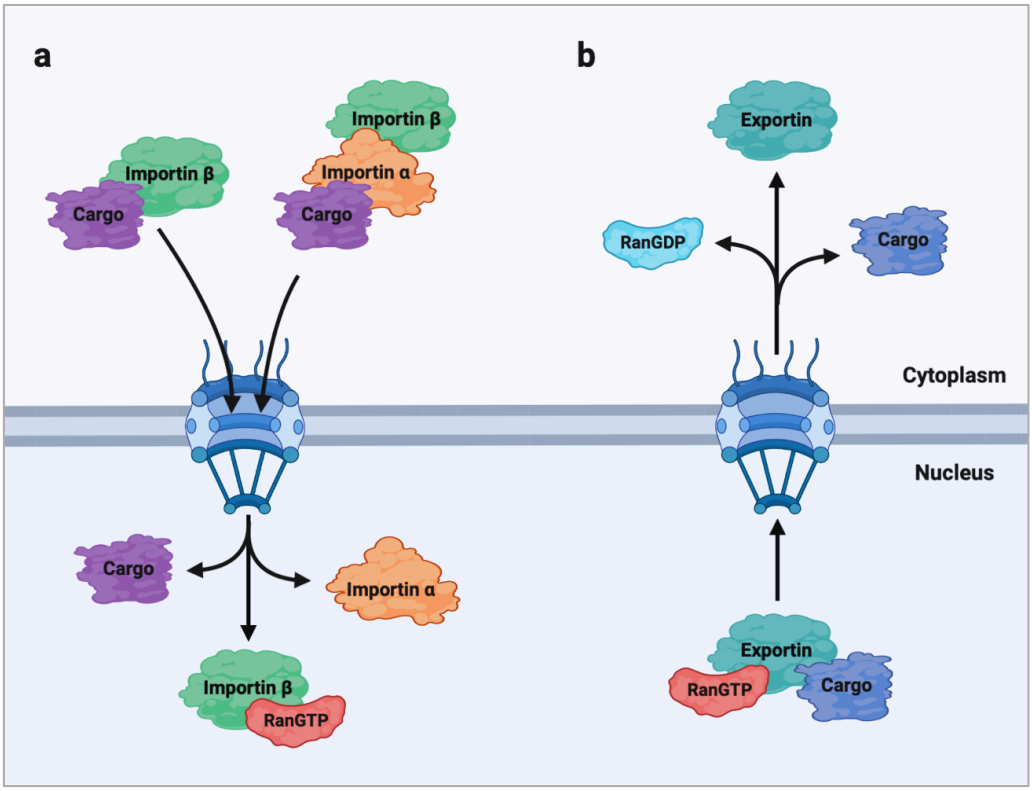

Figure 1.6 Nucleocytoplasmic transport of protein cargos. (**a**) Nuclear import of cargos containing a nuclear localization signal (NLS) is mediated by the importin α/β heterodimer or importin βs alone. An importin/cargo complex is formed in the cytoplasm and imported into the nucleus via the transient interaction of importin β with nucleoporins (Nups) within the nuclear pore complex (NPC). In the nucleus, RanGTP binds to importin β, leading to the release of cargo. (**b**) Cargos that possess a nuclear export signal (NES) bind to exportins in the presence of RanGTP in the nucleus. The exportin/cargo/RanGTP complex is exported into the cytoplasm through an NPC. The cargo is released from the complex after the hydrolysis of GTP to GDP, facilitated by RanGAP1, leading to the dissociation of the nuclear export complex in the cytoplasm. Created with BioRender.com. Modified from Sekimoto and Yoneda, 2012.

1.3.6 Nucleocytoplasmic transport and neurodegeneration

The appropriate subcellular localization of proteins and transcripts is extremely essential for their physiological functions and the maintenance of cellular homeostasis (Ding and Sepehrimanesh, 2021). Dysregulation of nucleocytoplasmic transport machinery has detrimental effects on cells and is associated with several diseases. Recently, a large body of

evidence supports the involvement of defective nucleocytoplasmic transport in aging and neurodegenerative diseases, including ALS (Aizawa et al., 2019; Burk and Pasterkamp, 2019), FTD (Zhang et al., 2015), AD (Eftekharzadeh et al., 2018), HD (Gasset-Rosa et al., 2017; Grima et al., 2017), PD (Chen et al., 2020), SCA (Zhang et al., 2020), and dystonia (Ding et al., 2021). Nonetheless, the molecular mechanisms by which impaired nucleocytoplasmic transport contributes to the pathogenesis of neurodegenerative diseases are poorly understood.

An impairment of nucleocytoplasmic transport interferes with the normal distribution of proteins and RNAs, leading to their mislocalization in the cells, particularly in the neurons. Alteration of the subcellular distribution of the local protein reservoir results in abnormal protein-protein interactions, which further stimulates the formation of protein aggregates (Figure 1.8). On the other hand, these protein aggregates can sequester the components of nucleocytoplasmic transport machinery, such as nucleoporins, driving further aggregation and defects in neuronal functions (Tamburrino and Decressac, 2016; Woerner et al., 2016). In this regard, evaluation of nucleocytoplasmic transport machinery and its involvement in the process of neurodegenerative diseases has focused attention in recent years. For example, it has been demonstrated that aggregation of TDP-43 or poly-dipeptides encoded by C9orf72 repeat expansion in ALS/FTD and tau protein in AD leads to disruption of nucleocytoplasmic transport (Burk and Pasterkamp, 2019). It has been displayed that tau can directly interact with nucleoporin Nup98, leading to its mislocalization, failure of nuclear transport, and alteration in Ran localization (Eftekharzadeh et al., 2018). Growing evidence indicates that dysregulation of nucleocytoplasmic transport is implicated in the pathophysiology of HD. Cytoplasmic mislocalization of Ran, which is due to disruption of NPCs and abnormal protein-protein interactions between expanded HTT and nucleocytoplasmic transport components, such as RanGAP1, has been detected in HD (Grima et al., 2017; Hosp et al., 2015). Alteration in the localization of multiple components of the nuclear transport machinery, including NUP98 and NUP62, has been indicated in an SCA1 mouse model, which highlights deficits in nucleocytoplasmic trafficking (Zhang et al., 2020). Beside the recruitment of nucleoporins into aggregates and perturbed Ran gradient, modulation in the protein levels and/or mislocalization of karyopherins appear to be linked to impaired nucleocytoplasmic transport in neurodegenerative diseases. For instance, nuclear depletion and cytosolic accumulation of karyopherin β-1 (KPNB1) have been observed in the spinal motor neurons of ALS patients and

in an SCA1 mouse model (Aizawa et al., 2019; Kinoshita et al., 2009; Zhang et al., 2020). Additionally, nuclear depletion and reduction of karyopherin α-4 (KPNA4) protein levels have been reported in the frontal cortex of FTD patients (Solomon et al., 2018).

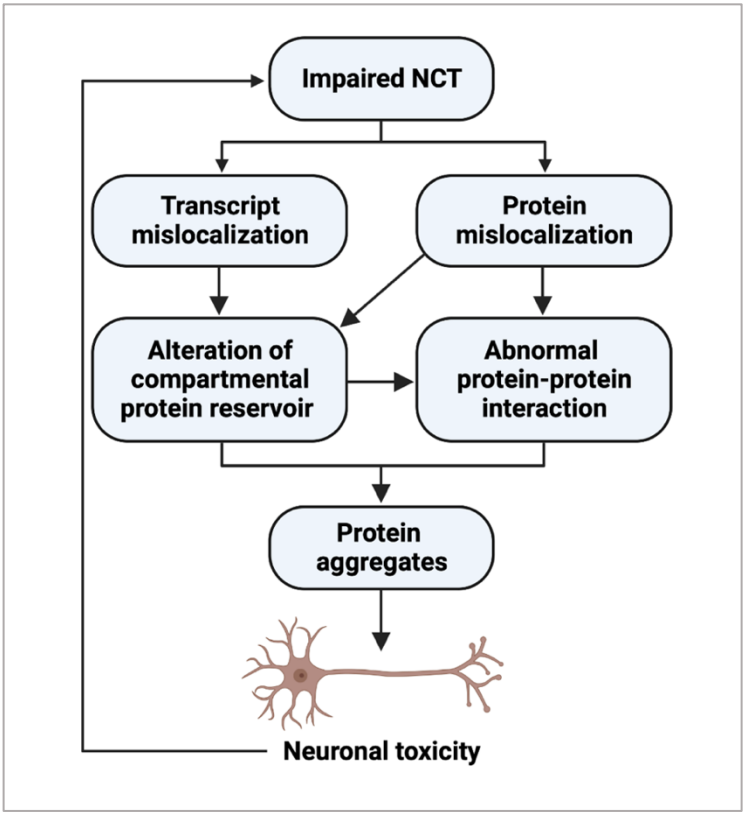

Figure 1.7 Linkages between impaired nucleocytoplasmic transport and neuronal toxicity. Impairment of nucleocytoplasmic transport results in protein and RNA mislocalization, disruption of the homeostasis of local protein reservoirs, and abnormal protein-protein interactions, leading to protein aggregation and neuronal toxicity. NCT = nucleocytoplasmic transport. Created with BioRender.com. Modified from Ding and Sepehrimanesh, 2021.

1.4 Aim of the thesis

Spinocerebellar ataxia type 3 (SCA3) is an autosomal dominant neurodegenerative disease that belongs to the class of polyglutamine (polyQ) diseases (Hersheson et al., 2012; Klockgether et al., 2019; Zoghbi and Orr, 2000). It is caused by a CAG trinucleotide expansion in the coding region of the *ATXN3/MJD1* gene, leading to a polyQ expansion in the ataxin-3 protein (Kawaguchi et al., 1994; Schöls et al., 2004). PolyQ diseases are progressive neurodegenerative diseases that principally affect the CNS and lead to neurological and physical impairments (McLoughlin et al., 2020; Rudnicki and Margolis, 2003).

Introduction

A common pathological feature of polyQ diseases is the nuclear accumulation of disease proteins as intraneuronal aggregates, which is due to the failure to adopt their native and functional conformation. It is believed that these intraneuronal aggregates perturb crucial cellular functions and compromise cellular homeostasis, leading to neurotoxicity and the manifestation of the disease. Elucidating the mechanisms behind the nuclear localization of polyQ-expanded proteins and its contribution to neurotoxicity could provide insight into the pathogenesis of these diseases and the development of effective therapeutic strategies (Havel et al., 2009; Klockgether et al., 2019). Like other polyQ diseases, aggregation of polyQ-expanded ataxin-3 occurs mainly in the form of intranuclear inclusions; however, cytoplasm is its primary site of location. The accumulation of expanded ataxin-3 in the nuclei of neurons is evident in both SCA3 patients and animal models (Bichelmeier et al., 2007; Schmidt et al., 1998; Yang et al., 2002). It has been shown that inhibition of nuclear localization of expanded ataxin-3 alleviates the disease symptoms (Bichelmeier et al., 2007). Accumulating evidence revealed that dysregulation of nucleocytoplasmic transport machinery is associated with several neurodegenerative diseases and can be an explanation for the nuclear accumulation of polyQ-expanded proteins (Cornett et al., 2005; Ding and Sepehrimanesh, 2021).

An *in vitro* study indicated that nuclear shuttling of ataxin-3 is mediated by the classical transport pathway (Macedo-Ribeiro et al., 2009). Previously, our group reported that karyopherin α-3 (KPNA3) is a key player in the nuclear transport of ataxin-3 and implicated in the pathogenesis and progression of SCA3 (Sowa et al., 2018). KPNA3 functions as an adaptor protein for KPNB1 in the nuclear transport of various cargos, and this raises the possibility that KPNB1 could be implicated in the modulation of ataxin-3 as well. Accordingly, the current study focused on three main aspects: (1) What is the impact of KPNB1 dysregulation on ataxin-3 modulation in an SCA3 cellular model? What are the impacts of KPNB1 overexpression as well as KPNB1 knockdown and pharmacological inhibition on wild-type and polyQ-expanded ataxin-3 protein levels, subcellular localization, and aggregates formation? (2) What are the upstream regulators or pathways implicated in the modulation of ataxin-3 via KPNB1 overexpression? (3) Is there any alteration of KPNB1 protein levels in SCA3 transgenic mouse models?

2. Materials and Methods

2.1 Cell culture and transfection

2.1.1 Culture and maintenance of HEK 293T cells

Wild-type HEK 293T (ATCC: CRL-11268) as well as *ATXN3* KO HEK 293T cells previously generated in our lab (Weishäupl et al., 2019), were maintained in Dulbecco's modified Eagle's medium (DMEM) supplemented with 10% fetal bovine serum (FBS) and 1% antibiotic-antimycotic (all Gibco, Thermo Fisher Scientific) in a mycoplasma-free and humidified incubator at 37 °C and 5% CO_2. The cells were split once or twice a week. The cell culture medium was discarded, and the cells were washed using 5 ml of pre-warmed Dulbecco's phosphate-buffered saline (DPBS; Gibco, Thermo Fisher Scientific). Afterward, cells were incubated with 1–2 ml of pre-warmed TrypLE Express (Gibco, Thermo Fisher Scientific) at room temperature for 2 min. When ~90% of the cells detached, 9–8 ml (at least twice the volume used for the dissociation reagent) of pre-warmed medium was added into the flask to inactivate TrypLE Express, and the cells were totally detached from the flask by pipetting over the cell layer several times. 1 ml of cell suspension was kept, and 9 ml of medium was pipetted into the flask and returned to the incubator.

2.1.2 Generation of induced pluripotent stem cells from fibroblasts

Fibroblasts of three SCA3 patients and three healthy, age- and gender-matched individuals were reprogrammed to induced pluripotent stem cells (iPSCs) (Hayer et al., 2018). Briefly, the skin biopsies were left undistributed in a medium consisting of Dulbecco's modified Eagle medium (DMEM) high glucose supplemented with 10% fetal calf serum (FCS) (all Gibco, Thermo Fisher Scientific, Karlsruhe, Germany) at 37 °C and 5% CO2 for 10 days. To expand the cells, the medium was changed every 2–3 days. For reprogramming, the cells were electroporated (Nucleofector 2D, Lonza) with 1 mg per plasmid carrying hOCT4, hSOX2, hKLF4, hLMYC, and hLIN28 genes and cultured for 1 further day. After a period of 2 days of cultivation in medium supplemented with 2 ng/l FGF-2 (Peprotech), fibroblasts were transferred to Essential 8 (E8) medium supplemented with 100 µM sodium butyrate (Sigma-Aldrich, St. Louis, MO, US). 3–4 weeks after reprogramming, the iPSC colonies were picked

and further expanded. At passage 5, iPSCs were harvested for analysis or frozen in E8 medium with 40% KnockOut Serum Replacement (KOSR; Gibco, Thermo Fisher Scientific) and 10% DMSO (Sigma-Aldrich).

2.1.3 Transient transfection of HEK 293T cells with TurboFectin 8.0

Transient transfection of cells with constructs was carried out using TurboFectin 8.0 (OriGene Technologies, Rockville, US) transfection reagent according to the manufacturer's instructions. Briefly, cells were seeded at a density of 400,000 cells/well in a 6-well plate at 37 °C for 24 h prior to transfection. 1 µg DNA construct was added to 250 µl serum-free medium or Opti-MEM I Reduced Serum Media (Gibco, Thermo Fisher Scientific), and then was mixed with 3 µl TurboFectin 8.0 transfection reagent. The complex was incubated for 15 min at room temperature and subsequently added to the cells in a drop-wise manner. Before returning the plate to the incubator, it was swirled in a ∞ shape to ensure that the distribution of complexes was even. The cells were harvested for further assessments 72 h post-transfection.

2.1.3.1 Plasmid preparation

A specimen from a bacterial glycerol stock (stored at –80 °C) was taken and inoculated with a culture of 7.5–10 ml of autoclaved Luria-Bertani (LB) medium (DB Difco) containing the appropriate selective antibiotic. Dependent on plasmid resistance, 7.5–10 µl (1:1000) ampicillin (100 mg/ml), kanamycin (50 mg/ml), and/or tetracycline (10 mg/ml) were applied. The bacteria were grown at 37 °C for 16 h with vigorous shaking. All used plasmids are listed in Table 2.1.

Plasmid preparation was performed using the QIAprep Spin Miniprep Kit (Qiagen, Hilden, Germany) according to the manufacturer's instructions, and all steps were carried out at room temperature. The bacterial cells were harvested by centrifugation at 4000 rpm for 5 min at 4 °C. The pelleted bacterial cells were resuspended in 250 µl Buffer P1 (supplemented with RNase A) and transferred to a fresh 1.5 ml reaction tube. 250 µl Buffer P2 was added and mixed thoroughly by inverting the tube 4–6 times (the lysis reaction should not proceed for more than 5 min). Afterwards, 350 µl Buffer N3 was added, and the tube was immediately inverted 4–6 times. It was followed by centrifugation for 10 min at ~17,900×*g*, and 800 µl supernatant was applied to a QIAprep 2.0 Spin Column by pipetting. The QIAprep 2.0 Spin

Column was centrifuged at ~17,900×*g* for 30–60 s, and the flow-through was discarded. Subsequently, it was washed using 750 µl Buffer PE (supplemented with ethanol) and centrifuged at ~17,900×*g* for 30–60 s, and the flow-through was discarded. To remove the residual of wash buffer, the QIAprep 2.0 Spin Column was centrifuged at ~17,900×*g* for 1 min (Residual ethanol from Buffer PE may inhibit subsequent enzymatic reactions). Eventually, the QIAprep 2.0 Spin Column was placed in a fresh 1.5 ml reaction tube, and maximum 50 µl buffer EB (10 mM Tris-Cl pH 8.5) was added to the center of it. After 1 min, it was centrifuged at ~17,900×*g* for 1 min. The concentration of plasmids was measured using a BioPhotometer (Eppendorf) at 260 and 280 nm, and the ratio of A_{260}/A_{280} was used to analyze DNA purity.

Table 2.1 Expression constructs. Kana = kanamycin; Amp = ampicillin; Tet = tetracycline.

Plasmid	Promoter	Resistance	Provider/Company
pcDNA3.1/Xpress	CMV	Amp	Thermo Fisher Scientific, Karlsruhe, Germany
pcDNA3.1/Xpress-MJD15Q	CMV	Amp	Internal
pcDNA3.1/Xpress-MJD77Q	CMV	Amp	Internal
pcDNA3.1/Xpress-MJD148Q	CMV	Amp, Kana, Tet	Internal
pCMV6-Entry/myc-DDK-CLPP	CMV	Amp	OriGene Technologies, Rockville, US
pCMV6-XL5-KPNA2	CMV	Amp	OriGene Technologies
pCMV6- XL5 -KPNA3	CMV	Amp	OriGene Technologies
pCMV6-XL5-KPNB1	CMV	Amp	OriGene Technologies
pEGFP-N2	CMV	Kana	Clontech, Mountain View, CA, US
pEGFP-N2-MJD15Q	CMV	Kana	Internal
pEGFP-N2-MJD148Q	CMV	Kana	Internal
pGEX-6P-1	Tac	Amp	GE Healthcare, Munich, Germany
pGEX-6P-1-MJD15Q	Tac	Amp	Internal
pGEX-6P-1-MJD77Q	Tac	Amp	Internal
pTRE-MJD15Q	-	Amp	Gossen and Bujard, 1992
pTRE-MJD77Q	-	Amp	Gossen and Bujard, 1992
pTET-RCA2	-	Amp	Gossen and Bujard, 1992

2.1.4 Transient transfection of HEK 293T cells with Attractene

Transient transfection of cells with endoribonuclease-prepared siRNAs (esiRNAs) was conducted using Attractene (Qiagen) transfection reagent according to the manufacturer's instructions. Cells were plated at a density of 400,000 cells/well in a 6-well plate at 37 °C for 24 h prior to transfection. 1.2 µg DNA construct was added to 100 µl serum-free medium or Opti-MEM I Reduced Serum Media, and then was mixed with 4.5 µl Attractene transfection reagent. The complex was incubated for 15 min at room temperature followed as mentioned above. All used esiRNAs are listed in Table 2.2.

Table 2.2 Endoribonuclease-prepared siRNAs (esiRNAs). LUC = Renilla luciferase.

esiRNA	**Company**
esiRNA-CLPP (MISSION esiRNA EHU011941)	Sigma-Aldrich, St. Louis, MO, US
esiRNA-KPNA3 (MISSION esiRNA EHU038741)	Sigma-Aldrich
esiRNA-KPNB1 (MISSION esiRNA EHU043151)	Sigma-Aldrich
esiRNA-LUC (MISSION esiRNA EHURLUC)	Sigma-Aldrich

2.1.5 Cell viability assay

The PrestoBlue Cell Viability Reagent is a resazurin-based reagent that is blue and can irreversibly convert into pink-colored resorufin during aerobic respiration. Cell viability was evaluated using the PrestoBlue assay (Thermo Fisher Scientific) according to the manufacturer's instructions. In brief, cells were seeded at a density of 400,000 cells/well in a 6-well plate at 37 °C and transfected for 48 h. Afterwards, the cells were transferred into a 96-well plate containing fresh medium and further cultured for 24 h. The cell medium was removed, and fresh medium containing PrestoBlue reagent in a ratio of 1:10 was added to the cells at 37 °C and 5% CO_2 for 30 min. Fluorescence signals were measured at 535 nm (excitation) and 620 nm (emission) using an EnVision Multimode Plate Reader and the EnVision Manager software version 1.13.3009.1401 (both PerkinElmer).

2.2 HEK 293T cells treatment

2.2.1 Importazole treatment

Importazole (IPZ; a 2,4-diaminoquinazoline) (Figure 2.1) is a specific and reversible inhibitor of karyopherin β function, likely via altering the interaction of karyopherin β with RanGTP (Soderholm et al., 2011). To inhibit the function of KPNB1, cells were seeded at a density of 400,000 cells/well in a 6-well plate and transfected for 72 h and maintained under standard culturing conditions. Cells were incubated with 16 µM IPZ (Sigma-Aldrich) for 48 h prior to harvesting. DMSO-treated cells were applied as control.

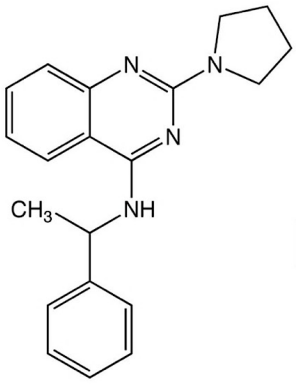

Figure 2.1 The chemical structure of importazole (a 2,4-diaminoquinazoline). Modified from Soderholm et al., 2011.

2.2.2 Bafilomycin A1 treatment

Bafilomycin A1 (BafA1) blocks the fusion of autophagosomes with lysosomes in the cells (Mizushima et al., 2010). To inhibit autophagy and analyze its effect, cells were seeded at a density of 400,000 cells/well in a 6-well plate at 37 °C and 5% CO_2 and transfected for 72 h. Cells were treated with 50 nM vacuolar H^+ ATPase inhibitor bafilomycin A1 (InvivoGen, Toulouse, France) for 24 h prior to harvesting. DMSO-treated cells were used as a control.

2.2.3 Lactacystin treatment

To inhibit proteasomal degradation and analyze its effect, cells were seeded at a density of 400,000 cells/well in a 6-well plate at 37 °C and 5% CO_2 and transfected for 72 h. 24 h prior to harvesting, cells were incubated with 10 µM of the proteasome inhibitor lactacystin (Enzo Lifescience, Lausen, Switzerland). DMSO-treated cells were used as a control.

2.2.4 Calpain inhibitor III treatment

To decrease the baseline activity of calpains in the cells, cells were seeded at a density of 400,000 cells/well in a 6-well plate at 37 °C and 5% CO_2 and transfected for 72 h. Cells were treated with 10 µM of calpain inhibitor III (CI-III; carbobenzoxy-valinyl-phenylalaninal) (Sigma-Aldrich) for 24 h prior to harvesting. DMSO-treated cells were used as a control.

2.2.5 Caspase inhibitor Q-VD-OPh treatment

To block the activation of caspases in cells, cells were seeded at a density of 400,000 cells/well in a 6-well plate at 37 °C and 5% CO_2 and transfected for 72 h. 24 h prior to harvesting, cells were incubated with 10 µM of the broad-spectrum caspase inhibitor Q-VD-OPh (Sigma-Aldrich). DMSO-treated cells were used as a control.

2.2.6 Ionomycin treatment

A cell-based calpain activation assay was conducted using ionomycin (IM). Cells were seeded at a density of 400,000 cells/well in a 6-well plate, transfected for 72 h, and maintained under standard culturing conditions. The cell medium was aspirated and replaced by Opti-MEM I Reduced Serum Media; afterwards, endogenous calpains were activated by incubating cells with 1 µM Ca^{2+} ionophore ionomycin (Sigma-Aldrich) and 5 mM $CaCl_2$ for 1 h at 37 °C and 5% CO_2. DMSO-treated cells were applied as a control.

2.2.7 Doxycycline treatment

To analyze the stability of ataxin-3, the Tet-Off system was applied. Cells were seeded at a density of 400,000 cells/well in a 6-well plate at 37 °C and 5% CO_2 and transfected for 72 h. To turn off the expression of the Tet-Off system, 4.5 µM doxycycline (Sigma-Aldrich) was applied for 0 h, 6 h, 24 h, and 48 h prior to harvesting the cells.

2.3 Protein analyses

2.3.1 Preparation of mouse brain lysate

To obtain mouse brain lysates, brain hemispheres were homogenized in RIPA buffer (50 mM Tris pH 7.5, 150 mM NaCl, 1% Triton X-100, 0.1% sodium dodecyl sulfate (SDS), 0.5% sodium deoxycholate) containing cOmplete protease inhibitor EDTA-free (Hoffmann-La Roche, Basel,

Switzerland) and 50 µM Thiamet G (TMG) using the ULTRA-TURRAX disperser (VWR International, Ulm, Germany). Subsequently, the homogenates were centrifuged at 16,000×*g* for 30 min at 4 °C. In the final step, the supernatant was transferred into a fresh reaction tube, supplemented with 10% glycerol, and stored at –80 °C for further analysis.

2.3.2 Preparation of HEK 293T cell lysate

To prepare HEK 293T cell lysates, cultured cells were harvested by removing the media and dissociating the cell layer using cold DPBS. The cell suspension was transferred into a 1.5 ml reaction tube, centrifuged at 300×*g* for 5 min, and the supernatant was discarded. RIPA buffer (50 mM Tris pH 7.5, 150 mM NaCl, 1% Triton X-100, 0.1% SDS, 0.5% sodium deoxycholate) containing cOmplete protease inhibitor EDTA-free was added to the cell pellet and it was resuspended by pipetting. It was incubated on ice for 25 minutes (vortexing every 5 min), and subsequently centrifuged at 16,000×*g* for 15 min at 4 °C. Finally, the supernatant was transferred into a fresh reaction tube and supplemented with 10% glycerol. The cell lysates were stored at –80 °C for later use.

2.3.3 Protein concentration measurement

The protein concentration of mouse brain and cell lysates was determined using the Bradford protein assay. The Bradford protein assay is a dye-binding assay in which the color of Coomassie Brilliant Blue G-250 dye changes from red to blue in response to various concentrations of proteins (Bradford, 1976). The absorbance of the acidic solution of this reagent shifts from 465 nm to 595 nm when it binds to proteins. 1 µg/µl bovine serum albumin (BSA) solution was applied for making the protein standard curve. 0 µl, 1 µl, 2 µl, 5 µl, 10 µl, 15 µl, and 20 µl of BSA solution were added to 800 µl H2O to prepare samples for making a standard curve. 2 µl cell lysate or homogenate was added to 798 µl H2O to reach the final volume of 800 µl. Ultimately, 200 µl Bio-Rad Protein Assay Dye Reagent Concentrate (Bio-Rad Laboratories, Hercules, CA, US) was added to the standard and target samples and thoroughly mixed by vortexing. 100 µl of each mixture was transferred to a 96-well plate, and the absorbance at 595 nm was measured using a Synergy HT plate reader.

2.3.4 Sodium dodecyl sulfate polyacrylamide gel electrophoresis (SDS-PAGE)

To prepare samples for running on a polyacrylamide gel, 30 µg protein extract was mixed with 4× LDS sample buffer (1 M Tris-base pH 8.5, 2 mM EDTA, 8% lithium dodecyl sulfate (LDS), 40% glycerol, 0.025% phenol red) supplemented with 100 mM Dithiothreitol (DTT) and heat-denatured for 10 min at 70 °C. Prepared samples and protein marker (Bio-Rad) were subjected to electrophoresis using 10% Bis-Tris gels (Table 2.3), and either MES SDS (50 mM MES, 50 mM Tris-base pH 7.3, 0.1% SDS, 1 mM EDTA) or MOPS SDS (50 mM MOPS, 50 mM Tris-Base pH 7.7, 0.1% SDS, 1 mM EDTA) running buffer. The gel was run at 80 V for 15 min and then increased to maximum of 120 V.

Table 2.3 Reagents and applied volumes for making 2 Bis-Tris gels (10%).

Reagent	Stacking gel (5%)	Separation gel (10%)
3.5× Bis-Tris buffer (pH 6.5–6.8)	1 ml	2.84 ml
ddH2O	1.9 ml	3.82 ml
30% Acrylamide-Solution (PanReac AppliChem)	0.6 ml	3.34 ml
10% APS	35 µl	50 µl
TEMED (PanReac AppliChem)	6.7 µl	14 µl

2.3.5 Western blot analysis

The gel was transferred on an Amersham Biosciences Protran Premium 0.2 µm nitrocellulose membrane (GE Healthcare, Freiburg, Germany) as illustrated in Figure 2.2, and it was made sure that there was no bubble between the layers. All used sponges and Whatman papers were pre-wetted with Bicine/Bis-Tris transfer buffer (25 mM Bicine, 25 mM Bis-Tris pH 7.2, 1 mM EDTA) containing 15% methanol. The transfer chamber was filled with transfer buffer, and blotting was conducted at 80 V for 90 min. Afterwards, the membrane was blocked using 5% skim milk (Sigma-Aldrich) in Tris-buffered saline (TBS; 10 mM Tris pH 7.5, 150 mM NaCl) for 1 h at room temperature (RT) and washed using TBS-T (TBS containing 0.1% Tween 20) for 5 min three times. The membrane was incubated with the primary antibody (Table 2.4) diluted in TBS-T overnight at 4°C. After three times washing the membrane with TBS-T for 5 min, fluorescence-conjugated secondary antibody (Table 2.5) diluted in TBS-T was added for

1 h at RT. The membrane was washed with TBS-T for 10 min three times, and fluorescence signals were detected using the LI-COR ODYSSEY FC system (LI-COR Biosciences, Bad Homburg, Germany). A ratio of target protein to loading control was calculated using Image Studio 5.2 software (LI-COR Biosciences). The primary and secondary antibodies were stripped from the membrane using stripping buffer (25mM glycine, 1% SDS pH 2.0) for 10 min twice, followed by washing with TBS-T for 5 min three times.

Table 2.4 Primary antibodies applied for immunodetection and immunostaining.

Primary antibody	Host specie	Dilution	Cat No.	Provider/Company
Anti-ataxin-3	Mouse	1:5000	1H9, MAB5360	Merck, Darmstadt, Germany
Anti-ataxin-3/C-terminal	Rabbit	1:2500	SA3637	Schmidt et al., 1998
Anti-α-spectrin	Mouse	1:1000	AA6	Merck
Anti-β-actin	Mouse	1:5000	AC-15, A5441	Sigma-Aldrich, St. Louis, MO, US
Anti-CLPP	Rabbit	1:2500	15698-1-AP	Proteintech, St. Leon-Rot, Germany
Anti-c-myc	Mouse	1:200	9E10, sc-40	Santa Cruz Biotechnology, Heidelberg, Germany
Anti-GAPDH	Mouse	1:5000	0411, sc-47724	Santa Cruz Biotechnology
Anti-GFP	Mouse	1:5000	B-2, sc-9996	Santa Cruz Biotechnology
Anti-GST	Mouse	1:2500	B-14, sc-138	Santa Cruz Biotechnology
Anti-KPNA2	Mouse	1:5000	G-11, sc-55537	Santa Cruz Biotechnology
Anti-KPNA3	Rabbit	1:5000	ab137446	Abcam, Cambridge, United Kingdom
Anti-KPNB1	Rabbit	1:5000	H-300, sc-11367	Santa Cruz Biotechnology
Anti-lamin A/C	Mouse	1:5000	346, sc-7293	Santa Cruz Biotechnology
Anti-LC3	Rabbit	1:1000	MBL-PD014	MBL International, Woburn, MA, US
Anti-p62	Rabbit	1:1000	5114	Cell Signaling Technologies, Frankfurt am Main, Germany
Anti-vinculin	Rabbit	1:1000	E1E9V, 13901	Cell Signaling Technologies

Table 2.5 Secondary antibodies used for immunodetection and immunostaining.

Secondary antibody	Host specie	Dilution	P/N	Lot/Cat No.	Company
IRDye 680LT	Goat anti-Mouse	1:10,000	926-68020	C50113-11	LI-COR Biosciences, Bad Homburg, Germany
IRDye 800CW	Goat anti-Mouse	1:10,000	926-32210	C50113-06	LI-COR Biosciences
IRDye 680LT	Goat anti-Rabbit	1:10,000	926-68021	C40916-01	LI-COR Biosciences
IRDye 800CW	Goat anti-Rabbit	1:10,000	926-32211	C50331-05	LI-COR Biosciences
Alexa Fluor 555	Goat anti-Rabbit	1:500	-	A32732	Thermo Fisher Scientific, Karlsruhe, Germany

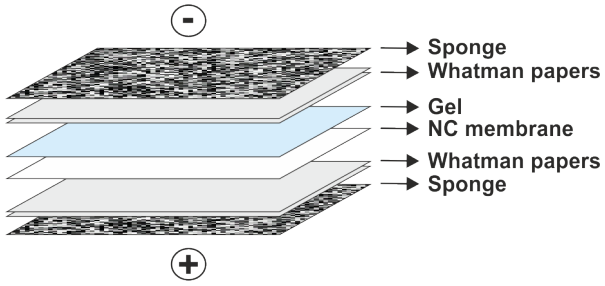

Figure 2.2 Schematic representation of protein transfer from a polyacrylamide gel on a nitrocellulose membrane. NC = nitrocellulose.

2.3.6 Subcellular fractionation assay

Cytoplasmic and nuclear fractions were separated according to the Rapid, Efficient And Practical (REAP) fractionation method (Suzuki et al., 2010), with minor modifications (Weber et al., 2017). Cells were seeded at a density of 400,000 cells/well in a 6-well plate and transfected for 72 h. The cells were harvested using cold DPBS and detached by pipetting. The cell suspension was centrifuged at 300×*g* for 5 min, and the supernatant was discarded. 100 µl micropipette tip was cut off at the 10 µl mark to enlarge the opening, and the cell pellet was triturated five times with cold lysis buffer (DPBS supplemented with 0.1% NP-40) containing cOmplete protease inhibitor EDTA-free (90 µl for sample from a 6-well plate). An aliquot of cell suspension (30 µl) was taken as the whole cell lysate and kept on ice. The rest was centrifuged at 10,000×*g* for 10 s, and the supernatant (60 µl) was considered cytoplasmic fraction. The remaining pellet was rinsed once with 100 µl cold lysis buffer and centrifuged at

10,000×*g* for 10 s. The supernatant was discarded, and the nuclear pellet was kept on ice. The whole cell lysate and cytoplasmic fraction were mixed with 30 µl and 60 µl 4× LDS sample buffer, respectively, and the nuclear pellet was resuspended in 36 µl 1× LDS sample buffer. 1 M DTT in a ratio of 1:10 was added to all samples and they were heat-denatured for 10 min at 70 °C, followed by ultra-sonication for 10 s with 5 intervals at 10% power. Ultimately, 10 µl of each sample was subjected to western blot analysis and immunodetection according to the standard protocol. GAPDH and Lamin A/C were served as cytoplasmic and nuclear loading controls, respectively.

2.3.7 Filter retardation assay

The formation of SDS-insoluble aggregates was analyzed by a filter retardation assay (Weber et al., 2017). Cells were plated at a density of 400,000 cells/well in a 6-well plate and transfected for 72 h. The cells were harvested using cold DPBS and centrifuged at 300×*g* for 5 min. The cell pellet was homogenized in lysis buffer (DPBS supplemented with 1% Triton X-100) containing cOmplete protease inhibitor EDTA-free by ultra-sonication for 10 s with 5 intervals at 10% power. The protein concentration of the homogenate was measured by the Bradford protein assay (as described before), and 10 µg homogenate was diluted in a total volume of 100 µl DPBS supplemented with 2% SDS and 50 mM DTT. Samples were boiled for 5 min at 95 °C and cooled down to room temperature (RT) to avoid precipitation of SDS. In the next step, filter trap apparatus (Minifold II Slot Blot System, GE Healthcare) was assembled, and an Amersham Biosciences Protran 0.45 µm nitrocellulose membrane (GE Healthcare) was placed on top of two whatman papers. The membrane was equilibrated by washing the wells with 100 µl DPBS, and 100 µl of each sample was run on it using a vacuum pump. Afterwards, the wells were washed using 100 µl DPBS, and the membrane was transferred into TBS for 5 min. Membrane was blocked using 5% skim milk in TBS for 1 h at RT, and immunodetection was conducted according to the standard protocol (as mentioned in the western blot analysis section).

2.3.8 Glutathione S-transferase (GST) pull-down assay

A GST pull-down assay was employed to detect protein-protein interactions. For this purpose, *E. coli* BL21 bacteria containing pGEX-6P-1-MJD15Q and pGEX-6P-1-MJD77Q were cultured in 10 ml 2× YT medium (Roth, X966.3) supplemented with 10 µl Ampicillin (100 mg/ml) (1:1000).

The bacteria were grown for 16 h at 37 °C with vigorous shaking (INFORS AG, Bottmingen, Switzerland), and protein expression was induced by adding 1 mM isopropyl β-D-1-thiogalactopyranoside (IPTG) for 2 h. The bacteria were centrifuged at 1500×*g* at 4 °C for 5 min, and the pellet was rinsed once and resuspended in 500 µl GST-binding/wash Buffer (4.2 mM NaH_2PO_4, 2 mM KH_2PO_4, 140 mM NaCl, and 10 mM KCl, 1% NP-40) containing cOmplete protease inhibitor EDTA-free. Bacterial lysate was prepared by ultra-sonication for 15 s with 5 intervals at 40% power, followed by centrifugation at 16,000×*g* for 10 min at 4 °C. The supernatant was transferred into a fresh 1.5 ml reaction tube and supplemented with 10% glycerol. Eukaryotic protein extract was obtained by harvesting wild-type HEK 293T cells using cold DPBS and centrifugation at 300×*g* for 5 min at 4 °C. The pellet was resuspended in 500 µl GST-binding/wash Buffer, lysed using a U-40 Insulin Syringe, and centrifuged at 16,000×*g* for 15 min at 4 °C. The supernatant was transferred into a fresh 1.5 ml reaction tube and supplemented with 10% glycerol. The protein concentration of HEK 293T cells and bacterial lysates was determined by the Bradford protein assay (as described before). 35 µl MagneGST Glutathione Particles (Promega, Walldorf, Germany) were applied and washed four times using 250 µl GST-binding/wash Buffer at room temperature and resuspended by flicking. 500 µg prokaryotic protein extract (in a volume of 250 µl) containing GST-15Q or GST-77Q ataxin-3 was immobilized on MagneGST Glutathione Particles for 1–2 h at 4 °C on a rotor, followed by a four-times-washing step using 500 µl GST-binding/wash Buffer for 5 min at 4 °C. Subsequently, MagneGST Glutathione Particles were incubated with 500 µg HEK 293T cells protein extract (in a volume of 250 µl) overnight at 4 °C on a rotor and washed five times with 500 µl GST-binding/wash Buffer. The trapped proteins were eluted from magnet particles by boiling in 40–50 µl 1× LDS sample buffer containing 100 mM DTT for 5 min at 95 °C and proceeded to western blot analysis and immunodetection.

2.3.9 Immunofluorescence staining

Cells were grown on poly-L-lysine (Sigma-Aldrich)-coated glass coverslips in a 24-well plate and transfected with respective constructs for 72 h. For prefixation, 50 µl 4% paraformaldehyde (PFA) solution (4% PFA in DPBS pH 7.5) was added to the medium, and it was incubated for 10 min at 37 °C with 5% CO_2. For cell fixation, medium was aspirated, and cells were incubated with 200 µl 4% PFA solution for 15 min at room temperature (RT),

shaking gently. Afterwards, cells were washed using DPBS three times for 5 min, and blocked and permeabilized using 200 µl blocking solution (DPBS supplemented with 10% BSA and 0.5% Triton X-100) for 1 h at RT. Blocking solution was removed, and 150 µl primary antibody in antibody diluent (DPBS supplemented with 1% BSA and 0.5% Triton X-100) was added over night at 4 °C. The cells were washed using cold DPBS four times for 5 min at RT and incubated with 150 µl secondary fluorescence-tagged antibody Alexa Fluor 555 (1:500; Thermo Fisher Scientific) in antibody diluent for 1 h at RT. Subsequently, cells were rinsed by cold DPBS four times for 5 min and mounted using VECTASHIELD Antifade Mounting Medium containing DAPI (Vector Laboratories, Peterborough, UK). Fluorescent images were taken with an Axioplan 2 Imaging System, AxioCam MRm (Carl Zeiss Microscopy, Jena, Germany), 400× magnification, and AxioVision version 4.8 imaging software (Carl Zeiss Microscopy). 20 fields of vision with at least 10 GFP-positive cells were photographed per coverslip under blinded conditions. The number of cells with aggregates was counted manually and calculated as the percentage of total GFP-positive cells.

2.4 Mass spectrometry (MS)

2.4.1 Protein in-gel digestion

Cells were seeded at a density of 400,000 cells/well in a 6-well plate and transfected for 72 h in three biological replicates. Cells were harvested using cold DPBS, and cell lysates were prepared using RIPA buffer as described in the preparation of the HEK 293T cell lysate section. The whole cell lysates were purified using SDS-PAGE (Thermo Fisher Scientific), and the gel was stained with Coomassie Brilliant Blue. Stained gel pieces were excised and in-gel digested using trypsin as described previously (Borchert et al., 2010). Tryptic peptides were desalted using C18 StageTips (Rappsilber et al., 2007) and subjected to liquid chromatography and tandem mass spectrometry (LC-MS/MS) analysis.

2.4.2 Liquid chromatography and tandem mass spectrometry (LC-MS/MS)

LC-MS/MS analysis was conducted on an Easy nano-LC (Thermo Fisher Scientific) coupled to an QExactiveHF mass spectrometer (Thermo Fisher Scientific) as described before (Franz-Wachtel et al., 2012). Peptides were eluted by applying a 60-min segmented gradient with a

flow rate of 200 nl/min. The 20 most intensive peaks were selected for fragmentation with HCD.

2.4.3 Mass spectrometry data processing

The MS data from all three replicates was processed utilizing MaxQuant software suite version 1.6.7.0 (Cox and Mann, 2008). Database search was carried out using the Andromeda search engine (Cox et al., 2011), which is integrated into MaxQuant. MS/MS spectra were searched against a target-decoy human Uniprot database comprising 96817 protein entries and 245 commonly observed contaminants. Full specificity was required for trypsin, and up to two missed cleavages were allowed in database searches. Cysteine carbamidomethylation was considered the static modification, while methionine oxidation and acetylation of N-terminal residues were set as variable modifications. Initial mass tolerance was set to 4.5 parts per million (ppm) for precursor ions and 0.5 Dalton (Da) for fragment ions. Peptide and modification site identifications were determined at a false discovery rate (FDR) of 0.01, interpreted by the target-decoy approach (Elias and Gygi, 2007). The label-free algorithm was enabled, as was the "match between runs" option for samples within one biological replicate (Luber et al., 2010). Label-free quantification (LFQ) protein intensities from the MaxQuant data output were employed for relative protein quantification. Bioinformatic analysis (Student's *t*-test) was performed using the Perseus software package version 1.6.2.3 (Tyanova et al., 2016). The data was filtered for contaminants, reversed, and only identified by site entries. A p-value ≤ 0.05 was considered statistically significant, and SO was set to 0 (SO = 0).

For canonical pathway analysis and identification of the upstream regulators, dysregulated proteins obtained from mass spectrometry were analyzed using the Ingenuity Pathway Analysis (IPA) software (v60467501) (Qiagen). Dysregulated proteins with a p-value ≤ 0.05 were considered for the analysis. A z-score, which describes how many standard deviations a value is above or below the mean of a given distribution, was calculated.

2.5 RNA sequencing

Cells were seeded at a density of 400,000 cells/well in a 6-well plate and transfected for 72 h. The cells were harvested using cold DPBS and centrifuged at 300×g for 5 min. Total RNA was isolated from cells using the QIAsymphony RNA Kit (Qiagen) according to the manufacturer's

instructions. In brief, the cell pellet was disrupted using 400 µl RLT Plus in a 2 mL microcentrifuge tube containing a 5 mm-diameter stainless steel bead (Qiagen) and agitated at 30 HZ for twice 2 minutes using the TissueLyser II (Qiagen). RNA isolation was performed on the QIAsymphony (Qiagen) following the platform standard protocol. The RNA concentration was measured using the Qubit Fluorometric Quantitation and RNA Broad-Range Assay Kit (ThermoFisher Scientific), and RNA purity was determined using the A_{260}/A_{280} and A_{260}/A_{230} ratios using a spectrophotometer (Nanodrop ND-1000; PEQLAB). The RNA Integrity Number (RIN) was estimated using the Fragment Analyzer 5300 and the Fragment Analyzer RNA Kit (Agilent Technologies).

For library preparation, the mRNA fraction was enriched using oligodT priming from 100 ng of total RNA using the QuantSeq 3' mRNA-Seq (Lexogen). Subsequently, mRNA libraries were prepared using the UMI Second Strand Synthesis Module according to the manufacturer's instructions, and the library amplification was carried out with 15 PCR cycles. Library molarity was determined by measuring the library size using the Fragment Analyzer 5300 and the Fragment Analyzer DNA HS NGS fragment Kit (Agilent Technologies). The concentration of library (> 1 ng/µl) was measured using Qubit Fluorometric Quantitation and dsDNA High Sensitivity Assay (Thermo Fisher Scientific). In the next step, the libraries were denaturated according to the manufacturer's instructions, diluted to 800 pM, and sequenced as dual 100 bp reads on an Illumina NovaSeq 6000 (Illumina) with a sequencing depth > 10 million clusters per sample.

Read quality of RNA-seq data in fastq files was assessed using ngs-bits (v2020_12-60) to identify sequencing cycles with low average quality, adaptor contamination, or repetitive sequences from PCR amplification. Reads were aligned using STAR (v2.7.3a) allowing gapped alignments to account for splicing against a custom-built genome composed of the Ensembl rat Rnor6, and alignment quality was analyzed using samtools (v1.11) and visually inspected in the Integrative Genome Viewer (v2.7.2). Normalized read counts for all genes were obtained using TMM normalized expression in edgeR (v3.32.0) on R(v4.0.2). Transcripts covered with less than 1 count-per-milion in at least 1 sample were excluded from the analysis leaving > 9,000 genes for determining differential expression in each of the pair-wise comparisons between experimental groups.

The distribution of logarithmized cpm-normalized expression values displayed similar characteristics over all samples. Based on the filtered data set, samples were investigated with respect to their pairwise similarity. Spearman's rank correlation coefficient was calculated for each pair of samples. Hierarchical clustering was conducted on the resulting similarity values. Differential gene expression analysis was done based on the filtered gene expression data set. A statistical model incorporating the group property of samples was tested by fitting a negative binomial distribution using a generalized linear model (GLM) approach. For each gene, gene expression fold change (log_2 fold change) was computed, and a statistical test was carried out to assess the significance, which is given as a raw *p*-value and adjusted an *p*-value (FDR, obtained by the Benjamini-Hochberg procedure).

For canonical pathway analysis, differentially expressed genes obtained from RNA sequencing were analyzed using the Ingenuity Pathway Analysis (IPA) software (v60467501) (Qiagen). Differentially expressed genes with log_2 fold change (log_2 FC) ≥ 0.5 and *p*-value ≤ 0.05 were considered for the analysis. A z-score, which describes how many standard deviations a value is above or below the mean of a given distribution, was calculated.

2.6 Molecular cloning

All enzymes applied for molecular cloning were purchased from New England Biolabs (Frankfurt am Main, Germany).

2.6.1 Amplification of mutation by polymerase chain reaction (PCR)

To introduce mutation (AAT to AGA) into a DNA construct containing human KPNB1, touchdown PCR was conducted according to Tables 2.6 and 2.7, applying the following primers: forward, 5'-ATGTCACAAACCCCAACAGC-3'; and reverse, 5'-GTAGCAGCTAGCTTCACATTATTACTAGGCTCTTCTTTCCTCATCCCCTGG**TC**TATGGCAGTCAGA ATC-3'.

Table 2.6 Reagents and applied volumes for PCR.

Reagent	Volume
ddH2O	13.5 µl
10× Reactions Buffer complete (includes 20 mM MgSO4)	2 µl
2 mM dNTPs	2 µl (200 µM)
pCMV6-XL5-KPNB1 (50 ng/µl)	0.5 µl (25 ng)
Primer/F	0.6 µl
Primer/R	0.6 µl
peqGOLD Pwo-DNA-Polymerase (peqlab) (1 U/µl)	0.8 µl (0.03–0.06 U/µl)
Total volume	20 µl

Table 2.7 The touchdown PCR program.

No. cycle	Time	Temperature
1×	2 min	94 °C
10×	15 s	94 °C
	30 s	65 °C –1 °C
	1 min	68 °C
25×	15 s	94 °C
	30 s	55 °C
	1 min	68 °C
1×	7 min	68 °C
1×	Infinite	10 °C

2.6.2 Purification of PCR products

Before digestion by restriction enzymes, the PCR products were purified using the QIAquick PCR Purification Kit (Qiagen) according to the manufacturer's instructions, and all centrifugations were done at ~17,900×*g*. Briefly, 5 volumes of Buffer PB (supplemented with 1:250 volume pH indicator I) were added to 1 volume of the PCR reaction and mixed. The yellow color of Buffer PB with pH indicator I indicated a pH ≤ 7.5, which is the effective pH. A QIAquick column was placed into a provided 2 ml collection tube. The sample was applied to the QIAquick column and centrifuged for 30–60 s, and the flow-through was discarded. Subsequently, the QIAquick column was washed using 750 µl Buffer PE (supplemented with ethanol) and centrifuged for 30–60 s, and the flow-through was discarded. The QIAquick

column was centrifuged once more for 1 min to remove the residual of wash buffer. The QIAquick column was placed into a fresh 1.5 ml reaction tube, and a maximum of 50 µl Buffer EB (10 mM Tris-Cl pH 8.5) was added to the center of it and centrifuged for 1 min.

2.6.3 Digestion with restriction enzymes and dephosphorylation

Plasmids (pCMV6-XL5-KPNB1) and purified PCR products (insert) were digested using SalI-HF and NheI restriction enzymes according to Table 2.8. They were incubated at 37 °C for 3 h, and subsequently inactivated at 65 °C for 20 min.

Table 2.8 Reagents and applied volumes for digestion of plasmids and PCR products.

Reagent	Plasmid	PCR product
10× CutSmart buffer	5 µl	5 µl
SalI-HF	0.5 µl	0.5 µl
NheI	0.5 µl	0.5 µl
DNA	1.5 µg	total (40 µl)
ddH2O	Adjust	4 µl
Total volume	50 µl	50 µl

Alkaline Phosphatase, Calf Intestinal (CIP) nonspecifically catalyzes the dephosphorylation of the 5´ and 3´ ends of DNA, RNA, and dNTPs. To inhibit the self-ligation of digested plasmids, 1 µl CIP was added to the reaction and incubated at 37 °C for 1 h. Afterwards, the enzyme was inactivated at 65 °C for 10 min.

2.6.4 TAE agarose gel electrophoresis

Digested plasmids and PCR products were separated by running on a 1% and 2% TAE agarose gel, respectively. For making a 1% and 2% TAE agarose gel, 0.5 g and 1 g agarose were dissolved in 50 ml 1× TAE buffer (40 mM Tris-Acetate, 1 mM EDTA pH 8), respectively. Subsequently, 0.5 µg/µl ethidium bromide was added to the solution and mixed thoroughly. The solution was applied to a gel tray, and after polymerization, it was placed into an electrophoresis chamber. The samples were mixed with 6× loading sample buffer (0.25% bromophenol blue, 0.25% xylene cyanol FF, 30% glycerol) and loaded on the gel as well as the DNA ladder (GeneRuler DNA Ladder Mix). The electrophoresis was performed using 1× TAE

buffer at 100 V for 40 min. Afterwards, the respective band was cut from the gel using a clean scalpel under UV light and put into a pre-weighted reaction tube.

2.6.5 DNA extraction from gel

Digested plasmids and PCR products were extracted from the agarose gel using the QIAquick Gel Extraction Kit (Qiagen) according to the manufacturer's instructions, and all centrifugations were done at ~17,900×*g*. 3 volumes of Buffer QG were added to 1 volume of gel (100 mg gel ~100 µl), and the reaction was incubated at 50 °C for 10 min. It was vortexed for 2–3 min until the gel was completely dissolved. Then, 1 gel volume of 100% isopropanol was added to the reaction and mixed thoroughly. The sample was applied to the QIAquick spin column and centrifuged for 1 min. Subsequently, the QIAquick spin column was washed using 750 µl Buffer PE (supplemented with ethanol) and centrifuged for 1 min and the flow-through was discarded. The QIAquick spin column was placed into a fresh 2 ml collection tube and centrifuged once more for 1 min to remove the residual of wash buffer. The QIAquick spin column was placed into a fresh 1.5 ml reaction tube, and 30 µl Buffer EB (10 mM Tris-Cl pH 8.5) was added to the center of it and centrifuged for 1 min to elute the extracted DNA. The concentration of extracted DNA was measured using a BioPhotometer at 260 and 280 nm, and the ratio of A_{260}/A_{280} was used to analyze DNA purity.

2.6.6 DNA ligation

The mass of insert required at several molar insert:vector ratios was calculated by the NEBioCalculator online tool (https://nebiocalculator.neb.com/#!/ligation). The ligation of the purified plasmid (pCMV6-XL5-KPNB1) and insert was carried out according to Table 2.9.

Table 2.9 Reagents and applied volumes for ligation of plasmid and insert.

Reagent	**Volume**
10× T4 DNA Ligase Reaction Buffer	1 µl
T4 DNA Ligase	1 µl
Plasmid (pCMV6-XL5-KPNB1)	20 ng
Insert	1.714 ng (3:1), 2.857 ng (5:1)
ddH2O	Adjust
Total volume	10 µl

The reaction was incubated at 16 °C overnight or at room temperature for 1–2 h. Afterwards, the enzyme was inactivated at 65 °C for 10 min. Plasmid without an insert was applied as the negative control.

2.6.7 Transformation of competent Bacteria

The transformation of competent bacteria was conducted by heat shock. In brief, competent DH5α bacteria (from a glycerol stock stored at –80 °C) were thawed on ice, and 100 µl of it was mixed gently with 10 µl (total) ligation mixture. The reaction was kept on ice for 30 min, followed by incubation at 42 °C for 45 s, and then placed back on ice for 2 min. Subsequently, the reaction, including bacteria, was pipetted gently into 900 µl pre-warmed Super Optimal Broth (SOC) medium (Sigma-Aldrich) and incubated at 37 °C for 1–2 h with shaking. In this step, LB medium can be used as well.

2.6.8 Culturing bacteria on agar plates

The obtained bacterial suspension was centrifuged briefly to pellet the bacteria. 800 µl supernatant was discarded, and the pellet was resuspended in the rest of the supernatant (200 µl). In the next step, 5–6 autoclaved glass beads were put in an agar plate supplemented with 100 µg/ml ampicillin, and 200 µl bacterial suspension was added to it. The agar plate was shaken until the supernatant was dried out and incubated at 37 °C overnight. The next day, the plate was checked for the colonies, and a tiny portion of individual colonies was scraped using a loop and immersed in autoclaved LB medium supplemented (1:1000) with 100 mg/ml ampicillin. The bacteria were grown at 37 °C for 16 h with vigorous shaking and proceeded with plasmid preparation (as described before).

2.7 Sanger sequencing

To confirm the respective mutation and to ensure that no other mutations have been generated, Sanger sequencing was performed using GenomeLab Dye Terminator Cycle Sequencing with Quick Start Kit (Beckman Coulter) according to the manufacturer’s instructions.

2.7.1 Preparation of DNA

The DNA template (plasmid) was diluted with water to the appropriate concentration according to the manufacturer's instructions. It was heated at 96 °C for 1 min and then cooled down to room temperature. All reagents were added into a reaction tube in the order listed in Table 2.10 and mixed thoroughly. Afterwards, it was proceeded to a thermal cycling program (Table 2.11). The following primers were applied in this step: forward, 5'-ACCAGTGGCCAGAACTCATT-3'; and reverse, 5'-AGTGCCTTTCAGACTCTTTATCA-3'.

Table 2.10 Reagents and applied volumes for DNA sequencing.

Reagent	**Volume**
ddH2O	Adjust
DNA template (plasmid)	0.5–10 µl
Sequencing Primer (1.6 pmol/µL or 1.6 µM)	2 µl
DTCS Quick Start Master Mix	8 µl
Total volume	20 µl

Table 2.11 The thermal cycling program used for DNA sequencing.

No. cycle	**Time**	**Temperature**
30×	20 s	6 °C
	20 s	50 °C
	4 min	60 °C
1×	Infinite	4 °C

2.7.2 Ethanol precipitation and sample loading

To prepare a fresh Stop Solution/Glycogen mixture (per sequencing reaction), 2 µl 3 M Sodium Acetate (pH 5.2), 2 µl 100 mM Na_2-EDTA (pH 8.0), and 1 µl 20 mg/ml glycogen (supplied with the kit) were mixed, and 5 µl Stop Solution/Glycogen mixture was added to the sequencing reaction from the last step. Afterwards, 60 µl of cold 95% ethanol from –20 °C freezer was added and mixed thoroughly, and immediately centrifuged at 14,000 rpm at 4 °C for 15 min. The supernatant was removed carefully, and the pellet was rinsed twice with 200 µl of cold 70% ethanol from –20 °C freezer. For each rinse, centrifugation was conducted immediately at 14,000 rpm at 4 °C for 2 min and the supernatant was removed carefully. Subsequently,

the sample was vacuum dried for 10 min, resuspended in 40 µl of the Sample Loading Solution (SLS), and incubated at 4 °C for 1 h. In the next step, the resuspended sample was transferred to the wells of a sample plate and overlaid with one drop of light mineral oil. The sample plate was loaded into the instrument (Beckman Coulter) and the sequencing program was started. Analysis of sequences was carried out by GenomeLab Software GeXP software (Beckman Coulter).

2.8 Animal research

2.8.1 Ethical statement on human and animal research

Informed consent was obtained for taking fibroblasts from SCA3 patients and healthy individuals. All research on human materials was carried out under the approval of the Ethics Committee of Tübingen University (598/2011BO1). Mouse tissue was obtained and applied for the experiments according to the German Animal Welfare Act and the guidelines of the Federation of European Laboratory Animal Science Associations, based on European Union legislation (Directive 2010/63/EU).

2.8.2 Mouse housing and tissue sampling

Wild-type mice as well as YAC transgenic mice (Cemal et al., 2002), and CaMKII/MJD77 transgenic mice previously generated in our lab (Schmidt et al., 2019), were housed under standard conditions and a 12-hour light-dark cycle with 50–55% relative air humidity. Mice were sacrificed using CO_2 inhalation and perfused transcardially with phosphate-buffered saline (PBS). Brains were immediately dissected on ice, snap-frozen in liquid nitrogen, and stored at –80 °C for further assessments.

2.9 Statistical analysis

Data are presented as mean ± SEM. Statistical analysis was conducted using GraphPad Prism 6.00 software (GraphPad Software Inc., La Jolla, CA, US). The statistical significance of data sets with a normal distribution was evaluated using one sample *t*-test and two-tailed Student's *t*-test. A comparison among multiple groups was performed using one-way ANOVA with Tukey's post-test. Significance was considered at p-value ≤ 0.05. Statistical outliers determined by the ROUT test (Q = 1%) were excluded from analysis.

2.10 Kits, compounds, and software

Table 2.12 Kits and reagents

Kit/Reagent	Cat No.	Company
GenomeLab Dye Terminator Cycle Sequencing with Quick Start Kit	P/N 608120	Beckman Coulter Inc., CA, USA
QIAquick Gel Extraction Kit	28706	Qiagen, Hilden, Germany
QIAquick PCR Purification Kit	28106	Qiagen
QIAprep Spin Miniprep Kit	27106	Qiagen
Attractene	301005	Qiagen
PrestoBlue Cell Viability Reagent	A13261	Thermo Fisher Scientific, Karlsruhe, Germany
TurboFectin 8.0	TF81001	OriGene Technologies, Rockville, US

Table 2.13 Compounds for cell treatment

Compound	Cat No.	Company
Bafilomycin A1	tlrl-baf1	InvivoGen, Toulouse, France
Calpain inhibitor III	MDL-28170	Sigma-Aldrich, St. Louis, MO, US
Caspase inhibitor Q-VD-OPh	SML0063	Sigma-Aldrich
Importazole/IPZ	SML0341	Sigma-Aldrich
Ionomycin	I0634	Sigma-Aldrich
Lactacystin	BML-PI104-0200	Enzo Lifescience, Lausen, Switzerland

Table 2.14 Software

Software	Provider/Company
AxioVision version 4.8 imaging software	Carl Zeiss Microscopy, Jena, Germany
Coreldraw X5	Corel Corporation, Ottawa, Ontario, Canada
GenomeLab Software GeXP software	Beckman Coulter, CA, USA
GraphPad Prism 6.00 software	GraphPad Software Inc., La Jolla, CA, US
Image Studio 4.0 software	LI-COR Biosciences, Bad Homburg, Germany
Ingenuity Pathway Analysis	Qiagen, Hilden, Germany
MaxQuant software suite version 1.6.7.0	Cox and Mann, 2008
Perseus software package version 1.6.2.3	Tyanova et al., 2016

3. Results

3.1 Wild-type and polyQ-expanded ataxin-3 interact with nuclear transport receptors

Ataxin-3 is primarily a cytoplasmic protein, even though polyQ-expanded ataxin-3 generates intranuclear aggregates in the neurons of SCA3 patients (Paulson et al., 1997b). The exact molecular mechanism implicated in the nuclear localization of polyQ-expanded ataxin-3 is not fully characterized; however, mounting evidence indicates that there is a direct link between the intracellular localization of ataxin-3 and its neurotoxicity (Bichelmeier et al., 2007; Tait et al., 1998). In the previous study in our group, it was shown that karyopherin α-3 (KPNA3), which is a nuclear transport receptor, has a leading role in the nucleocytoplasmic trafficking of ataxin-3, influencing its aggregation, toxicity, and the pathogenic development of SCA3 (Sowa et al., 2018). Given that KPNA3 is an adaptor protein for karyopherin β-1 (KPNB1) to execute its transport function in the cells (Cautain et al., 2015), we sought to study the impact of KPNB1 modulation on ataxin-3.

In the first step, we investigated whether ataxin-3 interacts directly with KPNB1 as well as karyopherin α-2 (KPNA2) and KPNA3, therefor, the glutathione S-transferase (GST) pull-down assay was performed. Accordingly, GST-tagged wild-type (15Q) and polyQ-expanded (77Q) ataxin-3 were overexpressed in *E. coli* and immobilized on glutathione beads. In the next step, glutathione beads were incubated with wild-type HEK 293T cell lysates, which endogenously express all three karyopherins. Western blot analysis of the GST pull-down defined that endogenous KPNB1, along with KPNA2 and KPNA3, were copurified with both 15Q and 77Q ataxin-3 (Figure 3.1), representing an important indication of a direct functional interaction between ataxin-3 and nuclear transport receptors.

Altogether, the GST pull-down assay demonstrated a direct interaction between both wild-type and polyQ-expanded ataxin-3 with three different karyopherins, KPNB1, KPNA2, and KPNA3. These findings provide evidence for the concept that nuclear transport of ataxin-3 is likely mediated by importin α and importin β.

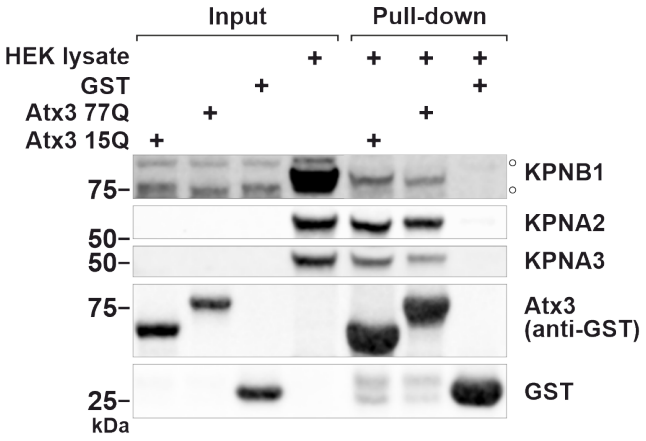

Figure 3.1 Wild-type and polyQ-expanded ataxin-3 interact with KPNB1, KPNA2, and KPNA3. The interaction of wild-type (15Q) and polyQ-expanded (77Q) ataxin-3 with KPNB1 and its partners KPNA2 and KPNA3 was validated by a GST pull-down assay. GST-tagged 15Q and 77Q ataxin-3 were overexpressed in *E. coli* and purified using glutathione beads, followed by incubation with wild-type HEK 293T cell protein extract overnight. Input as well as pull-down samples were subjected to western blot analysis, and blots were probed for KPNB1, KPNA2, KPNA3, and GST. Empty GST was utilized as a negative control. White bullets (o) indicate nonspecific bands. Modified from Abeditashi et al., 2022.

3.2 KPNB1 modulation does not alter the subcellular localization of wild-type and polyQ-expanded ataxin-3

Nucleocytoplasmic transport is a highly regulated process that controls the trafficking of various cargos between the nucleus and the cytoplasmic compartments. Appropriate nucleocytoplasmic transport is essential to maintain the cell homeostasis (Fallini et al., 2020). Regulation of nucleocytoplasmic transport involves the mechanisms that modulate the interaction of the nuclear transport receptors with their cargos. Disruption of this regulation can cause detrimental effects on the cells (McLane and Corbett, 2009).

The precise mechanisms implicated in the nuclear transport of ataxin-3 are not well understood. As karyopherins are known to transport cargos across the nuclear membrane and we were able to confirm the interaction of ataxin-3 with KPNB1, we decided to explore the effect of KPNB1 overexpression and knockdown on subcellular localization of ataxin-3.

To fulfill this purpose, we transfected *ATXN3* KO HEK 293T cells with either wild-type (15Q) or polyQ-expanded (148Q) ataxin-3 together with KPNB1 or empty vectors as control for 72 h. *ATXN3* KO HEK 293T cells were applied for most experiments to avoid the interference of endogenous ataxin-3. The intracellular localization of ataxin-3 was analyzed by a nucleocytoplasmic fractionation assay measuring the amount of protein located in the

nucleus and cytoplasmic compartments. Nucleocytoplasmic fractionation was performed using the Rapid, Efficient And Practical (REAP) method (Suzuki et al., 2010), which is a fast and non-ionic detergent-based purification technique and prevents protein degradation. The nuclear and cytoplasmic fractions were subjected to western blot analysis. Given that KPNB1 is an importin, we expected to detect an increase in the nuclear fraction of ataxin-3. To our surprise, quantification of the cytoplasmic and nuclear levels of 15Q and 148Q ataxin-3 relative to the total amount of ataxin-3 as well as the ratio of the nuclear and cytoplasmic ataxin-3 indicated that overexpression of KPNB1 does not induce any significant alteration in the intracellular localization of 15Q and 148Q ataxin-3. However, KPNB1 overexpression led to an apparent reduction of both nuclear and cytoplasmic levels of 15Q and 148Q ataxin-3 as observed in the western blot analysis of the nucleocytoplasmic fractionation assay (Figure 3.2). Furthermore, the detection of ataxin-3 using the 1H9 and C-terminal antibodies revealed the generation of specific ataxin-3 fragments upon KPNB1 overexpression, which was best visible in the cytoplasmic fraction of the transfected cells (Figure 3.2).

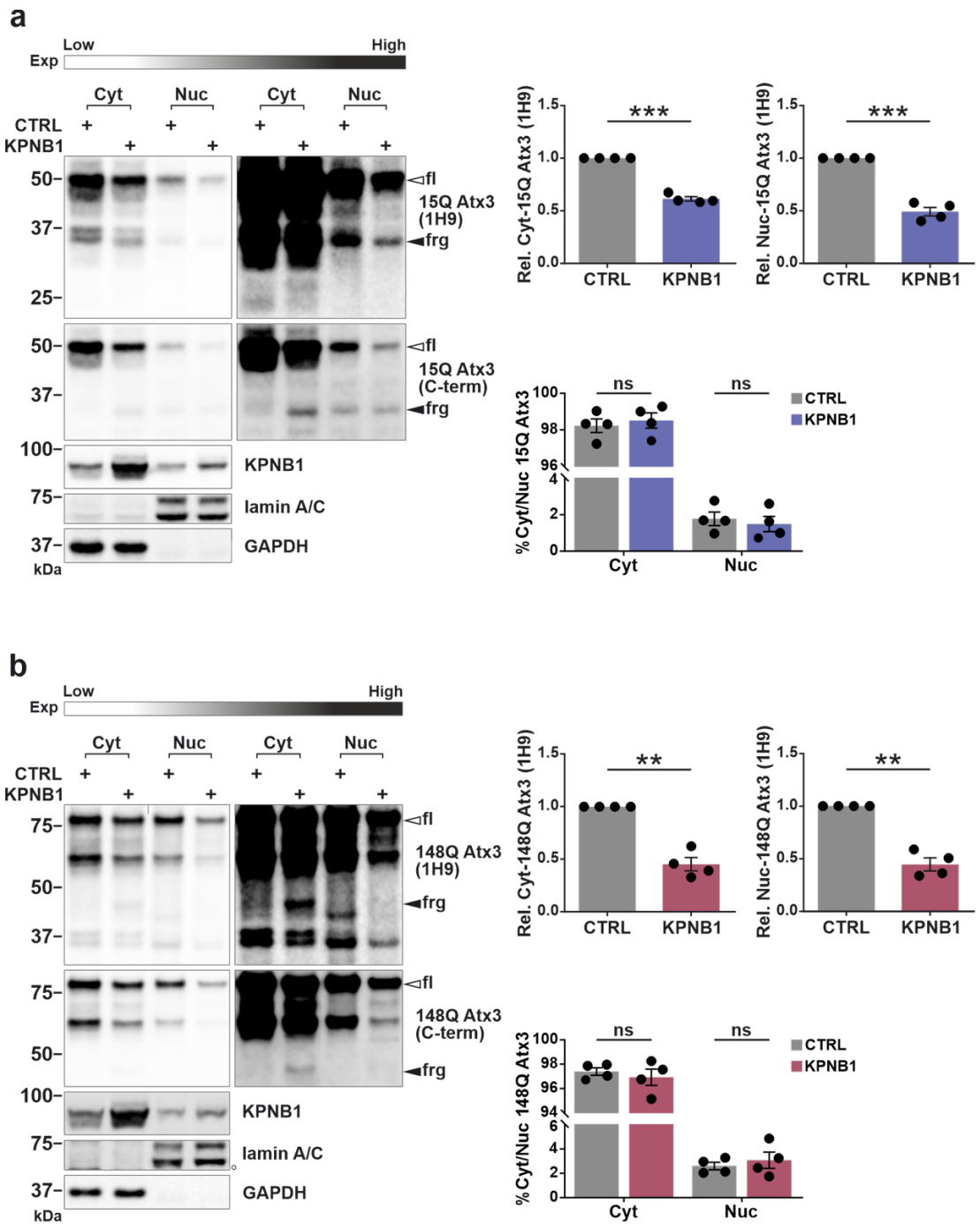

Figure 3.2 KPNB1 overexpression does not modulate the subcellular localization of neither wild-type nor polyQ-expanded ataxin-3. (**a**, **b**) The nucleocytoplasmic fractionation assay displays a significant decrease in cytoplasmic and nuclear wild-type (15Q) and polyQ-expanded (148Q) ataxin-3 upon KPNB1 overexpression (white arrowheads), whereas no alteration was observed in the subcellular localization of ataxin-3 in comparison to control. Additionally, it shows the accumulation of mainly cytoplasmic ataxin-3 fragments (black arrowheads) in KPNB1-overexpressing cells. *ATXN3* KO HEK 293T cells were cotransfected with either 15Q or 148Q ataxin-3 and KPNB1 or empty vectors as a control. 72 h post-transfection, transfected cells were harvested, and a nucleocytoplasmic fractionation assay was carried out according to the REAP method and proceeded to western blot analysis. Blots are shown in low and high exposures. The white bullet (o) marks nonspecific bands.

Ataxin-3 was detected using the 1H9 and C-terminal antibodies. Western blot analysis confirmed the overexpression of KPNB1 in transfected cells. The diagrams illustrate the relative cytoplasmic and nuclear levels of 15Q and 148Q ataxin-3, as well as the ratio of nuclear and cytoplasmic ataxin-3 as a percentage. GAPDH and lamin A/C were applied as cytoplasmic and nuclear loading controls, respectively. a, $n = 4$, Cyt-15Q, one sample *t*-test, $p = 0.0003$; Nuc-15Q, one sample *t*-test, $p = 0.0012$; Cyt/Nuc, unpaired *t*-test, $p = 0.6261$; b, $n = 4$, Cyt-148Q, one sample *t*-test, $p = 0.0033$; Nuc-148Q, one sample *t*-test, $p = 0.0027$; Cyt/Nuc, unpaired *t*-test, $p = 0.5443$. CTRL = empty vector; Cyt = cytoplasmic fraction; Nuc = nuclear fraction; fl = full-length; frg = fragment; C-term = C-terminal; Exp = exposure; Rel. = relative. Values are displayed as means ± SEM. ns = not significant; $*p \leq 0.05$; $**p \leq 0.01$; $***p \leq 0.001$. Modified from Abeditashi et al., 2022.

To further confirm our findings, we investigated the effect of KPNB1 overexpression on the subcellular localization of wild-type and polyQ-expanded ataxin-3 using fluorescence microscopy. ATXN3 KO HEK293T cells were cotransfected with either EGFP-ataxin-3 15Q or EGFP-ataxin-3 148Q together with KPNB1 or empty vectors as a respective control. The intracellular distribution of EGFP-ataxin-3 15Q or EGFP-ataxin-3 148Q was visualized with a fluorescence microscope. Figure 3.3 shows representative pictures of cells displaying both the cytoplasmic and nuclear distribution of ataxin-3. Consistent with the result of nucleocytoplasmic fractionation assay, manual quantification of the percentage of GFP-positive cells with predominantly nuclear ataxin-3 indicated that KPNB1 overexpression does not modulate the subcellular localization of neither 15Q nor 148Q ataxin-3 compared with control (Figure 3.3).

Since we observed a potential influence of KPNB1 overexpression on protein levels of both wild-type (15Q) and polyQ-expanded (148Q) ataxin-3 rather than their subcellular localization, we further assessed the effect of KPNB1 knockdown on localization of ataxin-3. In this respect, *ATXN3* KO HEK 293T cells were cotransfected with either 15Q or 148Q ataxin-3 and endoribonuclease-prepared siRNA (esiRNA) targeting KPNB1 or *Renilla* luciferase (esiLUC) as a respective control for 72 h. A nucleocytoplasmic fractionation assay was performed using the REAP method, followed by western blot analysis. Detection of membranes using an antibody specific for KPNB1 confirmed the knockdown of this protein in transfected cells (Figure 3.4). Western blot analysis of the nucleocytoplasmic fractionation assay demonstrated that KPNB1 knockdown using esiRNA did not modulate the localization of neither 15Q nor 148Q ataxin-3, although in contrast to KPNB1 overexpression, a significant increase in the levels of both nuclear and cytoplasmic ataxin-3 was detected in these cells compared to control (Figure 3.4).

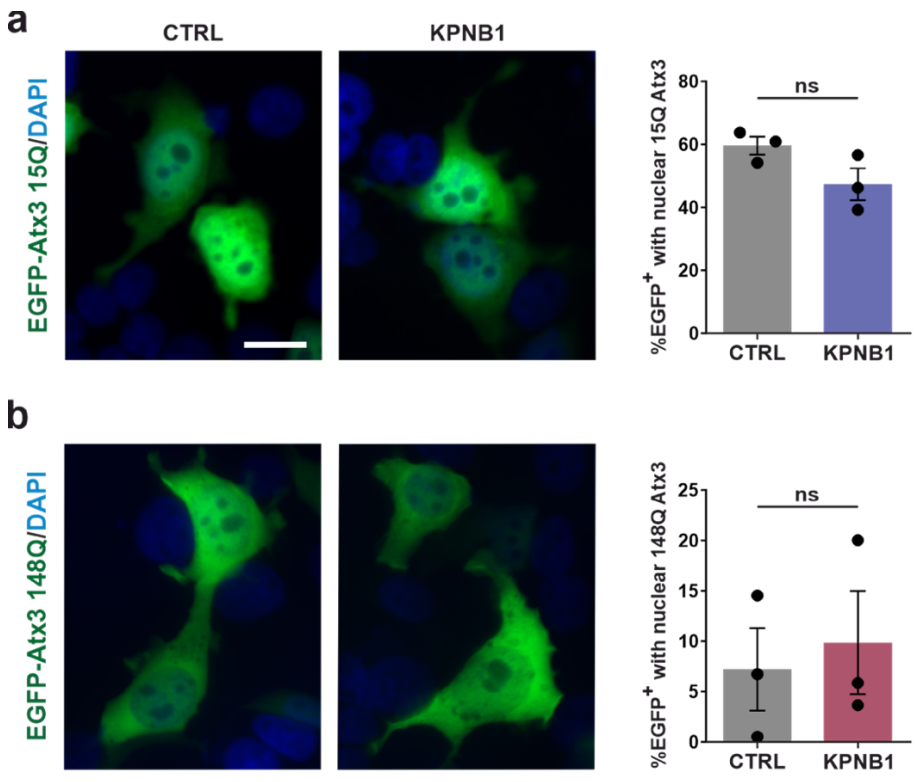

Figure 3.3 Overexpression of KPNB1 does not affect the intracellular distribution of EGFP-ataxin-3. (**a**, **b**) Fluorescence microscopy was performed to visualize the subcellular localization of wild-type and polyQ-expanded ataxin-3 upon KPNB1 overexpression. *ATXN3* KO HEK293T cells were cotransfected with either EGFP-ataxin-3 15Q or EGFP-ataxin-3 148Q together with KPNB1 and empty vectors (control). 72 h post-transfection, cells were fixed and mounted using a medium containing DAPI. The number of GFP-positive ($EGFP^+$) cells and cells with mainly nuclear localization of EGFP-ataxin-3 was counted manually in 20 fields of vision. The result displayed that the intracellular localization of neither wild-type (15Q) nor polyQ-expanded (148Q) ataxin-3 was altered upon KPNB1 overexpression compared with control. Blue and green channels show DAPI as a nuclear counterstain and GFP signals, respectively. 400 × magnification, scale bar = 20 µm. The diagrams show the percentage of GFP-positive ($EGFP^+$) cells with nuclear localization of ataxin-3. a, $n = 3$, unpaired t-test, $p = 0.1023$; b, $n = 3$, unpaired t-test, $p = 0.7075$. CTRL = empty vector. Values are displayed as means ± SEM. ns = not significant. Modified from Abeditashi et al., 2022.

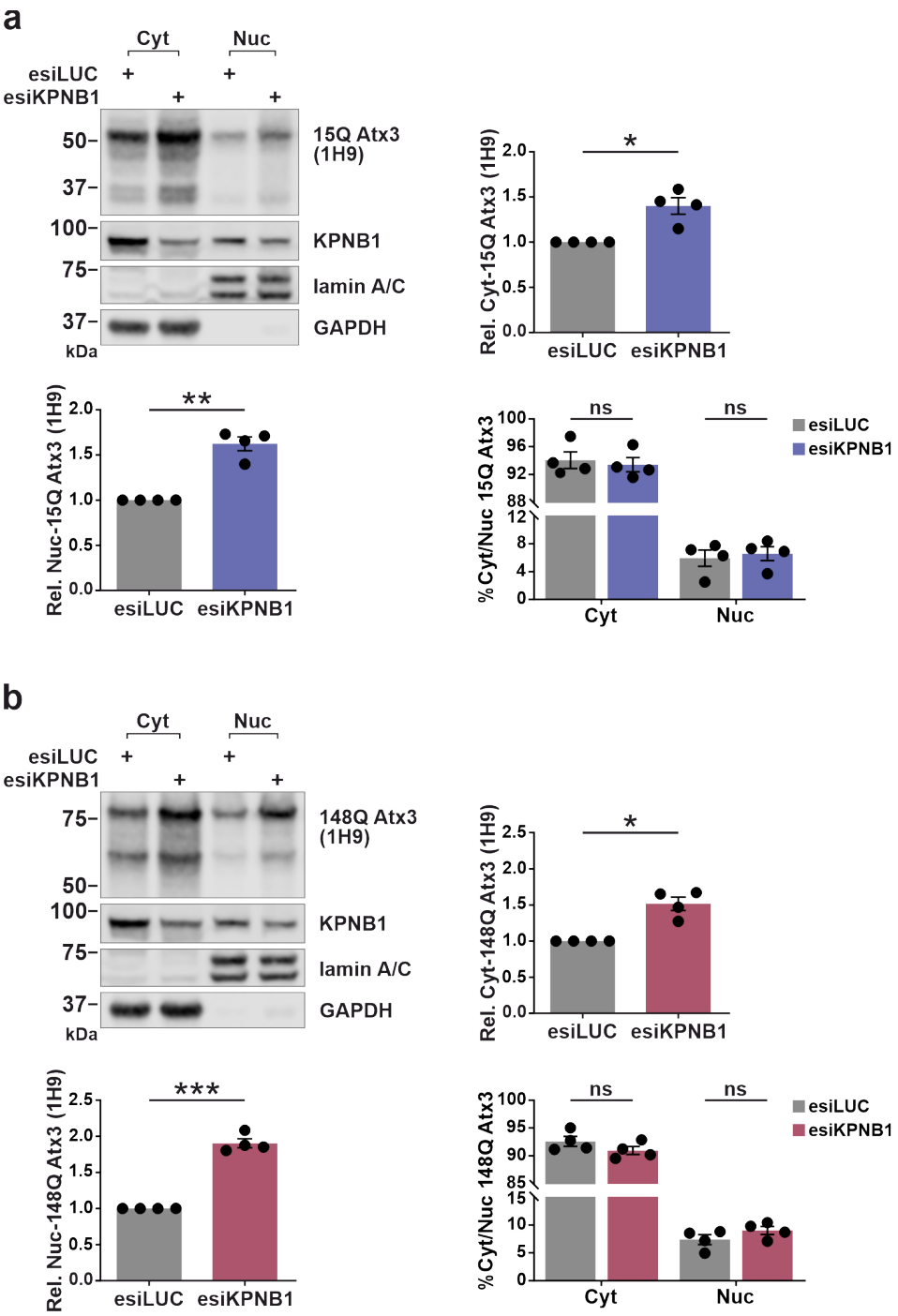

Figure 3.4 KPNB1 knockdown does not impact the intracellular localization of wild-type and polyQ-expanded ataxin-3. (**a**, **b**) The nucleocytoplasmic fractionation assay indicates an increase in cytoplasmic and nuclear levels of both wild-type (15Q) and polyQ-expanded (148Q) ataxin-3 upon KPNB1 knockdown compared to the control. However, no alteration was observed in the subcellular localization of ataxin-3. *ATXN3* KO HEK 293T cells were cotransfected with either 15Q or 148Q ataxin-3 and esiKPNB1 or esiLUC as a control. 72 h post-transfection, transfected cells were harvested, and a nucleocytoplasmic fractionation assay was performed, followed by western blot analysis. The diagrams illustrate the relative cytoplasmic and nuclear levels of 15Q and 148Q ataxin-3, as well as the ratio of nuclear and cytoplasmic ataxin-3 as a percentage. Ataxin-3 was detected using the 1H9 antibody. Western blot analysis confirmed the knockdown of KPNB1 in transfected cells. GAPDH and

lamin A/C were applied as cytoplasmic and nuclear loading controls, respectively. a, $n = 4$, Cyt-15Q, one sample *t*-test, $p = 0.0220$; Nuc-15Q, one sample *t*-test, $p = 0.0039$; Cyt/Nuc 15Q, unpaired *t*-test, $p = 0.6901$; b, $n = 4$, Cyt-148Q, one sample *t*-test, $p = 0.0116$; Nuc-148Q, one sample *t*-test, $p = 0.0007$; Cyt/Nuc, unpaired *t*-test, $p = 0.2029$. Cyt = cytoplasmic fraction; Nuc = nuclear fraction; Rel. = relative. Values are displayed as means ± SEM. ns = not significant; $*p \leq 0.05$; $**p \leq 0.01$; $***p \leq 0.001$. Modified from Abeditashi et al., 2022.

In summary, neither overexpression nor knockdown of KPNB1 alters the subcellular localization of ataxin-3, as analyzed by fluorescence microscopy and nucleocytoplasmic fractionation assay. However, these modulations can affect the protein levels of ataxin-3. Overall, these data suggest that modulation of KPNB1 protein levels has the potential to affect both wild-type and polyQ-expanded ataxin-3 protein levels through a mechanism that does not appear to implicate the localization of this protein.

3.3 KPNB1 overexpression decreases wild-type and polyQ-expanded ataxin-3 protein levels and enhances its cleavage

After observing the potential effects of KPNB1 overexpression on wild-type and polyQ-expanded ataxin-3 protein levels in the nucleocytoplasmic fractionation assays, we sought to investigate in detail whether increasing the levels of KPNB1 has any robust effect on ataxin-3 protein levels. Indeed, induction of protein clearance and thereby reducing the soluble levels of ataxin-3 has been considered as a potential therapeutic target for SCA3 and other polyQ diseases (Nascimento-Ferreira et al., 2011). Notably, many common mechanisms that play important roles in the pathogenesis of polyQ diseases are apparently consequences of the soluble polyQ-expanded proteins rather than aggregates.

In this connection, *ATXN3* KO HEK 293T cells were cotransfected with either wild-type (15Q) or polyQ-expanded (148Q) ataxin-3 together with KPNB1 or empty vectors as a control for 72 h. Cells were lysed and subjected to western blot analysis. The result revealed that overexpression of KPNB1 resulted in a significant reduction in protein levels of both wild-type and polyQ-expanded ataxin-3, which verified the result of nucleocytoplasmic fractionation (Figure 3.5). In addition to decreased protein levels of ataxin-3, we confirmed enhanced fragmentation of ataxin-3 upon KPNB1 overexpression. Notably, the fragmentation of wild-type ataxin-3 was more prominent than polyQ-expanded ataxin-3. By using two different antibodies (1H9 and C-terminal), recognizing different epitopes, we concluded that ataxin-3 fragments induced by KPNB1 overexpression are C-terminal and contain the polyQ tract

(Figure 3.5). Proteolytically derived breakdown products of ataxin-3 were reported both in the brains of SCA3 patients and SCA3 mouse models (Goti et al., 2004). Proteolytic cleavage of polyQ-expanded proteins mediated by proteolytic pathways and proteases has been suggested as an important mechanism in the molecular pathogenesis of polyQ diseases, leading to the generation of fragments that are able to promote nuclear accumulation and toxicity (Berke et al., 2004; Havel et al., 2009; Weber et al., 2017; Weber et al., 2014).

For better understanding of the modulation of ataxin-3 protein levels and fragmentation by KPNB1 overexpression, and to figure out whether this effect is time-dependent, *ATXN3* KO HEK 293T cells were cotransfected with either 15Q or 148Q ataxin-3 together with KPNB1 or empty vectors as control in different time intervals (24, 48, and 72 h). Western blot analysis presented that the accumulation of ataxin-3 fragments as well as the reduction of full-length ataxin-3 levels upon KPNB1 overexpression were time-dependent. The strongest effect both on ataxin-3 fragments and protein levels was observed after 72 h of KPNB1 overexpression compared with 24 h and 48 h overexpression (Figure 3.6).

The above findings highlight that KPNB1 overexpression lowers protein levels of both wild-type and polyQ-expanded ataxin-3 and enhances its fragmentation, suggesting the effect is not polyglutamine-specific. Additionally, it was revealed that the enhancement of ataxin-3 cleavage as well as the reduction of its soluble levels upon KPNB1 overexpression were time-dependent. These alterations present KPNB1 as a putative modulator of ataxin-3 protein levels and fragmentation.

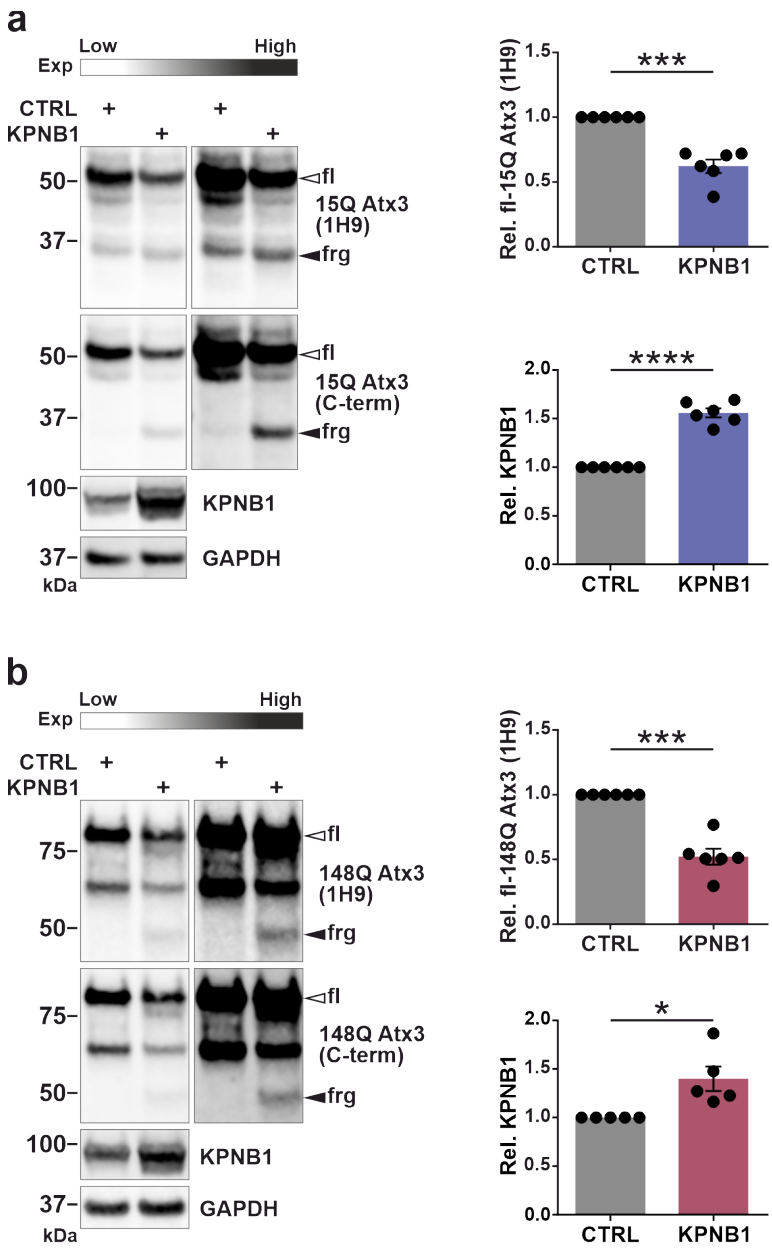

Figure 3.5 KPNB1 overexpression lowers protein levels of wild-type and polyQ-expanded ataxin-3 and promotes its fragmentation. (**a**, **b**) Western blot analysis of *ATXN3* KO HEK 293T cells cotransfected with either wild-type (15Q) or polyQ-expanded (148Q) ataxin-3 and KPNB1 or empty vectors as a control for 72 h. The result indicates that KPNB1 overexpression decreases the soluble levels of both 15Q and 148Q ataxin-3 (white arrowheads) and enhances fragmentation of ataxin-3 (black arrowheads) compared with control. Detection of ataxin-3 using two different antibodies (1H9 and C-terminal), which recognize different epitopes, reveals that ataxin-3 fragments are C-terminal breakdown products. Western blot analysis confirmed the overexpression of KPNB1. Blots are shown in low and high exposures. GAPDH was applied as a loading control. a, 15Q Atx3, $n = 6$, one sample *t*-test, $p = 0.0008$; KPNB1, $n = 6$, one sample *t*-test, $p < 0.0001$; b, $n = 6$, one sample *t*-test, $p = 0.0006$; KPNB1, $n = 5$, one sample *t*-test, $p = 0.0349$. CTRL = empty vector; fl = full-length; frg = fragment; C-term = C-terminal; Exp = exposure; Rel. = relative. Values are displayed as means ± SEM. ns = not significant; *$p \leq 0.05$; **$p \leq 0.01$; ***$p \leq 0.001$; ****$p \leq 0.0001$. Modified from Abeditashi et al., 2022.

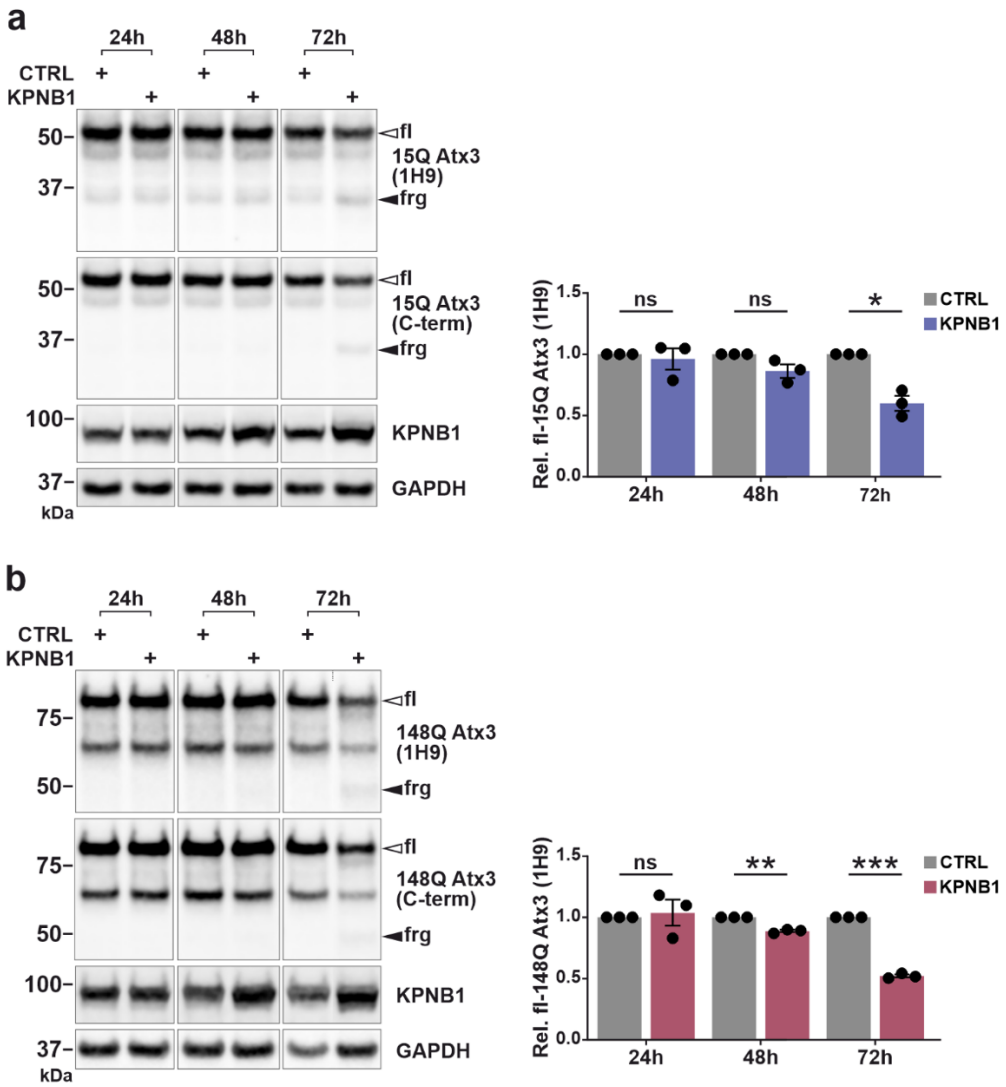

Figure 3.6 The reduction of ataxin-3 protein levels upon KPNB1 overexpression is time-dependent. (**a**, **b**) Western blot analysis of *ATXN3* KO HEK 293T cells transiently expressing either wild-type (15Q) or polyQ-expanded (148Q) ataxin-3. The cells were transfected with either KPNB1 or empty vectors (control) in different time intervals (24, 48, and 72 h). The cells were lysed using RIPA buffer and subjected to western blot analysis. The results reveal that the reduction of both 15Q and 148Q ataxin-3 protein levels is promoted by increasing the time of KPNB1 overexpression, and it is more obvious after 72 h of KPNB1 overexpression. Furthermore, the accumulation of ataxin-3 fragments is boosted after 72 h of KPNB1 overexpression compared with 24 h and 48 h of overexpression. White and black arrowheads indicate ataxin-3 full-length and fragments, respectively. Ataxin-3 was detected using the 1H9 and C-terminal antibodies. GAPDH was used as a loading control. a, $n = 3$, one sample *t*-test, CTRL *vs* KPNB1 (24 h), $p = 0.7083$; CTRL *vs* KPNB1 (48 h), $p = 0.1225$; CTRL *vs* KPNB1 (72 h), $p = 0.0229$; b, $n = 3$, one sample *t*-test, CTRL *vs* KPNB1 (24 h), $p = 0.7608$; CTRL *vs* KPNB1 (48 h), $p = 0.0065$; CTRL *vs* KPNB1 (72 h), $p = 0.0005$. CTRL = empty vector; fl = full-length; frg = fragment; C-term = C-terminal; Rel. = relative. Values are displayed as means ± SEM. ns = not significant; *$p \leq 0.05$; **$p \leq 0.01$; ***$p \leq 0.001$. Modified from Abeditashi et al., 2022.

3.4 KPNB1 overexpression reduces protein levels of endogenous ataxin-3, and its effect is specific

After confirming the reduction of overexpressed (15Q and 148Q) ataxin-3 protein levels in KPNB1-overexpressing cells, we were encouraged to investigate whether KPNB1 overexpression affects the protein levels of endogenous ataxin-3. For this purpose, wild-type HEK 293T cells were transfected with either KPNB1 or empty vectors as a respective control for 72 h because our previous experiments revealed that the effect of KPNB1 overexpression on ataxin-3 is time-dependent, and the strongest effect was observed after 72 h of KPNB1 overexpression. Cells were lysed, and cell lysates were subjected to western blot analysis. Our result displayed a significant decrease in the protein levels of endogenous ataxin-3 upon KPNB1 overexpression in comparison to cells transfected with empty vectors (Figure 3.7a). This is in line with our data showing that KPNB1 overexpression reduces protein levels of overexpressed ataxin-3.

Moreover, to determine if the impact of KPNB1 on ataxin-3 protein levels is substrate-specific, we analyzed the effect of KPNB1 overexpression on a control protein, such as GFP. Accordingly, wild-type HEK 293T cells were transfected with either GFP or empty vectors as a control for 72 h. In contrast to ataxin-3 protein levels, western blot analysis showed no alteration in the protein levels of GFP compared with the control (Figure 3.7b). The above results highlight that ataxin-3 protein levels are generally, yet specifically, decreased by KPNB1 overexpression.

In conclusion, beside its effect on overexpressed ataxin-3, KPNB1 overexpression decreases the protein levels of endogenous ataxin-3 as well. This effect is specific, as overexpression of KPNB1 in GFP-overexpressing cells does not modulate the protein levels of this control protein.

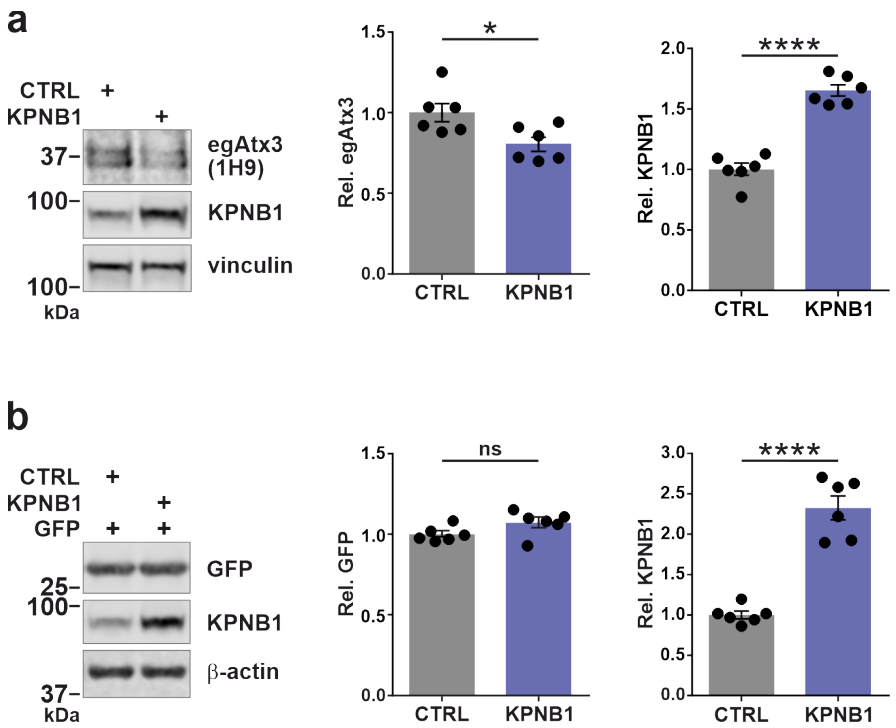

Figure 3.7 KPNB1 overexpression decreases endogenous ataxin-3 levels, whereas it does not affect GFP protein levels. (**a**) KPNB1 overexpression is accompanied by a reduction in the protein levels of endogenous ataxin-3. Wild-type HEK 293T cells were transfected with either KPNB1 or empty vectors (control) and harvested 72 h post-transfection. Cell lysates were subjected to western blot analysis and probed for ataxin-3 using the 1H9 antibody. Western blot analysis confirmed the overexpression of KPNB1. Vinculin was applied as a loading control. egAtx3, $n = 6$, unpaired t-test, $p = 0.0221$; KPNB1, $n = 6$, unpaired t-test, $p < 0.0001$. (**b**) Western blot analysis demonstrates that protein levels of GFP do not change upon KPNB1 overexpression compared with control. Wild-type HEK 293T cells were cotransfected with GFP and either KPNB1 or empty vectors as a control for 72 h. Cells were lysed using RIPA buffer and subjected to western blot analysis. β-actin was applied as a loading control. GFP, $n = 6$, unpaired t-test, $p = 0.0756$; KPNB1, $n = 6$, unpaired t-test, $p < 0.0001$. CTRL = empty vector; egAtx3 = endogenous ataxin-3; Rel. = relative. Values are displayed as means ± SEM. ns = not significant; *$p \leq 0.05$; **$p \leq 0.01$; ***$p \leq 0.001$; ****$p \leq 0.0001$. Modified from Abeditashi et al., 2022.

3.5 Cloning of KPNB1 I178D

Transport of protein cargos between the cytoplasm and nucleus, mediated by nuclear transport receptors, takes place along the central axis of the nuclear pore complexes (NPCs) and involves the interaction of karyopherin β with nucleoporins containing repeats rich in phenylalanine (FxFG). Indeed, these core motifs serve as docking sites for transport receptors and facilitate the shuttling of cargos through NPCs (Balasundaram et al., 1999; Damelin and Silver, 2000). Karyopherin β consists of 19 tandem “HEAT” repeats (Cingolani et al., 1999). Nucleoporin FxFG cores bind to a primary site between the A helices of HEAT repeats 5 and

6, and to a secondary site between HEAT repeats 6 and 7 (Figure 3.8) (Bayliss et al., 2000). Previous investigation has shown that mutation of isoleucine 178 (I178) of karyopherin β, a key component of the primary FxFG binding site of this protein, to aspartic acid (D), which is less hydrophobic, hampers the binding of karyopherin β to nucleoporins and disrupts its nuclear protein import function remarkably. However, this mutation does not introduce a major conformational change in karyopherin β (Bayliss et al., 2000).

```
         10          20          30          40          50          60
MELITILEKT VSPDRLELEA AQKFLERAAV ENLPTFLVEL SRVLANPGNS QVARVAAGLQ
         70          80          90         100         110         120
IKNSLTSKDP DIKAQYQQRW LAIDANARRE VKNYVLQTLG TETYRPSSAS QCVAGIACAE
        130         140         150.        160         170         180
IPVNQWPELI PQLVANVTNP NSTEHMKEST LEAIGYICQD IDPEQLQDKS NEILTAIIQG
        190         200.        210         220         230         240
MRKEEPSNNV KLAATNALLN SLEFTKANFD KESERHFIMQ VVCEATQCPD TRVRVAALQN
        250.        260         270         280         290         300
LVKIMSLYYQ YMETYMGPAL FAITIEAMKS DIDEVALQGI EFWSNVCDEE MDLAIEASEA
        310         320         330         340         350.        360
AEQGRPPEHT SKFYAKGALQ YLVPILTQTL TKQDENDDDD DWNPCKAAGV CLMLLATCCE
        370         380         390         400.        410         420
DDIVPHVLPF IKEHIKNPDW RYRDAAVMAF GCILEGPEPS QLKPLVIQAM PTLIELMKDP
        430         440         450.        460         470         480
SVVVRDTAAW TVGRICELLP EAAINDVYLA PLLQCLIEGL SAEPRVASNV CWAFSSLAEA
        490         500.        510         520         530         540
AYEAADVADD QEEPATYCLS SSFELIVQKL LETTDRPDGH QNNLRSSAYE SLMEIVKNSA
        550         560         570         580         590         600
KDCYPAVQKT TLVIMERLQQ VLQMESHIQS TSDRIQFNDL QSLLCATLQN VLRKVQHQDA
        610         620         630         640         650.        660
LQISDVVMAS LLRMFQSTAG SGGVQEDALM AVSTLVEVLG GEFLKYMEAF KPFLGIGLKN
        670         680         690         700         710         720
YAEYQVCLAA VGLVGDLCRA LQSNIIPFCD EVMQLLLENL GNENVHRSVK PQILSVFGDI
        730         740         750         760         770         780
ALAIGGEFKK YLEVVLNTLQ QASQAQVDKS DYDMVDYLNE LRESCLEAYT GIVQGLKGDQ
        790         800.        810         820         830         840
ENVHPDVMLV QPRVEFILSF IDHIAGDEDH TDGVVACAAG LIGDLCTAFG KDVLKLVEAR
        850.        860         870
PMIHELLTEG RRSKTNKAKT LATWATKELR KLKNQA
```

Figure 3.8 The amino acid sequence of KPNB1. The isoform 1 of KPNB1 (UniProt ID: Q14974-1) has 876 amino acids. The HEAT repeats 5 and 6, which construct the primary FxFG binding site of KPNB1, are marked with yellow and gray boxes, respectively. Mutation of isoleucine 178 (I178) of KPNB1, which is marked in red, can disrupt its nuclear transport function (Bayliss et al., 2000).

To introduce the target mutation (AAT to AGA) into the pCMV6-XL5 plasmid containing full-length human KPNB1, site-directed mutagenesis was performed (Figure 3.9). In brief, the DNA construct was amplified using the primers, which contain the mutation and restriction sites of the SalI-HF and NheI enzymes. Both the PCR product and the original vector were digested using the SalI-HF and NheI restriction enzymes. The vector and insert were purified using the

preparative TAE agarose gels, followed by ligation. Subsequently, the competent bacteria were transformed by heat shock and were cultured on an agar plate. The next day, the plate was checked for colonies, and individual colonies were grown. Finally, the respective mutation was verified by Sanger sequencing.

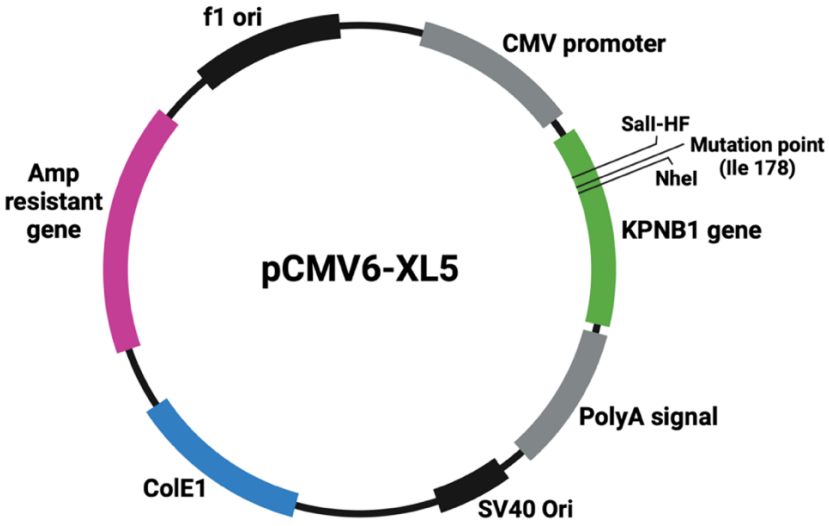

Figure 3.9 Schematic representation of the pCMV6-XL5 plasmid containing full-length human KPNB1. Mutation of isoleucine 178 (I178) of KPNB1 to aspartic acid (D) was carried out by site-directed mutagenesis. The pCMV6-XL5 plasmid containing full-length human KPNB1 was digested using SalI-HF and NheI restriction enzymes.

3.6 KPNB1 overexpression lowers wild-type and polyQ-expanded ataxin-3 protein levels independent of its nuclear transport function

As we observed a significant reduction in ataxin-3 protein levels upon KPNB1 overexpression, we postulated that this effect might be associated with the nuclear import function of KPNB1. Therefore, to allow disruption of the nuclear transport function of KPNB1, the mutation (AAT to AGA) was introduced on the FxFG binding site of KPNB1. To assess the influence of the KPNB1 mutation on ataxin-3 protein levels, KPNB1 I178D as well as wild-type KPNB1 were overexpressed in *ATXN3* KO HEK 293T cells transiently expressing either wild-type (15Q) or polyQ-expanded (148Q) ataxin-3 for 72 h. Cells cotransfected with empty vectors were considered as controls. The effect of KPNB1 I178D overexpression on full-length ataxin-3 protein levels was dissected by western blot analysis. Interestingly, no major difference was identified between the impact of KPNB1 I178D and wild-type KPNB1 on soluble levels of either

15Q or 148Q ataxin-3 (Figure 3.10). In fact, the overexpression of KPNB1 I178D was accompanied by a reduction in ataxin-3 protein levels as well as overexpression of wild-type KPNB1 (Figure 3.10).

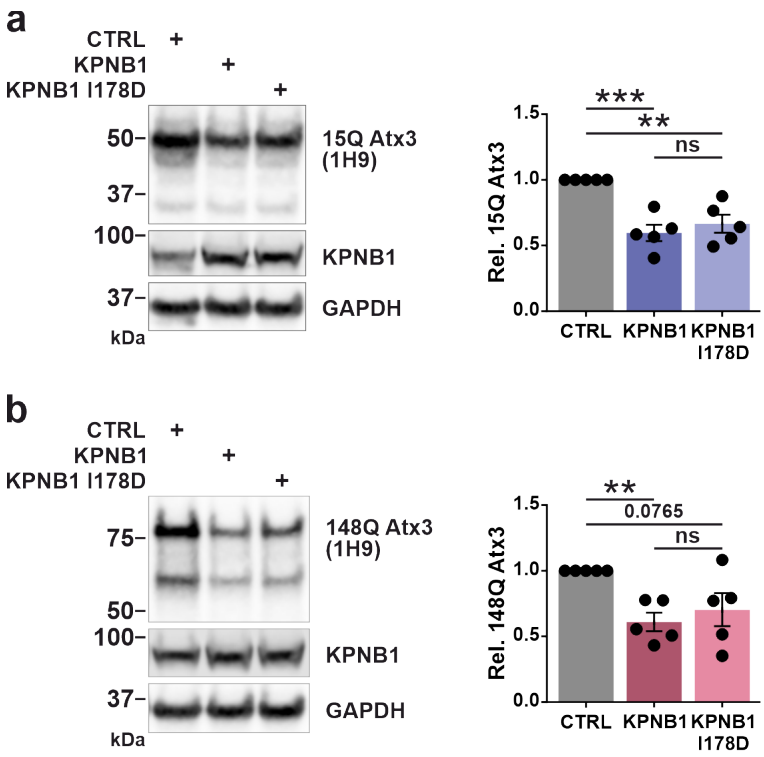

Figure 3.10 KPNB1 I178D overexpression decreases wild-type and polyQ-expanded ataxin-3 protein levels. (**a**, **b**) KPNB1 mutation (I178D) in the FxFG binding site does change the effect of KPNB1 overexpression on either wild-type (15Q) or polyQ-expanded (148Q) ataxin-3. *ATXN3* KO HEK 293T cells were cotransfected with either 15Q or 148Q ataxin-3 and wild-type KPNB1 or KPNB1 I178D constructs for 72 h. Cells cotransfected with empty vectors were considered a control. Western blot analysis displays that the ataxin-3-lowering effect of KPNB1 I178D is comparable to wild-type KPNB1, and it leads to a significant reduction of both 15Q and 148Q ataxin-3 protein levels. GAPDH was applied as a loading control. a, $n = 5$, one sample *t*-test, CTRL *vs* KPNB1, $p = 0.0030$; CTRL *vs* KPNB1 I178D, $p = 0.0086$; unpaired *t*-test, KPNB1 *vs* KPNB1 I178D, $p = 0.4784$; b, $n = 5$, one sample *t*-test, CTRL *vs* KPNB1, $p = 0.0052$; CTRL *vs* KPNB1 I178D, $p = 0.0765$; unpaired *t*-test, KPNB1 *vs* KPNB1 I178D, $p = 0.5367$. CTRL = empty vector; Rel. = relative. Values are displayed as means ± SEM. ns = not significant; *$p \leq 0.05$; **$p \leq 0.01$; ***$p \leq 0.001$. Modified from Abeditashi et al., 2022.

Our results provide evidence that mutation of the FxFG binding site of KPNB1 and disruption of its nuclear protein import function do not abolish its effect on ataxin-3 protein levels, implying that the observed ataxin-3 lowering effect of KPNB1 is a nuclear transport function-independent mechanism.

3.7 Knockdown or pharmacological inhibition of KPNB1 elevates protein levels of wild-type and polyQ-expanded ataxin-3

Given that KPNB1 overexpression resulted in the reduction of ataxin-3 protein levels, in the next step, we were motivated to explore if lowering KPNB1 levels has any consequences for wild-type and polyQ-expanded ataxin-3. In these conditions, *ATXN3* KO HEK 293T cells were transiently transfected with either wild-type (15Q) or polyQ-expanded (148Q) ataxin-3 together with endoribonuclease-prepared siRNA (esiRNA) targeting KPNB1 or *Renilla* luciferase (esiLUC) as a respective control for 72 h. Cells were lysed, and subjected to western blot analysis, and probed for ataxin-3 using the 1H9 antibody. Our results indicated that, in contrast to overexpression of KPNB1, knockdown of this protein resulted in a significant increase in the soluble levels of both full-length 15Q and 148Q ataxin-3 (Figure 3.11). These findings suggest that the effect of KPNB1 on ataxin-3 is not polyglutamine-specific. Moreover, transfection of cells with esiKPNB1 mitigated the protein levels of KPNB1 significantly compared with control (Figure 3.11).

To give validity to our findings, alteration of ataxin-3 protein levels was assessed upon pharmacological inhibition of KPNB1 using importazole. A high-throughput screening of small-molecule inhibitors revealed 2,4-diaminoquinazoline (importazole/IPZ) as a specific and reversible inhibitor of karyopherin β. Likely, this inhibition is via altering the interaction of karyopherin β with RanGTP; thus, this compound can be used to dissect the function and contribution of KPNB1/RanGTP in a variety of cellular mechanisms (Soderholm et al., 2011). In this experiment, *ATXN3* KO HEK 293T cells were transiently transfected with either wild-type (15Q) or polyQ-expanded (148Q) ataxin-3 for 72 h. 48 h prior to harvesting, transfected cells were treated using 16 µM IPZ or DMSO as a control. The modulation of ataxin-3 protein levels upon KPNB1 inhibition was assessed by western blot analysis. Our results displayed that the effect of KPNB1 knockdown could be recapitulated, and the protein levels of both 15Q and 148Q ataxin-3 increased significantly upon IPZ treatment in comparison to DMSO-treated cells (Figure 3.12a, b).

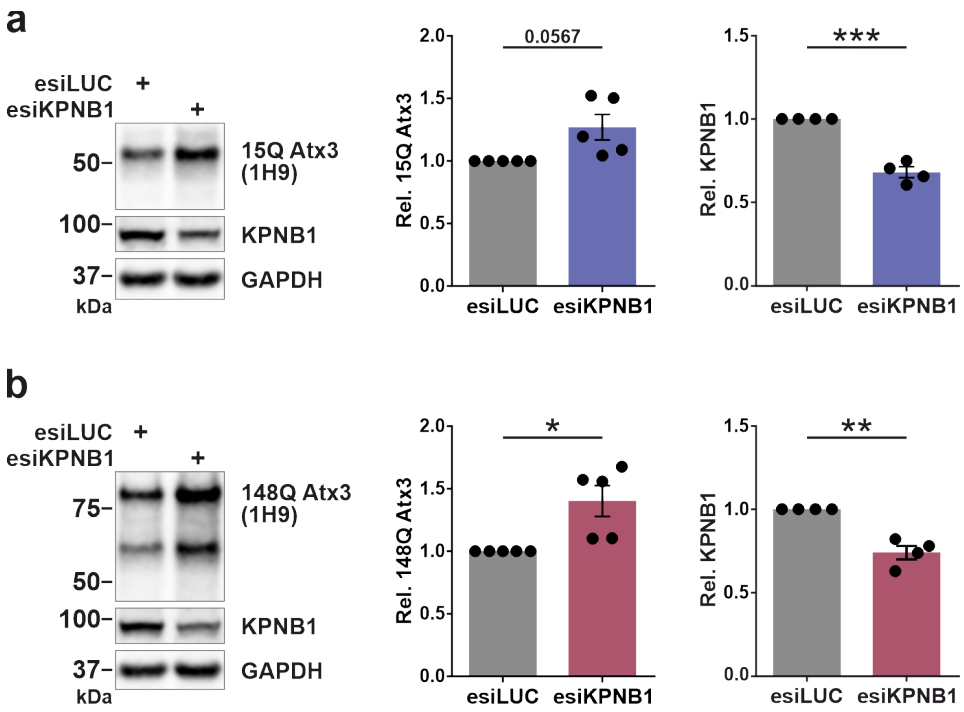

Figure 3.9 KPNB1 knockdown elevates soluble levels of wild-type and polyQ-expanded ataxin-3. (**a**, **b**) Western blot analysis reveals that knockdown of KPNB1 leads to an abundance of the soluble levels of both wild-type (15Q) and polyQ-expanded (148Q) ataxin-3 compared with control. *ATXN3* KO HEK 293T cells were cotransfected with either 15Q or 148Q ataxin-3 and esiKPNB1 or esiLUC as a control for 72 h. Transfected cells were lysed using RIPA buffer, subjected to western blot analysis, and probed for ataxin-3 using the 1H9 antibody. Western blot analysis confirmed the knockdown of KPNB1 in esiKPNB1-transfected cells. GAPDH was applied as a loading control. a, 15Q Atx3, $n = 5$, one sample *t*-test, $p = 0.0567$; KPNB1, $n = 4$, one sample *t*-test, $p = 0.0023$; b, 148Q Atx3, $n = 5$, one sample *t*-test, $p = 0.0315$; KPNB1, $n = 4$, one sample *t*-test, $p = 0.0083$. Rel. = relative. Values are displayed as means ± SEM. ns = not significant; *$p \leq 0.05$; **$p \leq 0.01$; ***$p \leq 0.001$. Modified from Abeditashi et al., 2022.

The effect of KPNB1 inhibition on the protein levels of overexpressed ataxin-3 prompted us to obtain evidence supporting the ability of this pharmacological inhibition to modulate the endogenous ataxin-3 levels. In this respect, we further investigated the effect of KPNB1 pharmacological inhibition on endogenous ataxin-3 protein levels. Wild-type HEK 293T cells were treated using 16 µM IPZ or DMSO as a control for 48 h. Western blot analysis demonstrated that inhibition of KPNB1 using IPZ is accompanied by an elevation in the protein levels of endogenous ataxin-3 compared with control (Figure 3.12c). These results indicated that KPNB1 inhibition could affect the protein levels of both overexpressed and endogenous ataxin-3.

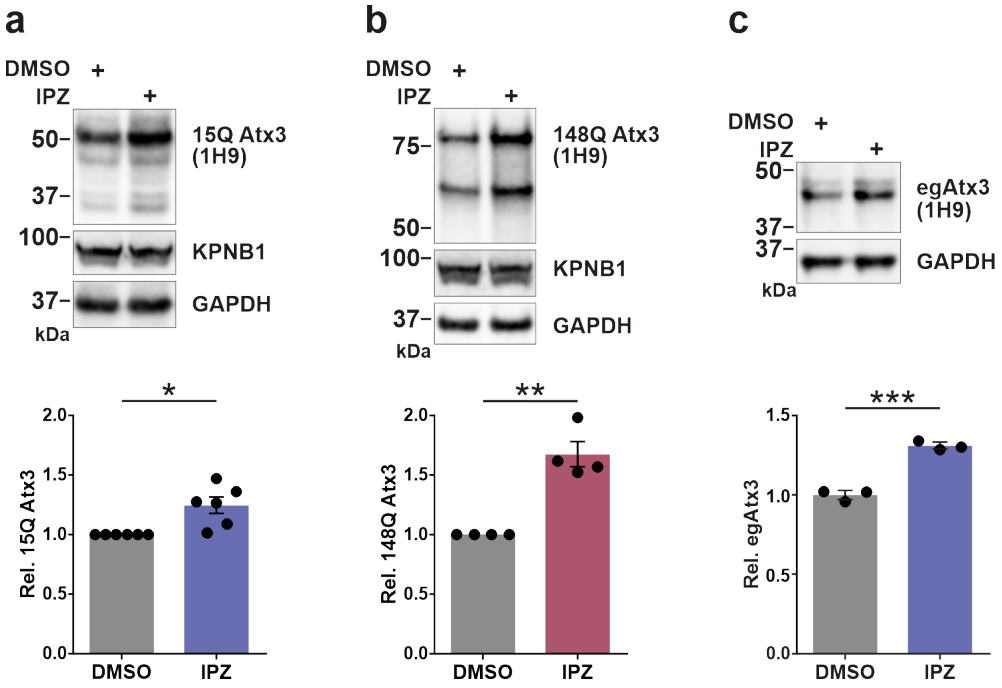

Figure 3.12 Pharmacological inhibition of KPNB1 increases wild-type and polyQ-expanded ataxin-3 protein levels. (**a**, **b**) Pharmacological inhibition of KPNB1 was performed using 16 µM importazole (IPZ) in either wild-type (15Q) or polyQ-expanded (148Q) ataxin-3 overexpressing cells. Quantification of blots indicates that the protein levels of both 15Q and 148Q ataxin-3 increase upon IPZ treatment in comparison to DMSO-treated cells (control). *ATXN3* KO HEK 293T cells were transfected with either 15Q or 148Q ataxin-3 constructs for 72 h. 48 h prior to harvesting, transfected cells were treated with either IPZ or DMSO as a control. Cell lysates were subjected to western blot analysis, and blots were detected using the 1H9 antibody. GAPDH was applied as a loading control. a, $n = 6$, one sample *t*-test, $p = 0.0162$; b, $n = 4$, one sample *t*-test, $p = 0.0077$. (**c**) Western blot analysis demonstrates that the amount of endogenous ataxin-3 enhances significantly upon IPZ treatment in comparison to DMSO-treated cells (control). Wild-type HEK 293T cells were treated using 16 µM IPZ or DMSO for 48 h. Cells were lysed using RIPA buffer and assessed by western blot analysis. The blots were detected using the 1H9 antibody. GAPDH was applied as a loading control. $n = 3$, unpaired *t*-test, $p = 0.0009$. IPZ = importazole; egAtx3 = endogenous ataxin-3; Rel. = relative. Values are displayed as means ± SEM. *$p \leq 0.05$; **$p \leq 0.01$; ***$p \leq 0.001$. Modified from Abeditashi et al., 2022.

Since we could observe a significant increase in protein levels of ataxin-3 in cells that KPNB1 was inhibited using IPZ, we expected to obtain evidence supporting the ability of this pharmacological inhibition to rescue ataxin-3 protein levels in KPNB1-overexpressing cells. In this connection and to enhance our understanding about the modulation of ataxin-3 protein levels by KPNB1, *ATXN3* KO HEK 293T cells were cotransfected with wild-type (15Q) ataxin-3 together with KPNB1 or empty vectors as a control for 72 h. 48 h prior to harvesting, transfected cells were treated using 16 µM IPZ or DMSO as a control. Interestingly, western

blot analysis indicated that the reduction of ataxin-3 protein levels upon KPNB1 overexpression was restored by IPZ administration in comparison to control (Figure 3.13).

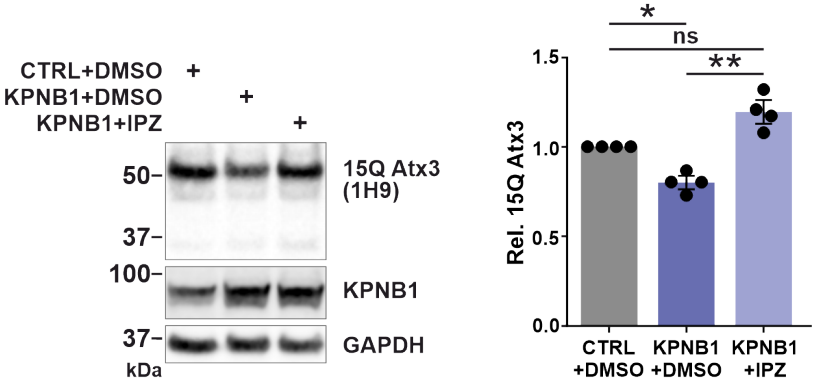

Figure 3.13 Reduction of ataxin-3 protein levels can be restored via IPZ treatment in KPNB1-overexpressing cells. Protein levels of wild-type (15Q) ataxin-3 are rescued by the administration of importazole (IPZ) in KPNB1-overexpressing cells. *ATXN3* KO HEK 293T cells were cotransfected with 15Q ataxin-3 and either KPNB1 or empty vectors (control). Transfected cells were incubated with 16 µM IPZ or DMSO as a control for 48 h prior to harvesting. Cells were lysed using RIPA buffer and assessed by western blot analysis. GAPDH was applied as a loading control. $n = 4$, one sample *t*-test, CTRL + DMSO *vs* KPNB1 + DMSO, $p = 0.0129$; CTRL + DMSO *vs* KPNB1 + IPZ, $p = 0.0615$; unpaired *t*-test, KPNB1 + DMSO *vs* KPNB1 + IPZ, $p = 0.0021$. CTRL = empty vector; IPZ = importazole; Rel. = relative. Values are displayed as means ± SEM. ns = not significant; $*p \leq 0.05$; $**p \leq 0.01$. Modified from Abeditashi et al., 2022.

Overall, in contrast to KPNB1 overexpression, either knockdown or pharmacological inhibition of KPNB1 using IPZ enhanced the soluble levels of both wild-type and polyQ-expanded ataxin-3, implying this effect is not polyglutamine-specific. In addition, the reduction of ataxin-3 protein levels in KPNB1-overexpressing cells can be rescued using importazole.

3.8 KPNB1 overexpression decreases the stability of wild-type and polyQ-expanded ataxin-3

Given that KPNB1 overexpression leads to the decrease of full-length levels of ataxin-3, we postulated that this effect might be associated with the alteration of ataxin-3 stability. Therefore, we applied the Tet-Off system (Gossen and Bujard, 1992) to abrogate the expression of wild-type (15Q) and polyQ-expanded (77Q) ataxin-3 by administering doxycycline in a time-dependent manner. The Tet-Off system allows differential control of the expression of genes of interest in mammalian cells as well as the creation of "on/off" situations for these genes in a reversible way (Gossen and Bujard, 1992). To investigate

whether KPNB1 overexpression influences ataxin-3 stability, *ATXN3* KO HEK 293T cells were cotransfected with either pTRE-15Q or pTRE-77Q ataxin-3 together with KPNB1 or empty vectors as a control. 24 h post-transfection, the expression of 15Q and 77Q ataxin-3 was turned off using doxycycline at different time points (0, 6, 24, and 48 h).

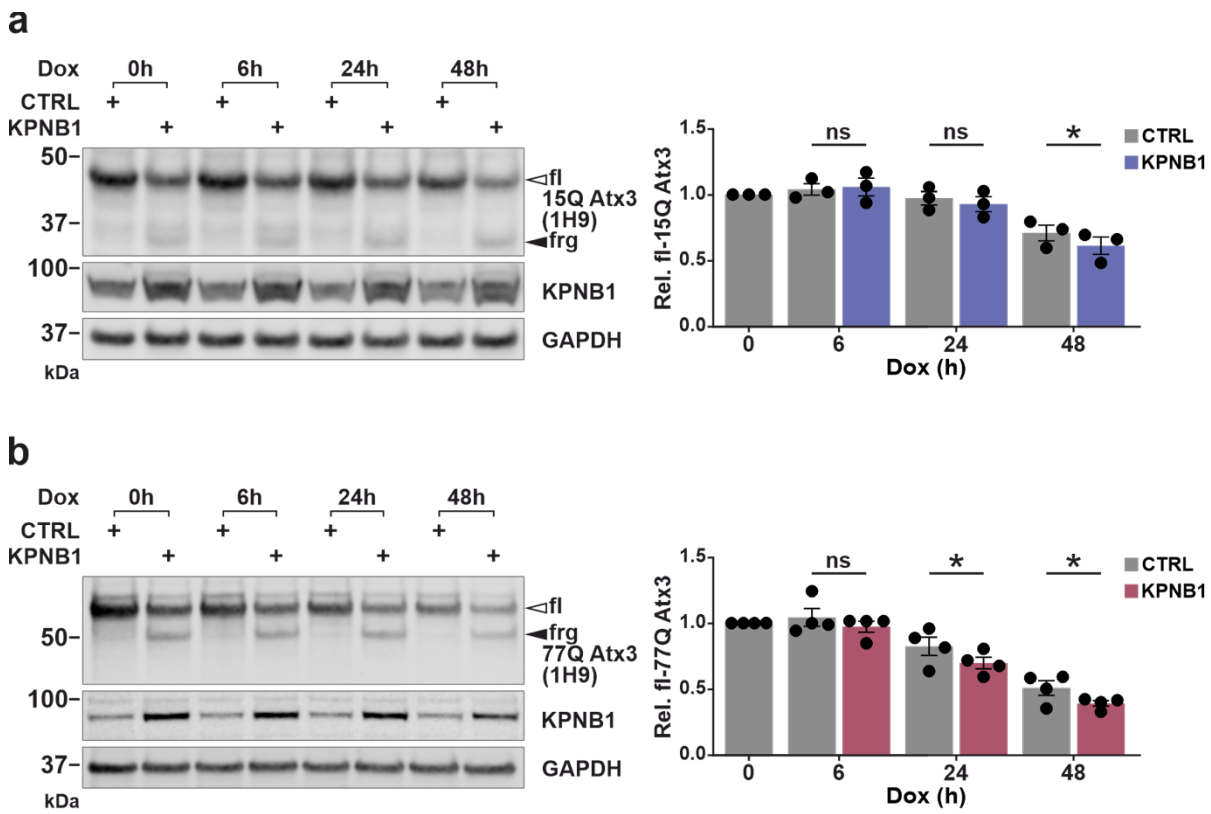

Figure 3.14 The stability of wild-type and polyQ-expanded ataxin-3 decreases upon KPNB1 overexpression. (**a**, **b**) Alteration of wild-type (15Q) and polyQ-expanded (77Q) ataxin-3 stability was assessed upon KPNB1 overexpression using the Tet-Off system. Western blot analysis reveals a significant reduction in the stability of ataxin-3 protein in KPNB1-overexpressing cells 48 h after termination of 15Q ataxin-3 expression, and 24 and 48 h after termination of 77Q ataxin-3 expression. *ATXN3* KO HEK 293T cells were cotransfected with either pTRE-15Q or pTRE-77Q ataxin-3 and KPNB1 or empty vectors (control). 24 h post-transfection, the expression of ataxin-3 was shut off using doxycycline at different time intervals (0, 6, 24, and 48 h). GAPDH was applied as a loading control. a, $n = 3$, paired *t*-test, CTRL *vs* KPNB1 (6 h), $p = 0.6029$; CTRL *vs* KPNB1 (24 h), $p = 0.6730$; CTRL *vs* KPNB1 (48 h), $p = 0.0132$; b, $n = 4$, paired *t*-test, CTRL *vs* KPNB1 (6 h), $p = 0.3859$; CTRL *vs* KPNB1 (24 h), $p = 0.0202$; CTRL *vs* KPNB1 (48 h), $p = 0.0427$. CTRL = empty vector; fl = full-length; frg = fragment; Dox = Doxycycline; Rel. = relative. Values are displayed as means ± SEM. ns = not significant; $*p \leq 0.05$. Modified from Abeditashi et al., 2022.

Western blot analysis revealed that the degradation of both wild-type and polyQ-expanded ataxin-3 accelerated significantly in KPNB1-overexpressing cells, as observed 48 h after termination of 15Q ataxin-3 expression (Figure 3.14a) and 24 and 48 h after termination of

77Q ataxin-3 expression (Figure 3.14b). However, no alteration was observed in the generation of ataxin-3 fragments, and they remained stable during the assay (Figure 3.14).

In short, KPNB1 overexpression promotes the degradation of wild-type and polyQ-expanded ataxin-3, leading to a reduction in the stability of this protein. These results stressed the importance of KPNB1 as a putative factor involved in the regulation of ataxin-3 protein levels and stability.

3.9 Ataxin-3 cleavage products induced by KPNB1 overexpression are not mediated by the activation of caspases or calpains

Proteolytic cleavage of polyQ-expanded proteins has been identified as a key event in the pathogenesis of polyQ diseases. This proteolytic processing of polyQ-expanded proteins is thought to result in the generation of cytotoxic fragments containing the expanded polyQ toxic entity, which are susceptible to aggregation and nuclear localization (Haacke et al., 2007; Havel et al., 2009; Takahashi et al., 2008). Notably, generation of the potentially toxic ataxin-3 fragments mediated mainly by two families of proteases, caspases and calpains, has been suggested extensively (Hübener et al., 2013; Ona et al., 1999), and activation of caspases and calpains has been indicated in different SCA3 models (Berke et al., 2004; Simões et al., 2012). The cysteine proteases of the caspase family play an important role in apoptosis and inflammatory pathways and can cleave proteins at specific aspartate residues (Earnshaw et al., 1999; Li and Yuan, 2008). The implication of caspases in the pathogenesis of other polyQ diseases besides SCA3 has been shown in several studies (Ellerby et al., 1999; Kim et al., 2001; Sánchez et al., 1999). Mounting evidence points to the involvement of calpains in SCA3 pathogenesis. Calpains are calcium-dependent cytosolic cysteine proteases that are ubiquitously expressed (Strobl et al., 2000). It has been shown that inhibition of calpains led to the reduction of polyQ-expanded ataxin-3 cleavage, nuclear localization, aggregation, and alleviated toxicity (Haacke et al., 2007; Simões et al., 2012).

To gain more insight into the promotion of cleavage of both wild-type and polyQ-expanded ataxin-3 observed in KPNB1-overexpressing cells, we decided to unravel whether this effect is mediated by the activation of caspases or calpains. To this point, the proteolytic cleavage of α-spectrin, which is a natural substrate of caspases and calpains (Yan et al., 2012), was assessed and quantified in KPNB1-overexpressing cells. Wild-type HEK 293T cells were

transfected with either KPNB1 or empty vectors as a control for 72 h. Cells were lysed and subjected to western blot analysis. Our result represented that neither full-length nor breakdown products of α-spectrin were modulated in KPNB1-overexpressing cells (Figure 3.15). In addition, the ratio between full-length and breakdown products of α-spectrin was comparable to the control (Figure 3.15). These results indicated that KPNB1 overexpression does not lead to the elevation of breakdown products of α-spectrin or the activation of caspases or calpains. The spectrin family are membrane-associated proteins that are ubiquitously expressed in various types of tissues, including the brain (Baines, 2009; Bennett and Lambert, 1991). Enhancement of breakdown products of α-spectrin has been identified in neuronal stress and death under acute and chronic degenerative conditions (Pineda et al., 2007; Zhang et al., 2009).

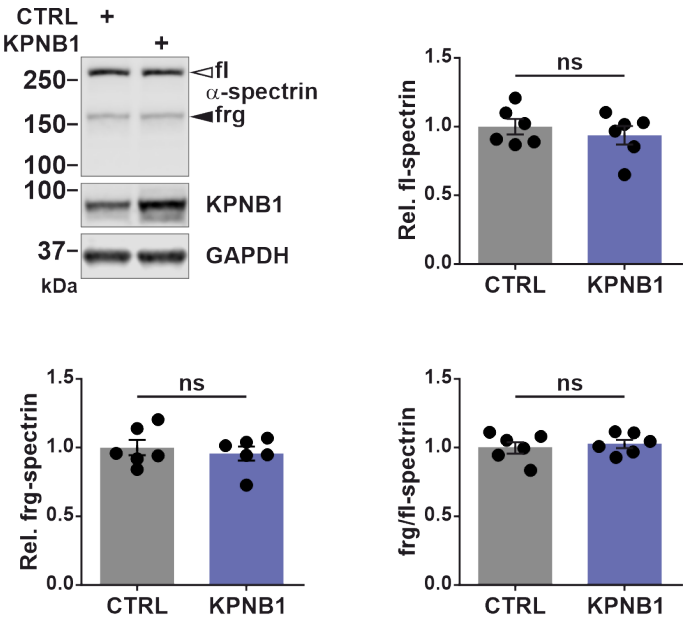

Figure 3.15 KPNB1 overexpression does not activate calpains or caspases. The activation of proteolytic enzymes, calpains and caspases, upon KPNB1 overexpression was evaluated by detecting cleavage of their common substrate, the α-spectrin protein. Wild-type HEK 293T cells were transfected with either KPNB1 or empty vectors (control) for 72 h. Western blot analysis indicates no alteration in the levels of either full-length α-spectrin (white arrowhead) or breakdown products of α-spectrin (black arrowhead) in KPNB1-overexpressing cells. In addition, the ratio between cleaved and full-length proteins remained comparable to the control. GAPDH was applied as a loading control. *n* = 6, unpaired *t*-test, fl-spectrin, $p = 0.4850$; frg-spectrin, $p = 0.5830$; frg/fl-spectrin, $p = 0.6296$. CTRL = empty vector; fl = full-length; frg = fragment; Rel. = relative. Values are displayed as means ± SEM. ns = not significant. Modified from Abeditashi et al., 2022.

In the follow-up analysis, we compared the cleavage pattern of wild-type and polyQ-expanded ataxin-3, followed by KPNB1 overexpression and calpains activation by western blotting. For this purpose, a cell-based calpain activation assay was carried out using ionomycin (IM). *ATXN3* KO HEK 293T cells were cotransfected with either wild-type (15Q) or polyQ-expanded (77Q) ataxin-3 together with KPNB1 or empty vectors as a control for 72 h. Transfected cells were incubated with 1 μM ionomycin at 37 °C for 1 h to trigger the activation of endogenous calpains and subjected to western blot analysis. Activation of endogenous calpains in ionomycin treated cells was confirmed by elevation of the breakdown products of α-spectrin (Figure 3.16a). Probing ataxin-3-derived fragments with two different antibodies (1H9 and C-terminal) recognizing distinct epitopes (Figure 3.16b), indicated that the cleavage pattern of 15Q and 77Q ataxin-3 induced by calpains activation (ataxin-3 calpain-derived fragments) was not comparable to ataxin-3-derived fragments promoted by KPNB1 overexpression (Figure 3.16c). These results provide evidence that neither caspases nor calpains are implicated in the promotion of ataxin-3 fragmentation upon KPNB1 overexpression.

To sum up, our findings provide evidence that KPNB1 overexpression does not induce the proteolytic cleavage of α-spectrin, which is a natural substrate of caspases and calpains. By comparing fragmentation of wild-type and polyQ-expanded ataxin-3 induced by activation of calpains using ionomycin and KPNB1 overexpression, we concluded that the enhancement of ataxin-3 fragmentation in KPNB1-overexpressing cells is not mediated by the activation of proteases, caspases, and calpains.

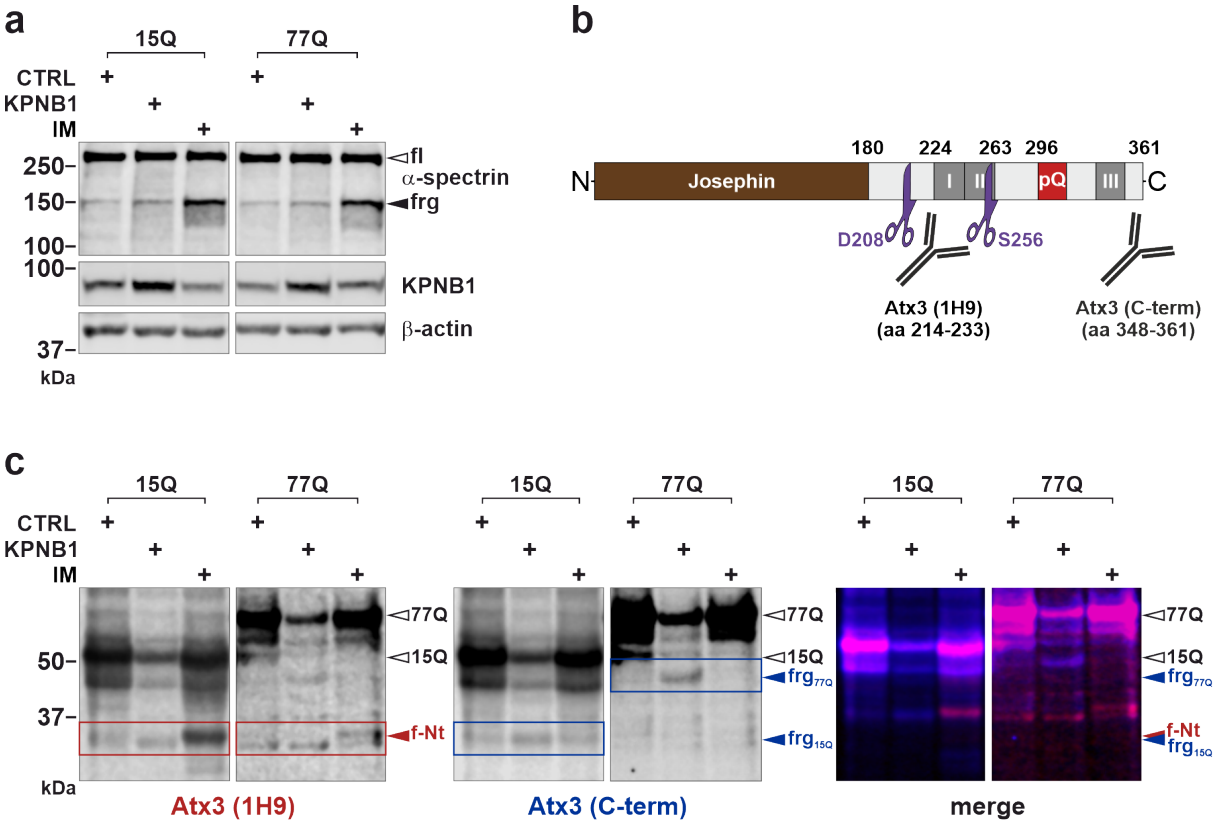

Figure 3.16 Calpains are not implicated in the cleavage of wild-type and polyQ-expanded ataxin-3 in KPNB1-overexpressing cells. (**a**) Breakdown products of α-spectrin (black arrowhead) are elevated in ionomycin (IM) treated cells, implying the activation of calpains compared with control. *ATXN3* KO HEK 293T cells were cotransfected with either wild-type (15Q) or polyQ-expanded (77Q) ataxin-3 together with KPNB1 or empty vectors (control) for 72 h. 1 h prior to harvesting, cells were treated with 1 µM ionomycin (IM), followed by cell lysis and western blotting. β-actin was applied as a loading control. (**b**) Schematic representation of ataxin-3 protein structure (UniProt ID: P54252-2) indicating calpain cleavage sites (purple scissors). The epitopes of ataxin-3 recognized by 1H9 and C-terminal antibodies are displayed in the figure. (**c**) Western blot analysis shows that ataxin-3 fragments induced by KPNB1 overexpression (blue boxes and arrowheads) are not comparable to ataxin-3 cleavage products mediated by calpains activation (red boxes and arrowheads). Ionomycin (IM) administration results in the activation of endogenous calpains and the cleavage of wild-type and polyQ-expanded ataxin-3. Red and blue channels indicate ataxin-3 detected by 1H9 and C-terminal antibodies, respectively. CTRL = empty vector; fl = full-length; frg = fragment; pQ = polyQ; aa = amino acids; f-Nt = fragment-N-terminal; IM = ionomycin; C-term = C-terminal. Modified from Abeditashi et al., 2022.

3.10 KPNB1 overexpression gives rise to fragments independent of proteolytic pathways

Protein homeostasis is a key element of cellular integrity and survival, which is achieved by the proper turnover of proteins and the degradation of misfolded or defective proteins in cells (Matyskiela and Martin, 2013). Dysfunction in protein homeostasis and impairment of protein

quality control pathways, including the ubiquitin-proteasome system and autophagy, are involved in the pathogenesis of polyQ diseases (Klockgether et al., 2019).

Autophagy is essential for proteostasis in cells, and there is strong evidence that it plays a crucial role in the degradation of insoluble aggregate-prone proteins, such as polyQ-expanded proteins (Levine and Kroemer, 2008). Autophagy impairment has been shown to be implicated in the pathogenesis of SCA3 (Onofre et al., 2016; Sittler et al., 2018).

The proteasome has an important role in the ubiquitin-dependent degradation of misfolded or damaged proteins (Ciechanover, 1994). The presence of ubiquitinated aggregates and sequestration of different components of the proteasomal machinery in SCA3 and other polyQ diseases implies the disruption of the ubiquitin-proteasome pathway, which may contribute to the pathogenesis of these diseases (Chai et al., 1999).

For better characterization of ataxin-3-derived fragments induced by KPNB1 overexpression and to figure out if the generation of these fragments is associated with the activation of autophagy or the ubiquitin-proteasome system, these two protein quality control pathways were inhibited using bafilomycin A1 and lactacystin, respectively. Moreover, to give validity to our previous finding regarding the involvement of calpains and caspases in ataxin-3 cleavage upon KPNB1 overexpression, these proteases were inhibited in these experiments as well. *ATXN3* KO HEK 293T cells were cotransfected with wild-type (15Q) ataxin-3 together with KPNB1 or empty vectors as a control for 72 h. As we found that the effect of KPNB1 modulation on ataxin-3 is not polyQ-dependent, this experiment was performed using only 15Q ataxin-3-expressing cells. Transfected cells were treated with calpain inhibitor III (CI-III), caspase inhibitor (Q-VD-OPh), autophagy inhibitor bafilomycin A1, proteasomal inhibitor lactacystin, or DMSO (control) for 16 h. Western blot analysis and quantification of ataxin-3-derived fragments demonstrated that inhibition of calpains and caspases or blocking of autophagic and proteasomal degradation did not prevent the formation of KPNB1 overexpression-associated fragments, and ataxin-3-derived fragments were detected in all samples (Figure 3.17). Interestingly, our result displayed an increase in the accumulation of ataxin-3-derived fragments in bafilomycin A1 treated cells compared with control, indicating these fragments are likely degraded via autophagy. However, quantification did not reach statistical significance (Figure 3.17).

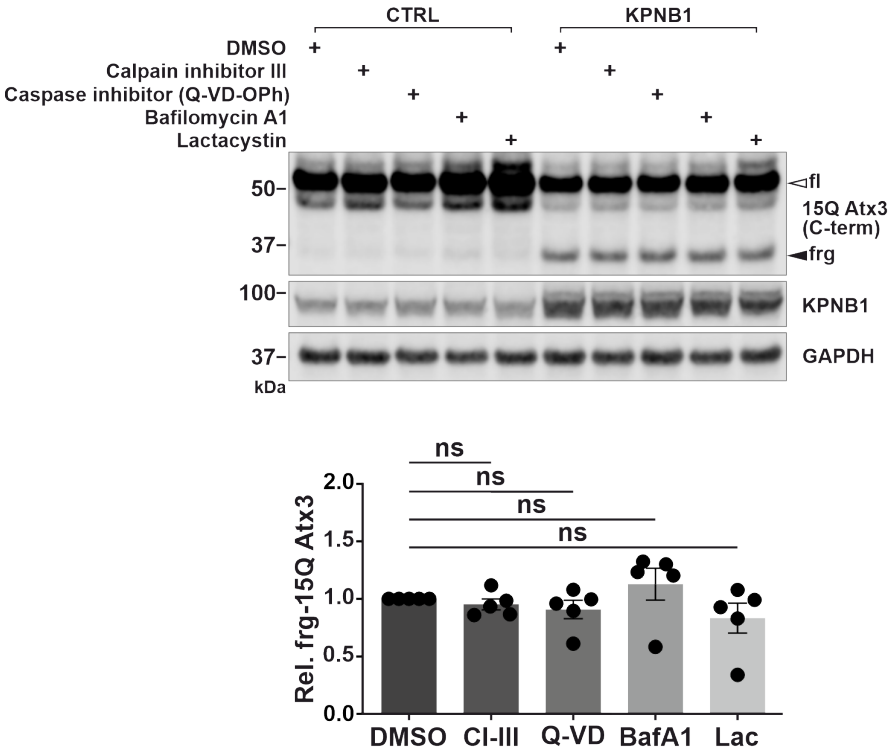

Figure 3.17 Ataxin-3-derived fragments are not mediated by activation of known SCA3-associated proteases or proteolytic pathways in KPNB1-overexpressing cells. Western blot analysis demonstrates that inhibition of calpains and caspases or blocking of autophagy and proteasomal degradation does not prevent the generation of ataxin-3-derived fragmentation in KPNB1-overexpressing cells. *ATXN3* KO HEK 293T cells were cotransfected with wild-type (15Q) ataxin-3 and KPNB1 or empty vectors (control) for 72 h. 16 h prior to harvesting, transfected cells were incubated with 10 µM calpain inhibitor III (CI-III), 10 µM caspase inhibitor (Q-VD-OPh), 50 nM autophagy inhibitor bafilomycin A1, or 10 µM proteasomal inhibitor lactacystin. Cells incubated with DMSO were considered a control. The diagram illustrates the quantification of ataxin-3 fragments in KPNB1-overexpressing cells. GAPDH was applied as a loading control. n = 5, one sample t-test, DMSO *vs* CI-III, p = 0.3708; DMSO *vs* Q-VD, p = 0.3136; DMSO *vs* BafA1, p = 0.4063; DMSO *vs* Lac, p = 0.2682. CTRL = empty vector; fl = full-length; frg = fragment; C-term = C-terminal; CI-III = calpain inhibitor III; BafA1 = bafilomycin A1; Lac = lactacystin; Rel. = relative. Values are displayed as means ± SEM. ns = not significant. Modified from Abeditashi et al., 2022.

Since we observed an elevation in ataxin-3 fragmentation upon KPNB1 overexpression, we postulated that this effect could be a consequence of altered autophagic flux within the cells. Protein levels of two widely used autophagy markers, autophagosomal microtubule-associated protein light chain 3 (LC3B-II) and p62, were analyzed to determine the potential of KPNB1 overexpression in inducing or inhibiting autophagy. p62 is an adapter protein target of autophagy that binds directly to LC3B and facilitates the degradation of protein aggregates. p62 accumulates upon the impairment of autophagy (Pankiv et al., 2007; Wong et al., 2012). LC3B-I is a cytosolic protein that conjugates to phosphatidylethanolamine (PE) to form LC3B-

II, which is recruited to the isolation membranes and autophagosomes, facilitating the fusion of autophagosomes with lysosomes (Kabeya et al., 2000). LC3B is the most widely used autophagosome marker because the amount of LC3B-II displays the number of autophagosomes within the cells (Yoshii and Mizushima, 2017). LC3B-II and p62 are selectively degraded by autophagy and accumulate upon bafilomycin A1 treatment. This inhibitor, which blocks the fusion of autophagosomes and lysosomes and the acidification of the lysosomes, is applied in the autophagic flux assay.

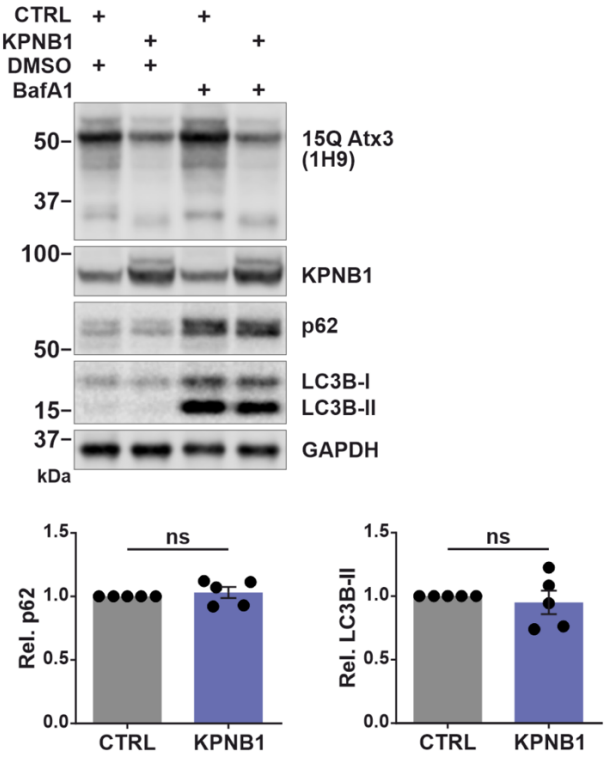

Figure 3.18 KPNB1 overexpression does not promote the autophagic flux. Western blot analysis indicates no alteration in the levels of autophagic markers, p62 and LC3B-II, upon KPNB1 overexpression. *ATXN3* KO HEK 293T cells were cotransfected with wild-type (15Q) ataxin-3 and KPNB1 or empty vectors (control) for 72 h. Transfected cells were incubated with 50 nM autophagy inhibitor bafilomycin A1 or DMSO (control) for 16 h prior to harvesting. The diagrams illustrate p62 and LC3B-II protein levels in bafilomycin A1 treated cells. GAPDH was applied as a loading control. n = 5, p62, one sample t-test, p = 0.5239; LC3B-II, one sample t-test, p = 0.6233. CTRL = empty vector; BafA1 = bafilomycin A1; Rel. = relative. Values are displayed as means ± SEM. ns = not significant. Modified from Abeditashi et al., 2022.

To analyze the effect of KPNB1 overexpression on autophagy, ATXN3 KO HEK 293T cells were cotransfected with wild-type (15Q) ataxin-3 together with KPNB1 and empty vectors for 72 h. 16 h prior to harvesting, transfected cells were treated with either bafilomycin A1 or DMSO

as a control. Western blot analysis and detection of membranes using specific antibodies for p62 and LC3B represented no alteration in protein levels of either LC3B-II or p62 upon KPNB1 overexpression, implying no stimulation or inhibition of autophagy in these cells (Figure 3.18).

In a nutshell, neither blocking of autophagic and proteasomal degradation nor inhibition of calpains and caspases could prevent the enhancement of ataxin-3 fragmentation in KPNB1-overexpressing cells. Moreover, KPNB1 overexpression does not alter the autophagic flux, as no change was detected in the levels of autophagy markers LC3B-II and p62. These results provide evidence that the enhancement of ataxin-3 lowering and fragmentation in KPNB1-overexpressing cells does not occur via the activation of known SCA3-associated proteases or proteolytic pathways.

3.11 KPNB1 overexpression decreases polyQ-expanded ataxin-3 aggregates and rescues cell viability

The formation of intraneuronal aggregates, which mainly consist of polyQ-expanded protein, is the pathological hallmark of SCA3 and other polyQ diseases (Taylor et al., 2002). Indeed, targeting and measuring the aggregation of disease proteins is employed to assess the disease progression and efficacy of treatments (Schmidt et al., 2016; Teixeira-Castro et al., 2011).

Given that we were able to observe a reduction in the soluble levels of both wild-type and polyQ-expanded ataxin-3 in KPNB1-overexpressing cells, we postulated that KPNB1 overexpression could reduce the aggregation and toxicity of poly-Q expanded ataxin-3 as well. Thus, in the first step, the aggregation of polyQ-expanded (148Q) ataxin-3 upon KPNB1 overexpression was evaluated by fluorescence microscopy. *ATXN3* KO HEK 293T cells were cotransfected with EGFP-ataxin-3 148Q together with KPNB1 or empty vectors as a control for 72 h. Transfected cells were fixed and immunostained using an antibody specific for KPNB1 to evaluate the efficacy of KPNB1 overexpression in these cells. The number of GFP-positive cells with and without aggregates was counted manually in 20 fields of vision under a fluorescence microscope, and the percentage of GFP-positive cells with aggregates was calculated. The result indicated that aggregation of EGFP-ataxin-3 148Q was impressively diminished upon KPNB1 overexpression compared with control (Figure 3.19a, b).

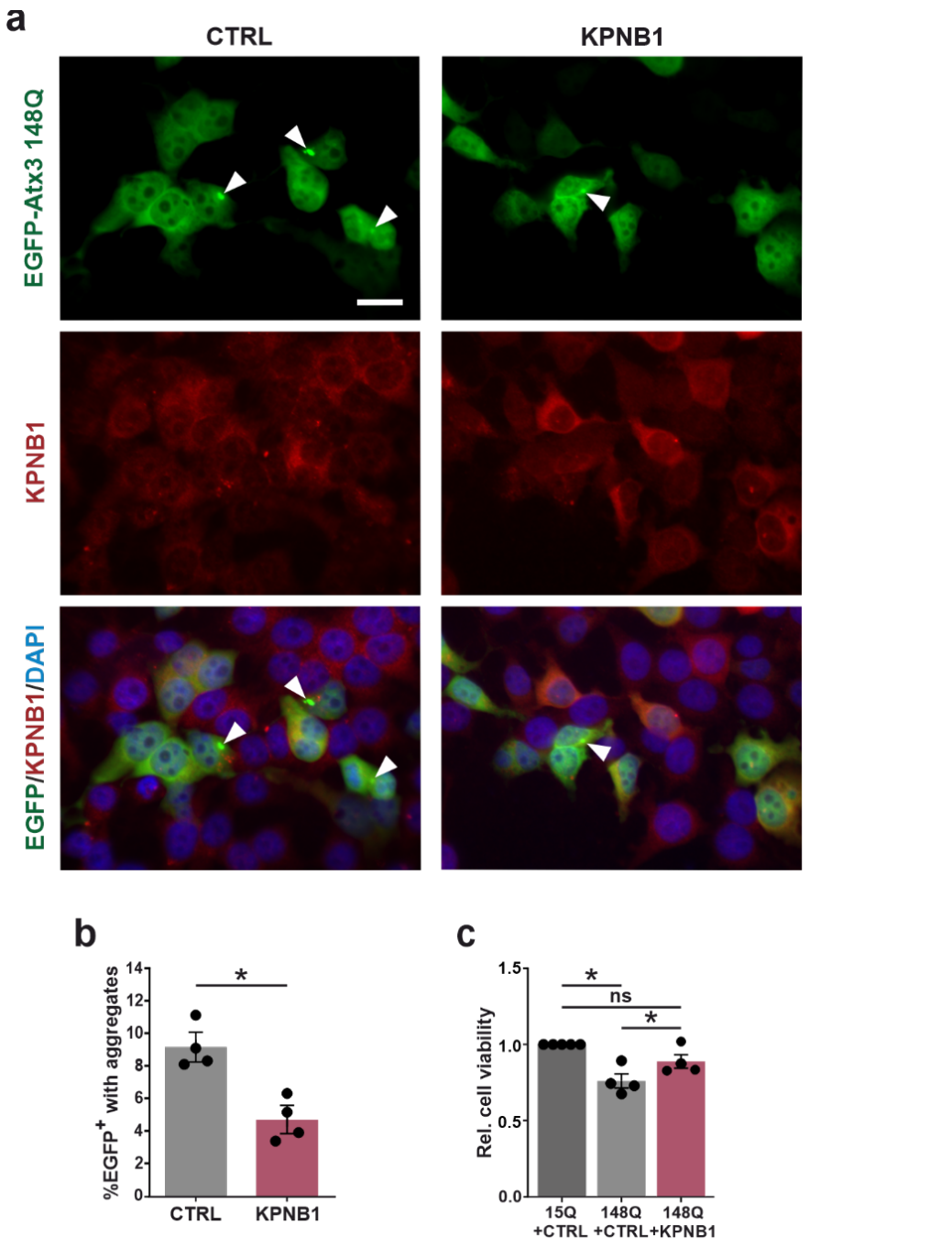

Figure 3.19 KPNB1 overexpression reduces cells with polyQ-expanded ataxin-3 aggregates and rescues cell viability. (**a**, **b**) Immunofluorescence staining was performed to visualize the modulation of polyQ-expanded ataxin-3 aggregation in KPNB1-overexpressing cells. *ATXN3* KO HEK 293T cells were transfected with EGFP-148Q ataxin-3 and either KPNB1 or empty vectors (control). 72 h post-transfection, cells were fixed and immunostained using an antibody specific for KPNB1. Subsequently, cells were mounted using a medium containing DAPI. The number of GFP-positive ($EGFP^+$) cells with and without aggregates was counted manually in 20 fields of vision. The result confirms the decrease of cells with polyQ-expanded ataxin-3 aggregates upon KPNB1 overexpression compared with control. Blue, green, and red channels are DAPI as nuclear counterstain, GFP, and KPNB1 signals, respectively. White arrowheads mark ataxin-3 aggregates (400 × magnification, scale bar = 20 µm). The diagram shows the percentage of aggregates in $EGFP^+$ cells. $n = 4$, unpaired *t*-test, $p = 0.0123$. (**c**) PrestoBlue

assay of *ATXN3* KO HEK 293T cells cotransfected with either wild-type (15Q) or polyQ-expanded (148Q) ataxin-3 and KPNB1 or empty vectors for 72 h. The viability of cells expressing 148Q ataxin-3 was rescued upon KPNB1 overexpression. Viability was normalized to 15Q ataxin-3-expressing cells. n = 4, one sample t-test, 15Q + CTRL *vs* 148Q + CTRL, $p = 0.0144$; 15Q + CTRL *vs* 148Q + KPNB1, $p = 0.0882$; paired t-test, 148Q + CTRL *vs* 148Q + KPNB1, $p = 0.0138$. CTRL = empty vector; Rel. = relative. Values are displayed as means ± SEM. ns = not significant; $*p \leq 0.05$. Modified from Abeditashi et al., 2022.

After evaluating the effect of KPNB1 overexpression on soluble levels and aggregation of ataxin-3, we were promoted to investigate if KPNB1 overexpression has any influence on cell viability. In this connection, *ATXN3* KO HEK 293T cells were cotransfected with either wild-type (15Q) or polyQ-expanded (148Q) ataxin-3 together with KPNB1 or empty vectors. The viability of cells was measured using the PrestoBlue assay 72 h post-transfection. In this analysis, cells are incubated with a non-toxic solution (PrestoBlue), which is reduced to a fluorescent product by metabolically active cells. This assay revealed that overexpression of 148Q ataxin-3 leads to a decrease in cellular viability in comparison to cells overexpressing 15Q ataxin-3. However, KPNB1 overexpression can rescue the impaired viability of *ATXN3* KO HEK 293T cells transiently expressing polyQ-expanded ataxin-3 (Figure 3.19c), which was presumably associated with attenuation of polyQ-expanded ataxin-3 aggregation propensity and cytotoxicity.

To further confirm our findings, the effect of KPNB1 overexpression on the aggregation load of polyQ-expanded ataxin-3 was measured using a filter retardation assay that traps and detects SDS-insoluble proteins and aggregates on a membrane. *ATXN3* KO HEK 293T cells were cotransfected with polyQ-expanded (148Q) ataxin-3 together with KPNB1 constructs. Cells cotransfected with 148Q ataxin-3 and empty vectors were considered a control. 72 h post-transfection, cells were lysed and subjected to a filter retardation assay. Our result showed that KPNB1 overexpression is accompanied by a significant mitigation of polyQ-expanded ataxin-3 aggregation in comparison to the control (Figure 3.20a). This finding can be explained by the lower concentration of misfolded ataxin-3 protein detected in KPNB1-overexpressing cells and is consistent with the result of fluorescence microscopy.

In line with the effects on soluble polyQ-expanded ataxin-3, overexpression of mutant KPNB1 (KPNB1 I178D) led to the reduction of ataxin-3 aggregation load as well as overexpression of wild-type KPNB1 (Figure 3.20b). *ATXN3* KO HEK 293T cells were cotransfected with polyQ-

expanded (148Q) ataxin-3 together with wild-type KPNB1 or KPNB1 I178D constructs for 72 h. Cells cotransfected with 148Q ataxin-3 and empty vectors were considered a control. Filter retardation assay indicated that mutation of the FxFG binding site of KPNB1 does not abolish its effect on ataxin-3 aggregation.

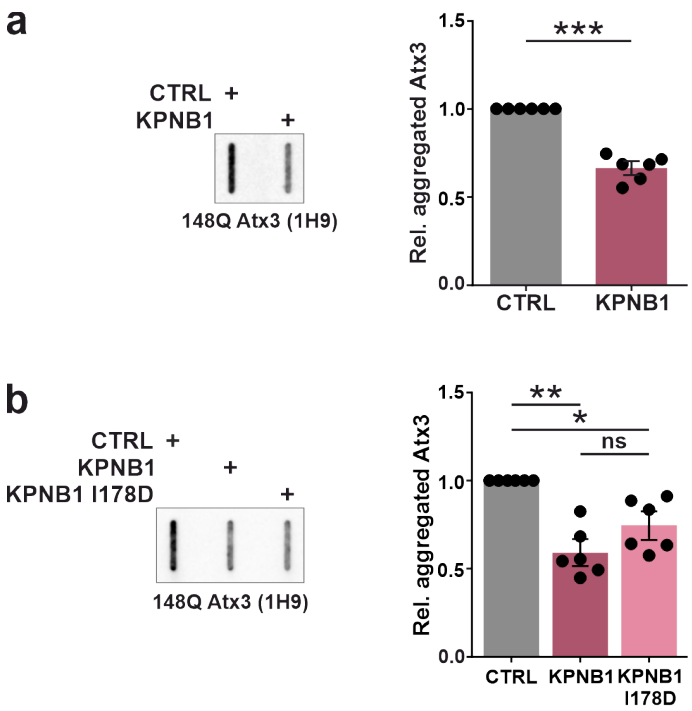

Figure 3.20 KPNB1 overexpression mitigates polyQ-expanded ataxin-3 aggregation, and this effect is not abolished with KPNB1 mutation. (**a**) Filter retardation assay demonstrates that KPNB1 overexpression is accompanied by a reduction of polyQ-expanded ataxin-3 aggregates in comparison to control. *ATXN3* KO HEK 293T cells were cotransfected with polyQ-expanded (148Q) ataxin-3 and either KPNB1 or empty vectors as a control for 72 h. Ataxin-3 aggregates were detected using the 1H9 antibody. Values represent the normalization to relative controls. $n = 6$, one sample *t*-test, $p = 0.0004$. (**b**) Filter retardation assay of *ATXN3* KO HEK 293T cells co-expressing polyQ-expanded (148Q) ataxin-3 and KPNB1 I178D for 72 h indicates a decrease in the aggregation of 148Q ataxin-3 as well as cells co-expressing wild-type KPNB1. Ataxin-3 aggregates were detected using the 1H9 antibody. Values represent the normalization to relative controls. $n = 6$, one sample *t*-test, CTRL *vs* KPNB1, $p = 0.0030$; CTRL *vs* KPNB1 I178D, $p = 0.0247$; unpaired *t*-test, KPNB1 *vs* KPNB1 I178D, $p = 0.1883$. CTRL = empty vector; Rel. = relative. Values are displayed as means ± SEM. ns = not significant; $*p \leq 0.05$; $**p \leq 0.01$; $***p \leq 0.001$. Modified from Abeditashi et al., 2022.

Altogether, beside the reduction of soluble levels of ataxin-3, we found that overexpression of KPNB1 can decrease the aggregation propensity of polyQ-expanded ataxin-3, as confirmed by fluorescence microscopy and filter retardation assay. This effect of KPNB1 could not be abolished by a mutation in the FxFG binding site of this protein, which disrupts the nuclear

transport function of KPNB1, implying that the observed effect is a nuclear transport function-independent mechanism. Additionally, KPNB1 overexpression can rescue the impaired viability of cells overexpressing polyQ-expanded ataxin-3, which can be related to the reduction of ataxin-3 aggregation in these cells.

3.12 KPNB1 knockdown or pharmacological inhibition promotes the aggregation of polyQ-expanded ataxin-3

Expansion of polyQ tract in disease proteins leads to abnormal and non-native conformations and ultimately formation of toxic oligomers and SDS-resistant aggregates, which play a crucial role in neurodegeneration (Breuer et al., 2010). The concentration of polyQ-expanded ataxin-3 plays an important role in the formation of aggregates which presented to be higher in the nuclear compartment of the cells (Pozzi et al., 2008).

Our results demonstrated that KPNB1 knockdown or pharmacological inhibition increases the soluble levels of ataxin-3. In this respect, we sought to investigate whether KPNB1 knockdown or pharmacological inhibition leads to an increase in ataxin-3 aggregation as well. To elucidate the propensity of polyQ-expanded (148Q) ataxin-3 to form aggregates upon KPNB1 knockdown, *ATXN3* KO HEK 293T cells were cotransfected with 148Q ataxin-3 and either esiKPNB1 or esiLUC as control for 72 h. Cell homogenates were subjected to filter retardation assay, and the result displayed that knockdown of KPNB1 using esiRNA promoted the formation of polyQ-expanded ataxin-3 aggregates remarkably (Figure 3.21a).

Furthermore, we investigated the impact of KPNB1 pharmacological inhibition using importazole (IPZ) on aggregation of polyQ-expanded ataxin-3. Filter retardation assay of *ATXN3* KO HEK 293T cells transfected with polyQ-expanded (148Q) ataxin-3 constructs disclosed an elevation in polyQ-expanded ataxin-3 aggregation upon 16 µM IPZ treatment compared with DMSO-treated cells (control) (Figure 3.21b). These results suggest that in contrast to KPNB1 overexpression, both KPNB1 knockdown and pharmacological inhibition lead to an increase in the aggregation and toxicity of polyQ-expanded ataxin-3, corresponding to the increased soluble levels of polyQ-expanded ataxin-3.

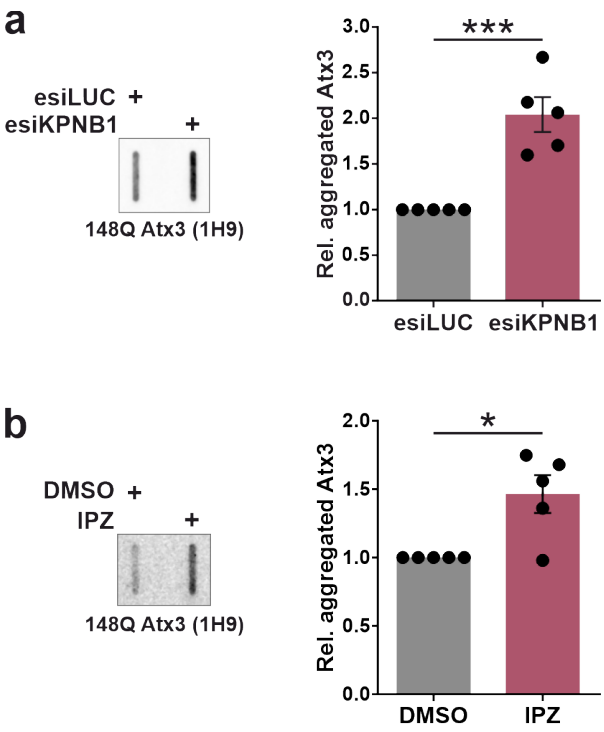

Figure 3.21 Knockdown or pharmacological inhibition of KPNB1 leads to an increase in polyQ-expanded ataxin-3 aggregates. (**a**) KPNB1 knockdown using esiRNA promotes the formation of polyQ-expanded (148Q) ataxin-3 aggregates. *ATXN3* KO HEK 293T cells were cotransfected with 148Q ataxin-3 construct and either esiKPNB1 or esiLUC (control). 72 h post-transfection, cells were harvested, and aggregation of 148Q ataxin-3 was analyzed using a filter retardation assay. The blots were probed for ataxin-3 using the 1H9 antibody. Values represent the normalization to relative controls. $n = 5$, one sample *t*-test, $p = 0.0054$. (**b**) KPNB1 pharmacological inhibition using importazole (IPZ) results in an increase in 148Q ataxin-3 aggregation. *ATXN3* KO HEK 293T cells were transfected with 148Q ataxin-3 constructs for 72 h. 48 h prior to harvesting, transfected cells were treated with either 16 µM IPZ or DMSO as a control. Cell homogenates were subjected to a filter retardation assay, and the blots were detected using the 1H9 antibody. Values represent the normalization to relative controls. $n = 5$, one sample *t*-test, $p = 0.0279$. IPZ = importazole; Rel. = relative. Values are displayed as means ± SEM. $*p \leq 0.05$; $**p \leq 0.01$; $***p \leq 0.001$. Modified from Abeditashi et al., 2022.

In conclusion, the filter retardation assay revealed that either KPNB1 knockdown or pharmacological inhibition using importazole can increase the aggregation propensity of polyQ-expanded ataxin-3 significantly, which can be related to the higher concentration of misfolded ataxin-3 protein in these cells. This finding is in agreement with the effect of KPNB1 knockdown or pharmacological inhibition on soluble levels of ataxin-3.

3.13 RNA sequencing indicated modulation of some canonical pathways upon KPNB1 overexpression

Given that KPNB1 overexpression leads to the decrease of ataxin-3 protein levels, a question remains concerning which factor contributes to this effect. To determine the cellular pathways that might be implicated in this process, we conducted 3' RNA sequencing of *ATXN3* KO HEK 293T cells contransfected with either wild-type (15Q) or polyQ-expanded (148Q) ataxin-3 and KPNB1 for 72 h. Cells cotransfected with ataxin-3 and empty vectors were considered a control. RNA sequencing revealed 565 and 653 differentially expressed genes in 15Q and 148Q ataxin-3-expressing cells, respectively (Table A.1–2). Statistical analysis demonstrated that 216 genes were upregulated and 349 genes were downregulated significantly in cells overexpressing 15Q ataxin-3 and KPNB1 compared with control (Figure 3.22a, c). Moreover, 304 upregulated and 349 downregulated genes were identified in cells expressing 148Q ataxin-3 upon KPNB1 overexpression, and amongst them, 222 genes were shared between 15Q and 148Q ataxin-3-expressing cells (Figure 3.22b, c). Importantly, RNA sequencing indicated that the gene expression of neither 15Q nor 148Q ataxin-3 was altered in KPNB1-overexpressing cells.

To get insight into the canonical pathways that have been activated or inhibited upon KPNB1 overexpression, we applied the Ingenuity Pathway Analysis (IPA). Ingenuity Pathway Analysis is a web-based functional analysis tool that allows comprehensive analysis of omics data. It predicts the downstream effects and discovers new targets or candidate biomarkers. Additionally, the most relevant signaling and metabolic pathways, activation and inhibition of upstream regulators, and interaction networks for the list of genes can be identified using the Ingenuity Pathway Analysis. Accordingly, modulation of some canonical pathways was predicted by the Ingenuity Pathway Analysis in both wild-type (15Q) and polyQ-expanded (148Q) ataxin-3-expressing cells upon KPNB1 overexpression (Figure 3.23). However, we could not link the modulated cellular pathways to the reduction of ataxin-3 levels upon KPNB1 overexpression.

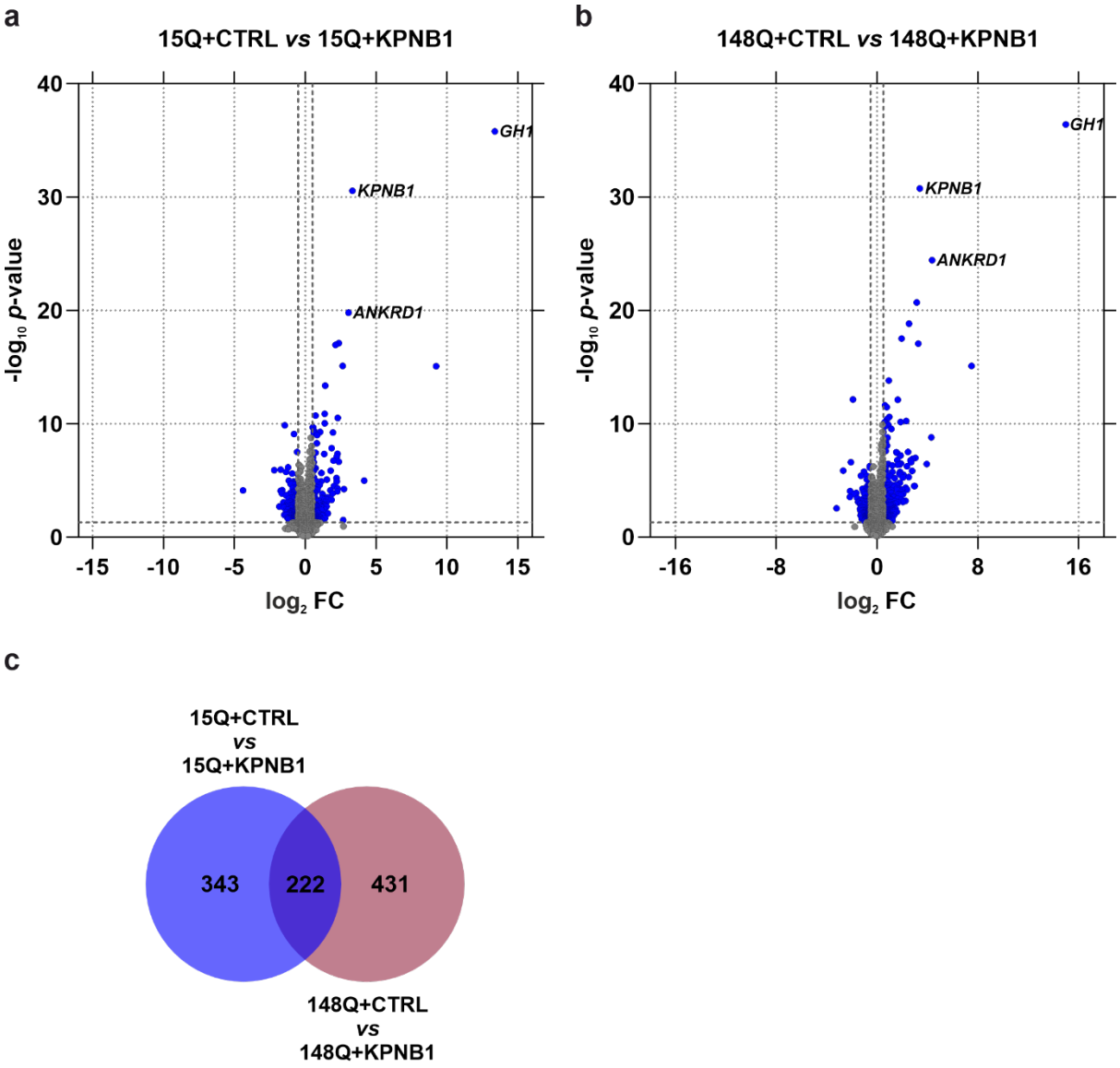

Figure 3.22 RNA sequencing of *ATXN3* KO HEK 293T cells overexpressing ataxin-3 and KPNB1. (**a**, **b**) Volcano plots illustrate the differentially expressed genes in cells expressing ataxin-3 upon KPNB1 overexpression. *ATXN3* KO HEK 293T cells were cotransfected with either wild-type (15Q) or polyQ-expanded (148Q) ataxin-3 and KPNB1 or empty vectors as a control. 72 h post-transfection, cells were lysed and subjected to 3' RNA sequencing in five biological replicates. Volcano plots indicate a direct comparison between the expression differences (log_2 FC) and significance ($-log_{10}$ *p*-value) of genes, highlighting the most upregulated genes. The blue circles show genes whose levels have changed significantly upon KPNB1 overexpression. $n = 5$, $p \leq 0.05$. (**c**) The Venn diagram displays the number of common and unique genes that have been dysregulated significantly in 15Q and 148Q atxain-3-expressing cells upon KPNB1 overexpression in comparison to the respective controls. CTRL = empty vector; FC = fold change.

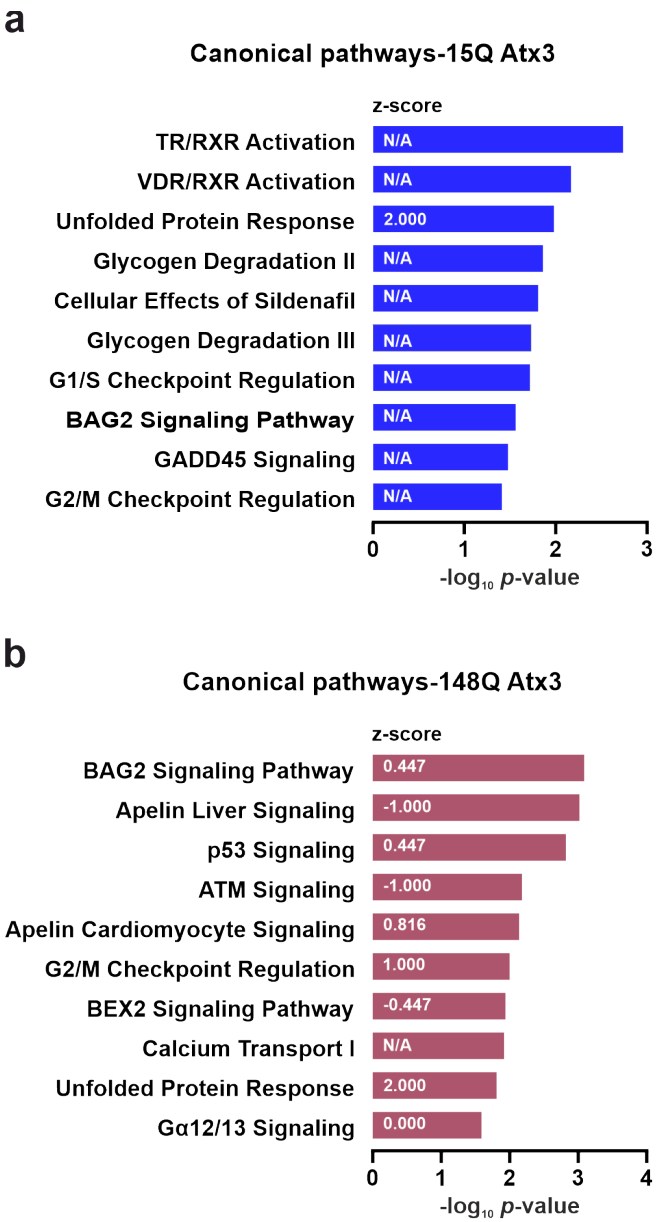

Figure 3.23 Modulation of canonical pathways in cells expressing ataxin-3 upon KPNB1 overexpression. (**a**, **b**) The top ten modulated canonical pathways in either wild-type (15Q) or polyQ-expanded (148Q) ataxin-3-expressing cells upon KPNB1 overexpression, as predicted by the Ingenuity Pathway Analysis of 3' RNA sequencing-based transcriptome data. The graphs illustrate -$\log_{10}$ *p*-values as well as the pathway-calculated z-scores. N/A = not applicable.

3.14 Mass spectrometry revealed activation of the mitochondrial protease CLPP in KPNB1-overexpressing cells

Our results demonstrated that KPNB1 overexpression leads to the decrease of ataxin-3 protein levels and aggregation, and it is able to promote fragmentation of ataxin-3. However, we could not link this process to the activation of one of the proteolytic pathways or modulation of canonical pathways revealed by RNA sequencing. Therefore, in the next step,

we carried out unbiased label-free quantitative proteomics to determine the upstream regulators or cellular pathways that might be implicated in this process. *ATXN3* KO HEK 293T cells were contransfected with either wild-type (15Q) or polyQ-expanded (148Q) ataxin-3 and KPNB1 for 72 h. Cells cotransfected with ataxin-3 and empty vectors were considered a control. The whole cell lysates were purified using SDS-PAGE, and gel pieces were excised and in-gel digested using trypsin. Tryptic peptides were subjected to liquid chromatography and tandem mass spectrometry (LC-MS/MS) analysis.

From triplicate analysis, we could identify 93 and 172 proteins in 15Q and 148Q ataxin-3-expressing cells, respectively, whose levels were significantly altered upon KPNB1 overexpression. Moreover, KPNB1 overexpression resulted in the modulation of levels of 215 proteins in ataxin-3-expressing cells (15Q and 148Q together) in comparison to control (Figure 3.24a–c and Table B.1–3). Statistical analysis of proteomics data indicated that 23 proteins were upregulated and 69 proteins were downregulated significantly in cells overexpressing 15Q ataxin-3 and KPNB1 compared with control (Figure 3.24a, d). In addition, 44 upregulated and 127 downregulated proteins were revealed in cells expressing 148Q ataxin-3 upon KPNB1 overexpression, and amongst them, 15 proteins (3 upregulated and 12 downregulated) were shared between 15Q and 148Q ataxin-3-expressing cells (Figure 3.24b, d, and Table 3.1).

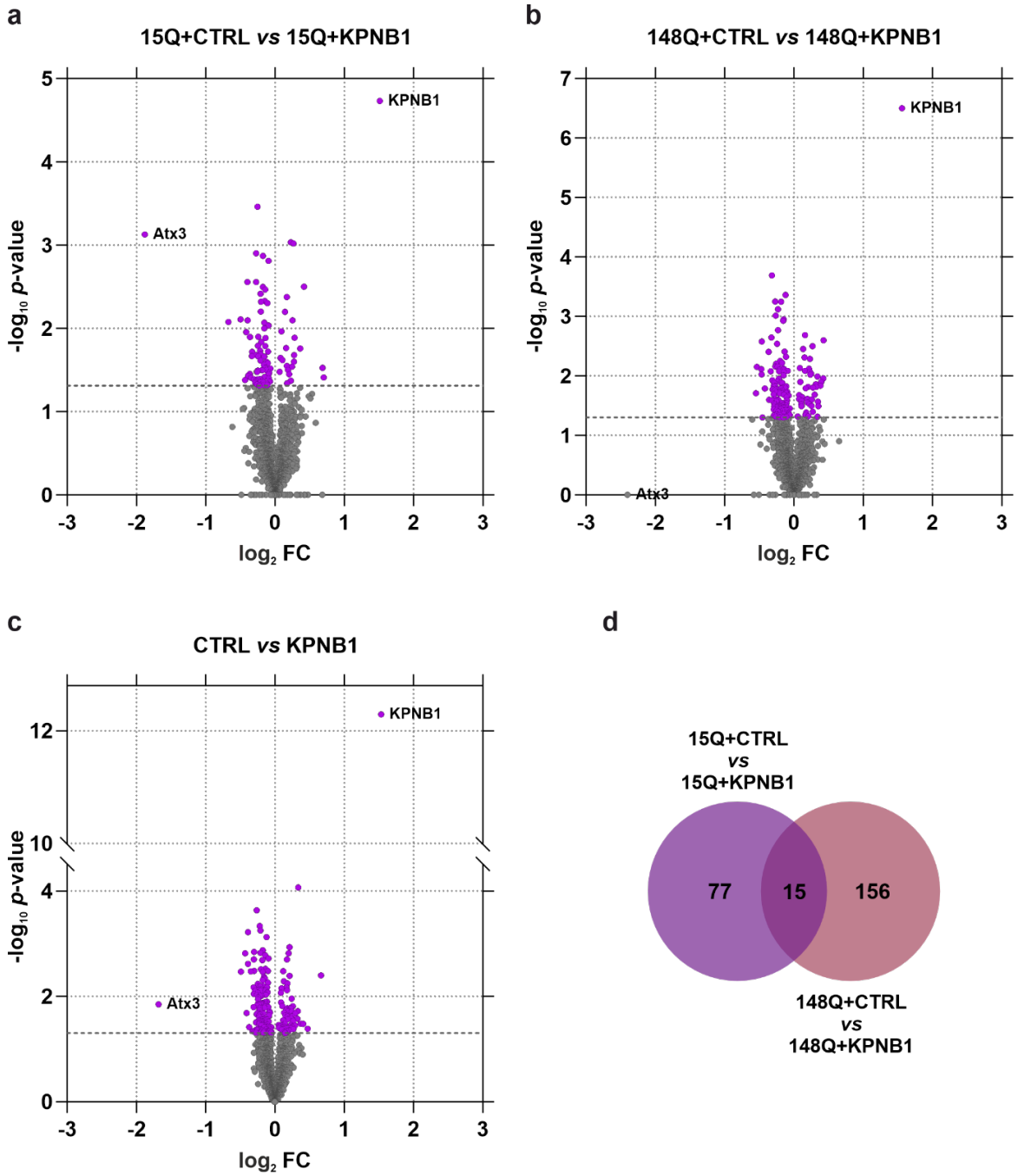

Figure 3.24 Label-free quantitative proteomics of *ATXN3* KO HEK 293T cells overexpressing ataxin-3 and KPNB1. (**a**, **b**, **c**) Volcano plots indicate the upregulated and downregulated proteins in KPNB1-overexpressing cells compared with control. *ATXN3* KO HEK 293T cells were cotransfected with either wild-type (15Q) or polyQ-expanded (148Q) ataxin-3 and KPNB1 or empty vectors as a control. 72 h post-transfection, cells were lysed and subjected to mass spectrometry in three biological replicates. Volcano plots illustrate a direct comparison between $\log_2$ FC and $-\log_{10}$ *p*-value of proteins. The purple circles show proteins whose levels have altered significantly upon KPNB1 overexpression. $n = 3$, two-sample *t*-test, $p \leq 0.05$. (**d**) The Venn diagram displays the number of common and unique proteins that have been modulated significantly in 15Q and 148Q atxain-3-expressing cells upon KPNB1 overexpression in comparison to control. CTRL = empty vector; FC = fold change. Modified from Abeditashi et al., 2022.

Table 3.1 15 common proteins between wild-type (15Q) and polyQ-expanded (148Q) ataxin-3-expressing cells were identified in mass spectrometry that their levels were significantly modified upon KPNB1 overexpression. FC = fold change. Modified from Abeditashi et al., 2022.

Gene name	Protein name	$-Log_{10}$ *p*-value	Log_2 FC	$-Log_{10}$ *p*-value	Log_2 FC
		15Q ataxin-3		**148Q ataxin-3**	
KPNA2	Importin α-1	1.8884	0.2815	1.9011	0.3919
RPA3	Replication protein A 14 kDa subunit	1.6005	0.2699	2.3108	0.1511
PPIA	Peptidyl-prolyl cis-trans isomerase A; Peptidyl-prolyl cis-trans isomerase A, N-terminally processed; Peptidyl-prolyl cis-trans isomerase	2.1972	0.1424	1.6160	0.1933
FLNB	Filamin-B	1.5187	-0.0694	2.3212	-0.1163
SUCLG2	Succinyl-CoA ligase [GDP-forming] subunit beta, mitochondrial	2.0348	-0.0959	1.7882	-0.1858
DARS2	Aspartate--tRNA ligase, mitochondrial	1.8837	-0.1395	1.4139	-0.2035
NUP155	Nuclear pore complex protein Nup155	1.4146	-0.1514	1.6854	-0.1444
HIBCH	3-hydroxyisobutyryl-CoA hydrolase, mitochondrial	1.3204	-0.1582	1.8878	-0.1885
MAP2K2	Dual specificity mitogen-activated protein kinase kinase 2	1.3529	-0.1644	1.3333	-0.1988
IDH2	Isocitrate dehydrogenase [NADP], mitochondrial	2.3184	-0.2038	2.0786	-0.2143
FDPS	Farnesyl pyrophosphate synthase	1.7910	-0.2457	1.7474	-0.1717
AMOT	Angiomotin	1.4788	-0.2578	2.1617	-0.2684
ERLIN2	Erlin-2	1.3274	-0.2602	1.7787	-0.2581
CYP51A1	Lanosterol 14-alpha demethylase	1.3446	-0.2841	2.9263	-0.1569
FAM98B	Protein FAM98B	1.7179	-0.3313	2.5785	-0.4639

To get insight into the upstream regulators and identify cellular processes that have been modulated in KPNB1-overexpressing cells, we employed the Ingenuity Pathway Analysis (IPA). Accordingly, modulation of some upstream regulators was predicted by the Ingenuity Pathway Analysis in both wild-type (15Q) and polyQ-expanded (148Q) ataxin-3-expressing cells upon KPNB1 overexpression (Table 3.2, Table 3.3). Intriguingly, activation of the ATP-dependent Clp protease proteolytic subunit (CLPP) was predicted by the Ingenuity Pathway Analysis amongst the top ten modulated upstream regulators in both 15Q (z-score = 2, *p* = 1.43e-04) and 148Q (z-score = 3.464, *p* = 7.52e-14) ataxin-3-expressing cells upon KPNB1

cotransfection. The Ingenuity Pathway Analysis predicted activation of the mitochondrial protease CLPP in these cells based on the modulation of target proteins of this protease (Table 3.2, Table 3.3).

Table 3.2 Prediction of upstream regulators modulation in wild-type (15Q) ataxin-3-expressing cells upon KPNB1 overexpression by Ingenuity Pathway Analysis.

Upstream regulator	**Molecule type**	**Predicted activation state**	**Activation z-score**	***P*-value**	**Target molecules**
SB203580	Chemical drug	Activated	2.219	4.70E-02	ACOT2, CCNB1, CYP51A1, NOL9, P4HA1
CLPP	Peptidase	Activated	2	1.43E-04	CYC1, IDH2, IDH3G, SDHA
ADRB	Group	Activated	2	2.70E-03	ANXA5, CYP51A1, FDPS, PCNA
Nitrofurantoin	Chemical drug	Activated	2	4.72E-03	ANXA5, MAPK3, PCNA, SCP2
Let-7a-5p (and other miRNAs w/seed GAGGUAG)	Mature microRNA	Activated	2	7.97E-03	CSDE1, SLC25A1, SLC25A13, SPCS3
Testosterone	Chemical - endogenous mammalian		-1.91	7.08E-02	CYP51A1, MGST1, PARP1, PCNA
Metribolone	Chemical reagent		-1.929	1.32E-05	CRYZ, CYC1, FDPS, HIBCH, IDH2, PPIA, SLC25A12, SLC25A13, SUCLG2, SUPV3L1
Mono-(2-ethylhexyl) phthalate	Chemical toxicant	Inhibited	-2	4.52E-03	CYC1, IDH3G, SDHA, SUCLG2
INSR	Kinase	Inhibited	-2.2	3.27E-03	ACOT2, CDC5L, CYC1, CYP51A1, FDPS, IQGAP1, SCP2
IL4	Cytokine	Inhibited	-2.874	7.25E-04	CKAP5, CLTC, DARS2, DCTN1, DDX46, FLNB, LMAN2, MAPK3, NUP155, SLC7A5, SYMPK, SYNJ2BP, UGGT1

Table 3.3 Prediction of upstream regulators modulation in polyQ-expanded (148Q) ataxin-3-expressing cells upon KPNB1 overexpression by Ingenuity Pathway Analysis.

Upstream regulator	**Molecule type**	**Predicted activation state**	**Activation z-score**	***P*-value**	**Target molecules**
CLPP	Peptidase	Activated	3.464	7.52E-14	ACADM, ALDH2, ATP5F1B, DLST, HADH, IDH2, LONP1, MDH2, PDHA1, PDHB, PHB2, UQCRC1
Gentamicin	Chemical drug	Activated	2.985	1.52E-03	ACADM, ACADSB, CUL2, EPB41L2, HSD17B4, HSPA1A/HSPA1B, IDH1, SEC22B, SSB
L-asparaginase	Biologic drug	Activated	2.646	3.10E-05	CYP51A1, DHCR7, FANCI, FDPS, HMGCS1, KIF11, SQLE
INSIG1	Other	Activated	2.573	1.43E-05	ACACA, CYP51A1, DHCR7, FDPS, HMGCS1, LSS, SQLE
ADRB	Group	Activated	2.449	7.88E-04	CDKN2A, CYP51A1, FDPS, HMGCS1, IDH1, LSS
Mono-(2-ethylhexyl) phthalate	Chemical toxicant	Inhibited	-2.891	5.09E-09	ACADM, ACADSB, ACO1, ATP5F1B, HADH, MDH2, NDUFS2, PDHB, PPA1, SUCLG2, UQCRC1, UQCRC2
SREBF2	Transcription regulator	Inhibited	-2.937	9.28E-09	ACACA, CYP51A1, DHCR7, FDPS, GTF2I, HMGCS1, IDH1, LSS, SQLE
Elaidic acid	Chemical - endogenous mammalian	Inhibited	-3.148	2.41E-09	ACACA, ATP5F1B, CYP51A1, DHCR7, FDPS, HMGCS1, LSS, SGPL1, SQLE, SUCLG2
Metribolone	Chemical reagent	Inhibited	-3.745	7.58E-17	ACACA, ACADSB, ALDH9A1, ATP5F1B, BPNT1, CPOX, FDPS, GRHPR, HADH, HIBCH, HMGCS1, HSD17B4, IDH2, MCCC2, MDH2, NDUFA9, NDUFB10, NDUFS2, PDHA1, PDHB, PFKP, PPA1, PPIA, SLC25A12, SUCLG2, UQCRC1, UQCRC2
INSR	Kinase	Inhibited	-3.825	4.61E-09	ACADM, ALDH2, ATP5F1B, CYP51A1, DHCR7, FDPS, GANAB, HMGCS1, HSD17B4, IDH1, IGF2R, LSS, MDH2, NDUFA9, PDHA1, PDHB, SQLE, UQCRC1, UQCRC2

The mitochondrial protease CLPP is an energy-dependent protease involved in protein degradation and homeostasis (Yu and Houry, 2007), thus, we assumed that activation of this mitochondrial protease might be implicated in the modulation of ataxin-3 levels and fragmentation in KPNB1-overexpressing cells. Indeed, we could not find any association between other predicted upstream regulators and modulation of ataxin-3 upon KPNB1 overexpression.

To sum up, KPNB1 overexpression leads to a significant reduction in ataxin-3 protein levels and aggregation. To figure out which upstream regulators or pathways might be involved in this effect, unbiased label-free quantitative proteomics was carried out, followed by the Ingenuity Pathway Analysis. Our findings indicated that mitochondrial protease CLPP has been activated in both wild-type and polyQ-expanded ataxin-3-expressing cells upon KPNB1 overexpression, which can be an explanation for the promotion of ataxin-3 cleavage and reduction of its soluble levels in these cells.

3.15 Knockdown of mitochondrial protease CLPP rescues protein levels of ataxin-3 in KPNB1-overexpressing cell

Mitochondrial proteases, or mitoproteases, play a critical role in the degradation of unfolded and damaged proteins, mitophagy, and apoptosis, and their dysregulation has been observed in aging and neurodegenerative diseases (Quirós et al., 2015; Rugarli and Langer, 2012). Given that CLPP is a nuclear-encoded mitochondrial protease implicated in the degradation of unfolded and misfolded proteins (Yu and Houry, 2007), we speculated that the decrease of wild-type and polyQ-expanded ataxin-3 protein levels and enhancement of its cleavage in KPNB1-overexpressing cells might be directly associated with the activation of this mitochondrial protease. To this point, we decided to validate our hypothesis by knockdown of mitochondrial protease CLPP using esiRNA in KPNB1-overexpressing cells. *ATXN3* KO HEK 293T cells were cotransfected with either wild-type (15Q) or polyQ-expanded (148Q) ataxin-3 together with KPNB1 or empty vectors as a control. Mitochondrial protease CLPP was depleted using esiCLPP in these cells, and cells cotransfected with esiLUC were considered a control. Cell lysates were analyzed using western blotting, and the result confirmed the reduction of CLPP protein levels in cells cotransfected with esiCLPP in comparison to cells cotransfected with esiLUC (Figure 3.25). Moreover, it revealed that knockdown of

mitochondrial protease CLPP in KPNB1-overexpressing cells counteracted the reduction of full-length wild-type and polyQ-expanded ataxin-3 protein levels in these cells (Figure 3.25).

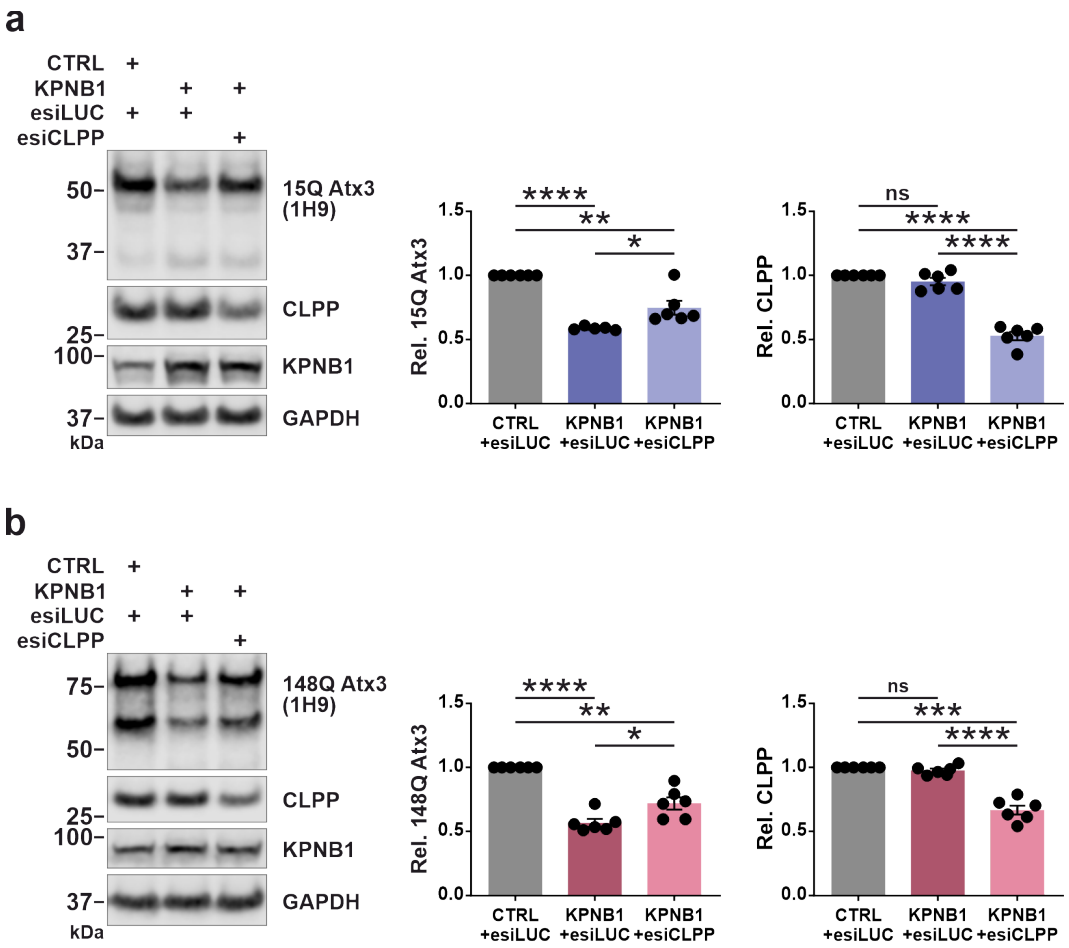

Figure 3.25 Knockdown of mitochondrial protease CLPP rescues wild-type and polyQ-expanded ataxin-3 protein levels in KPNB1-overexpressing cells. (**a**, **b**) Western blot analysis demonstrates that protein levels of both wild-type (15Q) and polyQ-expanded (148Q) ataxin-3 can be rescued partly by knockdown of the mitochondrial protease CLPP in KPNB1-overexpressing cells. *ATXN3* KO HEK 293T cells overexpressing either 15Q or 148Q ataxin-3 and KPNB1 were cotransfected with esiCLPP or esiLUC as control for 72 h. Western blot analysis confirmed knockdown of the mitochondrial protease CLPP. GAPDH was applied as a loading control. a, 15Q Atx3, $n = 6$, one sample *t*-test, CTRL + esiLUC *vs* KPNB1 + esiLUC, $p < 0.0001$; CTRL + esiLUC *vs* KPNB1 + esiCLPP, $p = 0.0056$; unpaired *t*-test, KPNB1 + esiLUC *vs* KPNB1 + esiCLPP, $p = 0.0264$; CLPP, $n = 6$, one sample *t*-test, CTRL + esiLUC *vs* KPNB1 + esiLUC, $p = 0.1619$; CTRL + esiLUC *vs* KPNB1 + esiCLPP, $p < 0.0001$; unpaired *t*-test, KPNB1 + esiLUC *vs* KPNB1 + esiCLPP, $p < 0.0001$; b, 148Q Atx3, $n = 6$, one sample *t*-test, CTRL + esiLUC *vs* KPNB1 + esiLUC, $p < 0.0001$; CTRL + esiLUC *vs* KPNB1 + esiCLPP, $p = 0.0020$; unpaired *t*-test, KPNB1 + esiLUC *vs* KPNB1 + esiCLPP, $p = 0.0219$; CLPP, $n = 6$, one sample *t*-test, CTRL + esiLUC *vs* KPNB1 + esiLUC, $p = 0.2175$; CTRL + esiLUC *vs* KPNB1 + esiCLPP, $p = 0.0003$; unpaired *t*-test, KPNB1 + esiLUC *vs* KPNB1 + esiCLPP, $p < 0.0001$. CTRL = empty vector; Rel. = relative. Values are displayed as means ± SEM. ns = not significant; *$p \leq 0.05$; **$p \leq 0.01$; ***$p \leq 0.001$; ****$p \leq 0.0001$. Modified from Abeditashi et al., 2022.

Since KPNB1 overexpression can affect the aggregation of ataxin-3 as well as its soluble levels and cleavage, in the next step, we sought to assess the propensity of polyQ-expanded ataxin-3 to form aggregates upon knockdown of mitochondrial protease CLPP in KPNB1-overexpressing cells. Accordingly, *ATXN3* KO HEK 293T cells were cotransfected with polyQ-expanded (148Q) ataxin-3 together with either KPNB1 or empty vectors. Mitochondrial protease CLPP was depleted using esiCLPP in these cells, and cells cotransfected with esiLUC were considered a control. Filter retardation assay demonstrated elevated polyQ-expanded ataxin-3 aggregation upon CLPP knockdown in KPNB1-overexpressing cells in comparison to control cells cotransfected with esiLUC (Figure 3.26).

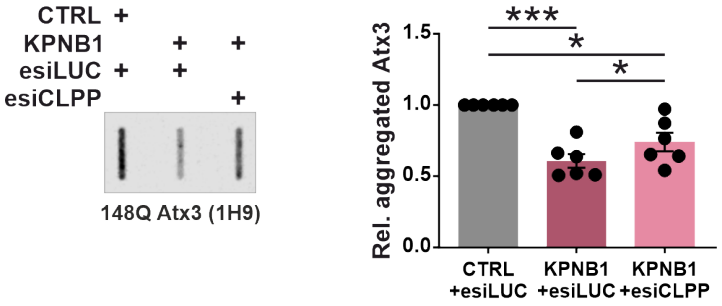

Figure 3.26 Knockdown of CLPP rescues aggregation of polyQ-expanded ataxin-3 in KPNB1-overexpressing cells. Knockdown of the mitochondrial protease CLPP counteracts the KPNB1-induced decrease of polyQ-expanded ataxin-3 aggregates compared with control. *ATXN3* KO HEK 293T cells overexpressing polyQ-expanded (148Q) ataxin-3 and KPNB1 were cotransfected with esiCLPP or esiLUC as a control. 72 h post-transfection, cells were lysed and subjected to a filter retardation assay. Ataxin-3 aggregates were detected using the 1H9 antibody. Values represent the normalization to relative controls. $n = 6$, one sample *t*-test, CTRL + esiLUC *vs* KPNB1 + esiLUC, $p = 0.0005$; CTRL + esiLUC *vs* KPNB1 + esiCLPP, $p = 0.0107$; paired *t*-test, KPNB1 + esiLUC *vs* KPNB1 + esiCLPP, $p = 0.0187$. CTRL = empty vector; Rel. = relative. Values are displayed as means ± SEM. ns = not significant; *$p \leq 0.05$; **$p \leq 0.01$; ***$p \leq 0.001$. Modified from Abeditashi et al., 2022.

Overall, knockdown of mitochondrial protease CLPP using esiRNA counteracted the reduction of protein levels and aggregation of ataxin-3 in KPNB1-overexpressing cells. These results provide evidence that mitigation of ataxin-3 protein levels and aggregates by KPNB1 overexpression is likely mediated by activation of the mitochondrial protease CLPP, and it can be restored by CLPP knockdown.

3.16 Modulation of mitochondrial protease CLPP alters the protein levels of ataxin-3

As mitochondrial protease CLPP knockdown could rescue the reduction of ataxin-3 protein levels and aggregates in KPNB1-overexpressing cells, we were encouraged to figure out if the modulation of CLPP protein levels has any direct effect on protein levels of wild-type and polyQ-expanded ataxin-3. For this purpose, *ATXN3* KO HEK 293T cells were transiently transfected with either wild-type (15Q) or polyQ-expanded (148Q) ataxin-3 together with esiCLPP or esiLUC as a respective control. 72 h post-transfection, cells were lysed and analyzed by western blotting. Interestingly, knockdown of mitochondrial protease CLPP using esiRNA led to an increase in soluble levels of both full-length 15Q and 148Q ataxin-3 compared with control (Figure 3.27).

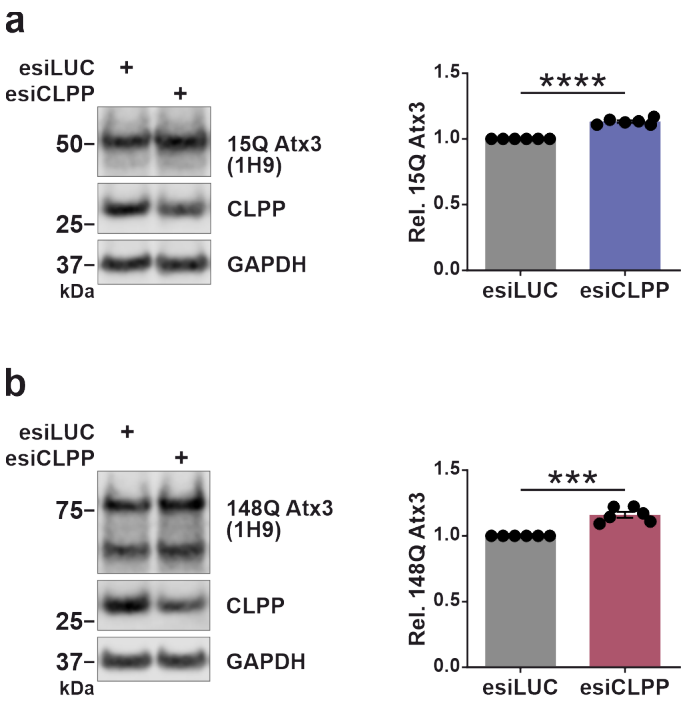

Figure 3.27 Knockdown of the mitochondrial protease CLPP increases wild-type and polyQ-expanded ataxin-3 protein levels. (**a**, **b**) Western blot analysis reveals that knockdown of mitochondrial protease CLPP is accompanied by a significant increase in protein levels of both wild-type (15Q) and polyQ-expanded (148Q) ataxin-3. *ATXN3* KO HEK 293T cells were cotransfected with either 15Q or 148Q ataxin-3 together with esiCLPP or esiLUC as a control for 72 h. Ataxin-3 was detected using the 1H9 antibody. GAPDH was used as a loading control. a, $n = 6$, one sample *t*-test, $p < 0.0001$; b, $n = 6$, one sample *t*-test, $p = 0.0009$. Rel. = relative. Values are displayed as means ± SEM. ***$p \leq 0.001$; ****$p \leq 0.0001$. Modified from Abeditashi et al., 2022.

To have a better understanding of the effect of mitochondrial protease CLPP modulation on ataxin-3, in the next step, we decided to investigate the impact of CLPP overexpression on ataxin-3 protein levels as well as CLPP knockdown. Accordingly, *ATXN3* KO HEK 293T cells were cotransfected with either 15Q or 148Q ataxin-3 together with either CLPP or both CLPP and KPNB1 constructs for 72 h. Cells cotransfected with ataxin-3 and empty vectors were considered a respective control.

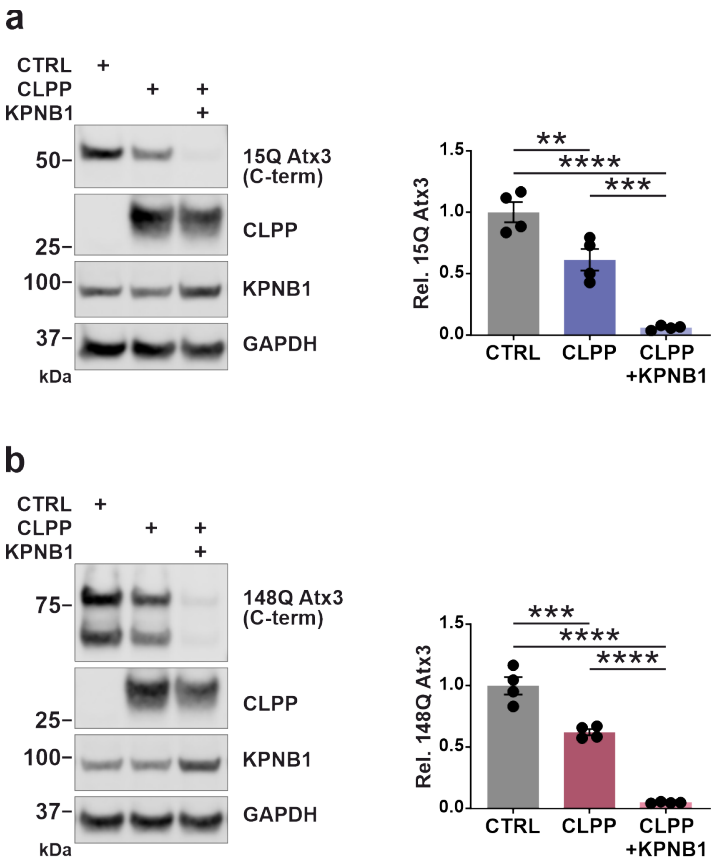

Figure 3.28 CLPP overexpression reduces wild-type and polyQ-expanded ataxin-3 protein levels. (**a**, **b**) Overexpression of the mitochondrial protease CLPP decreases protein levels of both wild-type (15Q) and polyQ-expanded (148Q) ataxin-3, and its effect is enhanced by KPNB1 overexpression. *ATXN3* KO HEK 293T cells were cotransfected with either 15Q or 148Q ataxin-3 and CLPP or both CLPP and KPNB1 constructs for 72 h. Cells cotransfected with ataxin-3 and empty vectors were considered a control. Ataxin-3 was detected using the C-terminal antibody. GAPDH was applied as a loading control. a, $n = 4$, one-way ANOVA with Tukey's post-test, CTRL *vs* CLPP, $p = 0.0089$; CTRL *vs* CLPP + KPNB1, $p < 0.0001$; CLPP *vs* CLPP + KPNB1, $p = 0.0009$; b, $n = 4$, one-way ANOVA with Tukey's post-test, CTRL *vs* CLPP, $p = 0.0004$; CTRL *vs* CLPP + KPNB1, $p < 0.0001$; CLPP *vs* CLPP + KPNB1, $p < 0.0001$. CTRL = empty vector; C-term = C-terminal; Rel. = relative. Values are displayed as means ± SEM. $^{**}p \leq 0.01$; $^{***}p \leq 0.001$; $^{****}p \leq 0.0001$. Modified from Abeditashi et al., 2022.

Western blot analysis revealed that overexpression of mitochondrial protease CLPP led to a significant reduction in protein levels of both wild-type and polyQ-expanded ataxin-3 in comparison to control (Figure 3.28). Interestingly, this effect was boosted upon additional overexpression of KPNB1 in these cells (Figure 3.28). These data are consistent with the effect of KPNB1 overexpression on wild-type and polyQ-expanded ataxin-3.

In summary, knockdown of mitochondrial protease CLPP increased the protein levels of wild-type and polyQ-expanded ataxin-3, whereas its overexpression lowered ataxin-3 protein levels. These results revealed the mitochondrial protease CLPP as a modulator of ataxin-3 protein levels and reinforced the idea that modulation of ataxin-3 by KPNB1 overexpression is likely mediated by the activation of this mitochondrial protease.

3.17 KPNB1 and CLPP protein levels are reduced in SCA3 models

Our findings revealed KPNB1 as an important modulator of protein levels, aggregation, and fragmentation of both wild-type and polyQ-expanded ataxin-3. These interesting and novel results motivated us to investigate the endogenous levels of KPNB1 in different models of SCA3. In this respect, we aimed to examine whether protein levels of KPNB1 are affected in two SCA3 transgenic mouse models (YAC and CaMKII/MJD77) and induced pluripotent stem cells (iPSCs) derived from SCA3 patients as a cell model of SCA3.

The YAC transgenic mice were generated with the use of yeast artificial chromosome (YAC) constructs carrying the full-length *MJD1* gene with expanded polyglutamine tracts (Cemal et al., 2002). The double transgenic mice (CamKII/MJD77) were previously developed in our lab (Schmidt et al., 2019) using the CaMKII (calcium-calmodulin-dependent kinase II) promoter (Mayford et al., 1996) and a MJD77Q responder in C57Bl/6 mice (Boy et al., 2009). Accordingly, the whole brain of 15-month-old YAC transgenic mice as well as the cerebral cortex of 5-month-old CaMKII/MJD77 transgenic mice were lysed and subjected to western blot analysis. Interestingly, our finding depicted a significant reduction in protein levels of KPNB1 in the neuronal tissue of both YAC and CaMKII/MJD77 transgenic mouse models in comparison to aged-matched control mice (Figure 3.29). The reduction of KPNB1 protein levels was more prominent in the YAC transgenic mouse model, which might be related to the older age of these animals compared with CaMKII/MJD77 transgenic mice. Serving two

different SCA3 mouse models corroborated that the attenuation of KPNB1 protein levels in their neuronal tissue is not associated with the mouse model.

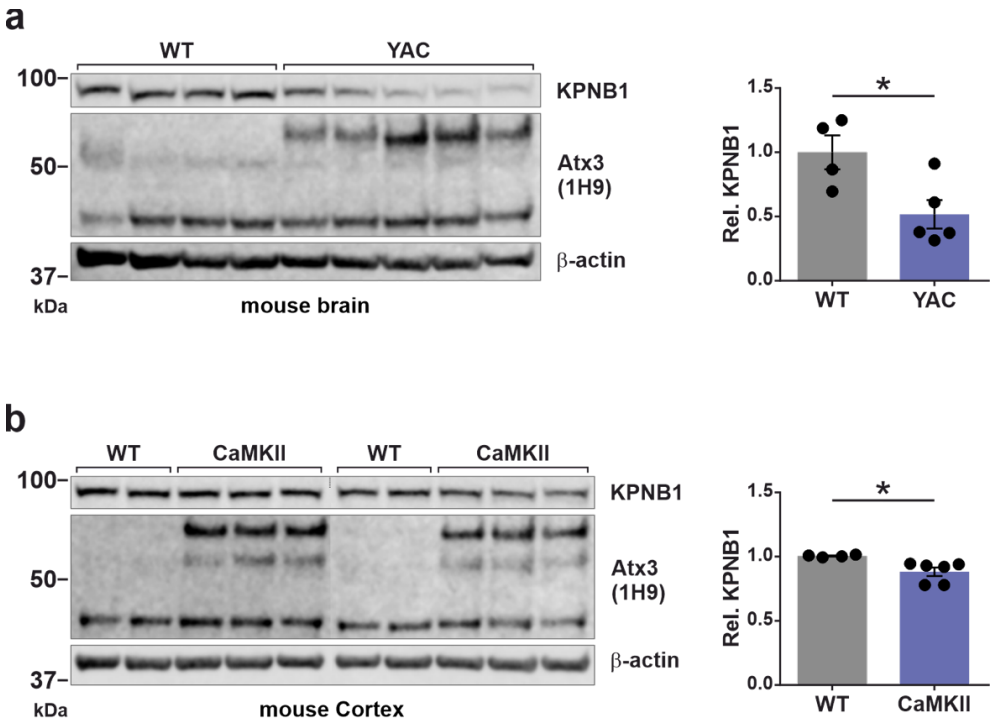

Figure 3.29 Decrease of KPNB1 protein levels in SCA3 transgenic mouse models. (**a**) Western blot analysis of whole brain protein extracts of 15-month-old YAC transgenic mice demonstrated a statistically significant decrease of KPNB1 protein levels in comparison to controls (15-month-old wild-type mice). Brain hemispheres were homogenized in RIPA buffer. β-actin was applied as a loading control. *n* = 4–5, unpaired *t*-test, *p* = 0.0257. (**b**) Western blot analysis of cortical lysates of 5-month-old CaMKII/MJD77 transgenic mice confirms attenuation of KPNB1 protein levels compared with controls (5-month-old wild-type mice). β-actin was used as a loading control. *n* = 4–6, unpaired *t*-test, *p* = 0.0175. WT = wild-type; Rel. = relative. Values are displayed as means ± SEM. **p* ≤ 0.05. Modified from Abeditashi et al., 2022.

We further explored protein levels of KPNB1 in a human cellular model of SCA3 as well as protein levels of mitochondrial protease CLPP, as modulation of levels of this mitochondrial protease could affect ataxin-3 protein levels. Thus, fibroblasts were obtained from three SCA3 patients and three healthy, age- and gender-matched individuals and reprogrammed to induced pluripotent stem cells (iPSCs). Control and SCA3 patient-derived iPSCs were lysed and assessed by western blot analysis. Our findings indicated that both KPNB1 and CLPP protein levels are decreased in iPSCs derived from SCA3 patients in comparison to healthy controls (Figure 3.30), and validated the result obtained from the analysis of the neuronal tissue of two different SCA3 mouse models.

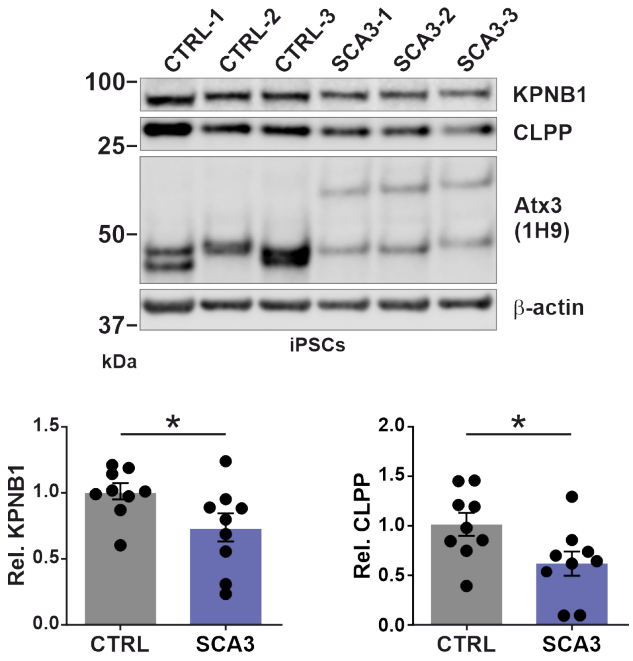

Figure 3.30 Reduction of protein levels of KPNB1 and mitochondrial protease CLPP in SCA3 patient-derived iPSCs. Western blot analysis of induced pluripotent stem cells (iPSCs) from three SCA3 patients and three healthy controls demonstrates a significant reduction of both KPNB1 and CLPP protein levels. β-actin was applied as a loading control. *n* = 3 replicates of 3 patients and 3 controls, KPNB1, unpaired *t*-test, $p = 0.0410$; CLPP, unpaired *t*-test, $p = 0.0325$. iPSCs = induced pluripotent stem cells; CTRL = healthy control; Rel. = relative. Values are displayed as means ± SEM. *$p \leq 0.05$. Modified from Abeditashi et al., 2022.

Our results demonstrated a reduction of KPNB1 levels in the brains of two different SCA3 mouse models. Moreover, decreased levels of both KPNB1 and CLPP were revealed in SCA3 patient-derived iPSCs. Altogether, the analysis of SCA3 patient-derived iPSCs and neuronal tissue from two different SCA3 mouse models emphasized presumptive dysregulation of KPNB1 and mitochondrial protease CLPP in SCA3.

3.18 Summary of findings

To sum up, our results revealed KPNB1 as a putative modulator of protein levels, cleavage, aggregation, and stability of ataxin-3. Our findings indicated that KPNB1 overexpression leads to the reduction of wild-type and polyQ-expanded ataxin-3 soluble levels and enhancement of their cleavage, although it does not modulate the subcellular localization of ataxin-3. Additionally, KPNB1 overexpression is accompanied by the decrease of polyQ-expanded ataxin-3 aggregates (Tables 3.4 and 3.5).

In contrast to overexpression of KPNB1, knockdown and pharmacological inhibition of this nuclear transport receptor result in the increase of soluble protein levels and the aggregation of wild-type and polyQ-expanded ataxin-3. However, no alteration of subcellular localization of ataxin-3 was observed in these cells (Tables 3.4 and 3.5).

Table 3.4 Summary of findings on the effects of KPNB1 overexpression and knockdown/ pharmacological inhibition on wild-type ataxin-3. ↑ = upregulation; ↓ = downregulation; ↕ = unchanged; N/A = not applicable.

Effects on wild-type ataxin-3	**KPNB1 overexpression**	**KPNB1 knockdown/ pharmacological inhibition**
Localization	↕	↕
Protein levels	↓	↑
Cleavage	↑	N/A
Stability	↓	N/A

Table 3.5 Summary of findings on the effects of KPNB1 overexpression and knockdown/ pharmacological inhibition on polyQ-expanded ataxin-3. ↑ = upregulation; ↓ = downregulation; ↕ = unchanged; N/A = not applicable.

Effects on polyQ-expanded ataxin-3	**KPNB1 overexpression**	**KPNB1 knockdown/ pharmacological inhibition**
Localization	↕	↕
Protein levels	↓	↑
Cleavage	↑	N/A
Stability	↓	N/A
Aggregation	↓	↑
Viability	↑	N/A

4. Discussion

Abnormal intracellular and/or extracellular inclusions in affected brain regions are a defining feature of neurodegenerative diseases. It is generally accepted that this dysregulation is directly involved in neurotoxicity, neurodegeneration, and the phenotypic presentation of these diseases (Ross and Poirier, 2004). The intracellular inclusions usually contain aggregates of mislocalized and misfolded disease-specific proteins, although the exact molecular mechanisms implicated in the formation of protein aggregates are poorly understood. It has been proposed that genetic mutations and environmental factors, such as oxidative or metabolic stress, play a critical role in the formation of protein aggregates in neurodegenerative diseases (Takalo et al., 2013).

Spinocerebellar ataxia type 3 (SCA3), also known as Machado-Joseph Disease (MJD), is the most common dominantly inherited form of spinocerebellar ataxia (SCA) worldwide. It is caused by a CAG repeat expansion mutation in the coding region of the *ATXN3*/*MJD1* gene, leading to the elongation of the polyglutamine (polyQ) tract in the C-terminus of the ataxin-3 protein (Kawaguchi et al., 1994; Schöls et al., 2004; Takiyama et al., 1997). SCA3 is an autosomal dominant neurodegenerative disorder of late onset and progressive, involving predominantly the cerebellar, pyramidal, extrapyramidal, motor neuron, and oculomotor systems, leading to neurological and physical impairments in patients (Bettencourt and Lima, 2011; Rudnicki and Margolis, 2003).

Ataxin-3 is a multi-faceted protein implicated in various cellular processes, such as deubiquitination, transcriptional regulation, and DNA repair (McLoughlin et al., 2020). The presence of an expanded polyQ tract evokes the production of insoluble protein aggregates, susceptibility to proteolysis, destabilization of functional conformation, leading to abnormal protein-protein interactions, and ultimately neuronal death (Costa Mdo and Paulson, 2012; Raj and Akundi, 2021). Although the precise underlying molecular mechanism by which polyQ-expanded ataxin-3 elicits neurotoxicity is still far from clear.

The right subcellular localization of proteins and the proper protein-protein interactions play important roles in the maintenance of cellular homeostasis, which is regulated by the nucleocytoplasmic transport across the nuclear envelope (Ding et al., 2020; Ding and

Sepehrimanesh, 2021). Under normal conditions of nucleocytoplasmic transport, protein cargos are able to reach and be retained in appropriate compartments, either the nucleus or cytoplasm. However, dysregulations of the nucleocytoplasmic transport machinery will interfere with the normal intracellular distribution of protein cargos, resulting in protein mislocalization, which can be observed in diseased or aged neurons. Mislocalization of protein cargos disrupts the hemostasis of the local protein reservoir and leads to abnormal protein-protein interactions, by which induces the formation of protein aggregates in cells, especially in post-mitotics such as neurons (Tamburrino and Decressac, 2016; Woerner et al., 2016). On the flip side, these protein aggregates have deleterious effects on the normal functions of the neurons by recruiting other proteins and factors that play a crucial role in signaling pathways or nucleocytoplasmic transport. It has been indicated that TDP-43 aggregates or poly-dipeptides encoded by C9orf72 repeat expansion in ALS/FTD interfere with the nucleocytoplasmic transport in affected neurons (Chou et al., 2018; Shi et al., 2017). These disruptions further deteriorate the impaired functions of nucleocytoplasmic transport machinery, leading to more severe mislocalization of proteins.

In addition to mislocalization of protein cargos, the nuclear export of transcripts can be defected in neurons, causing abnormal subcellular distribution of RNA molecules, such as nuclear RNA accumulation and mRNA mislocalization. Disruption of the normal distribution of RNA molecules can dysregulate protein synthesis and results in the abnormal compartmentalization of protein reservoirs (Lusk and King, 2017; Wang et al., 2016). Indeed, the impairment of nucleocytoplasmic transport in trafficking either protein cargos or RNA molecules will contribute to neuronal toxicity, leading to neurodegeneration and the manifestation of the disease (Ding and Sepehrimanesh, 2021).

4.1 KPNB1 modulates ataxin-3 levels and cleavage, whereas it does not affect its subcellular localization

Despite predominantly cytoplasmic localization of ataxin-3 (Antony et al., 2009), abnormal accumulation of ubiquitinated protein aggregates and formation of inclusions in neuronal nuclei containing the polyQ-expanded ataxin-3 is the pathological hallmark of SCA3 and other polyQ diseases (Ross and Poirier, 2004; Rüb et al., 2013; Taylor et al., 2002). Several lines of evidence point to the nucleus as the preferential site of aggregation, toxicity, and pathology

of polyQ-expanded ataxin-3 (Schmidt et al., 1998; Yang et al., 2002). It was shown that nuclear localization of ataxin-3 plays a crucial role in the manifestation of symptoms. Directing polyQ-expanded ataxin-3 into the nucleus promotes the formation of inclusions and the disease phenotype in an SCA3 mouse model, while preventing nuclear localization of polyQ-expanded ataxin-3 alleviates many disease features (Bichelmeier et al., 2007). It is proposed that the intrinsically lower activity of the neuronal nuclear ubiquitin-proteasome system (UPS) may account for the preferential nuclear accumulation of polyQ-expanded proteins in neurons (Tydlacka et al., 2008), although the exact underlying mechanisms remained enigmatic. In this regard, evaluation of the nucleocytoplasmic transport in SCA3 and other polyQ diseases might unravel its pathological implications and therapeutic targetability.

Nucleocytoplasmic transport of protein cargos between the cytoplasm and nucleus involves the recognition of nuclear localization signals (NLSs) or nuclear export signals (NESs) of protein cargos by a family of nuclear transport receptors referred to as karyopherins. The classical import pathway across the nuclear/cytoplasmic border is mediated by the karyopherin β family (KPNBs) that binds to the cargos directly or through adaptor proteins, the karyopherin α family (KPNAs) (Cautain et al., 2015; Chook and Blobel, 2001). Ataxin-3 is known to possess a putative NLS and two NESs, which might be implicated in the nuclear shuttling of this protein (Antony et al., 2009; Breuer et al., 2010). Nonetheless, the molecular mechanism implicated in the nucleocytoplasmic transport of ataxin-3 and its contribution to the pathogenesis of SCA3 is not fully understood.

Recently, there has been a growing appreciation for the idea that dysregulation of nucleocytoplasmic transport and defects in maintaining discrete nuclear and cytoplasmic compartments are involved in the pathogenesis of various neurodegenerative diseases. The impairment of nucleocytoplasmic transport machinery has been demonstrated in different models of neurodegenerative diseases, including Drosophila (Steyaert et al., 2018), mouse (Gasset-Rosa et al., 2017), and patient-derived induced pluripotent stem cells (iPSCs) (Gasset-Rosa et al., 2019). Previous studies demonstrated severe mislocalization and aggregation of nucleoporins and impairment of nucleocytoplasmic transport in HD (Gasset-Rosa et al., 2017; Grima et al., 2017). A close relationship between perturbed nuclear pore complexes (NPCs), changes in the nucleocytoplasmic transport, and the pathology of ALS has been revealed (Aizawa et al., 2019; Burk and Pasterkamp, 2019). Apart from this, defective

nucleocytoplasmic transport has been indicated in Alzheimer's disease (AD) (Eftekharzadeh et al., 2018), Parkinson's disease (PD) (Chen et al., 2020), frontotemporal dementia (FTD) (Zhang et al., 2015), and SCA1 (Zhang et al., 2020), which contributes to the neurotoxicity.

Previously, based on *in vitro* and *in vivo* studies, our group reported that karyopherin subunit alpha-3 (KPNA3) controls the localization of ataxin-3 and plays a key role in the SCA3-related phenotypes in Drosophila and mouse models. It was indicated that KPNA3 is involved in the pathogenesis and progression of SCA3, as modulation of this protein influences both pathogenic mechanisms, such as intracellular localization and aggregation of ataxin-3 (Figure 4.1), and manifestations of SCA3, such as anxiety, total activity, and gait abnormalities (Sowa et al., 2018). Importantly, KPNA3 functions as an adaptor protein for karyopherin subunit beta-1 (KPNB1) in the nuclear transport of various cargos (Cautain et al., 2015), raising the possibility that KPNB1 could be implicated in the subcellular localization and modulation of ataxin-3 protein, thereby pathogenesis of SCA3 as well. To test this hypothesis, we employed a GST pull-down assay to investigate whether wild-type (15Q) and polyQ-expanded (77Q) ataxin-3 interacts directly with nuclear transport receptor KPNB1 as well as karyopherin subunit alpha-2 (KPNA2) and KPNA3. The result indicated a direct interaction between both wild-type and polyQ-expanded ataxin-3 with three different nuclear transport receptors, KPNB1, KPNA2, and KPNA3. The interaction of ataxin-3 with nuclear transport receptors, both beta and alpha families, provides evidence for the concept that the classical import pathway mediated by importin α and importin β is likely involved in the nuclear transport of both wild-type and polyQ-expanded ataxin-3.

Given that KPNB1 is able to bind to protein cargos directly or through adaptor proteins importin α to transport cargos between the cytoplasm and nucleus through the nuclear pore complexes (Cautain et al., 2015; Chook and Blobel, 2001), and we could confirm the interaction of wild-type and polyQ-expanded ataxin-3 with KPNB1, we were encouraged to assess if modulation of KPNB1 can affect the subcellular localization of ataxin-3 using fluorescence microscopy and nucleocytoplasmic fractionation assay. KPNB1 is known as an importin that shuttles protein cargos from the cytoplasm into the nucleus; thereby, we expected that KPNB1 overexpression results in an increase in the amount of nuclear ataxin-3, whereas KPNB1 knockdown has an opposite effect, leading to a reduction in nuclear ataxin-3. To our surprise, our findings demonstrated that neither overexpression nor knockdown of

KPNB1 using esiRNA shows any significant alteration of the intracellular distribution of ataxin-3 in HEK293T cells, although modulation of KPNB1 levels can apparently affect protein levels of either wild-type or polyQ-expanded ataxin-3. Additionally, western blot analysis of the nucleocytoplasmic fractionation assay revealed the generation of specific ataxin-3 fragments upon KPNB1 overexpression, which was mainly visible in the cytoplasmic fraction of the cells. KPNB1 has been described as a multifunctional protein involved in various cellular processes and mechanisms (Harel and Forbes, 2004; Mosammaparast and Pemberton, 2004; Zhong et al., 2011), and these data indicate that KPNB1 has the potential to influence both wild-type and polyQ-expanded ataxin-3 through a mechanism that does not appear to implicate the intracellular localization of this protein, suggesting a new role for this nuclear transport receptor.

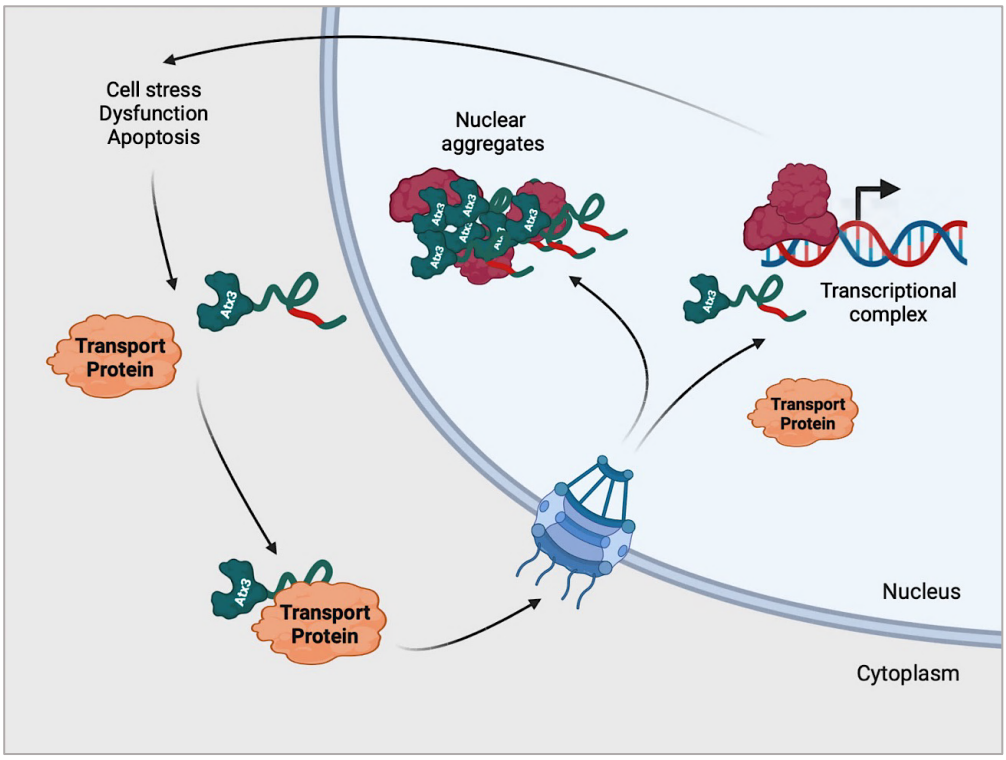

Figure 4.1 KPNA3 is a key player in the nuclear localization of ataxin-3 and is involved in the pathogenesis of SCA3. Modulation of KPNA3 affects pathogenic mechanisms, such as intracellular localization and aggregation of ataxin-3. Cell stress leads to expanded ataxin-3 being recruited into the nucleus, which is mediated by the transport protein KPNA3. Expanded ataxin-3 is not able to properly function as a transcriptional regulator and forms aggregates in the nucleus that recruit other proteins, leading to more cellular stress and damage. Created with BioRender.com. Modified from Sowa et al., 2018.

Observing the potential effects of KPNB1 modulation on ataxin-3 protein levels and cleavage in the nucleocytoplasmic fractionation assays motivated us to analyze in detail if alteration of KPNB1 levels with overexpression and knockdown of this protein has any robust effects on wild-type and polyQ-expanded ataxin-3. First, we investigated the effect of KPNB1 overexpression on ataxin-3 levels using western blotting. Our result revealed a marked reduction of both wild-type and polyQ-expanded ataxin-3 soluble levels and enhancement of ataxin-3 cleavage upon KPNB1 overexpression. Detection of ataxin-3 using specific antibodies displayed that ataxin-3 fragments induced by KPNB1 overexpression are C-terminal and contain the polyQ tract. Ataxin-3-derived C-terminal fragments have been identified both in the brains of SCA3 patients, mainly in the cerebellum and substantia nigra, and in the brain of a SCA3 mouse model (Goti et al., 2004).

Further analysis demonstrated that the enhancement of ataxin-3 fragmentation as well as the ataxin-3-lowering effect of KPNB1 were time-dependent. As these effects were observed on both wild-type and polyQ-expanded ataxin-3, we believe that the effect of KPNB1 overexpression on ataxin-3 is not polyglutamine-specific. KPNB1 overexpression lowered protein levels of ataxin-3, and this effect was not compromised by mutating the FxFG binding site of KPNB1, indicating a nuclear transport function-independent mechanism behind ataxin-3 reduction, which confirms the result of nucleocytoplasmic fractionation assays. In addition, our results highlighted that protein levels of ataxin-3 are generally yet specifically lowered by KPNB1 overexpression, as it was observed on both overexpressed and endogenous ataxin-3, whereas no effect was shown on GFP levels as a control protein. The above findings propose activation of a proteolytic pathway upon KPNB1 overexpression. However, KPNB1 does not have any protease function; therefore, we speculate that the effect of KPNB1 on ataxin-3 levels and cleavage might be an indirect effect.

We further explore the impact of KPNB1 knockdown and pharmacological inhibition on both wild-type and polyQ-expanded ataxin-3. In contrast to the result of KPNB1 overexpression, KPNB1 knockdown using esiRNA and its pharmacological inhibition using importazole led to an increase in ataxin-3 protein levels. Given that KPNB1 knockdown and pharmacological inhibition modulated both wild-type and polyQ-expanded ataxin-3, it seems to be a polyQ-independent and therefore physiological mechanism. These alterations yield KPNB1 as a

putative modulator of ataxin-3 protein levels, independent of the KPNB1 nuclear transport function.

4.2 The nature of KPNB1-induced ataxin-3 fragments

We confirmed that KPNB1 overexpression leads to the enhancement of ataxin-3 cleavage and the production of C-terminal fragments that were observed both in wild-type and polyQ-expanded ataxin-3, suggesting a polyQ-independent mechanism. However, these fragments were more prominent in wild-type ataxin-3, which can be explained by the sequestration of polyQ-expanded ataxin-3 into the aggregates and their lower availability to the proteolytic mechanisms. Proteolytic cleavage of polyQ-expanded ataxin-3 results in the production of fragments that are highly susceptible to aggregation, primarily in the nucleus, which induces cellular toxicity (Ross et al., 1999; Simões et al., 2012; Weber et al., 2017). Nucleocytoplasmic fractionation assays indicated that ataxin-3 fragments induced by KPNB1 overexpression localize in the cytoplasm, which might be degraded faster than fragments localized in the nucleus, thereby decreasing the toxicity of these fragments. Moreover, our results indicated that these fragments are likely degraded by autophagy, as inhibition of this protein quality control mechanism resulted in the accumulation of ataxin-3 fragments induced by KPNB1 overexpression.

Since KPNB1 is not a protease, we speculated that the enhancement of ataxin-3 cleavage upon KPNB1 overexpression is likely associated with the activation of proteases or proteolytic pathways. It is widely thought that activation of two classes of cysteine proteases, caspases and calpains, enhances the proteolytic cleavage of ataxin-3 and the generation of toxic fragments, eventually overwhelming protein quality control pathways and causing cell toxicity. Indeed, activation of caspases and calpains plays an important role in the pathogenesis of SCA3 and other polyQ diseases (Berke et al., 2004; Haacke et al., 2006; Matos et al., 2017). However, we could not substantiate an involvement of either class of proteases in ataxin-3 fragmentation upon KPNB1 overexpression, as proteolytic cleavage of α-spectrin, which is a natural substrate of caspases and calpains, was not promoted in KPNB1-overexpressing cells, and inhibition of these proteases could not prevent the generation of ataxin-3 fragments induced by KPNB1 overexpression. We further explored the implication of calpains by comparing the KPNB1-mediated fragmentation pattern of ataxin-3 with the

cleavage pattern of ataxin-3 induced by activation of calpains using ionomycin. Our results revealed that KPNB1 overexpression-induced ataxin-3 fragments are not linked to the activation of calpains, as they showed a different pattern from fragments induced by this protease, implying the contribution of a yet unknown proteolytic enzyme.

Damaged proteins are subjected to degradation by the ubiquitin-proteasome system (UPS) or autophagy, key components of the protein clearance mechanisms (Vilchez, 2014). Autophagy is essential for the maintenance of cellular survival and homeostasis, and impairment of autophagic activity has been indicated in many proteostasis disorders, such as neurodegenerative diseases, which contributes to their pathogenesis (Sridhar et al., 2012). Ataxin-3 has been described as a substrate for proteasomal degradation and autophagy, and disruption of both pathways has been associated with SCA3 pathogenesis (Blount et al., 2014; Chai et al., 1999; Onofre et al., 2016; Sittler et al., 2018).

We postulated that reduction of ataxin-3 levels and enhancement of its fragmentation might be linked to the activation of autophagic or proteasomal degradation in KPNB1-overexpressing cells. However, none of the classical proteolytic pathways appeared to be triggered by KPNB1 overexpression, as inhibition of autophagy and proteasomal degradation did not abolish the effect of KPNB1 overexpression on ataxin-3. Furthermore, KPNB1 overexpression did not affect the levels of autophagy markers LC3B-II and p62, implying no alteration in the autophagic flux in these cells. Altogether, it seems that the effect of KPNB1 overexpression on ataxin-3 does not occur via activation of the known SCA3-associated proteases or proteolytic pathways.

4.3 KPNB1 modulates the aggregation of ataxin-3

A common and prominent feature among polyglutamine diseases is the formation of neuronal inclusions mainly consist of the polyQ-expanded protein, suggesting protein misfolding and aggregation as a central mechanism in the pathogenesis of these diseases (Berke et al., 2004; Taylor et al., 2002; Williams and Paulson, 2008). Notably, the polyQ length threshold for aggregation determines the threshold length for polyglutamine diseases (Paulson, 2012). *In vitro* studies provide evidence that the expansion of polyQ tract alters the native conformation of polyQ proteins, leading to an increased amyloid-like structure and formation of aggregates (Chen et al., 2002; Kayed et al., 2003). Consistent with this

observation, polyQ-expanded ataxin-3 adopts amyloid-like conformations and forms aggregates *in vitro* (Bevivino and Loll, 2001).

It has been shown that the impairment of cellular quality control mechanisms including chaperone-mediated protein folding, ubiquitin-proteasome mediated protein degradation, and autophagy-lysosome, have a key role in protein misfolding and aggregation in SCA3 and other polyglutamine diseases. These mechanisms maintain a functional proteome and assist proteins in refolding or disaggregating in case that they fail to achieve their native conformation. If the concentration of misfolded proteins exceeds cellular folding and degradative capacity, these proteins can accumulate and form insoluble aggregates, which impair cell function and tissue homeostasis (Paulson, 2012; Vilchez et al., 2014; Williams and Paulson, 2008).

Our findings regarding the effect of KPNB1 modulation on ataxin-3 levels and cleavage, motivated us to investigate if modulation of this nuclear transporter might influence the aggregation propensity of polyQ-expanded ataxin-3 which is the main pathological hallmark of SCA3. Accordingly, fluorescence microscopy and filter retardation assay demonstrated that KPNB1 overexpression reduced aggregation load of polyQ-expanded ataxin-3. Further analysis indicated that this effect is a nuclear transport function-independent mechanism, as mutation of the FxFG binding site of KPNB1 did not abolish its effect on ataxin-3 aggregation. Additionally, overexpression of KPNB1 improved the viability of cells expressing polyQ-expanded ataxin-3 as analyzed by PrestoBlue assay. The enhancement of cell viability in these cells can be explained by less aggregation load of polyQ-expanded ataxin-3, leading to less cell toxicity. Contracting KPNB1 overexpression, either knockdown or pharmacological inhibition of this nuclear transporter using importazole increased ataxin-3 aggregates.

As we observed a modulation of full-length ataxin-3 upon KPNB1 overexpression or knockdown/pharmacological inhibition, we concluded that the alterations of polyQ-expanded ataxin-3 aggregates were due to the changes of soluble levels of this protein. It has been shown that concentration of polyQ-expanded ataxin-3 has direct consequences for formation of aggregates (Pozzi et al., 2008).

4.4 KPNB1 influences ataxin-3 levels and fragmentation via the mitochondrial protease CLPP

Our findings demonstrated that KPNB1 overexpression modulates the ataxin-3 protein. To figure out which regulators or cellular pathways might be involved in this effect, RNA sequencing was performed, and no alteration in the gene expression of ataxin-3 was detected upon KPNB1 overexpression, implying the reduction of ataxin-3 protein levels is not associated with the modulation of its gene expression. Additionally, we could not link the modulated canonical pathways revealed by the Ingenuity Pathway Analysis to the modulation of ataxin-3 in KPNB1-overexpressing cells.

To further dissect the KPNB1-mediated effects on levels and proteolysis of ataxin-3, we conducted unbiased label-free quantitative proteomics, followed by the Ingenuity Pathway Analysis to get insight into the activation and inhibition of upstream regulators or canonical pathways upon KPNB1 overexpression. Our analysis determined the potential activation of the ATP-dependent Clp protease proteolytic subunit (CLPP) upon KPNB1 overexpression in both wild-type and polyQ-expanded ataxin-3-expressing cells. This prediction was based on a significant down-regulation of some mitochondrial resident proteins, which can be cleaved by activation of the mitochondrial protease CLPP.

Mitochondrial proteases, or mitoproteases, are important regulatory components that perform highly regulated proteolytic reactions and degrade proteins that fail to fold or assemble properly. Mitoproteases are highly specific and are central regulatory components in quality control and mitochondrial function and integrity, such as activation of mitochondrial proteins, mitochondrial biogenesis, mitophagy, and apoptosis (Bulteau and Bayot, 2011; Quirós et al., 2015). Impaired function of mitoproteases is implicated in aging, metabolic syndromes, cancer, and neurodegenerative diseases including PD, SCA, and spastic paraplegia (Martinelli and Rugarli, 2010; Quirós et al., 2015; Rugarli and Langer, 2012).

The accumulation of unfolded or misfolded proteins in the mitochondria triggers a mitochondrial unfolded protein response (UPR^{mt}), leading to the induction of nuclear expression of mitochondrial protective genes, including mitochondrial chaperones and proteases. The ATP-dependent Clp protease proteolytic subunit (CLPP) is a mitoprotease that is highly conserved and plays a pivotal role in protein homeostasis and bioenergetic activity.

CLPP forms a proteasome-like cylinder together with the chaperone ATP-dependent Clp protease ATP-binding subunit ClpX-like (CLPX), which is called the CLPXP complex. CLPXP and Lon are ATPase Associated with diverse cellular Activities (AAA) proteases located within the mitochondrial matrix (Sauer and Baker, 2011; Tatsuta and Langer, 2009). This mitochondrial protease plays a pivotal role in UPR^{mt} signaling, and knockdown of CLPP perturbs the induction of mitochondrial chaperone genes during mitochondrial stress (Haynes et al., 2007; Pellegrino et al., 2013; Zhao et al., 2002). Mitochondrial protease CLPP is implicated in the degradation and regulation of the synthesis of proteins and enzymes that are related to mitochondrial translation, metabolic pathways such as the tricarboxylic acid cycle, and the electron transport chain (Fischer et al., 2015; Szczepanowska et al., 2016). Nonetheless, little is known about the substrates and involvement of this mitochondrial protease in cellular pathways and mechanisms in mammals.

The implication of the mitochondrial protease CLPP has been indicated in aging and disease (Fischer et al., 2015; Jenkinson et al., 2013; Rath et al., 2012). CLPP null mice presented accumulation of CLPX and mtDNA, leading to infertility, auditory deficits, and growth retardation (Gispert et al., 2013). Moreover, the protein levels of CLPP are reduced in PD patient post-mortem brains, induced neurons derived from PD patients, and α-synuclein-expressing cell cultures. In fact, loss of CLPP leads to the accumulation of misfolded proteins, disruption of the mitochondrial respiratory chain, promotion of oxidative products, and ultimately cell death (Hu et al., 2019).

We could corroborate our findings by esiRNA-mediated knockdown of CLPP in KPNB1-overexpressing cells, which resulted in the restoration of soluble and aggregated forms of ataxin-3. Not surprisingly, since the dysfunction of mitochondria and bioenergetic alterations are common features of neurodegenerative diseases, the implications of CLPP have been demonstrated in these diseases (Fischer et al., 2015; Guillon et al., 2009; Hu et al., 2019). Previous investigations have shown that loss of CLPP is implicated in α-synuclein-associated pathology in neurons derived from PD patient iPS cells. Conversely, overexpression of CLPP reduces α-synuclein-induced mitochondrial oxidative stress and inhibits the accumulation of S129-phosphorylated α-synuclein, leading to the promotion of neuronal morphology in these cells (Hu et al., 2019). In line with these findings, overexpression of CLPP decreased ataxin-3 protein levels, which was further enhanced by KPNB1 cotransfection in these cells, while

knockdown of CLPP increased ataxin-3 levels. These findings suggest that KPNB1 overexpression triggers proteolytic degradation of ataxin-3 via activation of the mitochondrial protease CLPP and consequently lowers protein levels and aggregation of this protein, whereas its knockdown or pharmacological inhibition has an opposite effect (Figure 4.2).

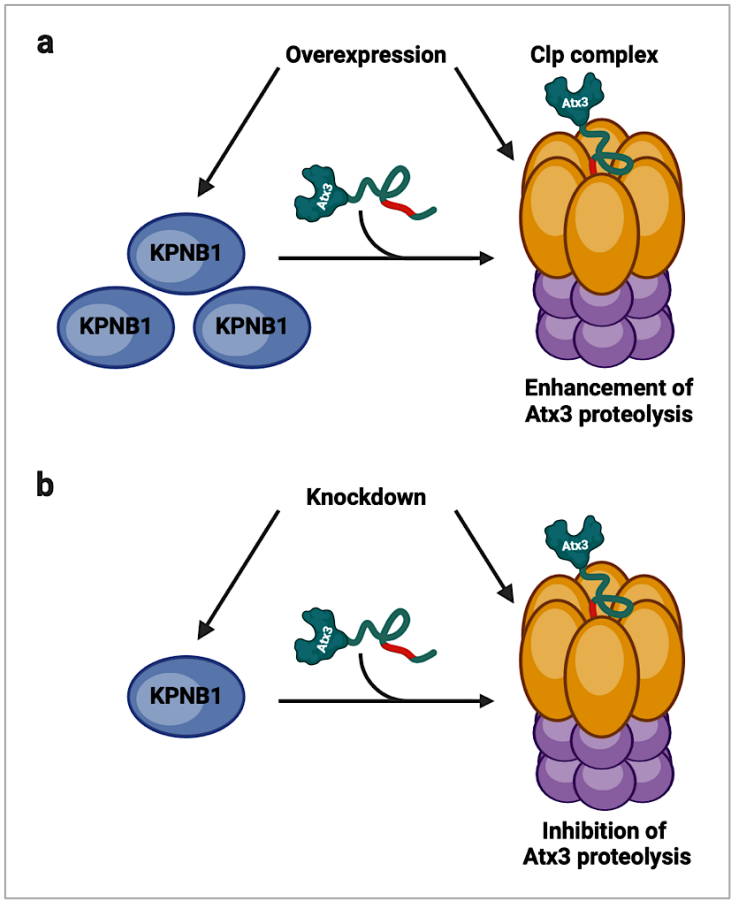

Figure 4.2 Schematic overview of the proposed ataxin-3 degrading pathway mediated by KPNB1 and mitochondrial protease CLPP. (**a**) Overexpression of KPNB1 triggers proteolytic degradation of ataxin-3 via mitochondrial protease CLPP activation, leading to the reduction of ataxin-3 protein levels. Additionally, CLPP overexpression impacts ataxin-3 protein levels in the same manner. Cleavage of the peptides by the protease component of the Clp complex is an ATP-dependent process (Bouchnak and van Wijk, 2021). (**b**) Either knockdown or pharmacological inhibition of KPNB1 as well as knockdown of CLPP prevent degradation of ataxin-3 via the suggested pathway. Created with BioRender.com. Modified from Abeditashi et al., 2022.

The potential site of intersection between the mitochondrially localized CLPP and the nucleocytoplasmic localization of ataxin-3 remains obscure. Although both wild-type and polyQ-expanded ataxin-3 have been shown to be associated with or localized in mitochondria (Kristensen et al., 2018; Pozzi et al., 2008). Importantly, some mitochondrial proteins have

been identified as interaction partners of wild-type and/or polyQ-expanded ataxin-3, such as cytochrome C oxidase subunit NDUFA4 (NDUFA4), succinate dehydrogenase complex subunits A and B (SDHA and SDHB), and cytochrome C oxidase assembly factor 7 (COA7) (Kristensen et al., 2018; Laço et al., 2012). In addition, ataxin-3 has been proposed as a crucial component of the canonical parkin-mediated mitophagy (Harmuth et al., 2022). These findings put emphasis on the possibility of ataxin-3 cleavage by the mitochondrial protease CLPP.

Aside from its role as a nuclear transport protein, KPNB1 has been described as a multifunctional protein involved in cell cycle control, mitosis and replication, promoting endoplasmic-reticulum-associated degradation (ERAD), and also functioning as a chaperone that prevents the aggregation of some proteins (Harel and Forbes, 2004; Mosammaparast and Pemberton, 2004; Zhong et al., 2011). The herein described activation of a mitochondrial protease, such as CLPP, and thereby the induction of proteolytic turnover would represent a new addition to the functional repertoire of KPNB1.

4.5 Dysregulation of KPNB1 and CLPP in SCA3 models

Karyopherin abnormalities have been identified in various neurodegenerative diseases, such as amyotrophic lateral sclerosis (ALS), frontotemporal dementia (FTD), Alzheimer's disease (AD), Parkinson's disease (PD), as well as in cell and animal models of polyQ diseases that vary from altered levels to intracellular mislocalization and aggregation (Chan et al., 2011; Chou et al., 2018; Lee et al., 2006; Ma et al., 2014; Nishimura et al., 2010; Solomon et al., 2018). Indeed, karyopherin abnormalities are associated with protein mislocalization and aggregate formation in neurodegenerative diseases (Pasha et al., 2021).

Defects in the nucleocytoplasmic shuttling of ataxin-3 were suggested as a pathological mechanism in SCA3 (Macedo-Ribeiro et al., 2009). Interestingly, we observed reduced KPNB1 protein levels in the neuronal tissue of two different SCA3 transgenic mouse models as well as iPSCs derived from SCA3 patients, which provides evidence for a pathological dysregulation of this karyopherin in SCA3. Dysregulation of KPNB1 has been linked to neurodegenerative diseases and several types of cancer (Pasha et al., 2021; van der Watt et al., 2009; Yang et al., 2015). In line with our findings, reduced levels of KPNB1 were found in the spinal cord of ALS patients (Yamashita et al., 2017). Additionally, it was demonstrated that knockdown of KPNB1

and cellular apoptosis susceptibility (CAS) can disrupt the classical nuclear import of TDP-43, leading to the cytoplasmic accumulation of this protein (Nishimura et al., 2010). Up-regulation of KPNB1 and XPO5/exportin-5 was detected in AD, and both karyopherins co-localized with hyperphosphorylated tau (Nuovo et al., 2018). Moreover, aggregation of KPNA2/Importin α-1 has been observed in AD tangles (Carter, 2011). These data suggest that karyopherin abnormalities play a pivotal role in the pathology related to neurodegenerative diseases, thereby highlighting karyopherins as candidates for the development of therapeutic strategies.

Since mitochondrial dysfunction has been shown in SCA3 (Laço et al., 2012; Yu et al., 2009), we investigated CLPP protein levels in iPSCs derived from SCA3 patients, and reduced levels of this mitochondrial protease were revealed in these cells. Down-regulation of CLPP mRNA and protein levels has been indicated in hereditary spastic paraplegia patients (Hansen et al., 2008). Furthermore, CLPP protein levels reduce in PD models *in vitro* and *in vivo*, as well as in PD patient postmortem brains (Hu et al., 2019). Loss of mitochondrial protease CLPP in mice results in mitochondrial dysfunction, diminished spontaneous motor activity, inflammatory response, infertility, respiratory deficiency caused by ineffective mitochondrial protein synthesis, and decreased survival (Gispert et al., 2013; Szczepanowska et al., 2016). These findings provide evidence for the implication of CLPP in both maintaining mitochondrial quality and neurodegenerative diseases such as SCA3 and suggest CLPP as a useful therapeutic target for neurodegenerative proteinopathies.

5. Conclusion

In conclusion, our study indicated KPNB1 as an interaction partner of wild-type and polyQ-expanded ataxin-3, although modulation of this nuclear transport receptor did not alter the subcellular localization of ataxin-3. Interestingly, KPNB1 modulation influenced protein levels and aggregate formation of ataxin-3 by a proteolytic event independent of known SCA3-associated proteolytic pathways. Unbiased label-free quantitative proteomics, followed by the Ingenuity Pathway Analysis (IPA), suggested activation of the ATP-dependent Clp protease proteolytic subunit (CLPP) upon KPNB1 overexpression. Consequently, esiRNA-mediated knockdown of CLPP counteracted the KPNB1 overexpression-induced reduction of ataxin-3 protein levels and aggregation, whereas CLPP overexpression promoted the KPNB1-mediated ataxin-3 lowering. In addition, we identified a reduction in KPNB1 protein levels in two different SCA3 transgenic mouse models and decreased levels of both KPNB1 and CLPP in induced pluripotent stem cells (iPSCs) of SCA3 patients. Our data suggest KPNB1 as a new putative modulator of soluble and aggregated ataxin-3, which triggers proteolytic degradation of this protein via activation of the mitochondrial protease CLPP. Therefore, it is reasonable to consider KPNB1 and CLPP as potential therapeutic targets for the treatment of SCA3 and other neurodegenerative proteinopathies.

References

Abeditashi, M., Weber, J.J., Pereira Sena, P., Velic, A., Kalimeri, M., Incebacak Eltemur, R.D., Schmidt, J., Hübener-Schmid, J., Hauser, S., Macek, B., et al. (2022). KPNB1 modulates the Machado-Joseph disease protein ataxin-3 through activation of the mitochondrial protease CLPP. Cell Mol Life Sci *79*, 401. 10.1007/s00018-022-04372-5.

Adanyeguh, I.M., Henry, P.G., Nguyen, T.M., Rinaldi, D., Jauffret, C., Valabregue, R., Emir, U.E., Deelchand, D.K., Brice, A., Eberly, L.E., et al. (2015). In vivo neurometabolic profiling in patients with spinocerebellar ataxia types 1, 2, 3, and 7. Mov Disord *30*, 662-670. 10.1002/mds.26181.

Aizawa, H., Yamashita, T., Kato, H., Kimura, T., and Kwak, S. (2019). Impaired Nucleoporins Are Present in Sporadic Amyotrophic Lateral Sclerosis Motor Neurons that Exhibit Mislocalization of the 43-kDa TAR DNA-Binding Protein. J Clin Neurol *15*, 62-67. 10.3988/jcn.2019.15.1.62.

Akçimen, F., Martins, S., Liao, C., Bourassa, C.V., Catoire, H., Nicholson, G.A., Riess, O., Raposo, M., França, M.C., Vasconcelos, J., et al. (2020). Genome-wide association study identifies genetic factors that modify age at onset in Machado-Joseph disease. Aging (Albany NY) *12*, 4742-4756. 10.18632/aging.102825.

Albrecht, M., Golatta, M., Wüllner, U., and Lengauer, T. (2004). Structural and functional analysis of ataxin-2 and ataxin-3. Eur J Biochem *271*, 3155-3170. 10.1111/j.1432-1033.2004.04245.x.

Alves-Rodrigues, A., Gregori, L., and Figueiredo-Pereira, M.E. (1998). Ubiquitin, cellular inclusions and their role in neurodegeneration. Trends Neurosci *21*, 516-520. 10.1016/s0166-2236(98)01276-4.

Andrade, M.A., and Bork, P. (1995). HEAT repeats in the Huntington's disease protein. Nat Genet *11*, 115-116. 10.1038/ng1095-115.

Antony, P.M., Mäntele, S., Mollenkopf, P., Boy, J., Kehlenbach, R.H., Riess, O., and Schmidt, T. (2009). Identification and functional dissection of localization signals within ataxin-3. Neurobiol Dis *36*, 280-292. 10.1016/j.nbd.2009.07.020.

Ashkenazi, A., Bento, C.F., Ricketts, T., Vicinanza, M., Siddiqi, F., Pavel, M., Squitieri, F., Hardenberg, M.C., Imarisio, S., Menzies, F.M., and Rubinsztein, D.C. (2017). Polyglutamine tracts regulate beclin 1-dependent autophagy. Nature *545*, 108-111. 10.1038/nature22078.

Baines, A.J. (2009). Evolution of spectrin function in cytoskeletal and membrane networks. Biochem Soc Trans *37*, 796-803. 10.1042/bst0370796.

Balasundaram, D., Benedik, M.J., Morphew, M., Dang, V.D., and Levin, H.L. (1999). Nup124p is a nuclear pore factor of Schizosaccharomyces pombe that is important for nuclear import and activity of retrotransposon Tf1. Mol Cell Biol *19*, 5768-5784. 10.1128/mcb.19.8.5768.

Bauer, P.O., and Nukina, N. (2009). The pathogenic mechanisms of polyglutamine diseases and current therapeutic strategies. J Neurochem *110*, 1737-1765. 10.1111/j.1471-4159.2009.06302.x.

Bayliss, R., Littlewood, T., and Stewart, M. (2000). Structural basis for the interaction between FxFG nucleoporin repeats and importin-beta in nuclear trafficking. Cell *102*, 99-108. 10.1016/s0092-8674(00)00014-3.

Bennett, V., and Lambert, S. (1991). The spectrin skeleton: from red cells to brain. J Clin Invest *87*, 1483-1489. 10.1172/jci115157.

Berke, S.J., Schmied, F.A., Brunt, E.R., Ellerby, L.M., and Paulson, H.L. (2004). Caspase-mediated proteolysis of the polyglutamine disease protein ataxin-3. J Neurochem *89*, 908-918. 10.1111/j.1471-4159.2004.02369.x.

Bettencourt, C., and Lima, M. (2011). Machado-Joseph Disease: from first descriptions to new perspectives. Orphanet Journal of Rare Diseases *6*, 35. 10.1186/1750-1172-6-35.

Bettencourt, C., Raposo, M., Ros, R., Montiel, R., Bruges-Armas, J., and Lima, M. (2013). Transcript diversity of Machado-Joseph disease gene (ATXN3) is not directly determined by SNPs in exonic or flanking intronic regions. J Mol Neurosci *49*, 539-543. 10.1007/s12031-012-9832-3.

Bettencourt, C., Santos, C., Montiel, R., Costa Mdo, C., Cruz-Morales, P., Santos, L.R., Simões, N., Kay, T., Vasconcelos, J., Maciel, P., and Lima, M. (2010). Increased transcript diversity: novel splicing variants of Machado-Joseph disease gene (ATXN3). Neurogenetics *11*, 193-202. 10.1007/s10048-009-0216-y.

Bevivino, A.E., and Loll, P.J. (2001). An expanded glutamine repeat destabilizes native ataxin-3 structure and mediates formation of parallel beta -fibrils. Proc Natl Acad Sci U S A *98*, 11955-11960. 10.1073/pnas.211305198.

Bichelmeier, U., Schmidt, T., Hübener, J., Boy, J., Rüttiger, L., Häbig, K., Poths, S., Bonin, M., Knipper, M., Schmidt, W.J., et al. (2007). Nuclear localization of ataxin-3 is required for the manifestation of symptoms in SCA3: in vivo evidence. J Neurosci *27*, 7418-7428. 10.1523/jneurosci.4540-06.2007.

Bilen, J., Liu, N., Burnett, B.G., Pittman, R.N., and Bonini, N.M. (2006). MicroRNA pathways modulate polyglutamine-induced neurodegeneration. Mol Cell *24*, 157-163. 10.1016/j.molcel.2006.07.030.

Birman, S. (2008). Neurodegeneration: RNA turns number one suspect in polyglutamine diseases. Curr Biol *18*, R659-r661. 10.1016/j.cub.2008.06.023.

Bischoff, F.R., Krebber, H., Kempf, T., Hermes, I., and Ponstingl, H. (1995). Human RanGTPase-activating protein RanGAP1 is a homologue of yeast Rna1p involved in mRNA processing and transport. Proceedings of the National Academy of Sciences *92*, 1749-1753. 10.1073/pnas.92.5.1749.

Bischoff, F.R., and Ponstingl, H. (1995). Catalysis of guanine nucleotide exchange of Ran by RCC1 and stimulation of hydrolysis of Ran-bound GTP by Ran-GAP1. Methods Enzymol *257*, 135-144. 10.1016/s0076-6879(95)57019-5.

Blount, J.R., Tsou, W.L., Ristic, G., Burr, A.A., Ouyang, M., Galante, H., Scaglione, K.M., and Todi, S.V. (2014). Ubiquitin-binding site 2 of ataxin-3 prevents its proteasomal degradation by interacting with Rad23. Nat Commun *5*, 4638. 10.1038/ncomms5638.

Boeddrich, A., Gaumer, S., Haacke, A., Tzvetkov, N., Albrecht, M., Evert, B.O., Müller, E.C., Lurz, R., Breuer, P., Schugardt, N., et al. (2006). An arginine/lysine-rich motif is crucial for VCP/p97-mediated modulation of ataxin-3 fibrillogenesis. Embo j *25*, 1547-1558. 10.1038/sj.emboj.7601043.

Borchert, N., Dieterich, C., Krug, K., Schütz, W., Jung, S., Nordheim, A., Sommer, R.J., and Macek, B. (2010). Proteogenomics of Pristionchus pacificus reveals distinct proteome structure of nematode models. Genome Res *20*, 837-846. 10.1101/gr.103119.109.

Bouchnak, I., and van Wijk, K.J. (2021). Structure, function, and substrates of Clp AAA+ protease systems in cyanobacteria, plastids, and apicoplasts: A comparative analysis. J Biol Chem *296*, 100338. 10.1016/j.jbc.2021.100338.

Boy, J., Schmidt, T., Wolburg, H., Mack, A., Nuber, S., Böttcher, M., Schmitt, I., Holzmann, C., Zimmermann, F., Servadio, A., and Riess, O. (2009). Reversibility of symptoms in a conditional mouse model of spinocerebellar ataxia type 3. Hum Mol Genet *18*, 4282-4295. 10.1093/hmg/ddp381.

Bradford, M.M. (1976). A rapid and sensitive method for the quantitation of microgram quantities of protein utilizing the principle of protein-dye binding. Anal Biochem *72*, 248-254. 10.1006/abio.1976.9999.

Breuer, P., Haacke, A., Evert, B.O., and Wüllner, U. (2010). Nuclear aggregation of polyglutamine-expanded ataxin-3: fragments escape the cytoplasmic quality control. J Biol Chem *285*, 6532-6537. 10.1074/jbc.M109.036335.

Browne, S.E., and Beal, M.F. (2006). Oxidative damage in Huntington's disease pathogenesis. Antioxid Redox Signal *8*, 2061-2073. 10.1089/ars.2006.8.2061.

Bulteau, A.L., and Bayot, A. (2011). Mitochondrial proteases and cancer. Biochim Biophys Acta *1807*, 595-601. 10.1016/j.bbabio.2010.12.011.

Burk, K., and Pasterkamp, R.J. (2019). Disrupted neuronal trafficking in amyotrophic lateral sclerosis. Acta Neuropathol *137*, 859-877. 10.1007/s00401-019-01964-7.

Burnett, B., Li, F., and Pittman, R.N. (2003). The polyglutamine neurodegenerative protein ataxin-3 binds polyubiquitylated proteins and has ubiquitin protease activity. Hum Mol Genet *12*, 3195-3205. 10.1093/hmg/ddg344.

Carter, C.J. (2011). Alzheimer's disease plaques and tangles: cemeteries of a pyrrhic victory of the immune defence network against herpes simplex infection at the expense of complement and inflammation-mediated neuronal destruction. Neurochem Int *58*, 301-320. 10.1016/j.neuint.2010.12.003.

Carvalho, D.R., La Rocque-Ferreira, A., Rizzo, I.M., Imamura, E.U., and Speck-Martins, C.E. (2008). Homozygosity enhances severity in spinocerebellar ataxia type 3. Pediatr Neurol *38*, 296-299. 10.1016/j.pediatrneurol.2007.12.006.

Cautain, B., Hill, R., de Pedro, N., and Link, W. (2015). Components and regulation of nuclear transport processes. Febs j *282*, 445-462. 10.1111/febs.13163.

Cemal, C.K., Carroll, C.J., Lawrence, L., Lowrie, M.B., Ruddle, P., Al-Mahdawi, S., King, R.H., Pook, M.A., Huxley, C., and Chamberlain, S. (2002). YAC transgenic mice carrying pathological alleles of the MJD1 locus exhibit a mild and slowly progressive cerebellar deficit. Hum Mol Genet *11*, 1075-1094. 10.1093/hmg/11.9.1075.

Chai, Y., Koppenhafer, S.L., Shoesmith, S.J., Perez, M.K., and Paulson, H.L. (1999). Evidence for proteasome involvement in polyglutamine disease: localization to nuclear inclusions in SCA3/MJD and suppression of polyglutamine aggregation in vitro. Hum Mol Genet *8*, 673-682. 10.1093/hmg/8.4.673.

Chai, Y., Shao, J., Miller, V.M., Williams, A., and Paulson, H.L. (2002). Live-cell imaging reveals divergent intracellular dynamics of polyglutamine disease proteins and supports a sequestration model of pathogenesis. Proc Natl Acad Sci U S A *99*, 9310-9315. 10.1073/pnas.152101299.

Chai, Y., Berke, S.S., Cohen, R.E., and Paulson, H.L. (2004). Poly-ubiquitin binding by the polyglutamine disease protein ataxin-3 links its normal function to protein surveillance pathways. J Biol Chem *279*, 3605-3611. 10.1074/jbc.M310939200.

Chan, W.M., Tsoi, H., Wu, C.C., Wong, C.H., Cheng, T.C., Li, H.Y., Lau, K.F., Shaw, P.C., Perrimon, N., and Chan, H.Y. (2011). Expanded polyglutamine domain possesses nuclear export activity which modulates subcellular localization and toxicity of polyQ disease protein via exportin-1. Hum Mol Genet *20*, 1738-1750. 10.1093/hmg/ddr049.

Chandel, N.S. (2015). Evolution of Mitochondria as Signaling Organelles. Cell Metab *22*, 204-206. 10.1016/j.cmet.2015.05.013.

Chatterjee, A., Saha, S., Chakraborty, A., Silva-Fernandes, A., Mandal, S.M., Neves-Carvalho, A., Liu, Y., Pandita, R.K., Hegde, M.L., Hegde, P.M., et al. (2015). The role of the mammalian DNA end-processing enzyme polynucleotide kinase 3'-phosphatase in spinocerebellar ataxia type 3 pathogenesis. PLoS Genet *11*, e1004749. 10.1371/journal.pgen.1004749.

Chen, S., Ferrone, F.A., and Wetzel, R. (2002). Huntington's disease age-of-onset linked to polyglutamine aggregation nucleation. Proc Natl Acad Sci U S A *99*, 11884-11889. 10.1073/pnas.182276099.

Chen, V., Moncalvo, M., Tringali, D., Tagliafierro, L., Shriskanda, A., Ilich, E., Dong, W., Kantor, B., and Chiba-Falek, O. (2020). The mechanistic role of alpha-synuclein in the nucleus: impaired nuclear function caused by familial Parkinson's disease SNCA mutations. Hum Mol Genet *29*, 3107-3121. 10.1093/hmg/ddaa183.

Choo, Y.S., Johnson, G.V., MacDonald, M., Detloff, P.J., and Lesort, M. (2004). Mutant huntingtin directly increases susceptibility of mitochondria to the calcium-induced permeability transition and cytochrome c release. Hum Mol Genet *13*, 1407-1420. 10.1093/hmg/ddh162.

Chook, Y.M., and Blobel, G. (2001). Karyopherins and nuclear import. Curr Opin Struct Biol *11*, 703-715. 10.1016/s0959-440x(01)00264-0.

Chook, Y.M., and Süel, K.E. (2011). Nuclear import by karyopherin-βs: recognition and inhibition. Biochim Biophys Acta *1813*, 1593-1606. 10.1016/j.bbamcr.2010.10.014.

Chou, A.H., Yeh, T.H., Ouyang, P., Chen, Y.L., Chen, S.Y., and Wang, H.L. (2008). Polyglutamine-expanded ataxin-3 causes cerebellar dysfunction of SCA3 transgenic mice by inducing transcriptional dysregulation. Neurobiol Dis *31*, 89-101. 10.1016/j.nbd.2008.03.011.

Chou, C.C., Zhang, Y., Umoh, M.E., Vaughan, S.W., Lorenzini, I., Liu, F., Sayegh, M., Donlin-Asp, P.G., Chen, Y.H., Duong, D.M., et al. (2018). TDP-43 pathology disrupts nuclear pore complexes and nucleocytoplasmic transport in ALS/FTD. Nat Neurosci *21*, 228-239. 10.1038/s41593-017-0047-3.

Chung, C.H., and Baek, S.H. (1999). Deubiquitinating enzymes: their diversity and emerging roles. Biochem Biophys Res Commun *266*, 633-640. 10.1006/bbrc.1999.1880.

Ciechanover, A. (1994). The ubiquitin-proteasome proteolytic pathway. Cell *79*, 13-21. 10.1016/0092-8674(94)90396-4.

Cingolani, G., Petosa, C., Weis, K., and Müller, C.W. (1999). Structure of importin-beta bound to the IBB domain of importin-alpha. Nature *399*, 221-229. 10.1038/20367.

Conti, E., and Izaurralde, E. (2001). Nucleocytoplasmic transport enters the atomic age. Curr Opin Cell Biol *13*, 310-319. 10.1016/s0955-0674(00)00213-1.

Cornett, J., Cao, F., Wang, C.E., Ross, C.A., Bates, G.P., Li, S.H., and Li, X.J. (2005). Polyglutamine expansion of huntingtin impairs its nuclear export. Nat Genet *37*, 198-204. 10.1038/ng1503.

Costa Mdo, C., and Paulson, H.L. (2012). Toward understanding Machado-Joseph disease. Prog Neurobiol *97*, 239-257. 10.1016/j.pneurobio.2011.11.006.

Coutinho, P., and Andrade, C. (1978). Autosomal dominant system degeneration in Portuguese families of the Azores Islands. A new genetic disorder involving cerebellar, pyramidal, extrapyramidal and spinal cord motor functions. Neurology *28*, 703-709. 10.1212/wnl.28.7.703.

Cox, J., and Mann, M. (2008). MaxQuant enables high peptide identification rates, individualized p.p.b.-range mass accuracies and proteome-wide protein quantification. Nat Biotechnol *26*, 1367-1372. 10.1038/nbt.1511.

Cox, J., Neuhauser, N., Michalski, A., Scheltema, R.A., Olsen, J.V., and Mann, M. (2011). Andromeda: a peptide search engine integrated into the MaxQuant environment. J Proteome Res *10*, 1794-1805. 10.1021/pr101065j.

Cronshaw, J.M., Krutchinsky, A.N., Zhang, W., Chait, B.T., and Matunis, M.J. (2002). Proteomic analysis of the mammalian nuclear pore complex. J Cell Biol *158*, 915-927. 10.1083/jcb.200206106.

Cummings, C.J., Mancini, M.A., Antalffy, B., DeFranco, D.B., Orr, H.T., and Zoghbi, H.Y. (1998). Chaperone suppression of aggregation and altered subcellular proteasome localization imply protein misfolding in SCA1. Nat Genet *19*, 148-154. 10.1038/502.

Cummings, C.J., and Zoghbi, H.Y. (2000). Trinucleotide repeats: mechanisms and pathophysiology. Annu Rev Genomics Hum Genet *1*, 281-328. 10.1146/annurev.genom.1.1.281.

Da Silva, J.D., Teixeira-Castro, A., and Maciel, P. (2019). From Pathogenesis to Novel Therapeutics for Spinocerebellar Ataxia Type 3: Evading Potholes on the Way to Translation. Neurotherapeutics *16*, 1009-1031. 10.1007/s13311-019-00798-1.

Damelin, M., and Silver, P.A. (2000). Mapping interactions between nuclear transport factors in living cells reveals pathways through the nuclear pore complex. Mol Cell *5*, 133-140. 10.1016/s1097-2765(00)80409-8.

De Strooper, B. (2010). Proteases and proteolysis in Alzheimer disease: a multifactorial view on the disease process. Physiol Rev *90*, 465-494. 10.1152/physrev.00023.2009.

Di Francesco, L., Verrico, A., Asteriti, I.A., Rovella, P., Cirigliano, P., Guarguaglini, G., Schininà, M.E., and Lavia, P. (2018). Visualization of human karyopherin beta-1/importin beta-1 interactions with protein partners in mitotic cells by co-immunoprecipitation and proximity ligation assays. Sci Rep *8*, 1850. 10.1038/s41598-018-19351-9.

Ding, B., Akter, M., and Zhang, C.L. (2020). Differential Influence of Sample Sex and Neuronal Maturation on mRNA and Protein Transport in Induced Human Neurons. Front Mol Neurosci *13*, 46. 10.3389/fnmol.2020.00046.

Ding, B., and Sepehrimanesh, M. (2021). Nucleocytoplasmic Transport: Regulatory Mechanisms and the Implications in Neurodegeneration. Int J Mol Sci *22*. 10.3390/ijms22084165.

Ding, B., Tang, Y., Ma, S., Akter, M., Liu, M.L., Zang, T., and Zhang, C.L. (2021). Disease Modeling with Human Neurons Reveals LMNB1 Dysregulation Underlying DYT1 Dystonia. J Neurosci *41*, 2024-2038. 10.1523/jneurosci.2507-20.2020.

Dingwall, C., Robbins, J., Dilworth, S.M., Roberts, B., and Richardson, W.D. (1988). The nucleoplasmin nuclear location sequence is larger and more complex than that of SV-40 large T antigen. J Cell Biol *107*, 841-849. 10.1083/jcb.107.3.841.

Dingwall, C., and Laskey, R.A. (1991). Nuclear targeting sequences--a consensus? Trends Biochem Sci *16*, 478-481. 10.1016/0968-0004(91)90184-w.

Duarte-Silva, S., and Maciel, P. (2018). Pharmacological Therapies for Machado-Joseph Disease. Adv Exp Med Biol *1049*, 369-394. 10.1007/978-3-319-71779-1_19.

Dugger, B.N., and Dickson, D.W. (2017). Pathology of Neurodegenerative Diseases. Cold Spring Harb Perspect Biol *9*. 10.1101/cshperspect.a028035.

Durcan, T.M., and Fon, E.A. (2011). Mutant ataxin-3 promotes the autophagic degradation of parkin. Autophagy *7*, 233-234. 10.4161/auto.7.2.14224.

Durcan, T.M., Kontogiannea, M., Bedard, N., Wing, S.S., and Fon, E.A. (2012). Ataxin-3 deubiquitination is coupled to Parkin ubiquitination via E2 ubiquitin-conjugating enzyme. J Biol Chem *287*, 531-541. 10.1074/jbc.M111.288449.

Dürr, A., Stevanin, G., Cancel, G., Duyckaerts, C., Abbas, N., Didierjean, O., Chneiweiss, H., Benomar, A., Lyon-Caen, O., Julien, J., et al. (1996). Spinocerebellar ataxia 3 and Machado-Joseph disease: clinical, molecular, and neuropathological features. Ann Neurol *39*, 490-499. 10.1002/ana.410390411.

Earnshaw, W.C., Martins, L.M., and Kaufmann, S.H. (1999). Mammalian caspases: structure, activation, substrates, and functions during apoptosis. Annu Rev Biochem *68*, 383-424. 10.1146/annurev.biochem.68.1.383.

Durr, A. (2010). Autosomal dominant cerebellar ataxias: polyglutamine expansions and beyond. Lancet Neurol *9*, 885-894. 10.1016/s1474-4422(10)70183-6.

Eftekharzadeh, B., Daigle, J.G., Kapinos, L.E., Coyne, A., Schiantarelli, J., Carlomagno, Y., Cook, C., Miller, S.J., Dujardin, S., Amaral, A.S., et al. (2018). Tau Protein Disrupts Nucleocytoplasmic Transport in Alzheimer's Disease. Neuron *99*, 925-940.e927. 10.1016/j.neuron.2018.07.039.

Elias, J.E., and Gygi, S.P. (2007). Target-decoy search strategy for increased confidence in large-scale protein identifications by mass spectrometry. Nat Methods *4*, 207-214. 10.1038/nmeth1019.

Ellerby, L.M., Hackam, A.S., Propp, S.S., Ellerby, H.M., Rabizadeh, S., Cashman, N.R., Trifiro, M.A., Pinsky, L., Wellington, C.L., Salvesen, G.S., et al. (1999). Kennedy's disease: caspase cleavage of the androgen receptor is a crucial event in cytotoxicity. J Neurochem *72*, 185-195. 10.1046/j.1471-4159.1999.0720185.x.

Emerit, J., Edeas, M., and Bricaire, F. (2004). Neurodegenerative diseases and oxidative stress. Biomedicine & Pharmacotherapy *58*, 39-46.

Evers, M.M., Toonen, L.J., and van Roon-Mom, W.M. (2014). Ataxin-3 protein and RNA toxicity in spinocerebellar ataxia type 3: current insights and emerging therapeutic strategies. Mol Neurobiol *49*, 1513-1531. 10.1007/s12035-013-8596-2.

Evert, B.O., Vogt, I.R., Kindermann, C., Ozimek, L., de Vos, R.A., Brunt, E.R., Schmitt, I., Klockgether, T., and Wüllner, U. (2001). Inflammatory genes are upregulated in expanded ataxin-3-expressing cell lines and spinocerebellar ataxia type 3 brains. J Neurosci *21*, 5389-5396. 10.1523/jneurosci.21-15-05389.2001.

Evert, B.O., Araujo, J., Vieira-Saecker, A.M., de Vos, R.A., Harendza, S., Klockgether, T., and Wüllner, U. (2006). Ataxin-3 represses transcription via chromatin binding, interaction with histone deacetylase 3, and histone deacetylation. J Neurosci *26*, 11474-11486. 10.1523/jneurosci.2053-06.2006.

Fallini, C., Khalil, B., Smith, C.L., and Rossoll, W. (2020). Traffic jam at the nuclear pore: All roads lead to nucleocytoplasmic transport defects in ALS/FTD. Neurobiol Dis *140*, 104835. 10.1016/j.nbd.2020.104835.

Fan, H.C., Ho, L.I., Chi, C.S., Chen, S.J., Peng, G.S., Chan, T.M., Lin, S.Z., and Harn, H.J. (2014). Polyglutamine (PolyQ) diseases: genetics to treatments. Cell Transplant *23*, 441-458. 10.3727/096368914x678454.

Fei, E., Jia, N., Zhang, T., Ma, X., Wang, H., Liu, C., Zhang, W., Ding, L., Nukina, N., and Wang, G. (2007). Phosphorylation of ataxin-3 by glycogen synthase kinase 3beta at serine 256 regulates the aggregation of ataxin-3. Biochem Biophys Res Commun *357*, 487-492. 10.1016/j.bbrc.2007.03.160.

Ferlazzo, M.L., Sonzogni, L., Granzotto, A., Bodgi, L., Lartin, O., Devic, C., Vogin, G., Pereira, S., and Foray, N. (2014). Mutations of the Huntington's disease protein impact on the ATM-dependent signaling and repair pathways of the radiation-induced DNA double-strand breaks: corrective effect of statins and bisphosphonates. Mol Neurobiol *49*, 1200-1211. 10.1007/s12035-013-8591-7.

Fischer, F., Langer, J.D., and Osiewacz, H.D. (2015). Identification of potential mitochondrial CLPXP protease interactors and substrates suggests its central role in energy metabolism. Sci Rep *5*, 18375. 10.1038/srep18375.

Fischer, U., Huber, J., Boelens, W.C., Mattaj, I.W., and Lührmann, R. (1995). The HIV-1 Rev activation domain is a nuclear export signal that accesses an export pathway used by specific cellular RNAs. Cell *82*, 475-483. 10.1016/0092-8674(95)90436-0.

Floer, M., Blobel, G., and Rexach, M. (1997). Disassembly of RanGTP-karyopherin beta complex, an intermediate in nuclear protein import. J Biol Chem *272*, 19538-19546. 10.1074/jbc.272.31.19538.

Fornerod, M., Ohno, M., Yoshida, M., and Mattaj, I.W. (1997). CRM1 is an export receptor for leucine-rich nuclear export signals. Cell *90*, 1051-1060. 10.1016/s0092-8674(00)80371-2.

Franz-Wachtel, M., Eisler, S.A., Krug, K., Wahl, S., Carpy, A., Nordheim, A., Pfizenmaier, K., Hausser, A., and Macek, B. (2012). Global detection of protein kinase D-dependent phosphorylation events in nocodazole-treated human cells. Mol Cell Proteomics *11*, 160-170. 10.1074/mcp.M111.016014.

Fried, H., and Kutay, U. (2003). Nucleocytoplasmic transport: taking an inventory. Cell Mol Life Sci *60*, 1659-1688. 10.1007/s00018-003-3070-3.

Friedman, J.E. (2011). Anticipation in hereditary disease: the history of a biomedical concept. Human Genetics *130*, 705-714. 10.1007/s00439-011-1022-9.

Friedman, M.J., Shah, A.G., Fang, Z.H., Ward, E.G., Warren, S.T., Li, S., and Li, X.J. (2007). Polyglutamine domain modulates the TBP-TFIIB interaction: implications for its normal function and neurodegeneration. Nat Neurosci *10*, 1519-1528. 10.1038/nn2011.

Gao, R., Liu, Y., Silva-Fernandes, A., Fang, X., Paulucci-Holthauzen, A., Chatterjee, A., Zhang, H.L., Matsuura, T., Choudhary, S., Ashizawa, T., et al. (2015). Inactivation of PNKP by mutant ATXN3 triggers apoptosis by activating the DNA damage-response pathway in SCA3. PLoS Genet *11*, e1004834. 10.1371/journal.pgen.1004834.

Gaspar, C., Lopes-Cendes, I., Hayes, S., Goto, J., Arvidsson, K., Dias, A., Silveira, I., Maciel, P., Coutinho, P., Lima, M., et al. (2001). Ancestral origins of the Machado-Joseph disease mutation: a worldwide haplotype study. Am J Hum Genet *68*, 523-528. 10.1086/318184.

Gasset-Rosa, F., Chillon-Marinas, C., Goginashvili, A., Atwal, R.S., Artates, J.W., Tabet, R., Wheeler, V.C., Bang, A.G., Cleveland, D.W., and Lagier-Tourenne, C. (2017). Polyglutamine-Expanded Huntingtin Exacerbates Age-Related Disruption of Nuclear Integrity and Nucleocytoplasmic Transport. Neuron *94*, 48-57.e44. 10.1016/j.neuron.2017.03.027.

Gatchel, J.R., and Zoghbi, H.Y. (2005). Diseases of unstable repeat expansion: mechanisms and common principles. Nat Rev Genet *6*, 743-755. 10.1038/nrg1691.

Gispert, S., Parganlija, D., Klinkenberg, M., Dröse, S., Wittig, I., Mittelbronn, M., Grzmil, P., Koob, S., Hamann, A., Walter, M., et al. (2013). Loss of mitochondrial peptidase Clpp leads to infertility, hearing loss plus growth retardation via accumulation of CLPX, mtDNA and inflammatory factors. Hum Mol Genet *22*, 4871-4887. 10.1093/hmg/ddt338.

Goll, D.E., Thompson, V.F., Li, H., Wei, W., and Cong, J. (2003). The calpain system. Physiol Rev *83*, 731-801. 10.1152/physrev.00029.2002.

Görlich, D., and Kutay, U. (1999). Transport between the cell nucleus and the cytoplasm. Annu Rev Cell Dev Biol *15*, 607-660. 10.1146/annurev.cellbio.15.1.607.

Gossen, M., and Bujard, H. (1992). Tight control of gene expression in mammalian cells by tetracycline-responsive promoters. Proc Natl Acad Sci U S A *89*, 5547-5551. 10.1073/pnas.89.12.5547.

Goti, D., Katzen, S.M., Mez, J., Kurtis, N., Kiluk, J., Ben-Haïem, L., Jenkins, N.A., Copeland, N.G., Kakizuka, A., Sharp, A.H., et al. (2004). A mutant ataxin-3 putative-cleavage fragment in brains of Machado-Joseph disease patients and transgenic mice is cytotoxic above a critical concentration. J Neurosci *24*, 10266-10279. 10.1523/jneurosci.2734-04.2004.

Goto, J., Watanabe, M., Ichikawa, Y., Yee, S.B., Ihara, N., Endo, K., Igarashi, S., Takiyama, Y., Gaspar, C., Maciel, P., et al. (1997). Machado-Joseph disease gene products carrying different carboxyl termini. Neurosci Res *28*, 373-377. 10.1016/s0168-0102(97)00056-4.

Grima, J.C., Daigle, J.G., Arbez, N., Cunningham, K.C., Zhang, K., Ochaba, J., Geater, C., Morozko, E., Stocksdale, J., Glatzer, J.C., et al. (2017). Mutant Huntingtin Disrupts the Nuclear Pore Complex. Neuron *94*, 93-107.e106. 10.1016/j.neuron.2017.03.023.

Guillon, B., Bulteau, A.L., Wattenhofer-Donzé, M., Schmucker, S., Friguet, B., Puccio, H., Drapier, J.C., and Bouton, C. (2009). Frataxin deficiency causes upregulation of mitochondrial Lon and ClpP proteases and severe loss of mitochondrial Fe-S proteins. Febs j *276*, 1036-1047. 10.1111/j.1742-4658.2008.06847.x.

Guo, L., Kim, H.J., Wang, H., Monaghan, J., Freyermuth, F., Sung, J.C., O'Donovan, K., Fare, C.M., Diaz, Z., Singh, N., et al. (2018). Nuclear-Import Receptors Reverse Aberrant Phase Transitions of RNA-Binding Proteins with Prion-like Domains. Cell *173*, 677-692.e620. 10.1016/j.cell.2018.03.002.

Haacke, A., Broadley, S.A., Boteva, R., Tzvetkov, N., Hartl, F.U., and Breuer, P. (2006). Proteolytic cleavage of polyglutamine-expanded ataxin-3 is critical for aggregation and sequestration of non-expanded ataxin-3. Hum Mol Genet *15*, 555-568. 10.1093/hmg/ddi472.

Haacke, A., Hartl, F.U., and Breuer, P. (2007). Calpain inhibition is sufficient to suppress aggregation of polyglutamine-expanded ataxin-3. J Biol Chem *282*, 18851-18856. 10.1074/jbc.M611914200.

Hansen, J., Corydon, T.J., Palmfeldt, J., Dürr, A., Fontaine, B., Nielsen, M.N., Christensen, J.H., Gregersen, N., and Bross, P. (2008). Decreased expression of the mitochondrial matrix proteases Lon and ClpP in cells from a patient with hereditary spastic paraplegia (SPG13). Neuroscience *153*, 474-482. 10.1016/j.neuroscience.2008.01.070.

Harel, A., and Forbes, D.J. (2004). Importin beta: conducting a much larger cellular symphony. Mol Cell *16*, 319-330. 10.1016/j.molcel.2004.10.026.

Harmuth, T., Weber, J.J., Zimmer, A.J., Sowa, A.S., Schmidt, J., Fitzgerald, J.C., Schöls, L., Riess, O., and Hübener-Schmid, J. (2022). Mitochondrial Dysfunction in Spinocerebellar Ataxia Type 3 Is Linked to VDAC1 Deubiquitination. Int J Mol Sci *23*. 10.3390/ijms23115933.

Harris, G.M., Dodelzon, K., Gong, L., Gonzalez-Alegre, P., and Paulson, H.L. (2010). Splice isoforms of the polyglutamine disease protein ataxin-3 exhibit similar enzymatic yet different aggregation properties. PLoS One *5*, e13695. 10.1371/journal.pone.0013695.

Havel, L.S., Li, S., and Li, X.J. (2009). Nuclear accumulation of polyglutamine disease proteins and neuropathology. Mol Brain *2*, 21. 10.1186/1756-6606-2-21.

Hayer, S.N., Schelling, Y., Huebener-Schmid, J., Weber, J.J., Hauser, S., and Schöls, L. (2018). Generation of an induced pluripotent stem cell line from a patient with spinocerebellar ataxia type 3 (SCA3): HIHCNi002-A. Stem Cell Res *30*, 171-174. 10.1016/j.scr.2018.06.006.

Haynes, C.M., Petrova, K., Benedetti, C., Yang, Y., and Ron, D. (2007). ClpP mediates activation of a mitochondrial unfolded protein response in C. elegans. Dev Cell *13*, 467-480. 10.1016/j.devcel.2007.07.016.

Hersheson, J., Haworth, A., and Houlden, H. (2012). The inherited ataxias: genetic heterogeneity, mutation databases, and future directions in research and clinical diagnostics. Hum Mutat *33*, 1324-1332. 10.1002/humu.22132.

Hipp, M.S., Kasturi, P., and Hartl, F.U. (2019). The proteostasis network and its decline in aging. Nature Reviews Molecular Cell Biology *20*, 421-435. 10.1038/s41580-019-0101-y.

Hofweber, M., Hutten, S., Bourgeois, B., Spreitzer, E., Niedner-Boblenz, A., Schifferer, M., Ruepp, M.D., Simons, M., Niessing, D., Madl, T., and Dormann, D. (2018). Phase Separation of FUS Is Suppressed by Its Nuclear Import Receptor and Arginine Methylation. Cell *173*, 706-719.e713. 10.1016/j.cell.2018.03.004.

Hosp, F., Vossfeldt, H., Heinig, M., Vasiljevic, D., Arumughan, A., Wyler, E., Landthaler, M., Hubner, N., Wanker, E.E., Lannfelt, L., et al. (2015). Quantitative interaction proteomics of neurodegenerative disease proteins. Cell Rep *11*, 1134-1146. 10.1016/j.celrep.2015.04.030.

Hu, D., Sun, X., Liao, X., Zhang, X., Zarabi, S., Schimmer, A., Hong, Y., Ford, C., Luo, Y., and Qi, X. (2019). Alpha-synuclein suppresses mitochondrial protease ClpP to trigger mitochondrial oxidative damage and neurotoxicity. Acta Neuropathol *137*, 939-960. 10.1007/s00401-019-01993-2.

Hübener, J., Weber, J.J., Richter, C., Honold, L., Weiss, A., Murad, F., Breuer, P., Wüllner, U., Bellstedt, P., Paquet-Durand, F., et al. (2013). Calpain-mediated ataxin-3 cleavage in the molecular pathogenesis of spinocerebellar ataxia type 3 (SCA3). Hum Mol Genet *22*, 508-518. 10.1093/hmg/dds449.

Ichikawa, Y., Goto, J., Hattori, M., Toyoda, A., Ishii, K., Jeong, S.Y., Hashida, H., Masuda, N., Ogata, K., Kasai, F., et al. (2001). The genomic structure and expression of MJD, the Machado-Joseph disease gene. J Hum Genet *46*, 413-422. 10.1007/s100380170060.

Jäkel, S., Mingot, J.M., Schwarzmaier, P., Hartmann, E., and Görlich, D. (2002). Importins fulfil a dual function as nuclear import receptors and cytoplasmic chaperones for exposed basic domains. Embo j *21*, 377-386. 10.1093/emboj/21.3.377.

Jans, D.A., Xiao, C.Y., and Lam, M.H. (2000). Nuclear targeting signal recognition: a key control point in nuclear transport? Bioessays *22*, 532-544. 10.1002/(sici)1521-1878(200006)22:6<532::Aid-bies6>3.0.Co;2-o.

Jardim, L.B., Pereira, M.L., Silveira, I., Ferro, A., Sequeiros, J., and Giugliani, R. (2001). Neurologic findings in Machado-Joseph disease: relation with disease duration, subtypes, and (CAG)n. Arch Neurol *58*, 899-904. 10.1001/archneur.58.6.899.

Jeffries, S., and Capobianco, A.J. (2000). Neoplastic Transformation by Notch Requires Nuclear Localization. Molecular and Cellular Biology *20*, 3928-3941. 10.1128/mcb.20.11.3928-3941.2000.

Jenkinson, E.M., Rehman, A.U., Walsh, T., Clayton-Smith, J., Lee, K., Morell, R.J., Drummond, M.C., Khan, S.N., Naeem, M.A., Rauf, B., et al. (2013). Perrault syndrome is caused by recessive mutations in CLPP, encoding a mitochondrial ATP-dependent chambered protease. Am J Hum Genet *92*, 605-613. 10.1016/j.ajhg.2013.02.013.

Joers, J.M., Deelchand, D.K., Lyu, T., Emir, U.E., Hutter, D., Gomez, C.M., Bushara, K.O., Eberly, L.E., and Öz, G. (2018). Neurochemical abnormalities in premanifest and early spinocerebellar ataxias. Ann Neurol *83*, 816-829. 10.1002/ana.25212.

Kabeya, Y., Mizushima, N., Ueno, T., Yamamoto, A., Kirisako, T., Noda, T., Kominami, E., Ohsumi, Y., and Yoshimori, T. (2000). LC3, a mammalian homologue of yeast Apg8p, is localized in autophagosome membranes after processing. Embo j *19*, 5720-5728. 10.1093/emboj/19.21.5720.

Kalab, P., Weis, K., and Heald, R. (2002). Visualization of a Ran-GTP gradient in interphase and mitotic Xenopus egg extracts. Science *295*, 2452-2456. 10.1126/science.1068798.

Kalderon, D., Richardson, W.D., Markham, A.F., and Smith, A.E. (1984). Sequence requirements for nuclear location of simian virus 40 large-T antigen. Nature *311*, 33-38. 10.1038/311033a0.

Kau, T.R., Way, J.C., and Silver, P.A. (2004). Nuclear transport and cancer: from mechanism to intervention. Nat Rev Cancer *4*, 106-117. 10.1038/nrc1274.

Kawaguchi, Y., Okamoto, T., Taniwaki, M., Aizawa, M., Inoue, M., Katayama, S., Kawakami, H., Nakamura, S., Nishimura, M., Akiguchi, I., and et al. (1994). CAG expansions in a novel gene for Machado-Joseph disease at chromosome 14q32.1. Nat Genet *8*, 221-228. 10.1038/ng1194-221.

Kawai, Y., Takeda, A., Abe, Y., Washimi, Y., Tanaka, F., and Sobue, G. (2004). Cognitive impairments in Machado-Joseph disease. Arch Neurol *61*, 1757-1760. 10.1001/archneur.61.11.1757.

Kayed, R., Head, E., Thompson, J.L., McIntire, T.M., Milton, S.C., Cotman, C.W., and Glabe, C.G. (2003). Common structure of soluble amyloid oligomers implies common mechanism of pathogenesis. Science *300*, 486-489. 10.1126/science.1079469.

Kazachkova, N., Raposo, M., Montiel, R., Cymbron, T., Bettencourt, C., Silva-Fernandes, A., Silva, S., Maciel, P., and Lima, M. (2013). Patterns of Mitochondrial DNA Damage in Blood and Brain Tissues of a Transgenic Mouse Model of Machado-Joseph Disease. Neurodegenerative Diseases *11*, 206-214. 10.1159/000339207.

Kim, Y.H., Han, M.E., and Oh, S.O. (2017). The molecular mechanism for nuclear transport and its application. Anat Cell Biol *50*, 77-85. 10.5115/acb.2017.50.2.77.

Kim, Y.J., Yi, Y., Sapp, E., Wang, Y., Cuiffo, B., Kegel, K.B., Qin, Z.H., Aronin, N., and DiFiglia, M. (2001). Caspase 3-cleaved N-terminal fragments of wild-type and mutant huntingtin are present in normal and Huntington's disease brains, associate with membranes, and undergo calpain-dependent proteolysis. Proc Natl Acad Sci U S A *98*, 12784-12789. 10.1073/pnas.221451398.

Kinoshita, Y., Ito, H., Hirano, A., Fujita, K., Wate, R., Nakamura, M., Kaneko, S., Nakano, S., and Kusaka, H. (2009). Nuclear contour irregularity and abnormal transporter protein distribution in anterior horn cells in amyotrophic lateral sclerosis. J Neuropathol Exp Neurol *68*, 1184-1192. 10.1097/NEN.0b013e3181bc3bec.

Kitada, T., Asakawa, S., Hattori, N., Matsumine, H., Yamamura, Y., Minoshima, S., Yokochi, M., Mizuno, Y., and Shimizu, N. (1998). Mutations in the parkin gene cause autosomal recessive juvenile parkinsonism. Nature *392*, 605-608. 10.1038/33416.

Klockgether, T., Mariotti, C., and Paulson, H.L. (2019). Spinocerebellar ataxia. Nat Rev Dis Primers *5*, 24. 10.1038/s41572-019-0074-3.

Koch, P., Breuer, P., Peitz, M., Jungverdorben, J., Kesavan, J., Poppe, D., Doerr, J., Ladewig, J., Mertens, J., Tüting, T., et al. (2011). Excitation-induced ataxin-3 aggregation in neurons from patients with Machado–Joseph disease. Nature *480*, 543-546. 10.1038/nature10671.

Köhler, M., Speck, C., Christiansen, M., Bischoff, F.R., Prehn, S., Haller, H., Görlich, D., and Hartmann, E. (1999). Evidence for distinct substrate specificities of importin alpha family members in nuclear protein import. Mol Cell Biol *19*, 7782-7791. 10.1128/mcb.19.11.7782.

Kristensen, L.V., Oppermann, F.S., Rauen, M.J., Fog, K., Schmidt, T., Schmidt, J., Harmuth, T., Hartmann-Petersen, R., and Thirstrup, K. (2018). Mass spectrometry analyses of normal and polyglutamine expanded ataxin-3 reveal novel interaction partners involved in mitochondrial function. Neurochem Int *112*, 5-17. 10.1016/j.neuint.2017.10.013.

Kroemer, G., and Reed, J.C. (2000). Mitochondrial control of cell death. Nat Med *6*, 513-519. 10.1038/74994.

La Spada, A.R., and Taylor, J.P. (2003). Polyglutamines placed into context. Neuron *38*, 681-684. 10.1016/s0896-6273(03)00328-3.

La Spada, A.R., Wilson, E.M., Lubahn, D.B., Harding, A.E., and Fischbeck, K.H. (1991). Androgen receptor gene mutations in X-linked spinal and bulbar muscular atrophy. Nature *352*, 77-79. 10.1038/352077a0.

Laço, M.N., Oliveira, C.R., Paulson, H.L., and Rego, A.C. (2012). Compromised mitochondrial complex II in models of Machado-Joseph disease. Biochim Biophys Acta *1822*, 139-149. 10.1016/j.bbadis.2011.10.010.

Lee, H.G., Ueda, M., Miyamoto, Y., Yoneda, Y., Perry, G., Smith, M.A., and Zhu, X. (2006). Aberrant localization of importin alpha1 in hippocampal neurons in Alzheimer disease. Brain Res *1124*, 1-4. 10.1016/j.brainres.2006.09.084.

Levine, B., and Kroemer, G. (2008). Autophagy in the pathogenesis of disease. Cell *132*, 27-42. 10.1016/j.cell.2007.12.018.

Li, F., Macfarlan, T., Pittman, R.N., and Chakravarti, D. (2002). Ataxin-3 is a histone-binding protein with two independent transcriptional corepressor activities. J Biol Chem *277*, 45004-45012. 10.1074/jbc.M205259200.

Li, J., and Yuan, J. (2008). Caspases in apoptosis and beyond. Oncogene *27*, 6194-6206. 10.1038/onc.2008.297.

Li, L.B., Yu, Z., Teng, X., and Bonini, N.M. (2008). RNA toxicity is a component of ataxin-3 degeneration in Drosophila. Nature *453*, 1107-1111. 10.1038/nature06909.

Li, X.J., Friedman, M., and Li, S. (2007). Interacting proteins as genetic modifiers of Huntington disease. Trends Genet *23*, 531-533. 10.1016/j.tig.2007.07.007.

Lin, M.T., and Beal, M.F. (2006). Mitochondrial dysfunction and oxidative stress in neurodegenerative diseases. Nature *443*, 787-795. 10.1038/nature05292.

Liu, H., Li, X., Ning, G., Zhu, S., Ma, X., Liu, X., Liu, C., Huang, M., Schmitt, I., Wüllner, U., et al. (2016). The Machado–Joseph Disease Deubiquitinase Ataxin-3 Regulates the Stability and Apoptotic Function of p53. PLOS Biology *14*, e2000733. 10.1371/journal.pbio.2000733.

Lopes, T.M., D'Abreu, A., França, M.C., Jr., Yasuda, C.L., Betting, L.E., Samara, A.B., Castellano, G., Somazz, J.C., Balthazar, M.L., Lopes-Cendes, I., and Cendes, F. (2013). Widespread neuronal damage and cognitive dysfunction in spinocerebellar ataxia type 3. J Neurol *260*, 2370-2379. 10.1007/s00415-013-6998-8.

Luber, C.A., Cox, J., Lauterbach, H., Fancke, B., Selbach, M., Tschopp, J., Akira, S., Wiegand, M., Hochrein, H., O'Keeffe, M., and Mann, M. (2010). Quantitative proteomics reveals subset-specific viral recognition in dendritic cells. Immunity *32*, 279-289. 10.1016/j.immuni.2010.01.013.

Lusk, C.P., and King, M.C. (2017). The nucleus: keeping it together by keeping it apart. Curr Opin Cell Biol *44*, 44-50. 10.1016/j.ceb.2017.02.001.

Ma, K.L., Song, L.K., Yuan, Y.H., Zhang, Y., Han, N., Gao, K., and Chen, N.H. (2014). The nuclear accumulation of alpha-synuclein is mediated by importin alpha and promotes neurotoxicity by accelerating the cell cycle. Neuropharmacology *82*, 132-142. 10.1016/j.neuropharm.2013.07.035.

Macara, I.G. (2001). Transport into and out of the nucleus. Microbiol Mol Biol Rev *65*, 570-594, table of contents. 10.1128/mmbr.65.4.570-594.2001.

Macedo-Ribeiro, S., Cortes, L., Maciel, P., and Carvalho, A.L. (2009). Nucleocytoplasmic shuttling activity of ataxin-3. PLoS One *4*, e5834. 10.1371/journal.pone.0005834.

Maciel, P., Costa, M.C., Ferro, A., Rousseau, M., Santos, C.S., Gaspar, C., Barros, J., Rouleau, G.A., Coutinho, P., and Sequeiros, J. (2001). Improvement in the molecular diagnosis of Machado-Joseph disease. Arch Neurol *58*, 1821-1827. 10.1001/archneur.58.11.1821.

Maciel, P., Gaspar, C., DeStefano, A.L., Silveira, I., Coutinho, P., Radvany, J., Dawson, D.M., Sudarsky, L., Guimarães, J., Loureiro, J.E., and et al. (1995). Correlation between CAG repeat length and clinical features in Machado-Joseph disease. Am J Hum Genet *57*, 54-61.

Maréchal, A., and Zou, L. (2013). DNA damage sensing by the ATM and ATR kinases. Cold Spring Harb Perspect Biol *5*. 10.1101/cshperspect.a012716.

Martinelli, P., and Rugarli, E.I. (2010). Emerging roles of mitochondrial proteases in neurodegeneration. Biochim Biophys Acta *1797*, 1-10. 10.1016/j.bbabio.2009.07.013.

Matos, C.A., Almeida, L.P., and Nobrega, C. (2017). Proteolytic Cleavage of Polyglutamine Disease-Causing Proteins: Revisiting the Toxic Fragment Hypothesis. Curr Pharm Des *23*, 753-775. 10.2174/1381612822666161227121912.

Mattaj, I.W., and Englmeier, L. (1998). Nucleocytoplasmic transport: the soluble phase. Annu Rev Biochem *67*, 265-306. 10.1146/annurev.biochem.67.1.265.

Matyskiela, M.E., and Martin, A. (2013). Design principles of a universal protein degradation machine. J Mol Biol *425*, 199-213. 10.1016/j.jmb.2012.11.001.

Mayford, M., Bach, M.E., Huang, Y.Y., Wang, L., Hawkins, R.D., and Kandel, E.R. (1996). Control of memory formation through regulated expression of a CaMKII transgene. Science *274*, 1678-1683. 10.1126/science.274.5293.1678.

McLane, L.M., and Corbett, A.H. (2009). Nuclear localization signals and human disease. IUBMB Life *61*, 697-706. 10.1002/iub.194.

McLoughlin, H.S., Moore, L.R., and Paulson, H.L. (2020). Pathogenesis of SCA3 and implications for other polyglutamine diseases. Neurobiol Dis *134*, 104635. 10.1016/j.nbd.2019.104635.

Mikhaleva, S., and Lemke, E.A. (2018). Beyond the Transport Function of Import Receptors: What's All the FUS about? Cell *173*, 549-553. 10.1016/j.cell.2018.04.002.

Milanese, C., Cerri, S., Ulusoy, A., Gornati, S.V., Plat, A., Gabriels, S., Blandini, F., Di Monte, D.A., Hoeijmakers, J.H., and Mastroberardino, P.G. (2018). Activation of the DNA damage response in vivo in synucleinopathy models of Parkinson's disease. Cell Death & Disease *9*, 818. 10.1038/s41419-018-0848-7.

Milles, S., Huy Bui, K., Koehler, C., Eltsov, M., Beck, M., and Lemke, E.A. (2013). Facilitated aggregation of FG nucleoporins under molecular crowding conditions. EMBO Rep *14*, 178-183. 10.1038/embor.2012.204.

Miyata, R., Hayashi, M., Tanuma, N., Shioda, K., Fukatsu, R., and Mizutani, S. (2008). Oxidative stress in neurodegeneration in dentatorubral-pallidoluysian atrophy. Journal of the Neurological Sciences *264*, 133-139.

Mizushima, N., Yoshimori, T., and Levine, B. (2010). Methods in mammalian autophagy research. Cell *140*, 313-326. 10.1016/j.cell.2010.01.028.

Mosammaparast, N., and Pemberton, L.F. (2004). Karyopherins: from nuclear-transport mediators to nuclear-function regulators. Trends Cell Biol *14*, 547-556. 10.1016/j.tcb.2004.09.004.

Mueller, T., Breuer, P., Schmitt, I., Walter, J., Evert, B.O., and Wüllner, U. (2009). CK2-dependent phosphorylation determines cellular localization and stability of ataxin-3. Hum Mol Genet *18*, 3334-3343. 10.1093/hmg/ddp274.

Mühlhäusser, P., Müller, E.C., Otto, A., and Kutay, U. (2001). Multiple pathways contribute to nuclear import of core histones. EMBO Rep *2*, 690-696. 10.1093/embo-reports/kve168.

Mykowska, A., Sobczak, K., Wojciechowska, M., Kozlowski, P., and Krzyzosiak, W.J. (2011). CAG repeats mimic CUG repeats in the misregulation of alternative splicing. Nucleic Acids Res *39*, 8938-8951. 10.1093/nar/gkr608.

Nascimento-Ferreira, I., Santos-Ferreira, T., Sousa-Ferreira, L., Auregan, G., Onofre, I., Alves, S., Dufour, N., Colomer Gould, V.F., Koeppen, A., Déglon, N., and Pereira de Almeida, L. (2011). Overexpression of the autophagic beclin-1 protein clears mutant ataxin-3 and alleviates Machado-Joseph disease. Brain *134*, 1400-1415. 10.1093/brain/awr047.

Nishimura, A.L., Zupunski, V., Troakes, C., Kathe, C., Fratta, P., Howell, M., Gallo, J.M., Hortobágyi, T., Shaw, C.E., and Rogelj, B. (2010). Nuclear import impairment causes cytoplasmic trans-activation

response DNA-binding protein accumulation and is associated with frontotemporal lobar degeneration. Brain *133*, 1763-1771. 10.1093/brain/awq111.

Nuovo, G., Amann, V., Williams, J., Vandiver, P., Quinonez, M., Fadda, P., Paniccia, B., Mezache, L., and Mikhail, A. (2018). Increased expression of importin-β, exportin-5 and nuclear transportable proteins in Alzheimer's disease aids anatomic pathologists in its diagnosis. Ann Diagn Pathol *32*, 10-16. 10.1016/j.anndiagpath.2017.08.003.

O'Brien, J., Hayder, H., Zayed, Y., and Peng, C. (2018). Overview of MicroRNA Biogenesis, Mechanisms of Actions, and Circulation. Front Endocrinol (Lausanne) *9*, 402. 10.3389/fendo.2018.00402.

Oka, M., and Yoneda, Y. (2018). Importin α: functions as a nuclear transport factor and beyond. Proc Jpn Acad Ser B Phys Biol Sci *94*, 259-274. 10.2183/pjab.94.018.

Ona, V.O., Li, M., Vonsattel, J.P., Andrews, L.J., Khan, S.Q., Chung, W.M., Frey, A.S., Menon, A.S., Li, X.J., Stieg, P.E., et al. (1999). Inhibition of caspase-1 slows disease progression in a mouse model of Huntington's disease. Nature *399*, 263-267. 10.1038/20446.

Onofre, I., Mendonça, N., Lopes, S., Nobre, R., de Melo, J.B., Carreira, I.M., Januário, C., Gonçalves, A.F., and de Almeida, L.P. (2016). Fibroblasts of Machado Joseph Disease patients reveal autophagy impairment. Sci Rep *6*, 28220. 10.1038/srep28220.

Osiewacz, H.D., and Bernhardt, D. (2013). Mitochondrial quality control: impact on aging and life span - a mini-review. Gerontology *59*, 413-420. 10.1159/000348662.

Pankiv, S., Clausen, T.H., Lamark, T., Brech, A., Bruun, J.A., Outzen, H., Øvervatn, A., Bjørkøy, G., and Johansen, T. (2007). p62/SQSTM1 binds directly to Atg8/LC3 to facilitate degradation of ubiquitinated protein aggregates by autophagy. J Biol Chem *282*, 24131-24145. 10.1074/jbc.M702824200.

Pasha, T., Zatorska, A., Sharipov, D., Rogelj, B., Hortobágyi, T., and Hirth, F. (2021). Karyopherin abnormalities in neurodegenerative proteinopathies. Brain *144*, 2915-2932. 10.1093/brain/awab201.

Patel, S.S., Belmont, B.J., Sante, J.M., and Rexach, M.F. (2007). Natively unfolded nucleoporins gate protein diffusion across the nuclear pore complex. Cell *129*, 83-96. 10.1016/j.cell.2007.01.044.

Paulson, H.L., Das, S.S., Crino, P.B., Perez, M.K., Patel, S.C., Gotsdiner, D., Fischbeck, K.H., and Pittman, R.N. (1997a). Machado-Joseph disease gene product is a cytoplasmic protein widely expressed in brain. Ann Neurol *41*, 453-462. 10.1002/ana.410410408.

Paulson, H.L., Perez, M.K., Trottier, Y., Trojanowski, J.Q., Subramony, S.H., Das, S.S., Vig, P., Mandel, J.L., Fischbeck, K.H., and Pittman, R.N. (1997b). Intranuclear inclusions of expanded polyglutamine protein in spinocerebellar ataxia type 3. Neuron *19*, 333-344. 10.1016/s0896-6273(00)80943-5.

Paulson, H.L. (2007). Dominantly inherited ataxias: lessons learned from Machado-Joseph disease/spinocerebellar ataxia type 3. Semin Neurol *27*, 133-142. 10.1055/s-2007-971172.

Paulson, H. (2012). Machado-Joseph disease/spinocerebellar ataxia type 3. Handb Clin Neurol *103*, 437-449. 10.1016/b978-0-444-51892-7.00027-9.

Pellegrino, M.W., Nargund, A.M., and Haynes, C.M. (2013). Signaling the mitochondrial unfolded protein response. Biochim Biophys Acta *1833*, 410-416. 10.1016/j.bbamcr.2012.02.019.

Pemberton, L.F., Blobel, G., and Rosenblum, J.S. (1998). Transport routes through the nuclear pore complex. Curr Opin Cell Biol *10*, 392-399. 10.1016/s0955-0674(98)80016-1.

Pemberton, L.F., and Paschal, B.M. (2005). Mechanisms of receptor-mediated nuclear import and nuclear export. Traffic *6*, 187-198. 10.1111/j.1600-0854.2005.00270.x.

Perez, M.K., Paulson, H.L., Pendse, S.J., Saionz, S.J., Bonini, N.M., and Pittman, R.N. (1998). Recruitment and the role of nuclear localization in polyglutamine-mediated aggregation. J Cell Biol *143*, 1457-1470. 10.1083/jcb.143.6.1457.

Pineda, J.A., Lewis, S.B., Valadka, A.B., Papa, L., Hannay, H.J., Heaton, S.C., Demery, J.A., Liu, M.C., Aikman, J.M., Akle, V., et al. (2007). Clinical significance of alphaII-spectrin breakdown products in cerebrospinal fluid after severe traumatic brain injury. J Neurotrauma *24*, 354-366. 10.1089/neu.2006.003789.

Pozzi, C., Valtorta, M., Tedeschi, G., Galbusera, E., Pastori, V., Bigi, A., Nonnis, S., Grassi, E., and Fusi, P. (2008). Study of subcellular localization and proteolysis of ataxin-3. Neurobiol Dis *30*, 190-200. 10.1016/j.nbd.2008.01.011.

Pumroy, R.A., and Cingolani, G. (2015). Diversification of importin-α isoforms in cellular trafficking and disease states. Biochem J *466*, 13-28. 10.1042/bj20141186.

Quimby, B.B., and Dasso, M. (2003). The small GTPase Ran: interpreting the signs. Curr Opin Cell Biol *15*, 338-344. 10.1016/s0955-0674(03)00046-2.

Quirós, P.M., Langer, T., and López-Otín, C. (2015). New roles for mitochondrial proteases in health, aging and disease. Nat Rev Mol Cell Biol *16*, 345-359. 10.1038/nrm3984.

Raj, K., and Akundi, R.S. (2021). Mutant Ataxin-3-Containing Aggregates (MATAGGs) in Spinocerebellar Ataxia Type 3: Dynamics of the Disorder. Mol Neurobiol. 10.1007/s12035-021-02314-z.

Rappsilber, J., Mann, M., and Ishihama, Y. (2007). Protocol for micro-purification, enrichment, pre-fractionation and storage of peptides for proteomics using StageTips. Nat Protoc *2*, 1896-1906. 10.1038/nprot.2007.261.

Rath, E., Berger, E., Messlik, A., Nunes, T., Liu, B., Kim, S.C., Hoogenraad, N., Sans, M., Sartor, R.B., and Haller, D. (2012). Induction of dsRNA-activated protein kinase links mitochondrial unfolded protein response to the pathogenesis of intestinal inflammation. Gut *61*, 1269-1278. 10.1136/gutjnl-2011-300767.

Reith, W. (2018). [Neurodegenerative diseases]. Radiologe *58*, 241-258. 10.1007/s00117-018-0363-y.

Rexach, M., and Blobel, G. (1995). Protein import into nuclei: association and dissociation reactions involving transport substrate, transport factors, and nucleoporins. Cell *83*, 683-692. 10.1016/0092-8674(95)90181-7.

Riley, B.E., and Orr, H.T. (2006). Polyglutamine neurodegenerative diseases and regulation of transcription: assembling the puzzle. Genes Dev *20*, 2183-2192. 10.1101/gad.1436506.

Ross, C.A., Wood, J.D., Schilling, G., Peters, M.F., Nucifora, F.C., Jr., Cooper, J.K., Sharp, A.H., Margolis, R.L., and Borchelt, D.R. (1999). Polyglutamine pathogenesis. Philos Trans R Soc Lond B Biol Sci *354*, 1005-1011. 10.1098/rstb.1999.0452.

Ross, C.A., and Poirier, M.A. (2004). Protein aggregation and neurodegenerative disease. Nat Med *10 Suppl*, S10-17. 10.1038/nm1066.

Rüb, U., Brunt, E.R., and Deller, T. (2008). New insights into the pathoanatomy of spinocerebellar ataxia type 3 (Machado-Joseph disease). Curr Opin Neurol *21*, 111-116. 10.1097/WCO.0b013e3282f7673d.

Rüb, U., Schöls, L., Paulson, H., Auburger, G., Kermer, P., Jen, J.C., Seidel, K., Korf, H.W., and Deller, T. (2013). Clinical features, neurogenetics and neuropathology of the polyglutamine spinocerebellar ataxias type 1, 2, 3, 6 and 7. Prog Neurobiol *104*, 38-66. 10.1016/j.pneurobio.2013.01.001.

Rudnicki, D.D., and Margolis, R.L. (2003). Repeat expansion and autosomal dominant neurodegenerative disorders: consensus and controversy. Expert Rev Mol Med *5*, 1-24. 10.1017/s1462399403006598.

Rugarli, E.I., and Langer, T. (2012). Mitochondrial quality control: a matter of life and death for neurons. Embo j *31*, 1336-1349. 10.1038/emboj.2012.38.

Ryan, K.J., and Wente, S.R. (2000). The nuclear pore complex: a protein machine bridging the nucleus and cytoplasm. Curr Opin Cell Biol *12*, 361-371. 10.1016/s0955-0674(00)00101-0.

Sakahira, H., Breuer, P., Hayer-Hartl, M.K., and Hartl, F.U. (2002). Molecular chaperones as modulators of polyglutamine protein aggregation and toxicity. Proc Natl Acad Sci U S A *99 Suppl 4*, 16412-16418. 10.1073/pnas.182426899.

Sakai, T., and Kawakami, H. (1996). Machado-Joseph disease: A proposal of spastic paraplegic subtype. Neurology *46*, 846-847.

Sánchez, I., Xu, C.J., Juo, P., Kakizaka, A., Blenis, J., and Yuan, J. (1999). Caspase-8 is required for cell death induced by expanded polyglutamine repeats. Neuron *22*, 623-633. 10.1016/s0896-6273(00)80716-3.

Sauer, R.T., and Baker, T.A. (2011). AAA+ proteases: ATP-fueled machines of protein destruction. Annu Rev Biochem *80*, 587-612. 10.1146/annurev-biochem-060408-172623.

Schmidt, J., Schmidt, T., Golla, M., Lehmann, L., Weber, J.J., Hübener-Schmid, J., and Riess, O. (2016). In vivo assessment of riluzole as a potential therapeutic drug for spinocerebellar ataxia type 3. J Neurochem *138*, 150-162. 10.1111/jnc.13606.

Schmidt, J., Mayer, A.K., Bakula, D., Freude, J., Weber, J.J., Weiss, A., Riess, O., and Schmidt, T. (2019). Vulnerability of frontal brain neurons for the toxicity of expanded ataxin-3. Hum Mol Genet *28*, 1463-1473. 10.1093/hmg/ddy437.

Schmidt, T., Landwehrmeyer, G.B., Schmitt, I., Trottier, Y., Auburger, G., Laccone, F., Klockgether, T., Völpel, M., Epplen, J.T., Schöls, L., and Riess, O. (1998). An isoform of ataxin-3 accumulates in the nucleus of neuronal cells in affected brain regions of SCA3 patients. Brain Pathol *8*, 669-679. 10.1111/j.1750-3639.1998.tb00193.x.

Schmitt, I., Linden, M., Khazneh, H., Evert, B.O., Breuer, P., Klockgether, T., and Wuellner, U. (2007). Inactivation of the mouse Atxn3 (ataxin-3) gene increases protein ubiquitination. Biochem Biophys Res Commun *362*, 734-739. 10.1016/j.bbrc.2007.08.062.

Schöls, L., Amoiridis, G., Epplen, J.T., Langkafel, M., Przuntek, H., and Riess, O. (1996). Relations between genotype and phenotype in German patients with the Machado-Joseph disease mutation. J Neurol Neurosurg Psychiatry *61*, 466-470. 10.1136/jnnp.61.5.466.

Schöls, L., Haan, J., Riess, O., Amoiridis, G., and Przuntek, H. (1998). Sleep disturbance in spinocerebellar ataxias: is the SCA3 mutation a cause of restless legs syndrome? Neurology *51*, 1603-1607. 10.1212/wnl.51.6.1603.

Schöls, L., Bauer, P., Schmidt, T., Schulte, T., and Riess, O. (2004). Autosomal dominant cerebellar ataxias: clinical features, genetics, and pathogenesis. Lancet Neurol *3*, 291-304. 10.1016/s1474-4422(04)00737-9.

Seidel, K., den Dunnen, W.F., Schultz, C., Paulson, H., Frank, S., de Vos, R.A., Brunt, E.R., Deller, T., Kampinga, H.H., and Rüb, U. (2010). Axonal inclusions in spinocerebellar ataxia type 3. Acta Neuropathol *120*, 449-460. 10.1007/s00401-010-0717-7.

Sequeiros, J., Martins, S., and Silveira, I. (2012). Epidemiology and population genetics of degenerative ataxias. Handb Clin Neurol *103*, 227-251. 10.1016/b978-0-444-51892-7.00014-0.

Shanbhag, N.M., Evans, M.D., Mao, W., Nana, A.L., Seeley, W.W., Adame, A., Rissman, R.A., Masliah, E., and Mucke, L. (2019). Early neuronal accumulation of DNA double strand breaks in Alzheimer's disease. Acta Neuropathol Commun *7*, 77. 10.1186/s40478-019-0723-5.

Shao, J., and Diamond, M.I. (2007). Polyglutamine diseases: emerging concepts in pathogenesis and therapy. Hum Mol Genet *16 Spec No. 2*, R115-123. 10.1093/hmg/ddm213.

Sherman, M.Y., and Goldberg, A.L. (2001). Cellular defenses against unfolded proteins: a cell biologist thinks about neurodegenerative diseases. Neuron *29*, 15-32. 10.1016/s0896-6273(01)00177-5.

Shi, K.Y., Mori, E., Nizami, Z.F., Lin, Y., Kato, M., Xiang, S., Wu, L.C., Ding, M., Yu, Y., Gall, J.G., and McKnight, S.L. (2017). Toxic PR(n) poly-dipeptides encoded by the C9orf72 repeat expansion block nuclear import and export. Proc Natl Acad Sci U S A *114*, E1111-e1117. 10.1073/pnas.1620293114.

Shimura, H., Hattori, N., Kubo, S., Mizuno, Y., Asakawa, S., Minoshima, S., Shimizu, N., Iwai, K., Chiba, T., Tanaka, K., and Suzuki, T. (2000). Familial Parkinson disease gene product, parkin, is a ubiquitin-protein ligase. Nat Genet *25*, 302-305. 10.1038/77060.

Simões, A.T., Gonçalves, N., Koeppen, A., Déglon, N., Kügler, S., Duarte, C.B., and Pereira de Almeida, L. (2012). Calpastatin-mediated inhibition of calpains in the mouse brain prevents mutant ataxin 3 proteolysis, nuclear localization and aggregation, relieving Machado-Joseph disease. Brain *135*, 2428-2439. 10.1093/brain/aws177.

Singh, A.N., Oehler, J., Torrecilla, I., Kilgas, S., Li, S., Vaz, B., Guérillon, C., Fielden, J., Hernandez-Carralero, E., Cabrera, E., et al. (2019). The p97–Ataxin 3 complex regulates homeostasis of the DNA damage response E3 ubiquitin ligase RNF8. The EMBO Journal *38*, e102361.

Sinha, M., Mukhopadhyay, S., and Bhattacharyya, N.P. (2012). Mechanism(s) of alteration of micro RNA expressions in Huntington's disease and their possible contributions to the observed cellular and molecular dysfunctions in the disease. Neuromolecular Med *14*, 221-243. 10.1007/s12017-012-8183-0.

Sittler, A., Muriel, M.P., Marinello, M., Brice, A., den Dunnen, W., and Alves, S. (2018). Deregulation of autophagy in postmortem brains of Machado-Joseph disease patients. Neuropathology *38*, 113-124. 10.1111/neup.12433.

Soderholm, J.F., Bird, S.L., Kalab, P., Sampathkumar, Y., Hasegawa, K., Uehara-Bingen, M., Weis, K., and Heald, R. (2011). Importazole, a small molecule inhibitor of the transport receptor importin-β. ACS Chem Biol *6*, 700-708. 10.1021/cb2000296.

Solomon, D.A., Stepto, A., Au, W.H., Adachi, Y., Diaper, D.C., Hall, R., Rekhi, A., Boudi, A., Tziortzouda, P., Lee, Y.B., et al. (2018). A feedback loop between dipeptide-repeat protein, TDP-43 and karyopherin-α mediates C9orf72-related neurodegeneration. Brain *141*, 2908-2924. 10.1093/brain/awy241.

Soniat, M., and Chook, Y.M. (2015). Nuclear localization signals for four distinct karyopherin-β nuclear import systems. Biochem J *468*, 353-362. 10.1042/bj20150368.

Soong, B.W., and Paulson, H.L. (2007). Spinocerebellar ataxias: an update. Curr Opin Neurol *20*, 438-446. 10.1097/WCO.0b013e3281fbd3dd.

Sowa, A.S., Martin, E., Martins, I.M., Schmidt, J., Depping, R., Weber, J.J., Rother, F., Hartmann, E., Bader, M., Riess, O., et al. (2018). Karyopherin α-3 is a key protein in the pathogenesis of spinocerebellar ataxia type 3 controlling the nuclear localization of ataxin-3. Proc Natl Acad Sci U S A *115*, E2624-e2633. 10.1073/pnas.1716071115.

Sridhar, S., Botbol, Y., Macian, F., and Cuervo, A.M. (2012). Autophagy and disease: always two sides to a problem. J Pathol *226*, 255-273. 10.1002/path.3025.

Stoffler, D., Fahrenkrog, B., and Aebi, U. (1999). The nuclear pore complex: from molecular architecture to functional dynamics. Current Opinion in Cell Biology *11*, 391-401.

Stoyas, C.A., and La Spada, A.R. (2018). The CAG-polyglutamine repeat diseases: a clinical, molecular, genetic, and pathophysiologic nosology. Handb Clin Neurol *147*, 143-170. 10.1016/b978-0-444-63233-3.00011-7.

Strobl, S., Fernandez-Catalan, C., Braun, M., Huber, R., Masumoto, H., Nakagawa, K., Irie, A., Sorimachi, H., Bourenkow, G., Bartunik, H., et al. (2000). The crystal structure of calcium-free human m-calpain

suggests an electrostatic switch mechanism for activation by calcium. Proc Natl Acad Sci U S A *97*, 588-592. 10.1073/pnas.97.2.588.

Sullivan, R., Yau, W.Y., O'Connor, E., and Houlden, H. (2019). Spinocerebellar ataxia: an update. J Neurol *266*, 533-544. 10.1007/s00415-018-9076-4.

Suzuki, K., Bose, P., Leong-Quong, R.Y., Fujita, D.J., and Riabowol, K. (2010). REAP: A two minute cell fractionation method. BMC Res Notes *3*, 294. 10.1186/1756-0500-3-294.

Szczepanowska, K., Maiti, P., Kukat, A., Hofsetz, E., Nolte, H., Senft, K., Becker, C., Ruzzenente, B., Hornig-Do, H.T., Wibom, R., et al. (2016). CLPP coordinates mitoribosomal assembly through the regulation of ERAL1 levels. Embo j *35*, 2566-2583. 10.15252/embj.201694253.

Tait, D., Riccio, M., Sittler, A., Scherzinger, E., Santi, S., Ognibene, A., Maraldi, N.M., Lehrach, H., and Wanker, E.E. (1998). Ataxin-3 is transported into the nucleus and associates with the nuclear matrix. Hum Mol Genet *7*, 991-997. 10.1093/hmg/7.6.991.

Takahashi, T., Kikuchi, S., Katada, S., Nagai, Y., Nishizawa, M., and Onodera, O. (2008). Soluble polyglutamine oligomers formed prior to inclusion body formation are cytotoxic. Hum Mol Genet *17*, 345-356. 10.1093/hmg/ddm311.

Takalo, M., Salminen, A., Soininen, H., Hiltunen, M., and Haapasalo, A. (2013). Protein aggregation and degradation mechanisms in neurodegenerative diseases. Am J Neurodegener Dis *2*, 1-14.

Takiyama, Y., Nishizawa, M., Tanaka, H., Kawashima, S., Sakamoto, H., Karube, Y., Shimazaki, H., Soutome, M., Endo, K., Ohta, S., and et al. (1993). The gene for Machado-Joseph disease maps to human chromosome 14q. Nat Genet *4*, 300-304. 10.1038/ng0793-300.

Takiyama, Y., Igarashi, S., Rogaeva, E.A., Endo, K., Rogaev, E.I., Tanaka, H., Sherrington, R., Sanpei, K., Liang, Y., Saito, M., and et al. (1995). Evidence for inter-generational instability in the CAG repeat in the MJD1 gene and for conserved haplotypes at flanking markers amongst Japanese and Caucasian subjects with Machado-Joseph disease. Hum Mol Genet *4*, 1137-1146. 10.1093/hmg/4.7.1137.

Takiyama, Y., Sakoe, K., Nakano, I., and Nishizawa, M. (1997). Machado-Joseph disease: cerebellar ataxia and autonomic dysfunction in a patient with the shortest known expanded allele (56 CAG repeat units) of the MJD1 gene. Neurology *49*, 604-606. 10.1212/wnl.49.2.604.

Takizawa, C.G., and Morgan, D.O. (2000). Control of mitosis by changes in the subcellular location of cyclin-B1–Cdk1 and Cdc25C. Current Opinion in Cell Biology *12*, 658-665.

Tamburrino, A., and Decressac, M. (2016). Aged and Diseased Neurons Get Lost in Transport. Trends Neurosci *39*, 199-201. 10.1016/j.tins.2016.02.007.

Tatsuta, T., and Langer, T. (2009). AAA proteases in mitochondria: diverse functions of membrane-bound proteolytic machines. Res Microbiol *160*, 711-717. 10.1016/j.resmic.2009.09.005.

Taylor, J., Grote, S.K., Xia, J., Vandelft, M., Graczyk, J., Ellerby, L.M., La Spada, A.R., and Truant, R. (2006). Ataxin-7 can export from the nucleus via a conserved exportin-dependent signal. J Biol Chem *281*, 2730-2739. 10.1074/jbc.M506751200.

Taylor, J.P., Hardy, J., and Fischbeck, K.H. (2002). Toxic proteins in neurodegenerative disease. Science *296*, 1991-1995. 10.1126/science.1067122.

Teixeira-Castro, A., Ailion, M., Jalles, A., Brignull, H.R., Vilaça, J.L., Dias, N., Rodrigues, P., Oliveira, J.F., Neves-Carvalho, A., Morimoto, R.I., and Maciel, P. (2011). Neuron-specific proteotoxicity of mutant ataxin-3 in C. elegans: rescue by the DAF-16 and HSF-1 pathways. Hum Mol Genet *20*, 2996-3009. 10.1093/hmg/ddr203.

Thrower, J.S., Hoffman, L., Rechsteiner, M., and Pickart, C.M. (2000). Recognition of the polyubiquitin proteolytic signal. Embo j *19*, 94-102. 10.1093/emboj/19.1.94.

Todi, S.V., Winborn, B.J., Scaglione, K.M., Blount, J.R., Travis, S.M., and Paulson, H.L. (2009). Ubiquitination directly enhances activity of the deubiquitinating enzyme ataxin-3. Embo j *28*, 372-382. 10.1038/emboj.2008.289.

Tokumaru, A.M., Kamakura, K., Maki, T., Murayama, S., Sakata, I., Kaji, T., Kohyama, S., Kusano, S., and Hasegawa, S. (2003). Magnetic resonance imaging findings of Machado-Joseph disease: histopathologic correlation. J Comput Assist Tomogr *27*, 241-248. 10.1097/00004728-200303000-00023.

Trottier, Y., Cancel, G., An-Gourfinkel, I., Lutz, Y., Weber, C., Brice, A., Hirsch, E., and Mandel, J.-L. (1998). Heterogeneous Intracellular Localization and Expression of Ataxin-3. Neurobiology of Disease *5*, 335-347.

Trushina, E., Dyer, R.B., Badger, J.D., 2nd, Ure, D., Eide, L., Tran, D.D., Vrieze, B.T., Legendre-Guillemin, V., McPherson, P.S., Mandavilli, B.S., et al. (2004). Mutant huntingtin impairs axonal trafficking in mammalian neurons in vivo and in vitro. Mol Cell Biol *24*, 8195-8209. 10.1128/mcb.24.18.8195-8209.2004.

Tsai, H.F., Tsai, H.J., and Hsieh, M. (2004). Full-length expanded ataxin-3 enhances mitochondrial-mediated cell death and decreases Bcl-2 expression in human neuroblastoma cells. Biochem Biophys Res Commun *324*, 1274-1282. 10.1016/j.bbrc.2004.09.192.

Tsai, Y.C., Fishman, P.S., Thakor, N.V., and Oyler, G.A. (2003). Parkin facilitates the elimination of expanded polyglutamine proteins and leads to preservation of proteasome function. J Biol Chem *278*, 22044-22055. 10.1074/jbc.M212235200.

Tu, Y., Liu, H., Zhu, X., Shen, H., Ma, X., Wang, F., Huang, M., Gong, J., Li, X., Wang, Y., et al. (2017). Ataxin-3 promotes genome integrity by stabilizing Chk1. Nucleic Acids Res *45*, 4532-4549. 10.1093/nar/gkx095.

Tu, Y., Li, X., Zhu, X., Liu, X., Guo, C., Jia, D., and Tang, T.-S. (2020). Determining the Fate of Neurons in SCA3: ATX3, a Rising Decision Maker in Response to DNA Stresses and Beyond. Frontiers in Cell and Developmental Biology *8*. 10.3389/fcell.2020.619911.

Tyanova, S., Temu, T., Sinitcyn, P., Carlson, A., Hein, M.Y., Geiger, T., Mann, M., and Cox, J. (2016). The Perseus computational platform for comprehensive analysis of (prote)omics data. Nat Methods *13*, 731-740. 10.1038/nmeth.3901.

Tydlacka, S., Wang, C.E., Wang, X., Li, S., and Li, X.J. (2008). Differential activities of the ubiquitin-proteasome system in neurons versus glia may account for the preferential accumulation of misfolded proteins in neurons. J Neurosci *28*, 13285-13295. 10.1523/jneurosci.4393-08.2008.

van de Warrenburg, B.P., Sinke, R.J., Verschuuren-Bemelmans, C.C., Scheffer, H., Brunt, E.R., Ippel, P.F., Maat-Kievit, J.A., Dooijes, D., Notermans, N.C., Lindhout, D., et al. (2002). Spinocerebellar ataxias in the Netherlands: prevalence and age at onset variance analysis. Neurology *58*, 702-708. 10.1212/wnl.58.5.702.

van de Warrenburg, B.P., Hendriks, H., Dürr, A., van Zuijlen, M.C., Stevanin, G., Camuzat, A., Sinke, R.J., Brice, A., and Kremer, B.P. (2005). Age at onset variance analysis in spinocerebellar ataxias: a study in a Dutch-French cohort. Ann Neurol *57*, 505-512. 10.1002/ana.20424.

van der Watt, P.J., Maske, C.P., Hendricks, D.T., Parker, M.I., Denny, L., Govender, D., Birrer, M.J., and Leaner, V.D. (2009). The Karyopherin proteins, Crm1 and Karyopherin beta1, are overexpressed in cervical cancer and are critical for cancer cell survival and proliferation. Int J Cancer *124*, 1829-1840. 10.1002/ijc.24146.

Vilchez, D., Saez, I., and Dillin, A. (2014). The role of protein clearance mechanisms in organismal aging and age-related diseases. Nat Commun *5*, 5659. 10.1038/ncomms6659.

Wang, E.T., Taliaferro, J.M., Lee, J.A., Sudhakaran, I.P., Rossoll, W., Gross, C., Moss, K.R., and Bassell, G.J. (2016). Dysregulation of mRNA Localization and Translation in Genetic Disease. J Neurosci *36*, 11418-11426. 10.1523/jneurosci.2352-16.2016.

Wang, Z. (2018). Experimental and Clinical Strategies for Treating Spinocerebellar Ataxia Type 3. Neuroscience *371*, 138-154. 10.1016/j.neuroscience.2017.11.051.

Weber, J.J., Sowa, A.S., Binder, T., and Hübener, J. (2014). From pathways to targets: understanding the mechanisms behind polyglutamine disease. Biomed Res Int *2014*, 701758. 10.1155/2014/701758.

Weber, J.J., Golla, M., Guaitoli, G., Wanichawan, P., Hayer, S.N., Hauser, S., Krahl, A.C., Nagel, M., Samer, S., Aronica, E., et al. (2017). A combinatorial approach to identify calpain cleavage sites in the Machado-Joseph disease protein ataxin-3. Brain *140*, 1280-1299. 10.1093/brain/awx039.

Weis, K. (2003). Regulating access to the genome: nucleocytoplasmic transport throughout the cell cycle. Cell *112*, 441-451. 10.1016/s0092-8674(03)00082-5.

Weishäupl, D., Schneider, J., Peixoto Pinheiro, B., Ruess, C., Dold, S.M., von Zweydorf, F., Gloeckner, C.J., Schmidt, J., Riess, O., and Schmidt, T. (2019). Physiological and pathophysiological characteristics of ataxin-3 isoforms. J Biol Chem *294*, 644-661. 10.1074/jbc.RA118.005801.

Wellington, C.L., and Hayden, M.R. (1997). Of molecular interactions, mice and mechanisms: new insights into Huntington's disease. Curr Opin Neurol *10*, 291-298. 10.1097/00019052-199708000-00003.

Wellington, C.L., Ellerby, L.M., Hackam, A.S., Margolis, R.L., Trifiro, M.A., Singaraja, R., McCutcheon, K., Salvesen, G.S., Propp, S.S., Bromm, M., et al. (1998). Caspase cleavage of gene products associated with triplet expansion disorders generates truncated fragments containing the polyglutamine tract. J Biol Chem *273*, 9158-9167. 10.1074/jbc.273.15.9158.

Wen, W., Meinkoth, J.L., Tsien, R.Y., and Taylor, S.S. (1995). Identification of a signal for rapid export of proteins from the nucleus. Cell *82*, 463-473. 10.1016/0092-8674(95)90435-2.

Wente, S.R., and Rout, M.P. (2010). The nuclear pore complex and nuclear transport. Cold Spring Harb Perspect Biol *2*, a000562-a000562. 10.1101/cshperspect.a000562.

Williams, A.J., and Paulson, H.L. (2008). Polyglutamine neurodegeneration: protein misfolding revisited. Trends Neurosci *31*, 521-528. 10.1016/j.tins.2008.07.004.

Williams, A.J., Knutson, T.M., Colomer Gould, V.F., and Paulson, H.L. (2009). In vivo suppression of polyglutamine neurotoxicity by C-terminus of Hsp70-interacting protein (CHIP) supports an aggregation model of pathogenesis. Neurobiol Dis *33*, 342-353. 10.1016/j.nbd.2008.10.016.

Winborn, B.J., Travis, S.M., Todi, S.V., Scaglione, K.M., Xu, P., Williams, A.J., Cohen, R.E., Peng, J., and Paulson, H.L. (2008). The deubiquitinating enzyme ataxin-3, a polyglutamine disease protein, edits Lys63 linkages in mixed linkage ubiquitin chains. J Biol Chem *283*, 26436-26443. 10.1074/jbc.M803692200.

Woerner, A.C., Frottin, F., Hornburg, D., Feng, L.R., Meissner, F., Patra, M., Tatzelt, J., Mann, M., Winklhofer, K.F., Hartl, F.U., and Hipp, M.S. (2016). Cytoplasmic protein aggregates interfere with nucleocytoplasmic transport of protein and RNA. Science *351*, 173-176. 10.1126/science.aad2033.

Wong, E., Bejarano, E., Rakshit, M., Lee, K., Hanson, H.H., Zaarur, N., Phillips, G.R., Sherman, M.Y., and Cuervo, A.M. (2012). Molecular determinants of selective clearance of protein inclusions by autophagy. Nat Commun *3*, 1240. 10.1038/ncomms2244.

Xilouri, M., Brekk, O.R., and Stefanis, L. (2013). α-Synuclein and protein degradation systems: a reciprocal relationship. Mol Neurobiol *47*, 537-551. 10.1007/s12035-012-8341-2.

Yamada, M., Hayashi, S., Tsuji, S., and Takahashi, H. (2001). Involvement of the cerebral cortex and autonomic ganglia in Machado-Joseph disease. Acta Neuropathologica *101*, 140-144. 10.1007/s004010000277.

Yamashita, T., Aizawa, H., Teramoto, S., Akamatsu, M., and Kwak, S. (2017). Calpain-dependent disruption of nucleo-cytoplasmic transport in ALS motor neurons. Sci Rep *7*, 39994. 10.1038/srep39994.

Yan, X.X., Jeromin, A., and Jeromin, A. (2012). Spectrin Breakdown Products (SBDPs) as Potential Biomarkers for Neurodegenerative Diseases. Curr Transl Geriatr Exp Gerontol Rep *1*, 85-93. 10.1007/s13670-012-0009-2.

Yang, L., Hu, B., Zhang, Y., Qiang, S., Cai, J., Huang, W., Gong, C., Zhang, T., Zhang, S., Xu, P., et al. (2015). Suppression of the nuclear transporter-KPNβ1 expression inhibits tumor proliferation in hepatocellular carcinoma. Med Oncol *32*, 128. 10.1007/s12032-015-0559-1.

Yang, W., Dunlap, J.R., Andrews, R.B., and Wetzel, R. (2002). Aggregated polyglutamine peptides delivered to nuclei are toxic to mammalian cells. Hum Mol Genet *11*, 2905-2917. 10.1093/hmg/11.23.2905.

Yoshii, S.R., and Mizushima, N. (2017). Monitoring and Measuring Autophagy. Int J Mol Sci *18*. 10.3390/ijms18091865.

Yoshizawa, T., Ali, R., Jiou, J., Fung, H.Y.J., Burke, K.A., Kim, S.J., Lin, Y., Peeples, W.B., Saltzberg, D., Soniat, M., et al. (2018). Nuclear Import Receptor Inhibits Phase Separation of FUS through Binding to Multiple Sites. Cell *173*, 693-705.e622. 10.1016/j.cell.2018.03.003.

Yu, A.Y., and Houry, W.A. (2007). ClpP: a distinctive family of cylindrical energy-dependent serine proteases. FEBS Lett *581*, 3749-3757. 10.1016/j.febslet.2007.04.076.

Yu, Y.C., Kuo, C.L., Cheng, W.L., Liu, C.S., and Hsieh, M. (2009). Decreased antioxidant enzyme activity and increased mitochondrial DNA damage in cellular models of Machado-Joseph disease. J Neurosci Res *87*, 1884-1891. 10.1002/jnr.22011.

Yushchenko, T., Deuerling, E., and Hauser, K. (2018). Insights into the Aggregation Mechanism of PolyQ Proteins with Different Glutamine Repeat Lengths. Biophys J *114*, 1847-1857. 10.1016/j.bpj.2018.02.037.

Zhang, K., Donnelly, C.J., Haeusler, A.R., Grima, J.C., Machamer, J.B., Steinwald, P., Daley, E.L., Miller, S.J., Cunningham, K.M., Vidensky, S., et al. (2015). The C9orf72 repeat expansion disrupts nucleocytoplasmic transport. Nature *525*, 56-61. 10.1038/nature14973.

Zhang, S., Williamson, N.A., Duvick, L., Lee, A., Orr, H.T., Korlin-Downs, A., Yang, P., Mok, Y.F., Jans, D.A., and Bogoyevitch, M.A. (2020). The ataxin-1 interactome reveals direct connection with multiple disrupted nuclear transport pathways. Nat Commun *11*, 3343. 10.1038/s41467-020-17145-0.

Zhang, Z., Larner, S.F., Liu, M.C., Zheng, W., Hayes, R.L., and Wang, K.K. (2009). Multiple alphaII-spectrin breakdown products distinguish calpain and caspase dominated necrotic and apoptotic cell death pathways. Apoptosis *14*, 1289-1298. 10.1007/s10495-009-0405-z.

Zhao, Q., Wang, J., Levichkin, I.V., Stasinopoulos, S., Ryan, M.T., and Hoogenraad, N.J. (2002). A mitochondrial specific stress response in mammalian cells. Embo j *21*, 4411-4419. 10.1093/emboj/cdf445.

Zhong, X., and Pittman, R.N. (2006). Ataxin-3 binds VCP/p97 and regulates retrotranslocation of ERAD substrates. Hum Mol Genet *15*, 2409-2420. 10.1093/hmg/ddl164.

Zhong, Y., Wang, Y., Yang, H., Ballar, P., Lee, J.G., Ye, Y., Monteiro, M.J., and Fang, S. (2011). Importin beta interacts with the endoplasmic reticulum-associated degradation machinery and promotes

ubiquitination and degradation of mutant alpha1-antitrypsin. J Biol Chem *286*, 33921-33930. 10.1074/jbc.M111.272906.

Zhou, Y.-F., Liao, S.-S., Luo, Y.-Y., Tang, J.-G., Wang, J.-L., Lei, L.-F., Chi, J.-W., Du, J., Jiang, H., Xia, K., et al. (2013). SUMO-1 Modification on K166 of PolyQ-Expanded aTaxin-3 Strengthens Its Stability and Increases Its Cytotoxicity. PLOS ONE *8*, e54214. 10.1371/journal.pone.0054214.

Zoghbi, H.Y., and Orr, H.T. (2000). Glutamine repeats and neurodegeneration. Annu Rev Neurosci *23*, 217-247. 10.1146/annurev.neuro.23.1.217.

Acknowledgments

First and foremost, I am extremely grateful to my supervisor, PD Dr. Thorsten Schmidt, for his valuable advice, consistent support, and trust during my PhD study. His immense knowledge and plentiful experience have encouraged me throughout my academic research. I would like to express my sincere gratitude and appreciation to Prof. Dr. Olaf Rieß for his unlimited support, unconditional guidance, and encouragement during my PhD journey. I would like to thank my project committee member, Prof. Dr. Ludger Schöls from German Center for Neurodegenerative Diseases (DZNE) in Tübingen, for his insightful comments and advice.

I gratefully acknowledge Dr. Ana Velic and Prof. Dr. Boris Macek from Proteome Center Tübingen for their collaboration in mass spectrometry and data processing. I would like to offer my special thanks to Dr. Nicolas Casadei from NGS Competence Center Tübingen (NCCT) for his collaboration in RNA sequencing and Ingenuity Pathway Analysis. I would like to thank Dr. Stefan Hauser from German Center for Neurodegenerative Diseases (DZNE) in Tübingen for providing SCA3 patient-derived iPSCs. Additionally, I am extremely grateful to Dr. Jana Schmidt, Dr. Jeannette Hübener-Schmid, and Rana Dilara Incebacak Eltemur for helping with this research project.

I would like to say a big thank you to my friends Dr. Jonasz Jeremiasz Weber and Priscila Pereira Sena, who guided me so positively and always made me feel confident in my abilities, and whose insight and knowledge into the subject matter steered me through this research. Thank you very much, Jonasz and Pri, for all the support you have shown me through this journey!

I would also like to thank my student, Maria Kalimeri, for her contribution to this work. I also appreciate all my friends, labmates, colleagues, and all the members of the Institute of Medical Genetics and Applied Genomics, in particular Dr. Daniel Weishäupl, Dr. Ilnaz Sepahi, Eva Haas, Dr. Yogesh Singh, Dr. Elisabeth Singer, Jaqueline Jung, Reema Chowdhury, Linda Sofan, Dr. Libo Yu-Täger, Dr. Rebecca Buchert-Lo, and Dr. Arianna Novati, for a cherished time spent together in the lab and in social settings.

Acknowledgments

I would like to extend my sincere thanks to the Deutscher Akademischer Austauschdienst (DAAD) for the financial support to undertake my PhD within the “Research Grants-Doctoral Programmes in Germany”.

Many thanks to Graduate Training Centre of Neuroscience, especially PD Dr. Marc Himmelbach and Dr. Monika Lam, for all their help and support during my PhD journey.

Most importantly, none of this could have happened without my beloved family. To my mother, who was a constant inspiration throughout my life and always believed in my ability to be successful but sadly did not live to see this journey finished. Thank you, Mom, for always loving me and guiding me. Even though you are no longer here with me, I can still feel your love guiding me. You will always be in my heart. I am also thankful to my father and my sister for their unconditional love and support. Lastly, I would like to thank my husband and best friend, Saeed Mazloom, for his tremendous understanding, encouragement, and love. Thank you for always being so supportive and helping me every step of the way!

Statement of contributions

The entire thesis was done by the PhD candidate, and some parts were performed with the collaboration of some colleagues.

The PhD candidate (Mahkameh Abeditashi) analyzed the interaction of nuclear transport receptors (KPNB1, KPNA2, and KPNA3) with wild-type and polyQ-expanded ataxin-3. Investigated the effects of modulation of KPNB1 levels on intracellular localization of ataxin-3. Studied the impacts of KPNB1 overexpression on protein levels, cleavage, and aggregation of ataxin-3 and knockdown/pharmacological inhibition of KPNB1 on protein levels and aggregation of ataxin-3. Generated mutated KPNB1 construct via molecular cloning, followed by Sanger sequencing to confirm it, and investigation of the effects of mutated KPNB1 on ataxin-3. Analyzed the effects of KPNB1 protein levels modulation on the stability of ataxin-3. Investigated the effects of inhibition of proteolytic pathways on ataxin-3 protein levels and cleavage. Analyzed the impacts of mitochondrial protease CLPP protein levels modulation on ataxin-3. Performed Ingenuity Pathway Analysis and interpretation of proteomics and transcriptomics data.

Dr. Jonasz Jeremiasz Weber performed analysis of the calpain activation and cell-based calpain cleavage assays and contributed to the Ingenuity Pathway Analysis. Priscila Pereira Sena performed cell viability assay and analysis of KPNB1 and CLPP protein levels in SCA3 models and contributed to the stability assay of ataxin-3. Rana Dilara Incebacak Eltemur contributed to the analysis of the effects of CLPP levels modulation.

Maria Kalimeri, under my supervision, contributed to the analysis of the effects of mutated KPNB1 on ataxin-3.

Dr. Nicolas Casadei from NGS Competence Center Tübingen (NCCT) conducted RNA sequencing and contributed to the Ingenuity Pathway Analysis of transcriptomics data. Dr. Ana Velic and Prof. Dr. Boris Macek from Proteome Center Tübingen carried out mass spectrometry and data processing.

Dr. Stefan Hauser from German Center for Neurodegenerative Diseases (DZNE) in Tübingen provided induced pluripotent stem cells. Dr. Jana Schmidt and Dr. Jeannette Hübener-Schmid provided brain tissues of transgenic mouse models.

Statement of contributions

Parts of the results of this PhD dissertation have been published in “Abeditashi, M., Weber, J. J., Pereira Sena, P., Velic, A., Kalimeri, M., Incebacak Eltemur, R. D., Schmidt, J., Hübener-Schmid, J., Hauser, S., Macek, B., Riess, O., & Schmidt, T. (2022). KPNB1 modulates the Machado-Joseph disease protein ataxin-3 through activation of the mitochondrial protease CLPP. *Cellular and molecular life sciences: CMLS*, *79*(8), 401”.

Appendix A: RNA sequencing

Table A.1 RNA sequencing revealed 565 differentially expressed genes in wild-type (15Q) ataxin-3-expressing cells upon KPNB1 overexpression (15Q + CTRL *vs* 15Q + KPNB1). The top 100 differentially expressed genes are listed in the table. FC = fold change; FDR = false discovery rate.

Gene name	Protein name	Log_2 FC	*P*-value	FDR
GH1	growth hormone 1	13.3796	0.0000	0.0000
GH2	growth hormone 2	9.2380	0.0000	0.0000
RNU4ATAC4P	RNA, U4atac small nuclear 4, pseudogene	4.1533	0.0000	0.0015
KPNB1	karyopherin (importin) beta 1	3.3313	0.0000	0.0000
ANKRD1	ankyrin repeat domain 1 (cardiac muscle)	3.0473	0.0000	0.0000
RP11-875O11.1		2.7314	0.0001	0.0044
MT-TA	mitochondrially encoded tRNA alanine	2.6839	0.0315	0.1915
RP11-386I14.4		2.6317	0.0000	0.0000
RP11-386I23.1		2.3590	0.0000	0.0001
HMOX1	heme oxygenase (decycling) 1	2.3561	0.0000	0.0000
RNU2-63P	RNA, U2 small nuclear 63, pseudogene	2.3002	0.0000	0.0000
SNX31	sorting nexin 31	2.2684	0.0000	0.0040
RNU11	RNA, U11 small nuclear	2.2671	0.0000	0.0000
ZBTB8OSP2	zinc finger and BTB domain containing 8 opposite strand pseudogene 2	2.2518	0.0001	0.0060
ARHGAP30	Rho GTPase activating protein 30	2.2316	0.0000	0.0016
RP11-386G11.5		2.2249	0.0000	0.0000
SCUBE2	signal peptide, CUB domain, EGF-like 2	2.2150	0.0000	0.0010
GDF15	growth differentiation factor 15	2.1358	0.0000	0.0000
U3	Small nucleolar RNA U3	2.0320	0.0000	0.0030
RNU1-60P	RNA, U1 small nuclear 60, pseudogene	1.9769	0.0000	0.0001
RNU1-85P	RNA, U1 small nuclear 85, pseudogene	1.9481	0.0000	0.0000
IQCA1P1	IQ motif containing with AAA domain 1 pseudogene 1	1.9204	0.0001	0.0078
SLC22A14	solute carrier family 22, member 14	1.8677	0.0000	0.0000
RNVU1-20	RNA, variant U1 small nuclear 20	1.8552	0.0005	0.0175
CYP4F3	cytochrome P450, family 4, subfamily F, polypeptide 3	1.7886	0.0000	0.0003
Y_RNA	Y RNA	1.7675	0.0001	0.0051
MSH4	mutS homolog 4	1.5882	0.0081	0.0906
CNTD2	cyclin N-terminal domain containing 2	1.5717	0.0003	0.0123
PTAFR	platelet-activating factor receptor	1.5550	0.0005	0.0173
ISG20	interferon stimulated exonuclease gene 20kDa	1.5200	0.0000	0.0013
RP3-340B19.2		1.5038	0.0008	0.0226
PYGM	phosphorylase, glycogen, muscle	1.5020	0.0020	0.0392
SNORD42	Small nucleolar RNA SNORD42	1.4670	0.0075	0.0872
C7orf61	chromosome 7 open reading frame 61	1.4251	0.0004	0.0154
ARRDC3	arrestin domain containing 3	1.4064	0.0000	0.0000

Gene name	Protein name	Log_2 FC	*P*-value	FDR
RN7SL336P	RNA, 7SL, cytoplasmic 336, pseudogene	1.4020	0.0221	0.1592
PLAC8L1	PLAC8-like 1	1.3808	0.0005	0.0166
NHLH2	nescient helix loop helix 2	1.3681	0.0000	0.0000
LMTK2	lemur tyrosine kinase 2	1.3653	0.0000	0.0000
RP3-326I13.1		1.3615	0.0017	0.0353
FOXQ1	forkhead box Q1	1.3458	0.0037	0.0580
ZNF669	zinc finger protein 669	1.3401	0.0000	0.0000
AC132192.1	LOC644656 protein; Uncharacterized protein	1.3134	0.0008	0.0230
RP4-607J23.2		1.2691	0.0012	0.0287
APC2	adenomatosis polyposis coli 2	1.2550	0.0013	0.0307
KIAA1614	KIAA1614	1.2468	0.0126	0.1148
RP11-372K14.2		1.2392	0.0115	0.1089
NPC1L1	NPC1-like 1	1.2349	0.0020	0.0391
IL20RB	interleukin 20 receptor beta	1.2206	0.0016	0.0350
ETV5	ets variant 5	1.2163	0.0022	0.0414
ARHGEF33	Rho guanine nucleotide exchange factor (GEF) 33	-1.0438	0.0078	0.0887
DNAH7	dynein, axonemal, heavy chain 7	-1.0460	0.0001	0.0073
SPDYC	speedy/RINGO cell cycle regulator family member C	-1.0506	0.0140	0.1229
AP001007.1		-1.0620	0.0008	0.0226
MEIG1	meiosis/spermiogenesis associated 1	-1.0709	0.0254	0.1700
KCNN4	potassium intermediate/small conductance calcium-activated channel, subfamily N, member 4	-1.0765	0.0408	0.2200
TXLNB	taxilin beta	-1.0791	0.0227	0.1624
LEKR1	leucine, glutamate and lysine rich 1	-1.0974	0.0058	0.0759
RNU1-124P	RNA, U1 small nuclear 124, pseudogene	-1.1290	0.0002	0.0095
RBP5	retinol binding protein 5, cellular	-1.1306	0.0083	0.0918
EPS8L2	EPS8-like 2	-1.1364	0.0010	0.0265
WDR93	WD repeat domain 93	-1.1402	0.0084	0.0921
KIAA1211L	KIAA1211-like	-1.1404	0.0019	0.0386
ABCD2	ATP-binding cassette, sub-family D (ALD), member 2	-1.1450	0.0090	0.0956
EPHA10	EPH receptor A10	-1.1473	0.0034	0.0556
FAXDC2	fatty acid hydroxylase domain containing 2	-1.1489	0.0000	0.0015
RP11-1038A11.3		-1.1695	0.0268	0.1752
ACVRL1	activin A receptor type II-like 1	-1.1732	0.0014	0.0313
FILIP1	filamin A interacting protein 1	-1.1835	0.0004	0.0155
AC145212.1		-1.1850	0.0267	0.1749
MTND4P12	MT-ND4 pseudogene 12	-1.1922	0.0209	0.1532
PM20D1	peptidase M20 domain containing 1	-1.1930	0.0202	0.1508
WDR31	WD repeat domain 31	-1.2095	0.0000	0.0002
RP11-389G6.3		-1.2182	0.0039	0.0604
C14orf79	chromosome 14 open reading frame 79	-1.2253	0.0009	0.0248
EFCAB6	EF-hand calcium binding domain 6	-1.2309	0.0109	0.1066
snoU13	Small nucleolar RNA U13	-1.2404	0.0204	0.1515
RPS3AP3	ribosomal protein S3A pseudogene 3	-1.2409	0.0036	0.0573

Gene name	Protein name	Log_2 FC	*P*-value	FDR
RP11-485G7.5		-1.2416	0.0103	0.1031
RP3-500L14.2		-1.2518	0.0173	0.1372
HIST1H4H	histone cluster 1, H4h	-1.2741	0.0022	0.0413
CCDC160	coiled-coil domain containing 160	-1.2896	0.0022	0.0418
RP5-1049N15.2		-1.3054	0.0037	0.0585
SSR4P1	signal sequence receptor, delta pseudogene 1	-1.3292	0.0022	0.0412
DEGS2	delta(4)-desaturase, sphingolipid 2	-1.3482	0.0117	0.1101
HIST1H2AG	histone cluster 1, H2ag	-1.3485	0.0002	0.0099
HIST1H2BJ	histone cluster 1, H2bj	-1.3605	0.0000	0.0004
LINC00853	long intergenic non-protein coding RNA 853	-1.3650	0.0062	0.0783
DHRS2	dehydrogenase/reductase (SDR family) member 2	-1.4411	0.0000	0.0000
ACKR2	atypical chemokine receptor 2	-1.4807	0.0111	0.1069
THSD7A	thrombospondin, type I, domain containing 7A	-1.4983	0.0024	0.0447
RUNDC3A	RUN domain containing 3A	-1.5019	0.0021	0.0402
RP11-1101H11.1		-1.5358	0.0009	0.0239
RP11-70C1.1		-1.6270	0.0001	0.0049
RP11-432J24.5		-1.6368	0.0001	0.0078
RPS10P28	ribosomal protein S10 pseudogene 28	-1.7315	0.0001	0.0057
PPL	periplakin	-1.7375	0.0000	0.0003
PACRG	PARK2 co-regulated	-1.8248	0.0020	0.0399
EDN2	endothelin 2	-2.1766	0.0000	0.0003
SNORD3B-2	small nucleolar RNA, C/D box 3B-2	-4.3946	0.0001	0.0053

Table A.2 RNA sequencing revealed 653 differentially expressed genes in polyQ-expanded (148Q) ataxin-3-expressing cells upon KPNB1 overexpression (148Q + CTRL *vs* 148Q + KPNB1). The top 100 differentially expressed genes are listed in the table. FC = fold change; FDR = false discovery rate.

Gene name	Protein name	Log_2 FC	*P*-value	FDR
GH1	growth hormone 1	14.9827	0.0000	0.0000
GH2	growth hormone 2	7.5075	0.0000	0.0000
ANKRD1	ankyrin repeat domain 1 (cardiac muscle)	4.3660	0.0000	0.0000
ZBTB8OSP2	zinc finger and BTB domain containing 8 opposite strand pseudogene 2	4.3095	0.0000	0.0000
RNU4ATAC4P	RNA, U4atac small nuclear 4, pseudogene	3.9416	0.0000	0.0001
KPNB1	karyopherin (importin) beta 1	3.3942	0.0000	0.0000
RP11-386I14.4		3.2841	0.0000	0.0000
HMOX1	heme oxygenase (decycling) 1	3.1640	0.0000	0.0000
SNX31	sorting nexin 31	3.0524	0.0000	0.0000
ALLC	allantoicase	2.9844	0.0000	0.0027
RP11-875O11.1		2.9493	0.0000	0.0027
Y_RNA	Y RNA	2.8086	0.0000	0.0000
RNVU1-20	RNA, variant U1 small nuclear 20	2.7831	0.0000	0.0003
RP11-44F14.8		2.7032	0.0000	0.0001
NPC1L1	NPC1-like 1	2.6708	0.0000	0.0000

Gene name	Protein name	Log_2 FC	*P*-value	FDR
GDF15	growth differentiation factor 15	2.5394	0.0000	0.0000
ARHGAP30	Rho GTPase activating protein 30	2.5226	0.0000	0.0007
RP11-386I23.1		2.4549	0.0000	0.0000
PTAFR	platelet-activating factor receptor	2.3845	0.0000	0.0001
AL589739.1	Uncharacterized protein	2.3707	0.0001	0.0044
RNU2-63P	RNA, U2 small nuclear 63, pseudogene	2.3127	0.0000	0.0000
RP3-486I3.4		2.2741	0.0000	0.0034
NKAPL	NFKB activating protein-like	2.2461	0.0006	0.0199
SCUBE2	signal peptide, CUB domain, EGF-like 2	2.0977	0.0000	0.0005
SNORD42	Small nucleolar RNA SNORD42	2.0666	0.0002	0.0077
KIAA1614	KIAA1614	2.0529	0.0008	0.0229
CNTD2	cyclin N-terminal domain containing 2	2.0453	0.0000	0.0008
AVIL	advillin	2.0008	0.0001	0.0045
CTSS	cathepsin S	1.9575	0.0005	0.0172
ARRDC3	arrestin domain containing 3	1.9538	0.0000	0.0000
RP11-372K14.2		1.9336	0.0001	0.0059
HUS1B	HUS1 checkpoint homolog b (S. pombe)	1.8979	0.0002	0.0090
RP11-386G11.5		1.8954	0.0000	0.0001
RNU1-60P	RNA, U1 small nuclear 60, pseudogene	1.8756	0.0000	0.0000
ZNF669	zinc finger protein 669	1.8733	0.0000	0.0000
FRZB	frizzled-related protein	1.8727	0.0001	0.0043
IL20RB	interleukin 20 receptor beta	1.8457	0.0000	0.0005
TAF7L	TAF7-like RNA polymerase II, TATA box binding protein (TBP)-associated factor, 50kDa	1.8293	0.0000	0.0003
SUMO4	small ubiquitin-like modifier 4	1.8076	0.0000	0.0018
CYP4F3	cytochrome P450, family 4, subfamily F, polypeptide 3	1.8025	0.0000	0.0001
RP11-791G15.2		1.7628	0.0000	0.0004
IQCA1P1	IQ motif containing with AAA domain 1 pseudogene 1	1.7515	0.0002	0.0076
RN7SKP274	RNA, 7SK small nuclear pseudogene 274	1.6694	0.0009	0.0243
RNU11	RNA, U11 small nuclear	1.6507	0.0000	0.0001
NHLH2	nescient helix loop helix 2	1.6497	0.0000	0.0000
RP3-326I13.1		1.6330	0.0004	0.0148
APC2	adenomatosis polyposis coli 2	1.6136	0.0000	0.0023
SLC22A14	solute carrier family 22, member 14	1.6125	0.0000	0.0000
PRDM1	PR domain containing 1, with ZNF domain	1.5956	0.0002	0.0087
SNORA42	small nucleolar RNA, H/ACA box 42	1.5811	0.0001	0.0046
DIRC3	disrupted in renal carcinoma 3	-1.0288	0.0015	0.0337
AGTR1	angiotensin II receptor, type 1	-1.0301	0.0341	0.2006
VAX2	ventral anterior homeobox 2	-1.0307	0.0067	0.0812
ACTA2	actin, alpha 2, smooth muscle, aorta	-1.0324	0.0000	0.0003
AC007690.1		-1.0488	0.0165	0.1354
RP11-723O4.9		-1.0586	0.0124	0.1139
SNAP25	synaptosomal-associated protein, 25kDa	-1.0630	0.0001	0.0061
RP11-717D12.1		-1.0660	0.0161	0.1331

Gene name	Protein name	Log_2 FC	*P*-value	FDR
COL6A4P2	collagen, type VI, alpha 4 pseudogene 2	-1.0700	0.0094	0.0976
RPL21P32	ribosomal protein L21 pseudogene 32	-1.0845	0.0160	0.1330
STPG2	sperm-tail PG-rich repeat containing 2	-1.0902	0.0208	0.1541
RAP2C-AS1	RAP2C antisense RNA 1	-1.0967	0.0011	0.0274
THAP10	THAP domain containing 10	-1.0985	0.0004	0.0153
RSPH4A	radial spoke head 4 homolog A (Chlamydomonas)	-1.1007	0.0062	0.0780
RP11-152N13.5		-1.1024	0.0008	0.0229
TSNAXIP1	translin-associated factor X interacting protein 1	-1.1073	0.0307	0.1889
ASTN1	astrotactin 1	-1.1140	0.0069	0.0822
AC018755.1	HCG2008157; Uncharacterized protein; cDNA FLJ30403 fis, clone BRACE2008480	-1.1237	0.0084	0.0914
TCEA3	transcription elongation factor A (SII), 3	-1.1278	0.0174	0.1396
USH1G	Usher syndrome 1G (autosomal recessive)	-1.1455	0.0015	0.0334
AP3B2	adaptor-related protein complex 3, beta 2 subunit	-1.1564	0.0001	0.0039
AC147651.3		-1.1590	0.0049	0.0678
RP11-23F23.2		-1.1856	0.0169	0.1370
SCGB1B2P	secretoglobin, family 1B, member 2, pseudogene	-1.1910	0.0084	0.0914
RP11-115D19.1		-1.1960	0.0045	0.0644
PACRG	PARK2 co-regulated	-1.2024	0.0254	0.1709
CTD-2377D24.6		-1.2255	0.0026	0.0471
KHDC1	KH homology domain containing 1	-1.2309	0.0020	0.0409
RBP5	retinol binding protein 5, cellular	-1.2353	0.0025	0.0458
RP11-345F18.1		-1.2573	0.0006	0.0196
EPS8L2	EPS8-like 2	-1.2612	0.0005	0.0172
RPSAP6	ribosomal protein SA pseudogene 6	-1.2801	0.0101	0.1019
FAXDC2	fatty acid hydroxylase domain containing 2	-1.2934	0.0000	0.0006
RNU6-228P	RNA, U6 small nuclear 228, pseudogene	-1.3039	0.0012	0.0293
RP11-125B21.2		-1.3143	0.0122	0.1127
RUNDC3A	RUN domain containing 3A	-1.3156	0.0043	0.0628
PTH1R	parathyroid hormone 1 receptor	-1.3293	0.0012	0.0291
RP5-933K21.3		-1.3533	0.0032	0.0535
LIMD1-AS1	LIMD1 antisense RNA 1	-1.3551	0.0011	0.0280
SORCS2	sortilin-related VPS10 domain containing receptor 2	-1.4649	0.0008	0.0233
EDN2	endothelin 2	-1.4965	0.0008	0.0223
RP11-421P23.1		-1.5566	0.0004	0.0141
FGD3	FYVE, RhoGEF and PH domain containing 3	-1.6398	0.0001	0.0067
CCDC160	coiled-coil domain containing 160	-1.8007	0.0002	0.0077
DHRS2	dehydrogenase/reductase (SDR family) member 2	-1.9103	0.0000	0.0000
PPL	periplakin	-2.0843	0.0000	0.0001
RP11-588H23.3		-2.1270	0.0001	0.0053
KCNN4	potassium intermediate/small conductance calcium-activated channel, subfamily N, member 4	-2.1604	0.0003	0.0118
RP11-70C1.1		-2.6810	0.0000	0.0003
MT-TA	mitochondrially encoded tRNA alanine	-3.2147	0.0029	0.0496

Appendix B: Mass spectrometry

Table B.1 Label-free quantitative proteomics identified 93 proteins that have been altered significantly in wild-type (15Q) ataxin-3-expressing cells upon KPNB1 overexpression (15Q + CTRL *vs* 15Q + KPNB1). FC = fold change.

Gene name	Protein name	Log_2 FC	*P*-value
KPNB1	Importin β-1	1.5114	0.0000
DUSP3	Dual specificity protein phosphatase 3	0.7018	0.0389
HIST1H2AJ; HIST1H2AH	Histone H2A type 1-J; Histone H2A type 1-H	0.6828	0.0297
CNBP	Cellular nucleic acid-binding protein	0.4154	0.0032
EEF1A2	Elongation factor 1-alpha 2	0.3624	0.0175
KPNA2	Importin α-1	0.2815	0.0129
TRMT112	Multifunctional methyltransferase subunit TRM112-like protein	0.2738	0.0209
RPA3	Replication protein A 14 kDa subunit	0.2699	0.0251
ATP6V1B2	V-type proton ATPase subunit B, brain isoform	0.2638	0.0010
BYSL	Bystin	0.2514	0.0080
CDC5L	Cell division cycle 5-like protein	0.2443	0.0288
PFN1	Profilin-1	0.2261	0.0009
PCNA	Proliferating cell nuclear antigen	0.2254	0.0425
ARFGAP1	ADP-ribosylation factor GTPase-activating protein 1	0.2049	0.0356
IST1	IST1 homolog	0.1857	0.0316
PRPF19	Pre-mRNA-processing factor 19	0.1719	0.0458
ANXA5	Annexin A5; Annexin	0.1700	0.0042
SLC25A12	Calcium-binding mitochondrial carrier protein Aralar1	0.1697	0.0282
SNX1	Sorting nexin-1	0.1602	0.0173
PPIA	Peptidyl-prolyl cis-trans isomerase A; Peptidyl-prolyl cis-trans isomerase A, N-terminally processed; Peptidyl-prolyl cis-trans	0.1424	0.0064
STIP1	Stress-induced-phosphoprotein 1	0.1058	0.0241
COPG1	Coatomer subunit gamma-1	0.0920	0.0109
IQGAP1	Ras GTPase-activating-like protein IQGAP1	0.0770	0.0227
PA2G4	Proliferation-associated protein 2G4	0.0642	0.0333
FLNB	Filamin-B	-0.0694	0.0303
CLTC	Clathrin heavy chain; Clathrin heavy chain 1	-0.0734	0.0435
CKAP5	Cytoskeleton-associated protein 5	-0.0860	0.0342
NUP93	Nuclear pore complex protein Nup93	-0.0923	0.0399
SMC2	Structural maintenance of chromosomes protein 2	-0.0947	0.0355
EEF1D	Elongation factor 1-delta	-0.0959	0.0015
SUCLG2	Succinyl-CoA ligase [GDP-forming] subunit beta, mitochondrial	-0.0959	0.0092

Gene name	Protein name	Log_2 FC	*P*-value
SLC25A13	Calcium-binding mitochondrial carrier protein Aralar2	-0.1021	0.0190
CRYZ	Quinone oxidoreductase	-0.1048	0.0262
UBE2M	NEDD8-conjugating enzyme Ubc12	-0.1108	0.0050
RPL4	60S ribosomal protein L4	-0.1122	0.0480
CSDE1	Cold shock domain-containing protein E1	-0.1181	0.0459
GDI1	Rab GDP dissociation inhibitor alpha	-0.1232	0.0253
RBM28	RNA-binding protein 28	-0.1279	0.0316
DARS2	Aspartate--tRNA ligase, mitochondrial	-0.1395	0.0131
AAAS	Aladin	-0.1416	0.0299
DCTN1	Dynactin subunit 1	-0.1417	0.0034
DDX46	Probable ATP-dependent RNA helicase DDX46	-0.1434	0.0163
SEPT9	Septin-9	-0.1503	0.0047
NUP155	Nuclear pore complex protein Nup155	-0.1514	0.0385
SYMPK	Symplekin	-0.1546	0.0218
QARS	Glutamine--tRNA ligase	-0.1550	0.0086
MAPK3	Mitogen-activated protein kinase 3	-0.1564	0.0100
HIBCH	3-hydroxyisobutyryl-CoA hydrolase, mitochondrial	-0.1582	0.0478
CYFIP1	Cytoplasmic FMR1-interacting protein 1	-0.1637	0.0274
MAP2K2	Dual specificity mitogen-activated protein kinase kinase 2	-0.1644	0.0444
SLC3A2	4F2 cell-surface antigen heavy chain	-0.1754	0.0013
SLC25A1	Tricarboxylate transport protein, mitochondrial	-0.1761	0.0032
MGST1	Microsomal glutathione S-transferase 1	-0.1864	0.0438
PARP1	Poly [ADP-ribose] polymerase 1	-0.1876	0.0318
BUB3	Mitotic checkpoint protein BUB3	-0.1992	0.0146
IDH2	Isocitrate dehydrogenase [NADP], mitochondrial	-0.2038	0.0048
ACOT2; ACOT1	Acyl-coenzyme A thioesterase 1; Acyl-coenzyme A thioesterase 2, mitochondrial	-0.2065	0.0063
LMAN2	Vesicular integral-membrane protein VIP36	-0.2084	0.0244
RPL11	60S ribosomal protein L11	-0.2092	0.0039
MYDGF	Myeloid-derived growth factor	-0.2095	0.0204
SDHA	Succinate dehydrogenase [ubiquinone] flavoprotein subunit, mitochondrial	-0.2126	0.0439
CYC1	Cytochrome c1, heme protein, mitochondrial	-0.2172	0.0406
VPS26A	Vacuolar protein sorting-associated protein 26A	-0.2174	0.0185
SUPV3L1	ATP-dependent RNA helicase SUPV3L1, mitochondrial	-0.2266	0.0487
PRTFDC1	Phosphoribosyltransferase domain-containing protein 1	-0.2435	0.0217
FDPS	Farnesyl pyrophosphate synthase	-0.2457	0.0162
SCPEP1	Retinoid-inducible serine carboxypeptidase	-0.2466	0.0323
UGGT1	UDP-glucose:glycoprotein glucosyltransferase 1	-0.2496	0.0409
STX12	Syntaxin-12	-0.2542	0.0003

Gene name	Protein name	Log_2 FC	*P*-value
IDH3G	Isocitrate dehydrogenase [NAD] subunit, mitochondrial; Isocitrate dehydrogenase [NAD] subunit gamma, mitochondrial	-0.2557	0.0323
AMOT	Angiomotin	-0.2578	0.0332
ERLIN2	Erlin-2	-0.2602	0.0471
NOL9	Polynucleotide 5-hydroxyl-kinase NOL9	-0.2676	0.0333
EPB41	Protein 4.1	-0.2700	0.0210
MRPL19	39S ribosomal protein L19, mitochondrial	-0.2731	0.0429
WDR18	WD repeat-containing protein 18	-0.2753	0.0028
DDX20	Probable ATP-dependent RNA helicase DDX20	-0.2756	0.0013
CYP51A1	Lanosterol 14-alpha demethylase	-0.2841	0.0452
TPP1	Tripeptidyl-peptidase 1	-0.3038	0.0408
FAM98B	Protein FAM98B	-0.3313	0.0191
DNAJC9	DnaJ homolog subfamily C member 9	-0.3363	0.0215
SRPR	Signal recognition particle receptor subunit alpha	-0.3494	0.0391
SCP2	Non-specific lipid-transfer protein	-0.3614	0.0127
NKRF	NF-kappa-B-repressing factor	-0.3672	0.0353
SLC7A5	Large neutral amino acids transporter small subunit 1	-0.3889	0.0370
SYNJ2BP; SYNJ2BP-COX16	Synaptojanin-2-binding protein	-0.3971	0.0080
CCNB1	G2/mitotic-specific cyclin-B1	-0.4004	0.0028
MAVS	Mitochondrial antiviral-signaling protein	-0.4164	0.0111
LSM1	U6 snRNA-associated Sm-like protein LSm1	-0.4352	0.0419
SPCS3	Signal peptidase complex subunit 3	-0.4971	0.0078
P4HA1	Prolyl 4-hydroxylase subunit alpha-1	-0.6746	0.0084
ATXN3	Ataxin-3	-1.8790	0.0007

Table B.2 Label-free quantitative proteomics identified 172 proteins that have been altered significantly in polyQ-expanded (148Q) ataxin-3-expressing cells upon KPNB1 overexpression (148Q + CTRL *vs* 148Q + KPNB1). FC = fold change.

Gene name	Protein name	Log_2 FC	*P*-value
KPNB1	Importin β-1	1.5582	0.0000
HIST1H4A	Histone H4	0.4271	0.0025
CDKN2A	Cyclin-dependent kinase inhibitor 2A; Cyclin-dependent kinase 4 inhibitor B	0.4229	0.0110
KPNA2	Importin α-1	0.3919	0.0126
CUL2	Cullin-2	0.3825	0.0146
MRPL47	39S ribosomal protein L47, mitochondrial	0.3516	0.0322
ENOPH1	Enolase-phosphatase E1	0.3450	0.0271
PTGES3	Prostaglandin E synthase 3	0.3385	0.0102
ARL8B	ADP-ribosylation factor-like protein 8B	0.3377	0.0484

Gene name	Protein name	Log_2 FC	*P*-value
ARL3	ADP-ribosylation factor-like protein 3	0.3222	0.0152
PWP1	Periodic tryptophan protein 1 homolog	0.3153	0.0138
ARF5	ADP-ribosylation factor 5	0.2971	0.0207
CSNK2B	Casein kinase II subunit beta	0.2734	0.0157
RPS15	40S ribosomal protein S15	0.2696	0.0402
ANXA2	Annexin A2; Annexin; Putative annexin A2-like protein	0.2673	0.0032
ATG3	Ubiquitin-like-conjugating enzyme ATG3	0.2587	0.0251
NDUFB10	NADH dehydrogenase [ubiquinone] 1 beta subcomplex subunit 10	0.2534	0.0319
UBE2L3	Ubiquitin-conjugating enzyme E2 L3	0.2467	0.0092
ACP1	Low molecular weight phosphotyrosine protein phosphatase	0.2385	0.0095
TNPO1	Transportin-1	0.2311	0.0085
SSB	Lupus La protein	0.2288	0.0052
DNAJB11	DnaJ homolog subfamily B member 11	0.2243	0.0296
PPA1	Inorganic pyrophosphatase	0.2162	0.0076
TSR1	Pre-rRNA-processing protein TSR1 homolog	0.2083	0.0476
HSP90AB2P	Putative heat shock protein HSP 90-beta 2	0.2018	0.0152
COPB1	Coatomer subunit beta	0.1976	0.0281
PPIA	Peptidyl-prolyl cis-trans isomerase A; Peptidyl-prolyl cis-trans isomerase A, N-terminally processed	0.1933	0.0242
PSMD10	26S proteasome non-ATPase regulatory subunit 10	0.1768	0.0410
SRRT	Serrate RNA effector molecule homolog	0.1764	0.0453
GTPBP4	Nucleolar GTP-binding protein 1	0.1688	0.0161
DIAPH1	Protein diaphanous homolog 1	0.1665	0.0450
IPO7	Importin-7	0.1590	0.0021
XPO1	Exportin-1	0.1578	0.0082
RPA3	Replication protein A 14 kDa subunit	0.1511	0.0049
DHX16	Putative pre-mRNA-splicing factor ATP-dependent RNA helicase DHX16	0.1307	0.0035
CSE1L	Exportin-2	0.1146	0.0225
TUBA1C	Tubulin alpha-1C chain	0.1102	0.0299
LAP3	Cytosol aminopeptidase	0.1083	0.0322
LTA4H	Leukotriene A-4 hydrolase	0.1069	0.0262
BPNT1	3(2),5-bisphosphate nucleotidase 1	0.1033	0.0298
DHX9	ATP-dependent RNA helicase A	0.0917	0.0126
EPB41L2	Band 4.1-like protein 2	0.0861	0.0074
HSPA4	Heat shock 70 kDa protein 4	0.0759	0.0246
HSPA1B; HSPA1A	Heat shock 70 kDa protein 1B; Heat shock 70 kDa protein 1A	0.0733	0.0210
BAG6; BAT3	Large proline-rich protein BAG6	0.0541	0.0481
RPS6	40S ribosomal protein S6	-0.0599	0.0454

Gene name	Protein name	Log_2 FC	*P*-value
LRPPRC	Leucine-rich PPR motif-containing protein, mitochondrial	-0.0622	0.0351
LONP1	Lon protease homolog, mitochondrial	-0.0763	0.0434
DARS	Aspartate-tRNA ligase, cytoplasmic	-0.0766	0.0453
ALDH7A1	Alpha-aminoadipic semialdehyde dehydrogenase	-0.0787	0.0213
DDB1	DNA damage-binding protein 1	-0.0817	0.0417
FANCI	Fanconi anemia group I protein	-0.0901	0.0375
RPS9	40S ribosomal protein S9	-0.0926	0.0082
SF3B3	Splicing factor 3B subunit 3	-0.0949	0.0342
MDH2	Malate dehydrogenase, mitochondrial; Malate dehydrogenase	-0.0982	0.0184
DYNC1H1	Cytoplasmic dynein 1 heavy chain 1	-0.0986	0.0341
AP1G1	AP-1 complex subunit gamma-1	-0.1029	0.0258
GRHPR	Glyoxylate reductase/hydroxypyruvate reductase	-0.1083	0.0286
GCN1L1	Translational activator GCN1	-0.1096	0.0229
ATP5B	ATP synthase subunit beta, mitochondrial; ATP synthase subunit beta	-0.1105	0.0315
SLC25A17	Peroxisomal membrane protein PMP34	-0.1110	0.0194
HMBS	Porphobilinogen deaminase	-0.1118	0.0150
MTHFD1L	Monofunctional C1-tetrahydrofolate synthase, mitochondrial	-0.1133	0.0484
MRPS2	28S ribosomal protein S2, mitochondrial	-0.1147	0.0422
CAD	CAD protein; Glutamine-dependent carbamoyl-phosphate synthase; Aspartate carbamoyltransferase; Dihydroorotase	-0.1153	0.0380
FLNB	Filamin-B	-0.1163	0.0048
PDHB	Pyruvate dehydrogenase E1 component subunit beta, mitochondrial	-0.1206	0.0004
NHP2L1	NHP2-like protein 1; NHP2-like protein 1, N-terminally processed	-0.1253	0.0162
GANAB	Neutral alpha-glucosidase AB	-0.1271	0.0312
GTF3C5	General transcription factor 3C polypeptide 5	-0.1308	0.0482
PHB2	Prohibitin-2	-0.1347	0.0345
UQCRC1	Cytochrome b-c1 complex subunit 1, mitochondrial	-0.1362	0.0378
HDLBP	Vigilin	-0.1362	0.0039
NDUFS2	NADH dehydrogenase [ubiquinone] iron-sulfur protein 2, mitochondrial	-0.1370	0.0078
HSD17B4	Peroxisomal multifunctional enzyme type 2; (3R)-hydroxyacyl-CoA dehydrogenase; Enoyl-CoA hydratase 2	-0.1404	0.0336
NUP155	Nuclear pore complex protein Nup155	-0.1444	0.0206
STT3A	Dolichyl-diphosphooligosaccharide--protein glycosyltransferase subunit STT3A	-0.1453	0.0302
FLNA	Filamin-A	-0.1466	0.0085
RPRD1A	Regulation of nuclear pre-mRNA domain-containing protein 1A	-0.1469	0.0439
WDR1	WD repeat-containing protein 1	-0.1480	0.0078
ACACA	Acetyl-CoA carboxylase 1; Biotin carboxylase	-0.1484	0.0098
ATAD3A	ATPase family AAA domain-containing protein 3A	-0.1485	0.0011
EIF3H	Eukaryotic translation initiation factor 3 subunit H	-0.1498	0.0291

Gene name	Protein name	Log_2 FC	*P*-value
BCAP31	B-cell receptor-associated protein 31	-0.1539	0.0343
ALDH9A1	4-trimethylaminobutyraldehyde dehydrogenase	-0.1542	0.0500
PFKP	ATP-dependent 6-phosphofructokinase, platelet type	-0.1547	0.0075
CYP51A1	Lanosterol 14-alpha demethylase	-0.1569	0.0012
CPOX	Oxygen-dependent coproporphyrinogen-III oxidase, mitochondrial	-0.1593	0.0290
NDUFA9	NADH dehydrogenase [ubiquinone] 1 alpha subcomplex subunit 9, mitochondrial	-0.1612	0.0157
TECR	Very-long-chain enoyl-CoA reductase	-0.1639	0.0287
DAP3	28S ribosomal protein S29, mitochondrial	-0.1641	0.0311
ACAT1	Acetyl-CoA acetyltransferase, mitochondrial	-0.1643	0.0300
ESYT1	Extended synaptotagmin-1	-0.1677	0.0381
GTF2I	General transcription factor II-I	-0.1695	0.0131
FDPS	Farnesyl pyrophosphate synthase	-0.1717	0.0179
RPS23	40S ribosomal protein S23	-0.1743	0.0060
HADH	Hydroxyacyl-coenzyme A dehydrogenase, mitochondrial	-0.1752	0.0383
MCCC2	Methylcrotonoyl-CoA carboxylase beta chain, mitochondrial	-0.1755	0.0330
ACO1	Cytoplasmic aconitate hydratase	-0.1762	0.0191
SUCLG2	Succinyl-CoA ligase [GDP-forming] subunit beta, mitochondrial	-0.1858	0.0163
CCAR2	Cell cycle and apoptosis regulator protein 2	-0.1875	0.0006
NUP160	Nuclear pore complex protein Nup160	-0.1877	0.0355
HIBCH	3-hydroxyisobutyryl-CoA hydrolase, mitochondrial	-0.1885	0.0129
EMC3	ER membrane protein complex subunit 3	-0.1964	0.0080
NELFCD; TH1L	Negative elongation factor C/D	-0.1970	0.0078
MAP2K2	Dual specificity mitogen-activated protein kinase kinase 2	-0.1988	0.0464
MPDU1	Mannose-P-dolichol utilization defect 1 protein	-0.1994	0.0056
IDH1	Isocitrate dehydrogenase [NADP] cytoplasmic	-0.2030	0.0198
DARS2	Aspartate--tRNA ligase, mitochondrial	-0.2035	0.0386
DHCR7	7-dehydrocholesterol reductase	-0.2059	0.0320
UQCRC2	Cytochrome b-c1 complex subunit 2, mitochondrial	-0.2069	0.0398
RTN4	Reticulon-4; Reticulon	-0.2083	0.0493
APMAP	Adipocyte plasma membrane-associated protein	-0.2086	0.0448
NCSTN	Nicastrin	-0.2139	0.0078
ARL6IP5	PRA1 family protein 3	-0.2141	0.0336
IDH2	Isocitrate dehydrogenase [NADP], mitochondrial	-0.2143	0.0083
HMGCS1	Hydroxymethylglutaryl-CoA synthase, cytoplasmic	-0.2147	0.0189
BSG	Basigin	-0.2154	0.0111
DLST	Dihydrolipoyllysine-residue succinyltransferase component of 2-oxoglutarate dehydrogenase complex, mitochondrial	-0.2165	0.0320
SEH1L	Nucleoporin SEH1	-0.2226	0.0397

Gene name	Protein name	Log_2 FC	*P*-value
TMX4	Thioredoxin-related transmembrane protein 4	-0.2246	0.0256
TBRG4	Protein TBRG4	-0.2265	0.0401
SNRPB2	U2 small nuclear ribonucleoprotein B	-0.2296	0.0250
RPL35A	60S ribosomal protein L35a	-0.2308	0.0008
IKBKAP	Elongator complex protein 1	-0.2315	0.0017
MRPL38	39S ribosomal protein L38, mitochondrial	-0.2358	0.0248
ALDH2	Aldehyde dehydrogenase, mitochondrial	-0.2384	0.0070
GNAS	Guanine nucleotide-binding protein G(s) subunit alpha isoforms XLas; Guanine nucleotide-binding protein G(s) subunit alpha isoforms short	-0.2388	0.0441
GAA	Lysosomal alpha-glucosidase; 76 kDa lysosomal alpha-glucosidase	-0.2407	0.0123
RPL22L1	60S ribosomal protein L22-like 1	-0.2410	0.0446
PRKDC	DNA-dependent protein kinase catalytic subunit	-0.2427	0.0029
MRPS27	28S ribosomal protein S27, mitochondrial	-0.2483	0.0339
NNT	NAD(P) transhydrogenase, mitochondrial	-0.2493	0.0332
EXOSC7	Exosome complex component RRP42	-0.2501	0.0380
RPS10; RPS10P5	40S ribosomal protein S10; Putative 40S ribosomal protein S10-like	-0.2502	0.0359
RPL28	60S ribosomal protein L28	-0.2507	0.0267
CLPB	Caseinolytic peptidase B protein homolog	-0.2562	0.0063
THEM6	Protein THEM6	-0.2575	0.0190
ERLIN2	Erlin-2	-0.2581	0.0166
AFG3L2	AFG3-like protein 2	-0.2598	0.0192
ACADM	Medium-chain specific acyl-CoA dehydrogenase, mitochondrial	-0.2633	0.0010
ADAR	Double-stranded RNA-specific adenosine deaminase	-0.2648	0.0480
AMOT	Angiomotin	-0.2684	0.0069
POLR2B	DNA-directed RNA polymerase II subunit RPB2	-0.2696	0.0155
NOC3L	Nucleolar complex protein 3 homolog	-0.2713	0.0006
SLC25A12	Calcium-binding mitochondrial carrier protein Aralar1	-0.2725	0.0148
CDS2	Phosphatidate cytidylyltransferase 2	-0.2739	0.0244
RNF2	E3 ubiquitin-protein ligase RING2	-0.2743	0.0310
KIF11	Kinesin-like protein KIF11	-0.2761	0.0168
PDHA1	Pyruvate dehydrogenase E1 component subunit alpha, somatic form, mitochondrial	-0.2786	0.0177
SMU1	WD40 repeat-containing protein SMU1; WD40 repeat-containing protein SMU1, N-terminally processed	-0.2852	0.0329
SYNGR2	Synaptogyrin-2	-0.2861	0.0291
ACADSB	Short/branched chain specific acyl-CoA dehydrogenase, mitochondrial	-0.2868	0.0129
DPYSL5	Dihydropyrimidinase-related protein 5	-0.2868	0.0458
QPRT	Nicotinate-nucleotide pyrophosphorylase [carboxylating]	-0.2901	0.0364
SURF4	Surfeit locus protein 4	-0.2901	0.0147

Gene name	Protein name	Log_2 FC	*P*-value
SEC22B	Vesicle-trafficking protein SEC22b	-0.2909	0.0204
TMEM14C	Transmembrane protein 14C	-0.3068	0.0168
FAM213A	Redox-regulatory protein FAM213A	-0.3102	0.0118
NUP210	Nuclear pore membrane glycoprotein 210	-0.3195	0.0002
TBL3	Transducin beta-like protein 3	-0.3198	0.0255
SACM1L	Phosphatidylinositide phosphatase SAC1	-0.3269	0.0023
SQLE	Squalene monooxygenase	-0.3345	0.0084
SGPL1	Sphingosine-1-phosphate lyase 1	-0.3576	0.0251
TKFC; DAK	Bifunctional ATP-dependent dihydroxyacetone kinase/FAD-AMP lyase (cyclizing); ATP-dependent dihydroxyacetone kinase; FAD-AMP lyase (cyclizing)	-0.3674	0.0039
GHITM	Growth hormone-inducible transmembrane protein	-0.4197	0.0163
IGF2R	Cation-independent mannose-6-phosphate receptor	-0.4554	0.0497
FAM98B	Protein FAM98B	-0.4639	0.0026
RCC1	Regulator of chromosome condensation	-0.4675	0.0095
PTGFRN	Prostaglandin F2 receptor negative regulator	-0.4707	0.0077
PDCD11	Protein RRP5 homolog	-0.5345	0.0070
LSS	Lanosterol synthase	-0.5474	0.0195

Table B.3 Label-free quantitative proteomics identified 215 proteins that have been altered significantly upon KPNB1 overexpression (CTRL *vs* KPNB1). FC = fold change.

Gene name	Protein name	Log_2 FC	*P*-value
KPNB1	Importin β-1	1.5348	0.0000
HIST1H2AJ; HIST1H2AH	Histone H2A type 1-J; Histone H2A type 1-H	0.6668	0.0040
PAFAH1B2	Platelet-activating factor acetylhydrolase IB subunit beta	0.4742	0.0409
H3F3B; H3F3A	Histone H3; Histone H3.2; Histone H3.1t; Histone H3.3	0.4085	0.0332
HIST1H4A	Histone H4	0.3715	0.0328
KPNA2	Importin α-1	0.3367	0.0001
SF3B6	Splicing factor 3B subunit 6	0.3289	0.0190
GLUL	Glutamine synthetase	0.3235	0.0263
HSP90AB2P	Putative heat shock protein HSP 90-beta 2	0.2917	0.0209
PWP1	Periodic tryptophan protein 1 homolog	0.2915	0.0357
PSMA2	Proteasome subunit alpha type; Proteasome subunit alpha type-2	0.2671	0.0414
PPME1	Protein phosphatase methylesterase 1	0.2623	0.0289
CNBP	Cellular nucleic acid-binding protein	0.2595	0.0152
PURA	Transcriptional activator protein Pur-alpha	0.2500	0.0376
KPNA1	Importin α-5; Importin α-5, N-terminally processed	0.2436	0.0191
ACP1	Low molecular weight phosphotyrosine protein phosphatase	0.2423	0.0110

Gene name	Protein name	Log_2 FC	*P*-value
ACTR10	Actin-related protein 10	0.2414	0.0239
SNRPF	Small nuclear ribonucleoprotein F	0.2371	0.0397
PPA1	Inorganic pyrophosphatase	0.2360	0.0263
EIF3K	Eukaryotic translation initiation factor 3 subunit K	0.2325	0.0169
CDKN2A; CDKN2B	Cyclin-dependent kinase inhibitor 2A; Cyclin-dependent kinase 4 inhibitor B	0.2320	0.0350
ATG3	Ubiquitin-like-conjugating enzyme ATG3	0.2126	0.0167
BYSL	Bystin	0.2107	0.0041
CDC5L	Cell division cycle 5-like protein	0.2107	0.0012
RPA3	Replication protein A 14 kDa subunit	0.2105	0.0168
DDX39B	Spliceosome RNA helicase DDX39B	0.2023	0.0236
EEF1A2	Elongation factor 1-alpha 2	0.2015	0.0441
TRMT112	Multifunctional methyltransferase subunit TRM112-like protein	0.1973	0.0015
SRSF7	Serine/arginine-rich splicing factor 7	0.1926	0.0234
CA2	Carbonic anhydrase 2	0.1896	0.0270
IDE	Insulin-degrading enzyme	0.1889	0.0191
UBA3	NEDD8-activating enzyme E1 catalytic subunit	0.1830	0.0242
SSB	Lupus La protein	0.1814	0.0193
COPB1	Coatomer subunit beta	0.1809	0.0056
PCNA	Proliferating cell nuclear antigen	0.1775	0.0167
CSNK2A1; CSNK2A3	Casein kinase II subunit alpha; Casein kinase II subunit alpha 3	0.1769	0.0466
TNPO1	Transportin-1	0.1754	0.0020
TSR1	Pre-rRNA-processing protein TSR1 homolog	0.1739	0.0076
LAS1L	Ribosomal biogenesis protein LAS1L	0.1733	0.0180
RPS15	40S ribosomal protein S15	0.1684	0.0399
PPIA	Peptidyl-prolyl cis-trans isomerase A; Peptidyl-prolyl cis-trans isomerase A, N-terminally processed	0.1678	0.0067
IPO7	Importin-7	0.1621	0.0185
CFL1	Cofilin-1	0.1496	0.0229
U2AF2	Splicing factor U2AF 65 kDa subunit	0.1477	0.0495
NANS	Sialic acid synthase	0.1462	0.0494
ACTA1; ACTC1	Actin, alpha skeletal muscle; Actin, alpha cardiac muscle 1; Actin, gamma-enteric smooth muscle; Actin, aortic smooth muscle	0.1437	0.0327
CAPRIN1	Caprin-1	0.1403	0.0470
GTPBP4	Nucleolar GTP-binding protein 1	0.1335	0.0203
UBA2	SUMO-activating enzyme subunit 2	0.1318	0.0371
XPO1	Exportin-1	0.1298	0.0051
IPO11	Importin-11	0.1235	0.0415
PRMT1	Protein arginine N-methyltransferase 1	0.1221	0.0390
STIP1	Stress-induced-phosphoprotein 1	0.1210	0.0033

Gene name	Protein name	Log_2 FC	*P*-value
SRRT	Serrate RNA effector molecule homolog	0.1189	0.0282
HSP90AA1	Heat shock protein HSP 90-alpha	0.1058	0.0152
PRPF19	Pre-mRNA-processing factor 19	0.1001	0.0439
NAP1L1	Nucleosome assembly protein 1-like 1	0.0996	0.0424
EEF1A1; EEF1A1P5	Elongation factor 1-alpha 1; Putative elongation factor 1-alpha-like 3; Elongation factor 1-alpha	0.0989	0.0353
CSE1L	Exportin-2	0.0976	0.0070
IPO5	Importin-5	0.0887	0.0130
LTA4H	Leukotriene A-4 hydrolase	0.0865	0.0085
COPG1	Coatomer subunit gamma-1	0.0678	0.0369
LAP3	Cytosol aminopeptidase	0.0583	0.0396
IQGAP1	Ras GTPase-activating-like protein IQGAP1	0.0554	0.0350
SMC4	Structural maintenance of chromosomes protein 4; Structural maintenance of chromosomes protein	-0.0491	0.0472
CLTC	Clathrin heavy chain; Clathrin heavy chain 1	-0.0523	0.0381
SMC2	Structural maintenance of chromosomes protein 2	-0.0560	0.0483
PCBP1	Poly(rC)-binding protein 1	-0.0696	0.0419
HSPA8	Heat shock cognate 71 kDa protein	-0.0733	0.0202
PSMC6	26S protease regulatory subunit 10B	-0.0790	0.0464
AP1G1	AP-1 complex subunit gamma-1	-0.0794	0.0192
EEF1D	Elongation factor 1-delta	-0.0814	0.0228
RAB1A	Ras-related protein Rab-1A	-0.0847	0.0239
CAD	CAD protein; Glutamine-dependent carbamoyl-phosphate synthase; Aspartate carbamoyltransferase; Dihydroorotase	-0.0866	0.0448
VCL	Vinculin	-0.0881	0.0401
IRS4	Insulin receptor substrate 4	-0.0894	0.0300
FLNB	Filamin-B	-0.0928	0.0019
DDX3X; DDX3Y	ATP-dependent RNA helicase DDX3X; ATP-dependent RNA helicase DDX3Y	-0.0963	0.0158
RPL5	60S ribosomal protein L5	-0.0968	0.0369
HSD17B4	Peroxisomal multifunctional enzyme type 2; (3R)-hydroxyacyl-CoA dehydrogenase; Enoyl-CoA hydratase 2	-0.0979	0.0452
PFKP	ATP-dependent 6-phosphofructokinase, platelet type	-0.0999	0.0033
CSDE1	Cold shock domain-containing protein E1	-0.1005	0.0055
PABPC4	Polyadenylate-binding protein 4; Polyadenylate-binding protein	-0.1021	0.0342
AP2B1	AP-2 complex subunit beta	-0.1032	0.0280
RPS6	40S ribosomal protein S6	-0.1061	0.0082
NDUFS2	NADH dehydrogenase [ubiquinone] iron-sulfur protein 2, mitochondrial	-0.1081	0.0380
QARS	Glutamine--tRNA ligase	-0.1095	0.0085
PYCR1	Pyrroline-5-carboxylate reductase 1	-0.1101	0.0338
MAP4	Microtubule-associated protein; Microtubule-associated protein 4	-0.1107	0.0274

Gene name	Protein name	Log_2 FC	*P*-value
FARSB	Phenylalanine--tRNA ligase beta subunit	-0.1123	0.0126
DCTN1	Dynactin subunit 1	-0.1135	0.0283
MAPK3	Mitogen-activated protein kinase 3; Mitogen-activated protein kinase	-0.1136	0.0068
MDN1	Midasin	-0.1195	0.0415
HDLBP	Vigilin	-0.1196	0.0007
RFC4	Replication factor C subunit 4	-0.1220	0.0368
CYFIP1	Cytoplasmic FMR1-interacting protein 1	-0.1238	0.0381
PDHB	Pyruvate dehydrogenase E1 component subunit beta, mitochondrial	-0.1257	0.0155
CPNE1	Copine-1	-0.1265	0.0363
RPL10	60S ribosomal protein L10	-0.1273	0.0147
SRP54	Signal recognition particle 54 kDa protein	-0.1292	0.0093
SEPT9	Septin-9	-0.1316	0.0267
SLC25A11	Mitochondrial 2-oxoglutarate/malate carrier protein	-0.1324	0.0138
IDH1	Isocitrate dehydrogenase [NADP] cytoplasmic	-0.1345	0.0077
ALDH9A1	4-trimethylaminobutyraldehyde dehydrogenase	-0.1367	0.0127
SEC61A1	Protein transport protein Sec61 subunit alpha isoform 1	-0.1372	0.0444
CPOX	Oxygen-dependent coproporphyrinogen-III oxidase, mitochondrial	-0.1375	0.0030
DDX20	Probable ATP-dependent RNA helicase DDX20	-0.1393	0.0296
VPS26A	Vacuolar protein sorting-associated protein 26A	-0.1402	0.0147
SUCLG2	Succinyl-CoA ligase [GDP-forming] subunit beta, mitochondrial	-0.1409	0.0016
RTN4	Reticulon-4; Reticulon	-0.1415	0.0394
CCAR2	Cell cycle and apoptosis regulator protein 2	-0.1417	0.0350
FLNA	Filamin-A	-0.1437	0.0046
EXOSC2	Exosome complex component RRP4	-0.1447	0.0390
MLEC	Malectin	-0.1450	0.0465
NUP155	Nuclear pore complex protein Nup155	-0.1479	0.0319
POLR2B	DNA-directed RNA polymerase II subunit RPB2	-0.1486	0.0267
PARP1	Poly [ADP-ribose] polymerase 1	-0.1509	0.0044
ACO2	Aconitate hydratase, mitochondrial	-0.1522	0.0391
IKBKAP	Elongator complex protein 1	-0.1523	0.0163
CLPB	Caseinolytic peptidase B protein homolog	-0.1549	0.0384
STT3A	Dolichyl-diphosphooligosaccharide--protein glycosyltransferase subunit STT3A	-0.1552	0.0135
RAB21	Ras-related protein Rab-21	-0.1571	0.0042
MRPL46	39S ribosomal protein L46, mitochondrial	-0.1575	0.0467
POLDIP3	Polymerase delta-interacting protein 3	-0.1576	0.0352
APMAP	Adipocyte plasma membrane-associated protein	-0.1578	0.0489
MRPS27	28S ribosomal protein S27, mitochondrial	-0.1619	0.0273

Gene name	Protein name	Log_2 FC	*P*-value
GTF2I	General transcription factor II-I	-0.1626	0.0268
SCRN1	Secernin-1	-0.1641	0.0484
SLC25A1	Tricarboxylate transport protein, mitochondrial	-0.1647	0.0136
DHCR7	7-dehydrocholesterol reductase	-0.1657	0.0210
HYOU1	Hypoxia up-regulated protein 1	-0.1687	0.0337
NCSTN	Nicastrin	-0.1707	0.0439
NNT	NAD(P) transhydrogenase, mitochondrial	-0.1709	0.0330
DARS2	Aspartate--tRNA ligase, mitochondrial	-0.1715	0.0077
ABCD3	ATP-binding cassette sub-family D member 3	-0.1724	0.0340
HIBCH	3-hydroxyisobutyryl-CoA hydrolase, mitochondrial	-0.1733	0.0049
PRKDC	DNA-dependent protein kinase catalytic subunit	-0.1739	0.0013
DECR1	2,4-dienoyl-CoA reductase, mitochondrial	-0.1742	0.0293
HMGCS1	Hydroxymethylglutaryl-CoA synthase, cytoplasmic	-0.1746	0.0034
MYDGF	Myeloid-derived growth factor	-0.1761	0.0063
TBL3	Transducin beta-like protein 3	-0.1798	0.0276
MAP2K2	Dual specificity mitogen-activated protein kinase kinase 2	-0.1816	0.0020
CPSF7	Cleavage and polyadenylation specificity factor subunit 7	-0.1822	0.0135
PHF6	PHD finger protein 6	-0.1830	0.0304
SDHA	Succinate dehydrogenase [ubiquinone] flavoprotein subunit, mitochondrial	-0.1838	0.0244
DLST	Dihydrolipoyllysine-residue succinyltransferase component of 2-oxoglutarate dehydrogenase complex, mitochondrial	-0.1863	0.0445
PRPF31	U4/U6 small nuclear ribonucleoprotein Prp31	-0.1872	0.0331
MRPL19	39S ribosomal protein L19, mitochondrial	-0.1877	0.0142
ACOT2; ACOT1	Acyl-coenzyme A thioesterase 1; Acyl-coenzyme A thioesterase 2, mitochondrial	-0.1907	0.0073
DOCK7	Dedicator of cytokinesis protein 7	-0.1912	0.0464
SCPEP1	Retinoid-inducible serine carboxypeptidase	-0.1930	0.0205
TBRG4	Protein TBRG4	-0.1946	0.0097
QPRT	Nicotinate-nucleotide pyrophosphorylase [carboxylating]	-0.1969	0.0463
UQCRC2	Cytochrome b-c1 complex subunit 2, mitochondrial	-0.1973	0.0354
ALDH2	Aldehyde dehydrogenase, mitochondrial	-0.2008	0.0077
ACADM	Medium-chain specific acyl-CoA dehydrogenase, mitochondrial	-0.2022	0.0030
PITRM1	Presequence protease, mitochondrial	-0.2064	0.0422
FDPS	Farnesyl pyrophosphate synthase	-0.2087	0.0006
IDH2	Isocitrate dehydrogenase [NADP], mitochondrial	-0.2090	0.0015
TST	Thiosulfate sulfurtransferase	-0.2100	0.0299
WDR18	WD repeat-containing protein 18	-0.2111	0.0064
UGGT1	UDP-glucose: glycoprotein glucosyltransferase 1	-0.2128	0.0072
AFG3L2	AFG3-like protein 2	-0.2160	0.0098

Gene name	Protein name	Log_2 FC	*P*-value
RPL28	60S ribosomal protein L28	-0.2160	0.0219
RPL35A	60S ribosomal protein L35a	-0.2175	0.0005
NOC3L	Nucleolar complex protein 3 homolog	-0.2176	0.0282
TMX4	Thioredoxin-related transmembrane protein 4	-0.2183	0.0186
CYP51A1	Lanosterol 14-alpha demethylase	-0.2205	0.0181
BSG	Basigin	-0.2227	0.0166
CDIPT	CDP-diacylglycerol--inositol 3-phosphatidyltransferase	-0.2227	0.0331
GNAI3	Guanine nucleotide-binding protein G(k) subunit alpha	-0.2237	0.0217
FAR1	Fatty acyl-CoA reductase 1	-0.2245	0.0246
GNAS	Guanine nucleotide-binding protein G(s) subunit alpha isoforms XLas; Guanine nucleotide-binding protein G(s) subunit alpha isoforms short	-0.2255	0.0323
PAFAH1B1	Platelet-activating factor acetylhydrolase IB subunit alpha	-0.2292	0.0232
CTNNB1	Catenin beta-1	-0.2300	0.0432
PDHA1	Pyruvate dehydrogenase E1 component subunit alpha, somatic form, mitochondrial	-0.2333	0.0144
DDI2	Protein DDI1 homolog 2	-0.2341	0.0424
ADAR	Double-stranded RNA-specific adenosine deaminase	-0.2368	0.0143
TMEM14C	Transmembrane protein 14C	-0.2399	0.0105
DHRS7	Dehydrogenase/reductase SDR family member 7	-0.2415	0.0114
NUP210	Nuclear pore membrane glycoprotein 210	-0.2416	0.0137
LMNB1	Lamin-B1	-0.2447	0.0405
GAA	Lysosomal alpha-glucosidase; 76 kDa lysosomal alpha-glucosidase	-0.2460	0.0058
SYNJ2BP; SYNJ2BP-COX16	Synaptojanin-2-binding protein	-0.2463	0.0296
SGPL1	Sphingosine-1-phosphate lyase 1	-0.2482	0.0207
ACADSB	Short/branched chain specific acyl-CoA dehydrogenase, mitochondrial	-0.2485	0.0064
SQLE	Squalene monooxygenase	-0.2485	0.0085
EIF2AK2	Interferon-induced, double-stranded RNA-activated protein kinase	-0.2528	0.0436
KIF11	Kinesin-like protein KIF11	-0.2572	0.0076
SLC7A5	Large neutral amino acids transporter small subunit 1	-0.2577	0.0094
ERLIN2	Erlin-2	-0.2591	0.0148
AMOT	Angiomotin	-0.2631	0.0002
NKRF	NF-kappa-B-repressing factor	-0.2632	0.0218
PTPN1	Tyrosine-protein phosphatase non-receptor type 1	-0.2696	0.0427
SLC25A17	Peroxisomal membrane protein PMP34	-0.2724	0.0313
PCK2	Phosphoenolpyruvate carboxykinase [GTP], mitochondrial	-0.2733	0.0486
DPYSL5	Dihydropyrimidinase-related protein 5	-0.2863	0.0078
TRAM1	Translocating chain-associated membrane protein 1	-0.2953	0.0471
SACM1L	Phosphatidylinositide phosphatase SAC1	-0.2992	0.0033

Gene name	Protein name	Log_2 FC	*P*-value
MAVS	Mitochondrial antiviral-signaling protein	-0.3010	0.0014
CCNB1	G2/mitotic-specific cyclin-B1	-0.3035	0.0020
PDCD11	Protein RRP5 homolog	-0.3035	0.0090
THEM6	Protein THEM6	-0.3070	0.0160
DPM1	Dolichol-phosphate mannosyltransferase subunit 1	-0.3085	0.0068
MRPS7	28S ribosomal protein S7, mitochondrial	-0.3161	0.0457
GHITM	Growth hormone-inducible transmembrane protein	-0.3215	0.0456
RPL22L1	60S ribosomal protein L22-like 1	-0.3489	0.0033
PTGFRN	Prostaglandin F2 receptor negative regulator	-0.3713	0.0384
RCC1	Regulator of chromosome condensation	-0.3871	0.0024
FAM98B	Protein FAM98B	-0.3893	0.0006
PLOD3	Procollagen-lysine,2-oxoglutarate 5-dioxygenase 3	-0.4076	0.0207
SPCS3	Signal peptidase complex subunit 3	-0.4291	0.0015
P4HA1	Prolyl 4-hydroxylase subunit alpha-1	-0.4891	0.0034
ATXN3	Ataxin-3	-1.6792	0.0141